CRUISE REPORT: 06MT19941230

Downloaded from NCEI: November 2024 Created: January 2025

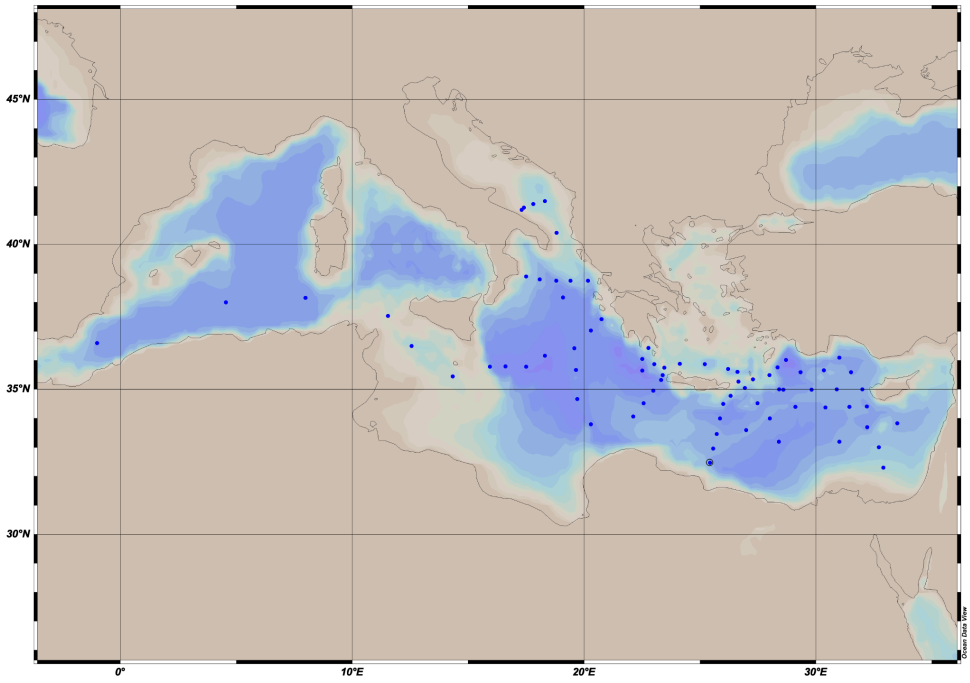

Highlights

Cruise Summary Information

Section Designation	M31/1
Expedition Designation (ExpoCode)	**06MT19941230**
Chief Scientist	**Christof Hemleben, (GPI Tü)**
Dates	30 December 1994 – 22 March 1995
Ship	R/V METEOR
Ports of Call	Hamburg, Germany Port Said, Egypt
Geographic Boundaries	41° 30' 0" N 1° 0' 36"W 33° 30' 7"E 32° 18' 7" N
Stations	75 (Leg 1)
Floats and Drifters Deployed	0
Moorings Deployed and Recovered	0

Contact Information:

Prof. Dr. Christoph Hemleben
Geologisch-Paläontologisches Institut, Universität Tübingen
Sigwartstraße 10, D-72076 Tübingen, Germany

Report assembled by Andre Dos Santos

METEOR-BERICHTE
96-4

Östliches Mittelmeer, Rotes Meer, Arabisches Meer
Cruise No. 31
30 December 1994 - 22 March 1995

Edited by:
Christoph Hemleben, Wolfgang Roether, Peter Stoffers

Editorial Assistance:
Dr. Sylvia Kemle-von Mücke

Universität Bremen, Fachbereich Geowissenschaften

Leitstelle METEOR
Institut für Meereskunde der Universität Hamburg

1996

Table of Contents

Page

Abstract

The METEOR - Cruise no. 31 included scientific programs of more than 15 working groups, which dealed with the response of oceanic environments to past and recent climates. On Leg 1 a set of physical and biochemical parameters was obtained by measuring on a grit of hydrographic sites that comprises all main water masses of the eastern Mediterranean, the southern Adriatic Sea and the southern Aegean Sea. This happens in cooperation with the working groups of M. T. P. (Mediterranean Target Project) and the POEM-BC - program (Physical Oceanography of the Eastern Mediterranean - Biology and Chemistry). The goals of these programs ranged from the investigation of oceanic circulations to ecologic modelling. Legs 2 and 3 mainly focused on the targets of the "International Geosphere-Biosphere" programs PAGES and JGOFS. Further geochemical processes, which control the metallogenesis in the northern Red Sea, was intensively studied. Two working groups investigate the taphonomy and biogeography of shelly macrobenthos of the Red Sea and the Arabian Sea. The benthopelagic coupling and biogeochemical fluxes within the benthic boundary layer are studied in the monsoonal influenced Arabian Sea.

Zusammenfassung

Die METEOR - Reise 31 wurde mit 15 verschiedenen Arbeitsgruppen durchgeführt, deren Programme darauf abgestimmt waren, die Kopplung Ozeans-Klima heute und in der Vergangenheit zu untersuchen. Der erste Abschnitt dieser Reise war einem Netz von Stationen im östlichen Mittelmeer gewidmet, um die verschiedenen Wassermassen zu charakterisieren. Dies geschah in enger Zusammenarbeit mit MTP und POEM. Die Ziele dieser Programme reichen von der ozeanischen Zirkulation bis hin zu Modellierungen ökologischer Zusammenhänge. Die Reiseabschnitte 2 und 3 im Roten und Arabischen Meer waren hauptsächlich den Zielen der IGB Programme PAGES und JGOFS gewidmet. Bis zu 24 m lange Kerne wurden gezogen, um die Paläoozeanographie und das Paleoklima zu erforschen. Weiterhin wurden die metallogenetischen Prozesse im Roten Meer ausführlich untersucht. Zwei weitere Gruppen haben sich mit der Taphonomie und Biogeographie des hartschaligen Makrobenthos im Roten Meer und dem Golf von Aden befaßt. Die benthisch-pelagische Kopplung und biogeochemische Flüsse in der bodennahen Grenzschicht wurden im monsun-beeinflußten Teil des Arabischen Meer auf dem Abschnitt 3 ausführlich studiert.

1 Research Objectives

Leg M31/1

The research area of Leg 1 of the cruise METEOR 31 was the Eastern Mediterranean and the topics included (i) the study of thermohaline circulation using hydrography and tracers, (ii) to serve as a preconditioning survey of a multiship investigation of the formation of Levantine Intermediate Water, (iii) to observe the distribution of biogeochemical parameters in a winter situation, and (iv) to collect long sediment cores to study the climate and hydrography of the Adriatic Sea during the Last Interglacial.

Leg M31/2

Based on several earlier expeditions the METEOR-cruise 31/2 constitutes a continuation of research of several scientists who recognized the Red Sea as a key region for regarding several important scientific questions. (i), this Leg was focused on hydrothermalism and volcanism in the deep basins of the northern Red Sea. (ii) the paleoclimatic and paleoceanographic history of the Red Sea. (iii) and the macrobenthos was investigated to characterize the Red Sea fauna in respect to adjacent marine environments (eastern Mediterranean and Gulf of Aden). Data and samples were taken by CTD, boxcoring, multicorer, gravity corer, piston corer, OFOS and dredges.

Leg M31/3

The Arabian Sea is strongly influenced by the monsoonal system and can therefore be regarded as a key region to understand seasonal fluxes that are different in origin. During Leg 31/3, interactions between monsoon, climate, high saline Red Sea water masses, circulation patterns and ecology were investigated in the western Gulf of Aden and the Arabian Sea. The knowledge of recent particle fluxes will lead to a better understanding of interactions between the paleowind- system, sediment input and paleoecosystem.

Tab. 1: Legs and chief scientists of METEOR cruise no. 31

Leg M31/1

30.12.1994 - 05.02.1995
Hamburg - Port Said
Chief scientist: W. Roether

Leg M31/2

08.02.1995 - 03.03.1995
Port Said - Djibouti
Chief scientist: P. Stoffers

Leg M31/3

06.03.1995 - 22.03.1995
Djibouti - Djibouti
Chief scientist: Ch. Hemleben

Coordination:
Prof. Dr. Ch. Hemleben

Masters (R.V. METEOR):
Captain H. Bruns (31/1)
Captain M. Kull (31/2 - 3)

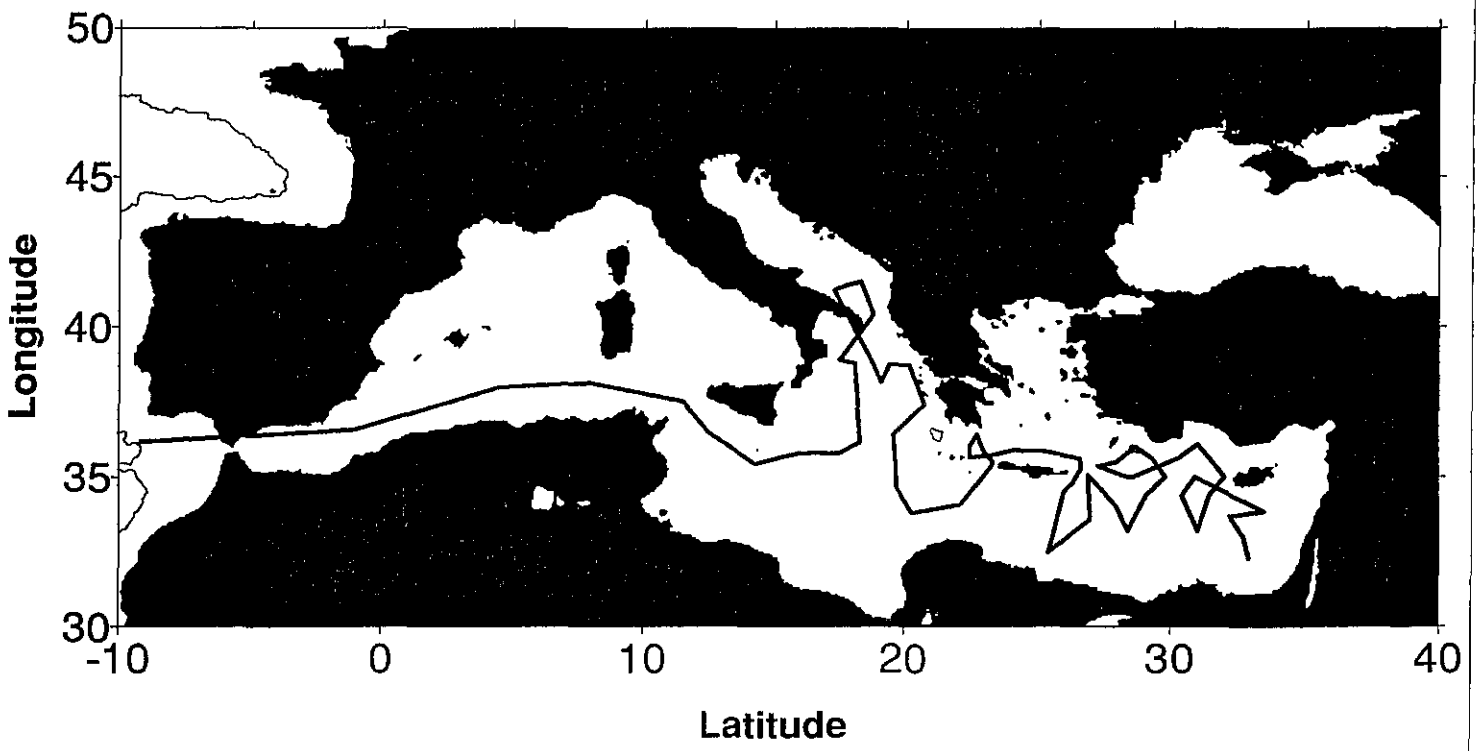

Fig. 1: Cruise track and sampling stations of METEOR leg M31/1.

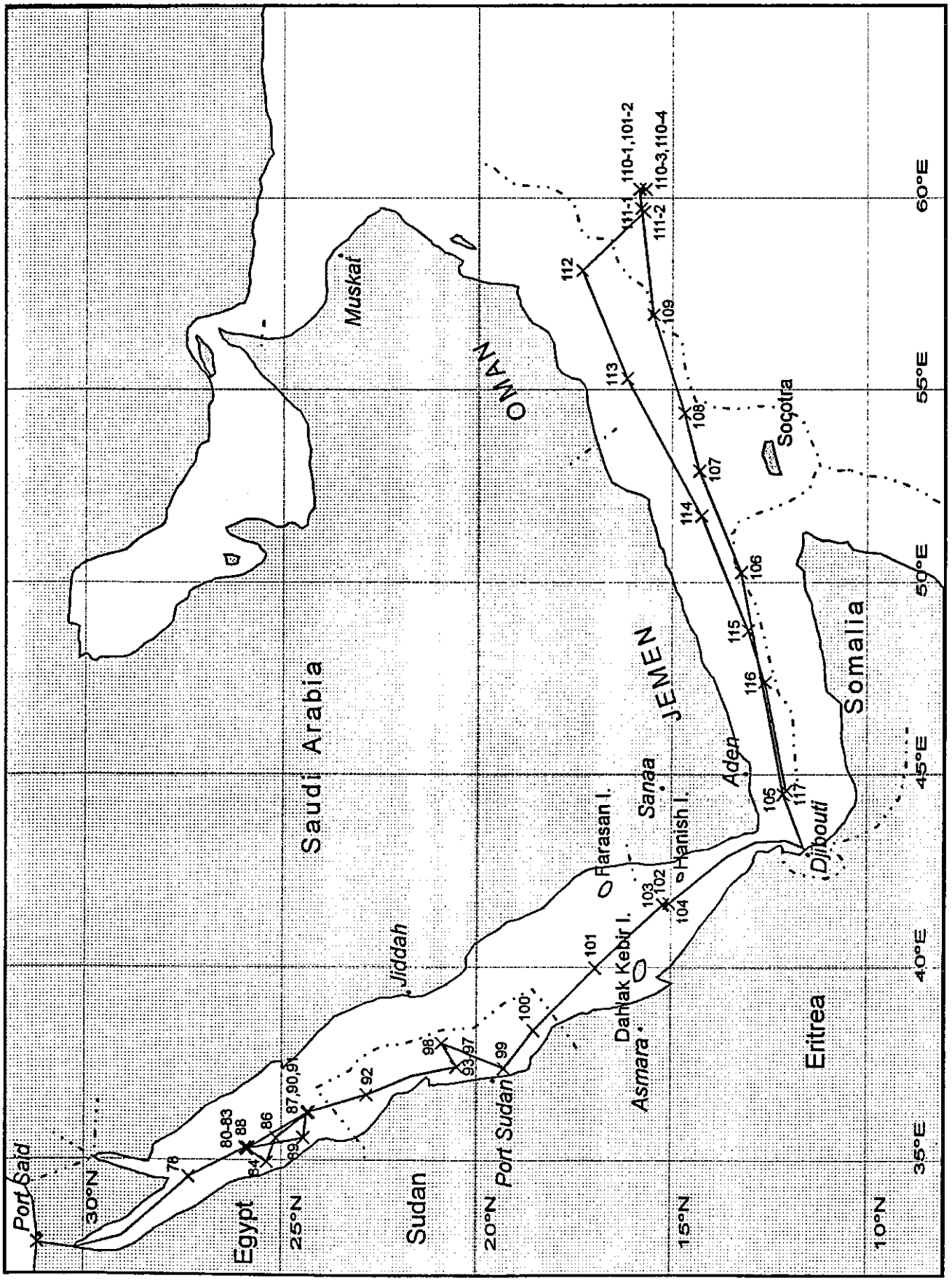

Fig. 2: Cruise track and sampling stations of METEOR leg M31/2 and M31/3.

2 Participants

Tab. 2: Participants of METEOR cruise no. 31

Leg M31/1

Name	Institute	Speciality	1	2	3
Roether, Wolfgang, Prof. Dr., (Chief Scientist)	TO HB	Tracer Physics	x	x	x
Arango, Hernan G., Dr.	HAU	Marine Physics	x	x	x
Auf dem Venne, Herbert, Dr.	IfM Ki	Plankton	x	x	x
Avril, Bernard, Dipl.-Oz.	CNRS	Geochemistry		x	x
Beitzel, Volker, Dipl.-Phys.	TO HB	Tracer Physics	x	x	x
Bregant, Davide, Dr.	ITT	Marine Chemistry		x	x
Bruns, Stefan, student	TO HB	Tracer Physics	x	x	
Bukowski, Tatjana, student	GPI Gö	Geology	x	x	
Bulsiewicz, Klaus, Dipl.-Phys.	TO HB	Tracer Physics	x	x	x
Candouna, Marina, Dipl.-Phys.		Cyprian Observer	x	x	x
Cecco, Roberto	OGS	Marine Physics	x	x	x
Copin-Montégut, Claire, Dr.	CNRS	Geochemistry	x		
Cozzi, Stefano, Dr.	ITT	Marine Chemistry	x	x	x
Dammer, Mark, Dr.	IfM Ki	Marine Biology			x
Drakopoulos, Panos, Dr.	NCMR	Greek Observer		x	x
Fleitmann, Dirk, student	GPI Gö	Geology	x	x	
Fraas, Gerhard, Dipl.	TO HB	Tracer Physics	x	x	x
Georgopoulos, Dimitris, Dr.	NCMR	Greek Observer		x	x
Hassan, Hassan Mostafa, Dr.	IOF	Egyptian Observer			x
Klatt, Uwe, student	TO HB	Tracer Physics	x	x	
Klein, Birgit, Dr.	TO HB	Tracer Physics	x	x	x
Kovacevic, Vedrana, Dr.	OGS	Marine Physics	x	x	x
Leslie, Wayne G.,	HAU	Marine Physics	x	x	x
Luchetta, Anna, Dr.	ITT	Marine Chemistry	x	x	x
Mahar, A.M.,	Navy	Egyptian Observer			x
Manca, Beniamino, Dr.	OGS	Marine Physics	x	x	x
Meischner, Dieter, Prof. Dr.	GPI Gö	Geology	x	x	
Meyer, Jürgen, student	GPI Gö	Geology	x	x	
Plep, Wilfried	TO HB	Tracer Physics	x	x	x
Robarts, Richard, Dr.	NHLR	Geochemistry			x
Robinson, Allan, Prof. Dr.	HAU	Marine Physics			x
Ruiz-Pino, Diana, Dr.	CNRS	Geochemistry		x	x
Sieverding, Hiltrud, Dipl.-Chem.	TO HB	Tracer Physics	x	x	x
Sußebach, Jürgen,	SWA	Meteorology	x	x	x
Vidussi, Francesca,	CNRS	Geochemistry	x	x	x
Yilmaz, Aysen, Dr.	METU	Marine Chemistry			x
Zohary, Tamar, Dr.	IOLR	Geochemistry			x

Leg M31/1 was subdivided into three sublegs. Subleg 1 started in Hamburg on December 30, 1994 and ended in Trapani on January 10, 1995; subleg 2 started in Trapani the same day and ended in Brindisi on January 17. The last subleg ended on February 5 in Port Said.

Leg M31/2

Name	Institute	Speciality
Dieter Bassek	SWA	Meteorology
Dr. Thomas Brachert	Geologie M	Paleontology
Tilmann Breetsch	GPI Ki	Technology
Dr. Rainer Botz	GPI Ki	Isotope geochemistry
Tanja Bukowski	GPI Tü	Geology
Peter Emmermann	Geomar Ki	Sedimentology
Dr. Eckhard Faber	BGR, Hannover	Isotop geochemistry
Mathias Fey	GPI Ki	Geology
Dominik Fleitmann	GPI Gö	Geology
Prof. Dr. Christoph Hemleben	GPI Tü	Geology
Dr. Martin Hartmann	GPI Ki	Geochemistry
Thomas Mühlstrasser	GPI Tü	Sedimentology
Jürgen Meyer	GPI Gö	Technology
Dr. James Nebelsick	GPI Tü	Paleontology
Prof. Dr. Wolfgang Oschmann	GPI Tü	Paleontology
Prof. Dr. W. Plüger	RWTH Aachen	Geochemistry
Prof. Dr. Harald Puchelt	IPG Ka	Vulkanology/Petrography
Wilmar Rehder	GPI Ki	Sedimentology
Dr. John Reijmer	Geomar Ki	Sedimentology
Dr. Gerhard Schmiedel	GPI Tü	Mikropaleontology
Dr. Jan Scholten	GPI Ki	Geology
Thorsten Schott	GPI Ki	Technology/Electronics
Prof. Dr. Peter Stoffers	GPI Ki	Geology (Chief-scientist)
Dr. Jürgen Sußebach	SWA	Meteorology
Frank Wehner	IFM Ki	Oceanography
Syee Weldeab	GPI Tü	Foraminifera
Dr. Frank Pieter Wesselingh	GPI Tü	Molluscs
Dr. Wolfgang Wranik	Bio Ro	Zoology
Khaled Abdel Aal Moussa	IOF	Geology
Prof. Dr. Abd Al-Malik Ali Al-Jebli	Yemen	
Dr. Gasim El Garafi	Sudan	Observer
Captain Nabil Ramadan	Egypt	Observer
Major Ahmed Mohamed Mahar	Egypt	Observer
Dr. Nabil Nasr El Din Saad	IOF	Oceanography

Leg M31/3

Name	Institute	Speciality
Dipl. Biol. Stefan Berg	GEOMAR Ki	Benthology
Dipl. Biol. Antje Boetius	AWI	Benthology
K. Dehning	Geo HB	Geology
Nikolai Delling	IBM HH	CO_2
Dr. Jochen Erbacher	GPI Tü	Planktology
Dominik Fleitmann	GPI Gö	Sedimentology
Prof. Dr. Gerd Graf	GEOMAR Ki	Benthology
Peer Helmke	Geo HB	Geology
Prof. Dr. Christoph Hemleben	GPI Tü	Chief-Scientist
Dipl. Biol. Birgit Hiller	GPI Tü	Planktology
Axel Hupe	IBM HH	CO_2
Britta Jahn	Geo HB	Geology
Anja Kähler	GEOMAR Ki	Benthology
Georg Kist	Geo HB	Geology
Prof. Dr. H. Kitazato	Univ. Shizuoka	Foraminifera
Ralf Lendt	IBM HH	CO_2
Jürgen Mayer	GPI Gö	Geology
Markus Molis	IfM Ki	Planktology
Wolf-Thilo Ochsenhirt	SWA	Meteorology
Dr. Olaf Pfannkuche	GEOMAR Ki	Benthology
Dr. Erhard Röd	SWA	Meteorology
Dr. Gerhard Schmiedl	GPI Tü	Sedimentology
Dr. Ralf Schneider	Geo HB	Geology
Maike Scholz	Geo HB	Geology
Katja Tölle	IfM Ki	Planktology
Dr. Klaus Wallmann	GEOMAR Ki	Geochemistry
Dipl. Oz. Frank Wehner	IfM Ki	Ozeanography
Dr. Frank Wesselingh	GPI Tü	Geology
Dipl. Biol. Ursula Witte	GEOMAR Ki	Benthology
Dipl. Geol. Alexandra Zeltner	GPI Tü	Planktology

Tab. 3: Participating Institutions

AWI	Alfred-Wegener-Institut für Polar- und Meeresforschung Postfach 120161 D - 27515 Bremerhaven, Germany
BGR Hannover	Bundesanstalt für Geowissenschaften und Rohstoffe Stilleweg 2 D - 30631 Hannover, Germany
BIO Ro	Fachbereich Biologie - Meeresbiologie Universität Rostock Freiligrathstraße 7/8 D - 18051 Rostock, Germany
CNRS	Lab. de Physique et Chimie Marines Université Paris 6, CNRS BP 8 F-06230 Villefrance sur Mer, France
GEO HB	Fachbereich Geowissenschaften Universität Bremen Postfach 33 04 40 D - 28359 Bremen, Germany
GPI Gö	Geologisches -Paläontologisches Institut der Universität Abt. Sediment-Geologie Goldschmidtstr. 3 D-37077 Göttingen, Germany
GEOMAR Ki	Forschungszentrum Geomar Wischhofstr.1-3 D- 24148 Kiel, Germany
GPI Ki	Geologisch-Paläontologisches Institut und Museum Universität Kiel D-24098 Kiel, Germany
Geologie M	Institut für Geowissenschaften Johannes Gutenberg-Universität Mainz Johann-Joachim-Becher-Weg 21 D-55099 Mainz, Germany

GPI Tü	Geologisch-Paläontologisches Institut Universität Tübingen Sigwartstr. 10 D-72076 Tübingen, Germany
HAU	Harvard University Division of Applied Sciences 29 Oxford Street Cambridge, MA 02138, USA
IBM HH	Institut für Biogeochemie u. Meereschemie Universität Hamburg, Geomatikum Bundesstr. 55 D - 20146 Hamburg, Germany
IfM Ki	Institut für Meereskunde Abt. Planktologie Düsternbrookerweg 20 D-24105 Kiel, Germany
IOF	Institute of Oceanography and Fisheries P.O. Box 1017 Alexandria, Egypt
IOLR	Israel Oceanography and Limnolog. Res. Ltd. The Yigal Allon Kinneret Limn. Lab. P.O. Box 345 Tiberias 14102, Israel
IPG Ka	Institut für Petrographie und Geochemie der Universität Kaiserstr. 12 D - 76128 Karlsruhe, Germany
ITT	Istituto Talssografico Sperimentale Viale R. Gessi 2 I-34123 Trieste, Italy
METU	Institute of Marine Sciences Middle East Technical University P.K. 28 Erdemly-Icel 33731, Turkey

NCMR	National Centre for Marine Research Dep. of Physical Oceanography Hellenikon, GR-16604 Athen, Greece
NHRL	National Hydrology Research Laboratory 11 Innovation Blvd. Saskatoon, Saskatchewan, Canada
OGS	Osservatorio Geofisico Sperimentale P.O. Box. 2011 (Opicina) I-34016 Trieste, Italy
RWTH Aachen	Angewandte Geochemie und Lagerstättenlehre der RWTH Aachen Süsterfeldstr. 22 D - 52072 Aachen, Germany
SWA	Seewetteramt / Deutscher Wetterdienst Bernhard-Nocht-Str. 76 20359 Hamburg Germany
TO HB	Tracer-Ozeanographie, Institut für Umweltphysik Universität Bremen Postfach 330440 D-28334 Bremen, Germany
Univ. Shizuoka	Institute of Geosciences Shizuoka University Oya 836 Shizuoka 422, Japan

3 Research Programme

3.1 Research Programme of Leg M31/1

3.1.1 Thermohaline Circulation of the Eastern Mediterranean

A major objective during the first leg of METEOR cruise M31/1 (Hamburg to Port Said, Dec. 30, 1994- Feb. 5, 1995, Figure 1) was to obtain a large scale survey of hydrographic and tracer properties in the entire Eastern Mediterranean Sea. This part of the program was carried out in cooperation with working groups of M.T.P. (Mediterranean Targeted Project, EU) and POEM-BC (Physical Oceanography of the Eastern Mediterranean, Biology and Chemistry). It was designed to provide information on structure, rates and interannual variations of the thermohaline circulation, to contribute to a physical understanding of the underlying processes and to improve the representation of thermohaline circulation in circulation models. Anthropogenic tracers are expected to provide valuable information also in the context of validating model circulations, especially in the Eastern Mediterranean.

Whereas all previous work in the Eastern Mediterranean had found a quasi-stationary situation in the deep waters, the new observations revealed that these waters had been subjected to a major transient after 1987. The scheduled station work was therefore modified during the cruise to allow us to study these changes in some detail.

Samples were taken from a medium-resolution grid of 77 hydrographic stations and comprised all main water masses of the Eastern Mediterranean, the southern Adriatic Sea and the Aegean, with some complementary sampling also in the Western Mediterranean. Parameters to be measured at hydrographic stations included nutrients, and the anthropogenic or natural tracers CFC-11, CFC-12, CFC-113, CCl4 , tritium, helium isotopes, neon, deuterium and ^{18}O. In addition, two velocity sections were obtained along the straits connecting the Aegean with the surrounding basins to measure the exchange of waters. The outflow of Adriatic waters through the Strait of Otranto was also monitored with an ADCP section.

3.1.2 Formation of Levantine Intermediate Water

Levantine Intermediate Water, with a formation site east of Rhodes and Crete, is the most active water mass in the Mediterranean. Leg M31/1 was part of an international observational program on the formation and early spreading of Levantine Intermediate Water (LIWEX-95), organized by POEM-BC. The observations made from METEOR during January and February provided large scale information about the preconditioning phase just prior to the onset of formation. The observed fields were used as guidance for the following regional experiments which studied the formation and spreading of Levantine Intermediate Water. METEOR data also served an intercalibration purpose for the following surveys. A major component of this study were XBT and ADCP measurements, besides hydrographic station data and

thermosalinograph recordings. The observations were used to initialize a dynamical model of the circulation and to obtain real-time forecasts of the circulation.

3.1.3 Winter Distribution of Biological Parameters

Ecosystem modelling requires extensive observations of a considerable number of biogeochemical parameters. To complement existing data and to obtain a comprehensive data set for a winter situation was one of the main objectives of the biogeochemical work during M31/1, again in cooperation with M.T.P. and POEM-BC. Measurements were restricted to the upper 200 m and concentrated on the low trophic levels. Only measurements of CO_2 parameters were conducted to greater depth. The biogeochemical parameters will be analyzed in combination with the hydrographic and nutrient data. The questions adressed in this study covers topics as response of microbial organisms to limitations in posphate, the carbon budget of the Eastern Mediterranean and studies of phytoplankton abundance.

3.1.4 Climate and Hydrography of the Adriatic during the Last Interglacial

The Adriatic Sea is regarded as the source of East Mediterranean Deep Waters. High saline Levantine Intermediate Water entering the Adriatic is involved in the formation of bottom water. The dense water leaves the Adriatic along the bottom of the Strait of Otranto and spreads over the Eastern Mediterranean.

Sediments in the region are known for their sapropelites or 'stagnant' sediments that are produced during phases of anoxic bottom water. The causes of such events are still controversial. Some authors explain the sapropelites by a general climatic warming, preventing the formation of cold, dense bottom waters. Anoxic phases in the southern Adriatic deep sea and in the Ionian should be coupled. The time of their beginning and their duration should be related to known climatic developments. Piston cores taken at both locations therefore should allow conclusions about the direct, physical or hydrographical causes and the global climatic context of the formation of sapropelites.

In order to test this hypothesis long piston cores (> 20 m) were to be taken from the center of the Ionian Sea and the center of the Adriatic, aiming at covering the sediments through isotopic stage (5). In substages 5e, 5c and 5a climatic optima of significance and duration have occured similar to the Holocene, but with decreasing intensity. The analysis of sapropelites from these three warm phases in addition to those in the Holocene are expected to lead to an understanding of the underlying mechanisms.

3.2 Research Programme of Leg M31/2

3.2.1 Physical Oceanography and Planktology

(F. Wehner and Ch. Hemleben)

Leg M31/2 was among other subjects dedicated to collections of hydrographical data sets along a north-south transect (Figure 2) in the Red Sea to support biological and geological research. As a desert enclosed marine environment, the Red Sea can be regarded as a key area for unravelling the Quaternary climatic history in the region. It is situated in the center of the wide spread low latitude desert belt. The climate in the Red Sea and its surrounding East African and Arabian landmasses (BROWN et al., 1989) are arid with a very low annual precipitation and river discharge in addition to a high evaporation rate. The water column properties are mainly controlled by an interplay between strait dynamics and the regional climatic regime; thus the north is influenced by the Mediterranean climate. In the south, the monsoonal regime plays the most important role. This results in north-south gradients which were investigated by means of CTD measurements and sampling the calcareous fauna with multiple-closening net tows.

3.2.2 Benthic Biology and Actuopalaeontology

(W. Oschmann, J. Nebelsick, F. Wesselingh and W. Wranik)

The investigations centered around the shelly remains of macrobenthic organisms with the aim of studying the changes in faunal composition, diversity, and density along the north-south transect and coast to basin transects in the Red Sea. In addition, we investigated diagenetic alterations (bioerosion, incrustation and solution) of biogenic hardparts including those of planktonic gastropods and phenomena of early diagenetic lithification of bathyal and abyssal carbonate sediments (steinkern and crust formation). The comparison of living and dead fauna should lead to a better understanding of the time averaging and of post-mortal (taphonomic) processes and early burial histories.

3.2.3 Marine Geoscience

3.2.3.1 Export of Shallow Water Carbonates

(P. Emmerman, J. Reijmer and T. Brachert)

The study areas are situated near the Abington Reef and the Sanganeb Atoll, both sites located off the coast of Sudan. The southernmost situated site, Sanganeb Atoll, was chosen as the main point of focus of our part of this scientific cruise (Figure 3).

The sediments deposited at the toe-of-slope and in the adjacent channels are the targets of our analysis. The cores collected are to answer a variety of questions listed in the next paragraph. The outcome of this research will be a perfect addition to existing datasets collected in the

Caribbean, mainly the Bahamas, the Indian Ocean, the Maledives, and near Australia, eastern Great Barrier Reef.

The sedimentary record found on the Bahamas is often used as being the one and only example of low latitude carbonate platforms. The Red Sea, however, also forms an interesting modern analogue for fossil deposits i.e. the Permian Trogkofelkalk ("Reef in the desert"; FLÜGEL 1980, 1984), and the Trias with its small western Tethys.

We expect that the sediments collected will enable us to prepare sea-level curves for each individual core that can be combined into a general curve for the study area. Other data such as direct submersible observations (BRACHERT and DULLO 1991, 1994) and the compositional analysis of calciturbidites, will give us a good insight in the polarity of sea-level variations, eustatic versus tectonic/subsidence (sediment load and waterload) in this part of the Red Sea. This study will also provide important new data to solve the question if the Red Sea became an isolated ocean basin during the Last Glacial Maximum. New observations obtained through submersible work indicate a sealevel drop of at least 120-130 m (BRACHERT and DULLO 1991, 1994) possibly exposing the shallow ridge of Bab el Mandeb and thus changing the palaeoceanographic conditions drastically during these times.

The toe-of-slope sediments will provide us with new data on the reaction-time, how long it takes before sediment export starts, and the production potential of biogene carbonate systems in response to relative changes in sealevel and associated changes in the general paleoceanographic changes in the area.

Do the existing slopes act as production areas during sealevel lowstands? In other words: Do the reefs step down the slope in these times? Submersible observations (Dullo pers. com.) indicate that carbonate production still must have taken place. We hope to solve the question what type of production still takes place and what are the relative quantities of sediment compared with the high-stand situations. Detailed facies analysis of the coarse fraction of the calciturbidites and the interbedding sediment will solve forementioned questions.

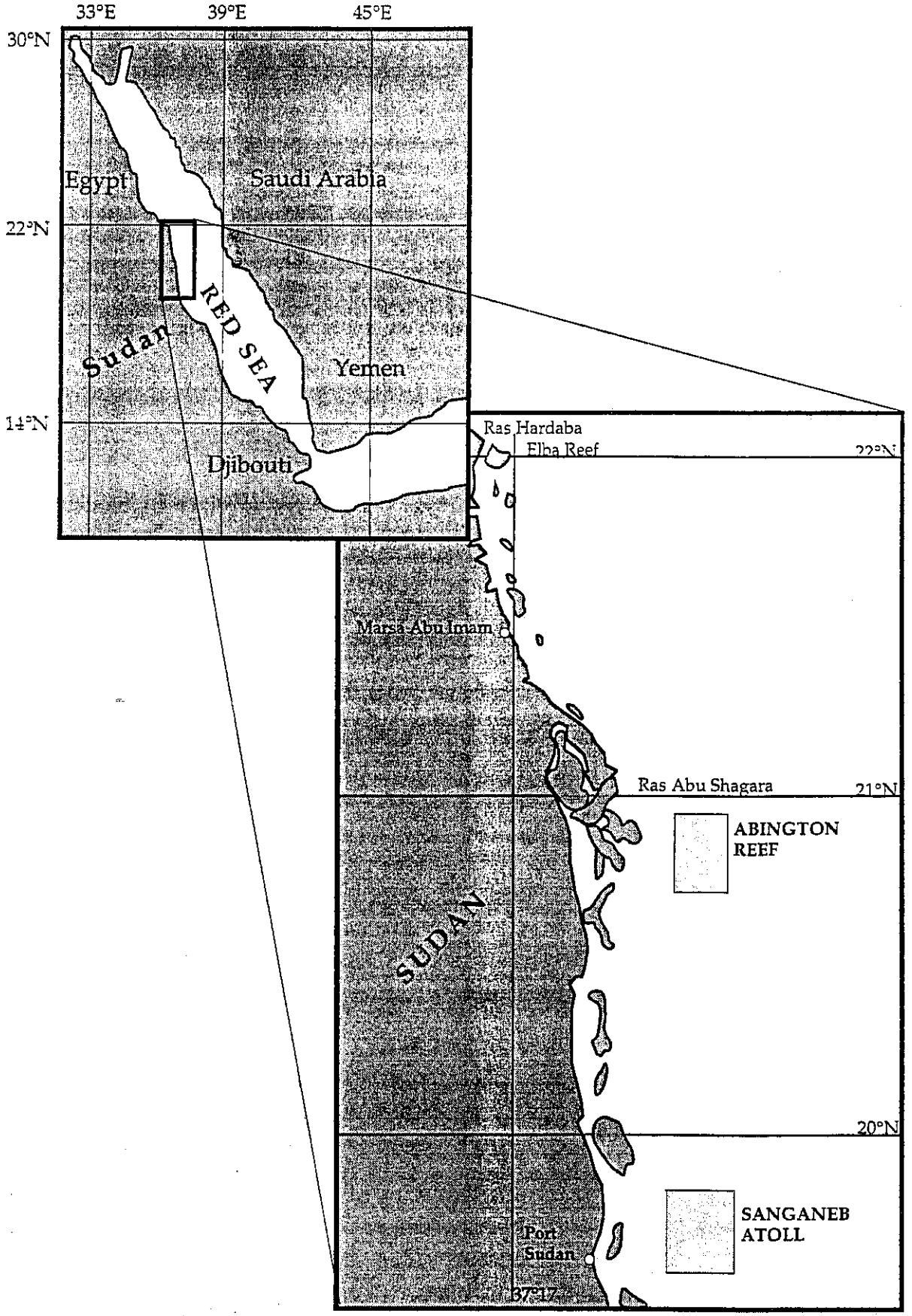

Fig. 3: Location map of the working areas.

In close co-operation with the laboratories of Prof. Bard (Marseilles) and Dr. Eisenhauer (Göttingen) different dating techniques, ^{14}C-AMS and U/Th-TIMS, will be applied to construct a very precise time-frame. Oxygen and carbon isotope analysis of planktonic foraminifera (G. *ruber*) will be another parameter that can be used to underbuilt the overall time-frame.

Calcite and aragonite variations along cores will be measured using X-ray diffraction (XRD) analysis. These variations can excellently be correlated with $\delta^{18}O$-logs as shown in a variety of studies: Pedro Bank situated south of Jamaica (GLASER, 1991), the Bahamas (DROXLER, 1984; DROXLER and SCHLAGER, 1985; DROXLER et al., 1983; ODP Leg 101, REIJMER et al., 1988), the Maldives (ODP Leg 115, DROXLER et al., 1990), and in Australia, Great Barrier Reef (ODP Leg 133, HADDAD et al., 1993). Ca-Ar logs and $\delta^{18}O$-logs show the same type of cyclic, climate-induced variations: Higher aragonite input during interglacials and reduced values in glacial times. To what extent is the aragonite input a result of sealevel-induced variations in the input of platform-derived carbonate mud in analogue with the studies of Pedro Bank (GLASER 1991) and the Bahamas (DROXLER, 1984) or is the input signal modified by depth and climate-dependent aragonite dissolution cycles (DROXLER et al., 1990). When comparing aragonite input curves and $\delta^{18}O$-curves it is clear that they run more or less parallel (DROXLER, 1984; DROXLER and SCHLAGER, 1985; DROXLER et al., 1983) or sometimes opposite (GLASER, 1991). They both show a typical asymmetric form which might be an indication that the aragonite signal registered resulted from the combination of sealevel dependent input and climatic induced dissolution cycles (GLASER and DROXLER, 1993). DROXLER et al. (1990) and HADDAD et al. (1993) showed that a clear correlation can be found between the aragonite super cycles with a duration of approx. 500 ka in NE Australia (Great Barrier Reef), the Maledives, and the Bahamas, and the carbonate preservation long-term cycles from the Pacific, Indian, and North Atlantic Oceans. The remaining question is to what extent our Red Sea aragonite input curves can be compared with the dissolution cycles seen in the pelagic realm in this area (see LOCKE and THUNELL, 1988) or if they are pure input cycles.

3.2.3.2 Paleoceanography and Monsoonal History of the Red Sea
(Ch. Hemleben)

Cores obtained from the central Red Sea during METEOR cruise 5 (1987) revealed a fossil record beginning with isotope stage 11 comprising approximately 370 ka. During this interval we were able to distinguish four stages of high aridity (isotope stages 2, 6, 8 and 10) and another four phases of relatively high humidity. Each of these phases can be subdivided (substages) to obtain a high resolution record (approximately 200 years). Based on these results, METEOR cruise 31 had planned to take long cores (>20 m) from the northern and southern Red Sea to unravel the paleoclimate based on gradients between these two regions. The northern Red Sea is characterized by highest evaporation rates and the formation of deep water, which influences the entire circulation pattern and thus the history of bottom water. This region is strongly influenced by the Mediterranean climate (rather than by monsoon). To the

contrary, the southern Red Sea is strongly influenced by the in- and outflow of waters through the Strait of Bab el Mandeb and also dominated by the monsoon. Paleoceanographical conditions and the role of monsoon will be examined by studying the sedimentary input, faunal distributions and stable C- and O-isotopes. Diversity and abundance of pteropods, benthic and planktic foraminifera and the growth forms of *Globigerinoides sacculifer* are used for palaeoecological analysis. Stable oxygen and carbon isotopes of planktic (mainly G. *ruber*) and benthic foraminifera (C. *mabahethi*) are used to establish glacial/interglacial cycles, to calculate salinities and to characterize the stratification of the water mass system.

3.2.3.3 Hydrothermal Activity and Volcanic Activity in the Northern Red Sea (P. Stoffers)

The Red Sea is an extraordinary example of an ocean which is presently being formed by the divergent movement of the Arabian and African continental plates. At the joint of the plates new oceanic crust is being formed. This process started about 4 million years ago in the southern Red Sea, and has since then, slowly propagated towards the north. As a consequence, a continuous oceanic basement is found in the southern Red Sea, whereas in the north only several small basins with oceanic crust occur; these are separated by inter-trough zones which have a continental basement. Very often connected with the formation of oceanic crusts are submarine ore forming hydrothermal processes, which can lead to submarine metalliferous deposits.

Since the late 60's detailed geological research work has been focussing on the distribution of metalliferous deposits in several basins of the Red Sea. The Atlantis II Deep was found to have ore concentrations of economic value. Further joint Saudi Arabian and German research cruises (MESEDA (1981); MENOR (1983); SONNE 29 (1984)) to the northern Red Sea discovered metalliferous deposits in the Kebrit and Shaban Deeps (Figure 4). Detailed investigations of the genesis and composition of these deposits were studied during METEOR cruise M31/2.

Shaban Deep

In the Shaban Deep the relation between the formation of sapropels in sediments and climatic and eustatic sea level changes shall be investigated. These studies will allow a comparison to the paleoclimate evolution of the eastern Mediterranean Sea.

The distribution of massive sulfides found during SONNE 29 (1984) and recent hydrothermal activity are of further scientific interests. Very young basalt intrusions centered in the middle of the basin should be sampled to investigate the evolution of the magma in an early stage of seafloor spreading.

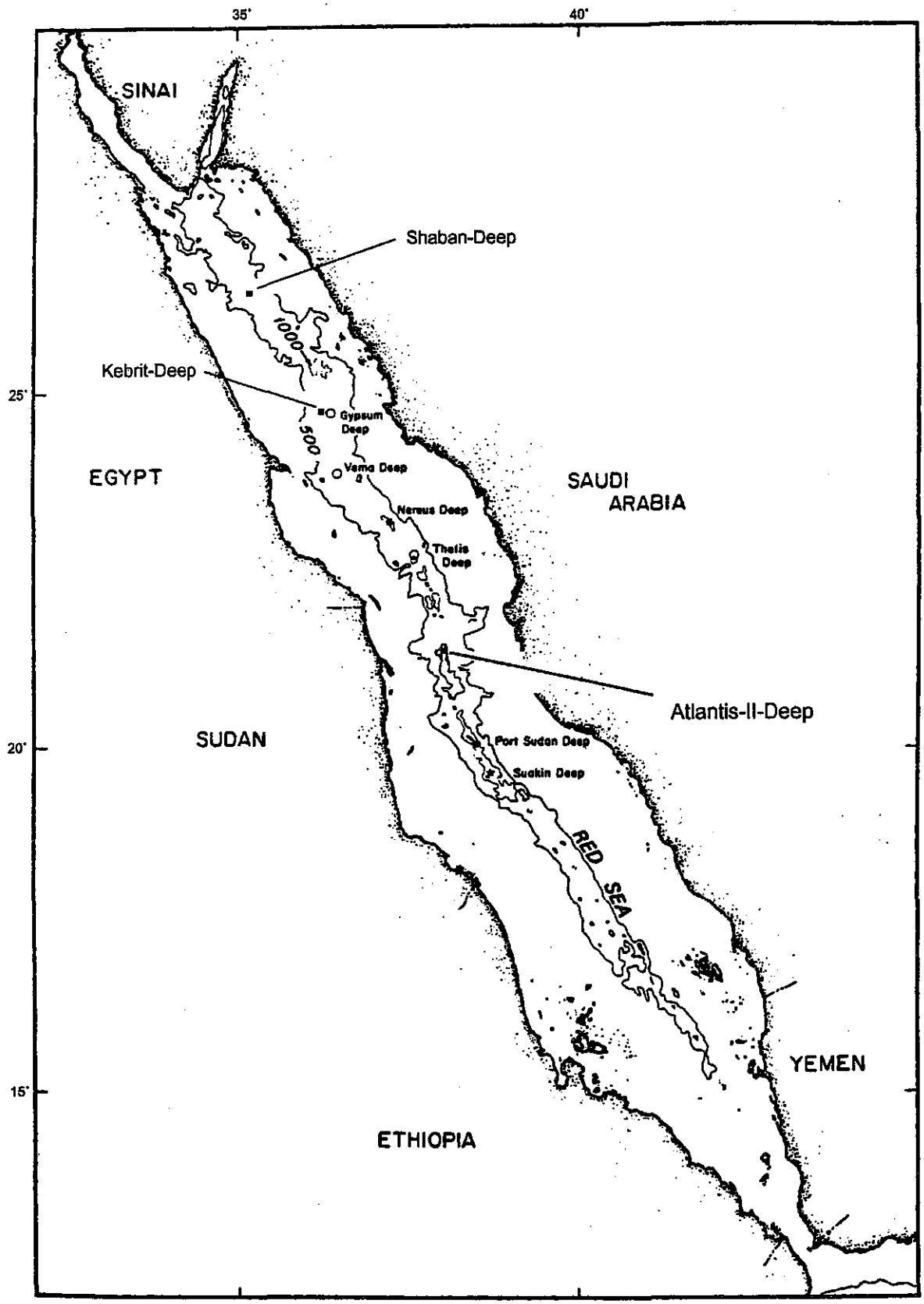

Fig. 4: Location of the Shaban-, Kebrit- and Atlantis II Deep in the Red Sea.

Kebrit Deep

The investigations in the Kebrit Deep, where massive sulfide deposits occur, shall center on establishing the extent to which these deposits are distributed in the basin and if there are any further indications for fossil and/or recent indications of hydrothermal activities to be found in the water column and in the sediments.

Hydrothermal gases

Hydrothermal gases such as CH_4, CO_2 and He are enriched within the water column of tectonically active regions of the world's oceans (WEISS et al., 1977; WELHAN, 1988). The origin of these gases may be attributed to mantle degassing processes. CH_4 (C_{2+}, CO_2) may, however, also derive from microbiological or thermal degradation of sedimentary organic matter as found in the Guaymas Basin (SIMONEIT and LONDSDALE, 1982) or the Bransfield Strait (WHITICAR and SUESS, 1985).

In the Red Sea - an ocean in statu nascendi - active rifting occurs. Petroleum-impregnated sediments are known from the Kebrit- and Shaban Deeps (MICHAELIS et al., 1990). Here, a high heat flux is responsible for thermal maturation of sedimentary organic matter probably incorporated in Miocene evaporitic sequences. BURKE et al. (1980) investigated light hydrocarbons in Red Sea brines and sediments from the Atlantis II-, Suakin-, Nereus- and Valdivia Deeps. They found CH_4 concentrations up to 155 ul/l and, based on the C_1/C_2+C_3 ratios, both a biogenic and a thermogenic source of the gas was assumed.

3.3 Research Programme of Leg M31/3

3.3.1 The CO_2 -System, Methane and Light Hydrocarbons in the Arabian Sea at the End of the Northeast Monsoon

(IBM HH)

The Joint Global Ocean Flux Study (JGOFS) intends to improve the understanding of the oceanic carbon cycle. For the time period 1994 to 1996, the Arabian Sea was chosen as the main working area for an internationally coordinated field study. The planktological subproject of the German JGOFS project "Indian Ocean" will participate in a series of expeditions to the Arabian Sea. The seasonal focus of this activities will be the SW-Monsun. During M31/3, additional research during the NE-monsun was carried out. One of the topics of JGOFS is to quantify sinks and sources of CO_2 and to describe the role of the "biological pump". The constant rise of the carbon dioxide concentration in the atmosphere and the related global warming is buffered 40 % dissolution of carbon dioxide (CO_2) in the ocean. Methan (CH_4) is also an important trace gas in the air which contributes to the "greenhouse-effect". The decisive CO_2 exchange processes between atmosphere, biosphere and hydrosphere occur in the euphotic sea surface. On M31/3, the exchange of CO_2 and volatile hydrocarbons through the air-sea interface of a highly productive area like the Arabian Sea has been investigated and the

effect of denitrification on the CO_2 and CH_4 concentration in the oxygen minimum zone will be described. The distribution of CH_4 and other light hydrocarbons is associated to bacterial processes in organic particles as well as to photosynthesis and respiration of plankton which also influences the marine CO_2 system. The light hydrocarbons were analysed onboard by gas chromatography. Total alkalinity (TA), total dissolved inorganic carbon (TCO_2) and pH has been measured by potentiometric precision titration and coulometry. These results are used to calculate the partial pressure of CO_2 (pCO_2) with the help of a thermodynamic program. The difference between the pCO_2 of the mixed layer and that of the air tells us whether the Arabian Sea is a potential CO_2 sink or source at the end of the NE monsoon. Underway, a pump system continuously supplied the laboratory and the connected instruments with seawater. This facilitates the measurement of the parameters mentioned above in very short time intervals. On CTD stations, the main emphasis is put on the investigation of the upper 1000 m of the water coulmn, that is, the oxygen minimum zone. Additionally, ^{13}C samples have been drawn to receive information about the origin of TCO_2 in this depth.

3.3.2 The History of the Monsoon during the Quaternary in the Western Arabian Sea
(GPI Tü, GPI Gö, GEO HB)

The western part of the Arabian Sea including the Gulf of Aden is completely influenced by the monsoon. The intensity of solar radiation at the monsoon cannot be correlated linearly (SIROCKO et al., 1993). We proved that already in the Red Sea, nutrient rich intermediate water reaches into the central Red Sea during the SW-monsoon. However, the situation differs from the western Arabian Sea. Here, upwelling causes nutrient-rich intermediate and surface waters. Thus the faunas are different from those of the Red Sea. In addition, the variability of the sedimentary input differs from the Red Sea. Stable isotope ratios of planktic and benthic foraminifera will be used to decipher the coupling of surface and deep circulation and the monsoon in this region. The intensity of high saline Red Sea waters should be seen in the stable isotope signal of benthic and planktic foraminifera. Several Sites shall help to document the paleoceanographic relationship between the Red Sea and the western Arabian Sea during the late Quaternary and the Holocene.

3.3.3 The Oxygen Minimum Zone (OMZ)
(GPI Tü)

One of the main targets is to reconstruct the OMZ during the late Quaternary and Holocene by investigating pteropods and benthic foraminifera. The ratio of meso- to epipelagic pteropods can be used as a proxy for the upper boundary of the OMZ. Benthic foraminifera (buliminids) characterize the lower boundary of the OMZ. The results of these investigations will give important informations to understand the paleoceanographic evolution of this region.

3.3.4 Ecology of Benthic Foraminifera
(GPI Tü)

Besides the investigation of the ecology of benthic foraminifera (trophic demands, benthic-pelagic coupling, distribution in the epibenthic zone, live horizons, distribution in the sediment, reaction on O_2-contents, high saline Red Sea waters) we performed experiments on living foraminifera, which are continued in our laboratory in Tübingen. The main goal was to get more informations on the ecology of deep marine benthic foraminifera. Only little is known on the ecology of benthic foraminifera from the North Atlantic or the Pacific near Japan, and almost nothing from the Arabian Sea/Indian Ocean. Therefore, it is of great interest to compare faunas from the rather extreme region of the Arabian Sea with those from other deep marine environments.

3.3.5 Biogeochemical Fluxes in the Deep Sea: Arabian Sea
(GEOMAR Ki, AWI)

In the area of the Arabian Sea, the input and turnover of organic matter was investigated in the upper sediment horizons of the deep sea. Aim of the investigation was the quantification of biogeochemical fluxes at the sea floor. Strong seasonal and regional variations in vertical flux have been documented by long-term sediment trap investigations. Due to the strong episodical sedimentation of organic matter this pattern of seasonality is likely to be reflected by the benthic activity and turnover of matter. In previous investigations in the NE-Atlantic we found that increased sedimentation after phytoplankton blooms caused a rise in benthic turnover rates and productivity. We expect that these processes of pelago-benthic coupling are more strongly expressed in the Arabian Sea.While the studies during M31/3 covered the end of the NE-monsoon, two further expeditions were targeted for the end of the SW-Monsoon and the spring intermonsoonal period.

4 Narrative of the Cruise

4.1 Narrative of Leg M31/1
(W. Roether)

METEOR sailed from Hamburg at 11:00 on December 30, 1994, with W. Roether being chief scientist. The Elbe was left at 17:00 the same day and METEOR continued its way westward towards the English Channel and the Bay of Biskay in rough weather. New years evening was spent in the North Sea. A first test of equipment was made in fair weather in the Bay of Biskay on January 3. The test revealed initial problems with the rosette systems. A first CTD profile was obtained on January 5 just outside of the Mediterranean at 36°10,0 N/009°10.0 W. The integrated system DVS to acquire navigational data, a continuosly recording thermosalino-graph and the shipborne ADCP were switched on. METEOR passed the Strait of Gibraltar during the night of January 5 and started station work in the western Mediterranean (Figure 1)

the following morning. Further tests were made on the functioning of the two rosette-water-sampler/CTD units. One unit was used to the bottom, and the second to 300 m only. Such a combination of a deep and a shallow cast was performed on most of the following CTD stations. Water samples from the deep cast were used for analysis of oxygen, nutrients, CFCs, helium isotopes and tritium. Water samples from the shallow casts were devoted to the biogeochemical studies including planktonic ciliates and carbon parameters. Four additional CTD profiles were obtained in the following days before METEOR went into Trapani on January 10.

The short stop at Trapani, Sicily, was used to exchange scientific personnel. Four scientists joined the cruise in Trapani while two members left. METEOR sailed from Trapani at noon and reached the next station at 18:36 the same day in the western Sicilian Passage, when also the XBT work was started. Again, stormy weather began to cause problems with the station work. Measurements at station 8 in the Ionian Sea had to be terminated on January 11 because winds increased to Bft 9-10. The work was picked up, at the same position, on January 12 when the weather improved slightly.

On January 13 the first geological station was performed in the central Ionian Sea (Sta. 13). A 12 m piston corer was sucessfully launched and a 11.5 m core was obtained. The larger piston corer could not be used due to weather conditions. After leaving the geological station, the wind picked up even more and reached hurricane strength the following day. Station work had to be suspended until January 15. The delay forced us to skip one scheduled section of hydrographic stations and a geological station in the Strait of Otranto. A second geological station was made on January 16 in the Adriatic. Both piston corers with lengths of 12 m respectively 24 m could be launched and an 11 m and a 22 m sediment core were recovered on deck.

On January 17 METEOR arrived at Brindisi, where 6 members of the scientic crew and one crew member left the ship; this included the geological group, which had to work hard on their sediment cores before leaving. 8 new scientists joined the cruise. METEOR sailed from Brindisi late the same day, resuming station work the next morning. The weather gradually calmed down and stayed favourable throughout the remainder of the leg, so that it became even possible to expand the scheduled work somewhat. Stations in the eastern Ionian Sea were completed before METEOR entered the Aegean on January 22. An ADCP section was performed covering the transect from the western end of Crete toward the Pelepones, followed by hydrographic stations in the Aegean. Further ADCP sections were made on January 24 and 28 across eastern straits between the Aegean and the Levantine.

The remaining station work was dedicated primarily to observations within LIWEX-95, with an increased density of hydrographic and XBT stations, and enhanced biogeochemical work. Intercomparison stations with succeeding LIWEX-95 cruises and accompanying sampling for intercomparison purposes were performed. The station work ended on February 3 (station 77). Apart from a moderate reservation for the work prior to Brindisi, the cruise was a full success.

It is worth mentioning that all observers took an active part in the work. METEOR reached Port Said early on February 5.

4.2 Narrative of Leg M31/2

(P. Stoffers)

The RV METEOR left Port Said on February 8, 1995 at 6 am. On board there were four scientists and/or observers from Egypt, one scientist from Sudan and 23 scientists from various German Universities.

METEOR reached the first research area (27°41,2 N/34°35,6 E) in the northern Red Sea (Figure 2) on February 10. In order to find a good coring site a continuous Hydrosweep and Parasound profile was started. Cores of 12 m and 24 m length were recovered containing 10 m and almost 19 m of sediments, which will provide information about the paleoclimatic evolution in the late Quaternary. Surface sediments were sampled using a multicorer. In addition, CTD water sampling was carried out to investigate the chemical properties of the water masses. Foraminifera and pteropods were sampled in the water column using multiple closure net.

After additional coring at location 26°26 N and 35°21 E METEOR reached the Shaban Deep (26°13,7 N/35°22,5 E) on 12 February and the work program began with Hydrosweep mapping, water and sediment sampling. The four basins of this Deep are filled with a brine (brine surface at 1290 m, temperature ranges between 22.7-25.3° C that is slightly higher than at greater depths (21.5° C), pH 5.7-6.16). In the area of this saline body there is methane present at 100 µl/l. In the water above the brine pool methane concentrations decrease by 2 to 3 decimal points to values of about 0.1 µl/l at the sea surface. In addition to methane there are also considerable amounts of ethane present, however, higher hydrocarbons are only present in small amounts. Suspended material was successfully taken from saline, intermediate layer, and brine pool. Gravity cores (between 3 and 11 m long) show interesting sequences of very different sediment types (carbonates, finely laminated diatomaceous slurry, sapropele, hydrothermal sediments).

In order to investigate the origin and chemical composition of the basement in the northern Red Sea six dredges were deployed. They recovered mostly carbonate crusts. Fresh basalts could only be recovered from one dredge. In order to locate basalt outcrops in the Shaban Deep the TV-grab was used. On the flank of the central edge pillow basalts could be targeted, and dredging at this location recovered fresh, vesicular, and dense basalts with beautiful glass rims. One dredge from the transitional zone brine/deep water contained small pieces of massive sulfides as well as carbonate crusts, which were also partially mineralised.

On the way to the Kebrit Deep the scientific crew was looking for a good coring site. Such sites are often very difficult to find as the seafloor consists of many small valleys and hills, each forming different sediment bodies. After an extensive search and extremely precise

manoevering, a core position was found at the edge of the Kebrit Deep, which was sampled with long gravity corers: 11 and 22 m of sediment were recovered.

Following a short period of hydrosweep mapping, station work started in the Kebrit Deep (24° 43 N/16°5 E) on February 15 with 5 hydrographic stations. As is the case in the Shaban Deep, the transition to the brine pool is at about 1468 m, with a temperature jump from 22.5° to 23.4°. This saline water is characterised by a strong hydrosulfuric odour. More than 100 l of water were collected from the saline body; there were up to ml-amounts of methane. Two 9 m long cores, pulled from inside and outside the saline body, show interesting sediment sequences (carbonates; coloured hydrothermal sediments; black, high organic layers with a strong oil odour). The TV-grab was deployed three times. By using the grab the brine surface could be observed directly. Judging by these observations, the transitional zone between normal seawater and brine pool seems to be only a few centimeters thick. Distinctive shadows on the surface of the brine indicate suspended particle enrichment in the bordering layer.

Above the saline body there are massive sulfides in a narrow zone (about 30 m wide). They stick out of the sediment like isolated chimneys or lie on the sediment like dark plates. Using dredges more than 200 kg of material was sampled, which mainly consisted of massive sulfides in a porous, lava-like form. The sulfides were partially soaked with an oil-like substance. In addition to carbonate crusts and fist size limestone crystals were found.

On February 20 sampling for paleoclimatic investigations (i. e. coring, CTD water sampling, multicorer, multiple closing net) was conducted on a transect from 24°45 N/36°13 E to 24°45 N/36°16,6 E.

On February 22 investigation of macro-benthos in shallow water began. Three near-shore-offshore profiles, which extended from 50 to 700 m depth were sampled with 3 dredges and 37 large grab-cores. Two profiles were located at 21° N/37°30 E near the Abingtom Reef, the third in the Sawakin archipelago at about 19° N/38°33 E. Samples show distinct sediment fazies types. Reef debris, coral sand, and large foraminiferas are indicative of shallow water regions. Starting at 100 m depth there is echinide-slurry, and at 200 to 250 m depth there is cuspidarien-slurry, which is found in different variations as far as the deep sea. All samples were rich in benthos, which were very diverse. Six box cores (6 m) and gravity cores (6 m) were recovered at water depths of between 500 and 700 m off the Sudanese coast at two locations - the Abington Reef (20°45 N/37°30 E) and the Sanganeb atoll (19°45 N/37°30 E). Sediments consisted predominantly of carbonate slurry, rich in foraminiferes and pteropodes. Interspersed in this slurry - in some of the cores of the Sanganeb region - were sandy (turbid-like) layers of shallow water material (bioclastic reef detritus).

METEOR reached the Atlantis II Deep (21°20,5 N/38°04 E) on February 24. This basin is filled with a brine pool and since its discovery in the sixties hydrothermal activity has been observed. CTD-profiles and water bottles were deployed in the SW-basin, the N-basin, and in the Discovery Deep. In the Atlantis II Deep these profiles showed a distinctly changed structure of the brine pool compared to earlier times: there are now three instead of two clearly

separated water bodies. Their temperatures were about 45°, 60° and 71° C, respectively, amounting to a rise in temperature by about 8° C for the lowest water body. A temperature maximum of about 72° C directly below the 60/71° C border shows that there is still an influx of fresh hydrothermal solutions.

The temperature has also increased in the Discovery Deep (from 45 to 50° C, max. near the bottom 50,78° C). Methane concentrations of the water stations show background concentrations above the brine bodies, while there is distinctive methane enrichment of up to 100 ul/l in the saline body. The occurrence of high ethane and propane contents is characteristic of the lower brine. This indicates complex hydrocarbon-genesis (biogene, thermal).

The TV-grab was used at the southern flank of the SW-Basin in the Atlantis II Deep. Slopes were covered with sediments to a depth of up to 2020 m. Occasionally, we observed basalts and crusts. There was no abrupt transition into the brine body. The video picture became increasingly diffuse until everything was blurred. The TV-grab sample consisted thick carbonate crusts. The first attempt to pull a 12 m core from the SW-basin failed. In a second attempt, a full core containing typically coloured hydrothermal sediments was recovered.

Sampling for paleoclimatic investigations (CTD, multiple closures net, multicorer, gravity corer) continued on two locations in the southern Red Sea (23°18,6 N/36°42 E; 15°33 N/ 41°40,5 E). Almost at the last station (sta. 102) a core of 23.65 m length was recovered.
METEOR cruise 31/2 ended on March 2, 1995 at noon in Djibouti.

4.3 Narrative of Leg M31/3

(Ch. Hemleben)

The RV METEOR left during the night of March 2./3. Djibouti harbour to anker on Reede. The day was used to unpack our laboratory equipment and to organize forthcoming stations. On March 3 we left Djibouti at 20:00 local time heading for our first research station off Aden (sta. 105, 12°27,6 N/44°25,3 E) were we sampled macrobenthos from various depths using the boxcorer and multicorer (Figure 2). Underway to the east we used the Parasound and Hydrosweep in order to become familiar with the sedimentary sequence in the area of the Gulf of Aden.

On March 6, METEOR arrived at our first coring station 13°29,1 N/50°17,9 E (sta. 106). At this station we used CTD followed by our multi-opening/closing net, the multicorer, and than using the 12 m gravity corer and the 24 m piston corer, recovering 10,5 m and 19 m of sediment respectively. At this station we realized by photospectrometry that the sediments recoverd may represent a time span of about 250 ka.(isotope stage 7 to 8). This will certainly help us to decipher the monsoonal history during this time slice. We arrived at the next station (sta.107, 14°36,3 N/52°55,2 E) on March 7. As we already experienced in the Red Sea, we utilized the Parasound for extensive search for excellent coring locations. After an extremely

precise manoevering, cores of 10.5 and 19.5 m were recovered. We obtained similar results (core recovery 11 m and 20 m respectively) while working at station 108 (14°58,3 N/54°22,2 E) on March 8. For the first time we used the photosledge to obtain deep sea fotos showing a rather dense population of brittle stars and large Xenophyophores. Both stations (107 and 108) were located in the Oman upwelling area. Chemical and biological data suggested the end of the NW monsoon. At station 109 (15°50,0 N/57°00,1 E) further east (March 10), the benthos-biologists were testing their laboratory equipment in order to be ready and well prepared for the next station. The methan measurements showed a pronounced maximum at 100 m decreasing down to 500 m. The coring activities resulted in 10.5 m and 17.10 m cores respectively. The deep sea winch caused more and more trouble thus captain M. Kull decided to spull the total lenght during the following night.

During afternoon on March 11, METEOR arrived at station 110-1, (16°13,0 N/60°16,0 E) east of the Owen Ridge over the abyssal plain,.with water depths of ca. 4000 m. Close by, the Hamburg-group under the guidance of Prof. Ittekkot is running a time series station over almost a decade called WAST (Western Arabian Sediment Trap). Therefore we decided to perform most of our deep sea activities in the neighborhood of WAST. CTD measurements, water chemistry analysis and plankton sampling were performed in the water column; photosledge, boxcorer and multicorer were deployed to discover the deep abysal plain. The sea floor was covered by a 1 cm thick phytodetrital layer with many xenophyophores. Early on March 12 we finished this station for the first time.

Station 111-1 (16°10,15 N/59°45,3 E) on the Owen Ridge at a water depth of approximately 2000 m and about 30 mi east of sta 110 was chosen as a contrast to the abyssal plain. With both gravity corer and piston corer we recovered only 8.90 and 6.20 m respectively. The multicorer has been used for obtaining samples for culturing experiments on benthic foraminifera. The fauna displays a typical species and a abundance pattern that was often been observed at low oxygen conditions. After having finished the "water exercises" we returned to station 110 (sta. 110-2, 16°13,1 N/60°16,0 E) were we started in the evening of March 12. Again multicorer and photosledge were used extensively. At each visit, we collected data with the CTD and Plankton net to investigate mainly the oxygen minimum zone.

On March 13, METEOR returned to station 111 (sta. 111-2, 16°05,4 N/59°41,0 E) in order to get longer cores from this location on the Owen Ridge. Our efforts resulted in 4,47 m and 11,69 m respectively. Therefore, we tried the 24 m piston corer. Unfortunately, strong currents influenced a stable position of the ship resulting in the first attempt which failed to obtain a long core. What happened was that the piston tube hit the trigger piston corer and broke. After this disaster we returned back to station 110 (sta. 110-3, 16°03,0 N/60°16,0 E), on March 14 to continue investigations in the abyssal plain by using CTD, multinet, photosledge, boxcorer and multicorer. The location of station 110-3 is situated a few miles south of station 110-1 and -2 and was chosen as another spot for sampling. During the late evening we moved back to station 110-2 (station 110-4, 16°13,0 N/60°16,1 E).where we employed the total suite of geares except of the coring devices. This lasted almost 24 hours.

During the morning of March 16, METEOR arrived at station 112 (17°44,9 N/58°07,7 E) rather close to the Oman coast. The water depth was almost 1000 m shallower compared to station 110. However, the benthos biologist could not detect general differences. Early morning on March 17 we started our way back to Djibouti.

Station 113 (16°32,0 N/55°19,8 E) was the last station where we tried to recover a long core. However, a hydrolic pressure tube blasted which was necessary for operating the jibboom with the core frame while handling the 24 m piston corer Since this has happened several times before, all spare parts were used up causing a non-functioning of the jibboom. From now on the gravity corer was handled without the core frame and the piston coring was stopped. At the following stations 114 (sta. 114: 14°32,4 N/51°44,7 E; sta. 115: 13°18,5 N/48°47,0 E ; sta. 116: 12°51,7 N/47°25,0 E) we completed our data sets by routinly running CTD, multinet, multicorer and gravity corer. The plankton fauna changed between sta. 113 and 114 from a NW monsoon influenced fauna to a more tropical intermonsoon fauna. The photosledge was used at station 115. In the evening of March 21 we obtained our last core off Aden (12°51,7 N/47°25,6 E). This core was taken to trace the outflow of highly saline Red Sea water. Also the photosledge was used for the last time. METEOR cruise 31/2 ended on March 23, 1995 at noon time in Djibouti.

5 Preliminary Results

5.1 Preliminary Results of Leg M31/1

5.1.1 Tracer Measurements in the Eastern Mediterranean

(W. Roether,V. Beitzel, S. Bruns, K. Bulsiewicz, G. Fraas, U. Katt, B. Klein, W. Plep, H. Sieverding)

Purpose:

Cruise M31/1 was a follow-up to previous tracer surveys in the Eastern Mediterranean in 1978 (M50/3, a few stations only), and a more extended one in 1987 (M5/6). In the case of transient tracers, repeated sampling is attractive, because it allows one to assess their gradual penetration into the subsurface waters, which "traces" the renewal of subsurface waters in detail. Furthermore, the tracers CFC-11, CFC-113, and CCl_4 were measured for the first time (Figure 6,7), in addition to ^3He, ^4He, Ne, and CFC-12 (the latter three were not measured in 1978). The main part of tritium, the radioactive hydrogen isotope which decays to ^3He, and the chlorofluorocarbons (CFCs), are of anthropogenic origin. Tritium input into the ocean peaked in the mid-1960ies. Input of CFC-11 and CFC-12 started in the 1940s and increased monotonically but with somewhat different rates. Atmospheric concentrations of CCl4 have been increasing since 1920 while CFC-113 has been released to the atmosphere only since about 1970. These different input functions allow one to interpret concentration ratios of different tracers in terms of water "age" (time since the water mass had last been in contact with the surface layer), yielding rates of water mass formation and mixing.

The hydrographic stations were planned on the basis of evaluations of the tracer data from the previous cruises (ROETHER and SCHLITZER, 1991, SCHLITZER et al., 1991; ROETHER et al., 1992, ROETHER et al., 1994), but were modified according to our findings (see below). CFC samples, to be analyzed aboard, were taken from virtually all hydrographic stations, whereas a reduced sampling program was used for the other tracers, for post-cruise measurement at Bremen. Like for the previous tracer surveys, supplementary sampling was carried out in in the Western Mediterranean (see station map Figure 5 and List 7.1.1). The work was performed in close cooperation with the other hydrographic groups (5.1.2 - 5.1.3) and with the Ocean Prediction Research group (5.1.4). An add-on were tests concerning the CFC measurement methodology.

Sampling and measurement

Water samples for the analysis of CFCs were taken in glass syringes and analyzed on board for all four CFCs by means of ECD capillary gas chromatography. Chromatograph and column are commercial units, connected to a non-commercial sample preparation part. The latter is used to prepare gas aliquots for calibration, and to transfer the gas from water samples (30 cm^3 volume) into the column by a purge-and-trap procedure. The trap is cooled by means of liquid CO_2 to -52° C, and the trapped gases are released to the chromatographic column by heating to 110° C. Measurement is by an electron capture detector (ECD). Detection sensitivity is approximately 0.01 pmol/kg, and precision for surface samples about 1 %. Preliminary data were available by the end of the cruise.

A new method of transferring water for CFC analysis, i.e. using through-flow glass ampoules in place of the syringes, was successfully tested. This method has since been introduced into our routine measurement procedure. The ampoules are furthermore suitable to store water samples for shore-based CFC measurement.

Helium samples were placed into clamped-off copper tubes, and tritium samples into 1-liter glass bottles, to be analyzed in the laboratory at Bremen after the cruise. The procedure is helium isotope mass spectrometry (precision 0.2 % in d^3He, 0.4 % in He isotope and Ne concentrations). Tritium is measured by determining ^3He grown in from tritium decay (typical ingrowth period 6 months). Helium isotope measurements have since been completed, while processing of the tritium samples is presently beginning.

Preliminary results

A station map is given in Figure 5 an List 7.1.2. The tracer distributions in the Western Mediterranean, according to the few hydrographic profiles obtained, were without surprises. In constrast, it became clear very soon during the cruise that in the Eastern Mediterranean a dramatic change had occurred since 1987. To demonstrate this, Figure 6 shows a CFC-12 section running from the Strait of Sicily through the Ionian Basin, across the area south of Crete and finally into the Levantine Basin (Figure 6a), in comparison with 1987 data (Figure 6b). Whereas in 1987 relatively CFC-rich, i. e. young, water below 1000 m depth was

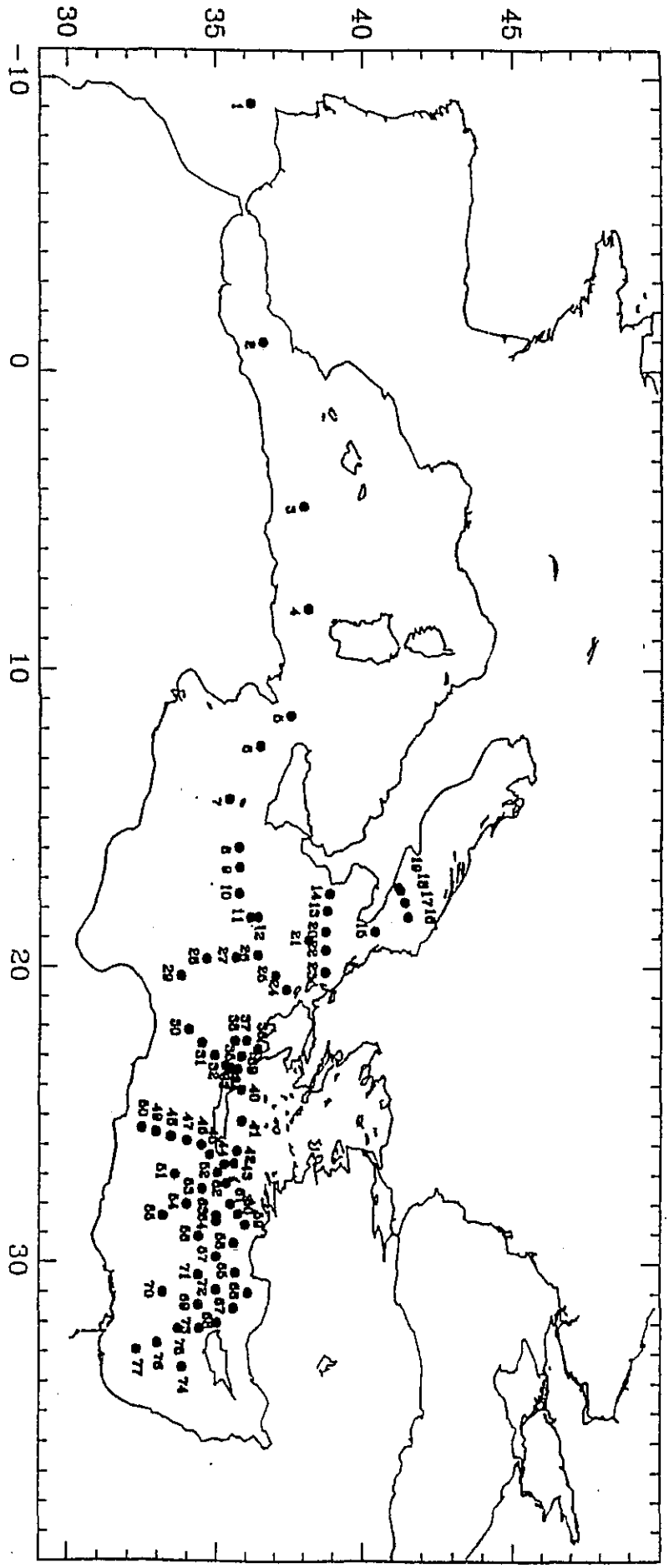

Fig. 5: Map of hydrographic stations, cruise M31/1.

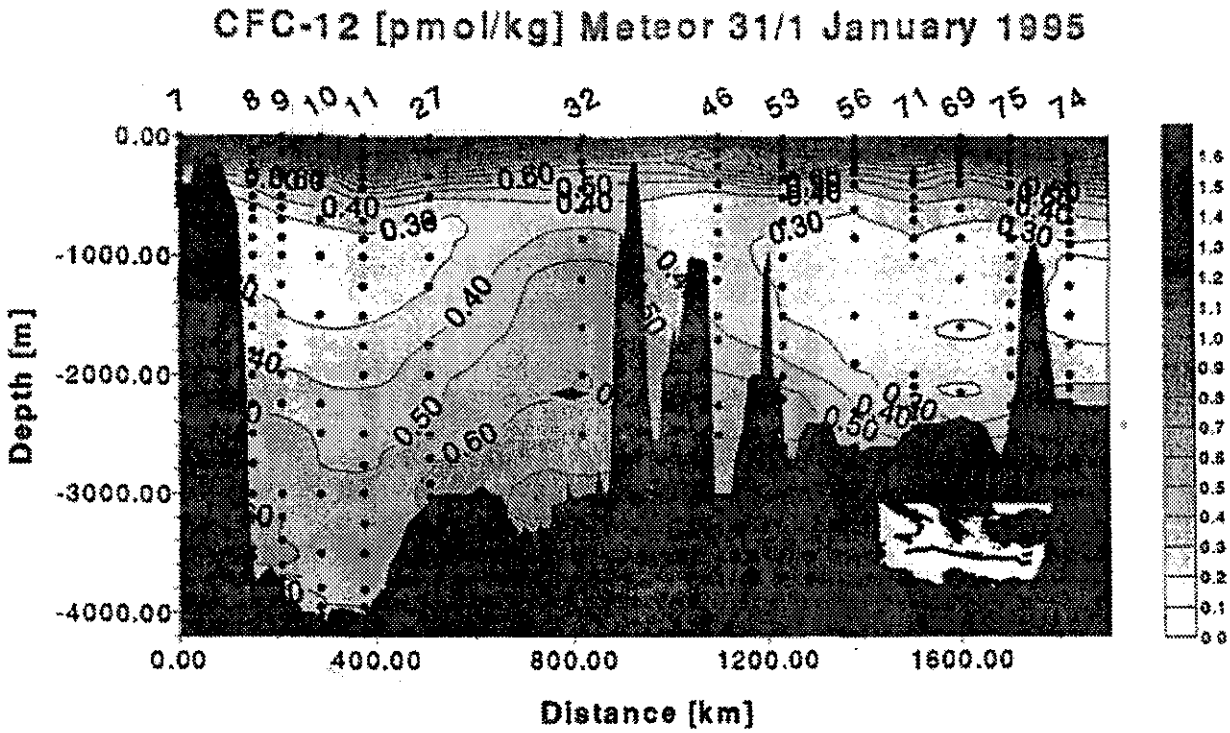

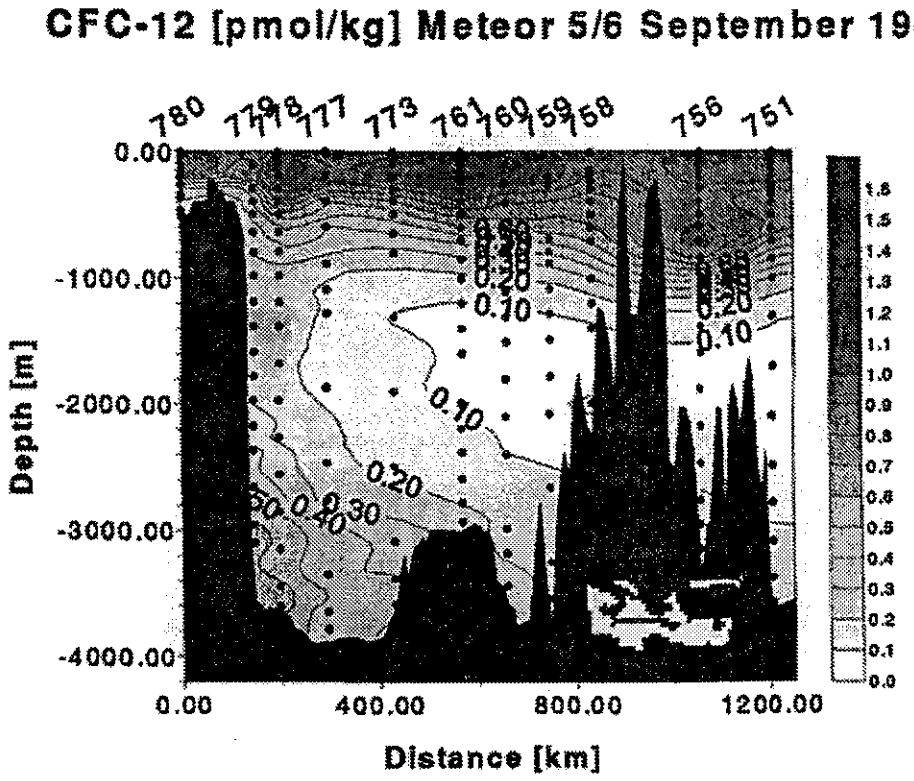

Fig. 6: Isolines of CFC-12 (pmol/kg) on sections from the Strait of Sicily toward the eastern Levantine Basin (see inset maps), data points indicated by dots, 1995, M31/1 (Figure 6a; stations see Figure 5) and 1987, M5/6 (Figure 6b).

restricted to the western end of the section, and mid-depth waters further east showed very low concentrations, in 1995 a plume of young water was found also in the vicinity of the Aegean Sea, and the mid-depth tracer minimum layer was partly filled in and occured at much shallower depth than previously. The explanation is that deep and bottom waters previously were generated only in the Adriatic, in accordance with classical assessments of water masses in Eastern Mediterranean (WÜST, 1961). The extended mid-depth tracer minimum represented old waters. Between 1987 and 1995, however, large amounts of dense water were added from the Aegean Sea. A further piece of evidence is presented in Figure 7, showing a CFC-113 section through the Aegean. Young water in the Aegean, and spilling out into the Eastern Mediterranean at large through passages in the Cretan Arc, is evident. Concentrations being largest at the bottom (Figures 6a, 7) mean that Aegean water was primarily added to near-bottom layers. Similar information is contained in the distributions of all parameters measured (see also 5.1.2, 5.1.3).

Our findings are confirmed by independent observations (e. g. inverted temperature gradients reported in sediments just below the water interface), and a first description is being published presently (ROETHER et al., 1996). Effects are found also at shallower depths at least into the Levantine Intermediate Water (about 250 m depth). Further work is in progress. Current deep water studies in the Eastern Mediterranean may be affected by the recent intrusion of dense Aegean Waters and must therefore take note of it.

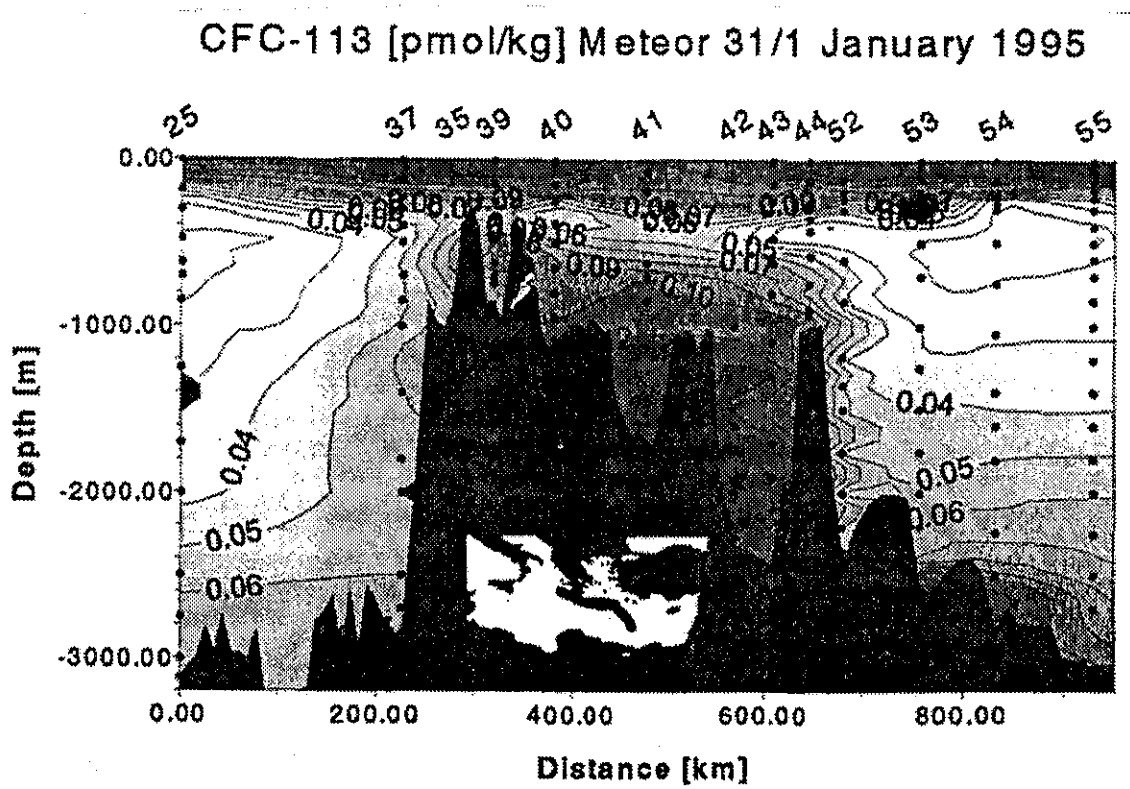

Fig. 7: Isolines of CFC-113 (pmol/kg) along a section through the Aegean Sea (stations see Figure 5).

5.1.2 CTD Work

(B.B. Manca, V. Kovacevic, R. Cecco, D. Georgopoulos,
P. Drakopoulos)

The cruise was carried out in the framework of the international POEM-BC (Physical and Biochemical Oceanography of the Eastern Mediterranean) program and especially in the framework of LIWIX-95 (Levantine Intermediate Water formation experiment) Experiment. The aim of the LIW experiment is to study the processes which dominate the formation of Intermediate Water in each of the three important phases (preconditioning, formation and spreading). The purpose of the METEOR M31/1 cruise was to cover the preconditioning phase in LIWEX-95.

CTD Data Acquisition and Quality Control

CTD measurements were performed with a Mark IIIC CTD (manufactured by Neil Brown) and a Sea Bird 911 plus CTD (manufactured by Sea Bird) equipped with fluorometer. Water samples were taken from two 24-bottle General Oceanics Rosette samplers with 10 liter bottles. For calibration purposes temperature readings were obtained from six SIS digital reversing thermometers and a protected mercury reversing thermometer attached to the bottles. An unprotected mercury thermometer and two SIS digital reversing pressure meters were used to obtain data for the pressure calibration. A Guildline Autosal salinometer 8400A was used to analyze the salinity samples. Three of the SIS thermometers and the mercury thermometers were provided by the Israeli and Turkish groups respectively, with the purpose to intercalibrate the data that will be collected in the framework of LIWEX-95, to ensure consistency of the data sets.

At most stations two CTD casts have been performed. In a first cast the Sea Bird CTD with fluorometer was lowered to 250-300 m (shallow rosette). The second cast was performed with the Neil Brown CTD lowering the instrument to the bottom (deep rosette). Salinity samples were taken from most of Niskin bottles of the deep casts and analysed on board by means of salinometer. Three to four water samples from the deep casts were collected additionally and stored away; they will be analyzed in the OGS laboratory after the cruise. The aim of the on board salinity analysis was to monitor a probable drift of the conductivity sensor of the CTD, to verify the proper closing sequence of the bottles in the rosette water sampler and to identify leaking bottles. For the same reasons a limited number of samples were also collected from the shallow casts.

During the oceanographic cruise 76 CTD casts were performed. One profile was obtained in the Atlantic ocean, just before entering the Strait of Gibraltar, 4 stations are situated in the western Mediterranean Sea up to the Strait of Sicily while the majority, 71 casts, were taken in the Eastern Mediterranean including the Adriatic Sea (see 5.1.1).

Parallel measurements of both CTDs to great depth were performed on 4 stations during the cruise. The aim of this intercomparison was to check the functioning of both instruments. At

the intercalibration stations water samples for salinity measurements were collected from both rosettes at all depths. Figure 8 shows the superimposed vertical profiles of temperature and salinity obtained by the Neil Brown and Sea Bird CTD at the station 3. The intercomparison from 1000 m down to the bottom, where a sufficient homogeneity of the water masses was met, revealed a difference in temperature of 0.0015 ±0.003° C and in salinity of 0.014 ±0.001 psu.

Preliminary Results

Figure 9 shows vertical profiles of temperature and salinity which are representative of the hydrological situation encountered in the Eastern Mediterranean during the cruise. The profiles shown here belong to station 8-69 carried out in the period from 11 to 31 of January. The stations are in the Ionian, Adriatic, Cretan Seas and in the Levantine Basin. The salinity profiles show the major characteristics of the different basins. In spite of the extreme vertical variability of the hydrographic characteristics encountered during the cruise, the Eastern Mediterranean is schematically described as a three-layer system.

The surface layer (0-200m) is dominated by intense dynamic features. We can distinguish the less saline Ionian Surface Water (ISW) from the very salty surface water of the Levantine Basin. The Eastern Mediterranean receives in fact relatively fresh Atlantic Water (AW) which is modified as it is moving eastward from the Strait of Gibraltar to the Strait of Sicily. The intermediate layer (200-800 m) is characterized by higher values in temperature and salinity of the Levantine Intermediate Water (LIW). At most of the stations in the Levantine Basin waters with LIW characteristics were observed, sometimes in the surface layer. These salty waters at the surface are clearly formed by intense evaporation and mixing processes during the previous summer period. The deep layer (800 m - to the bottom) is also dominated by strong variability in temperature and salinity with stronger gradients in the eastern Ionian basin. This represents a very new situation of the hydrological characteristics in the Ionian Sea (Figure 10). Detached from the main nucleous on the vertical profiles we can distinguish the less saline and colder water encountered in the Adriatic Sea down to 1200 m and the more saline and warmer waters of the Cretan Sea down to 2500 m.

T-S characteristics are plotted in Figure 9 separately for stations 7-14 in the western part of the Ionian sea and for stations 20-29 in the eastern part of the basin. Both diagrams show relatively fresh Atlantic Water near 14.5° C, and the LIW with a salinity maximum near to 38.87 psu. Besides these main similarities, there is a substantial difference in the deep water range for densities greater than of 29.2 kg/m^3. The profiles in the eastern part of the basin show an inversion in temperature and salinity in the deepest layers that is a clear evidence of the presence of dense waters from a source other than the Adriatic.

Figure 11 shows the salinity and temperature distribution along the transect at 35° N (from 25.5 to 31.5° E) in the Levantine basin. This transect is located across the Rhodes gyre. The existence of opposite flows is shown by the sloping isotherms and isolines in the upper layer down to 500 m. We can observe a layer of colder and less saline water masses underneath. The

core of this layer ranges from 1500 to 2000 m. The very deep layer is occupied by warm and saline waters creating an inversion of both temperature and salinity values. This is a clear evidence of Cretan Sea waters feeding the deepest part of the Levantine basin.

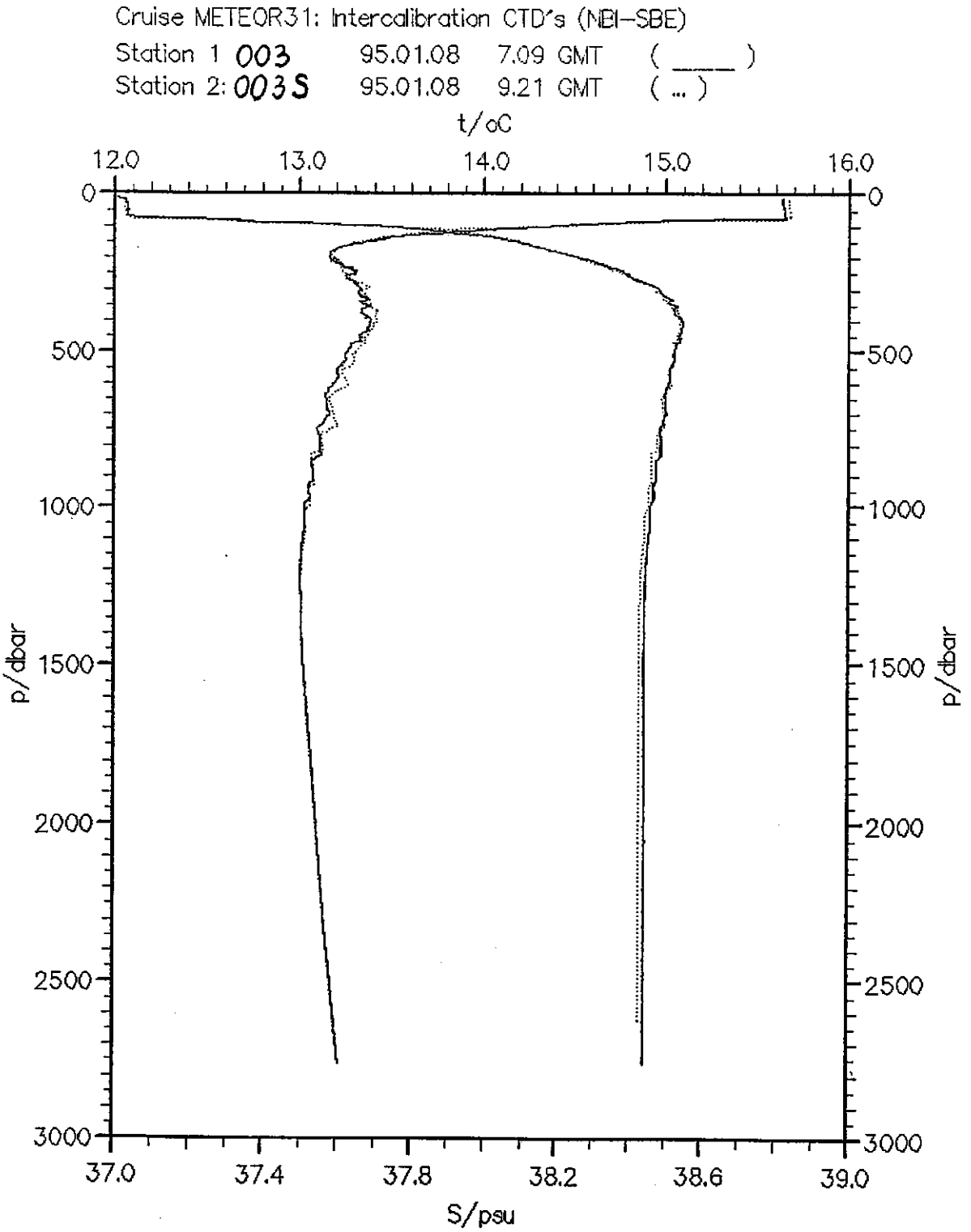

Fig. 8: Intercomparison of Neil Brown and Sea Bird vertical profiles at station 3.

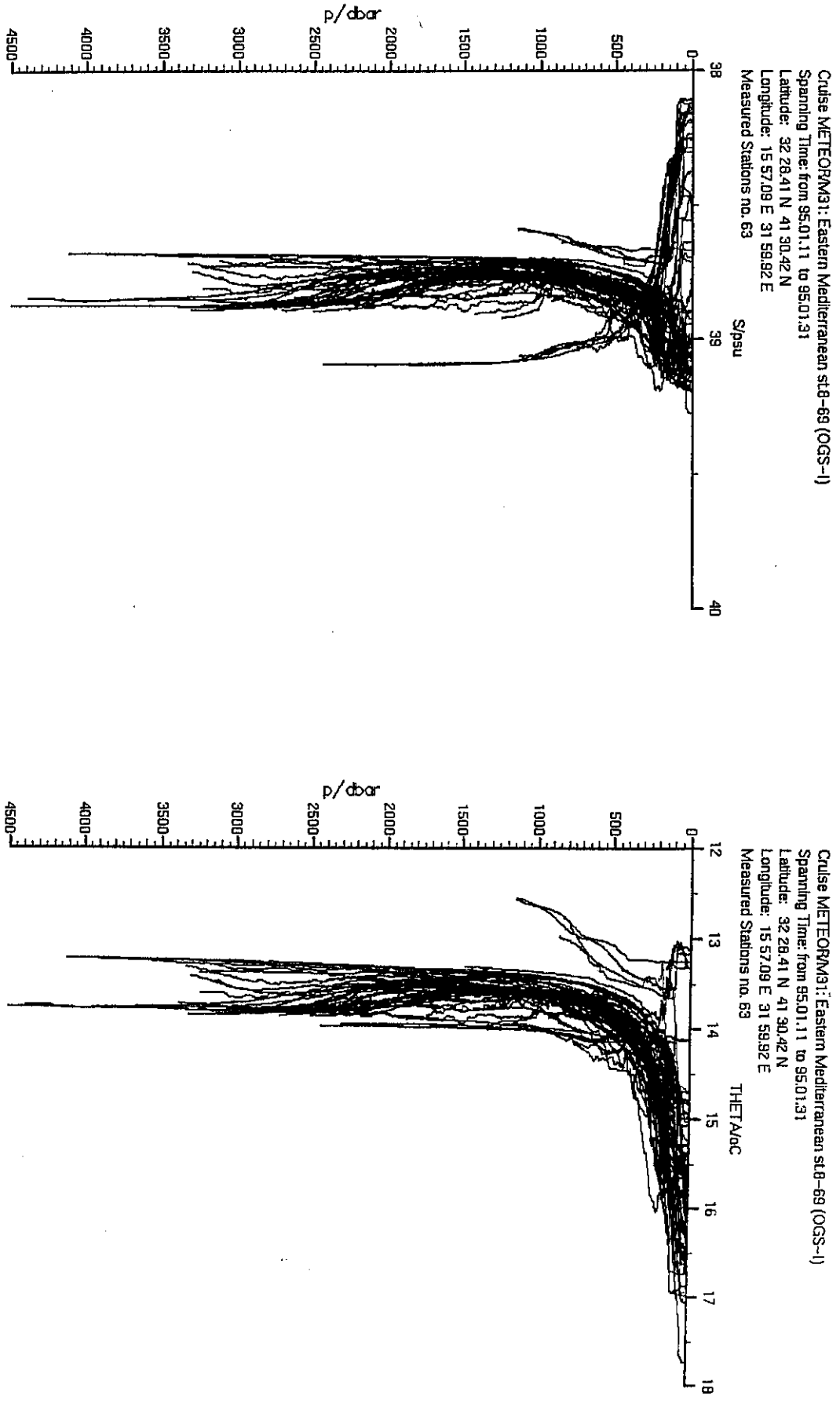

Fig. 9: Composite profiles of T and S for all the CTD stations in the the Eastern Mediterranean.

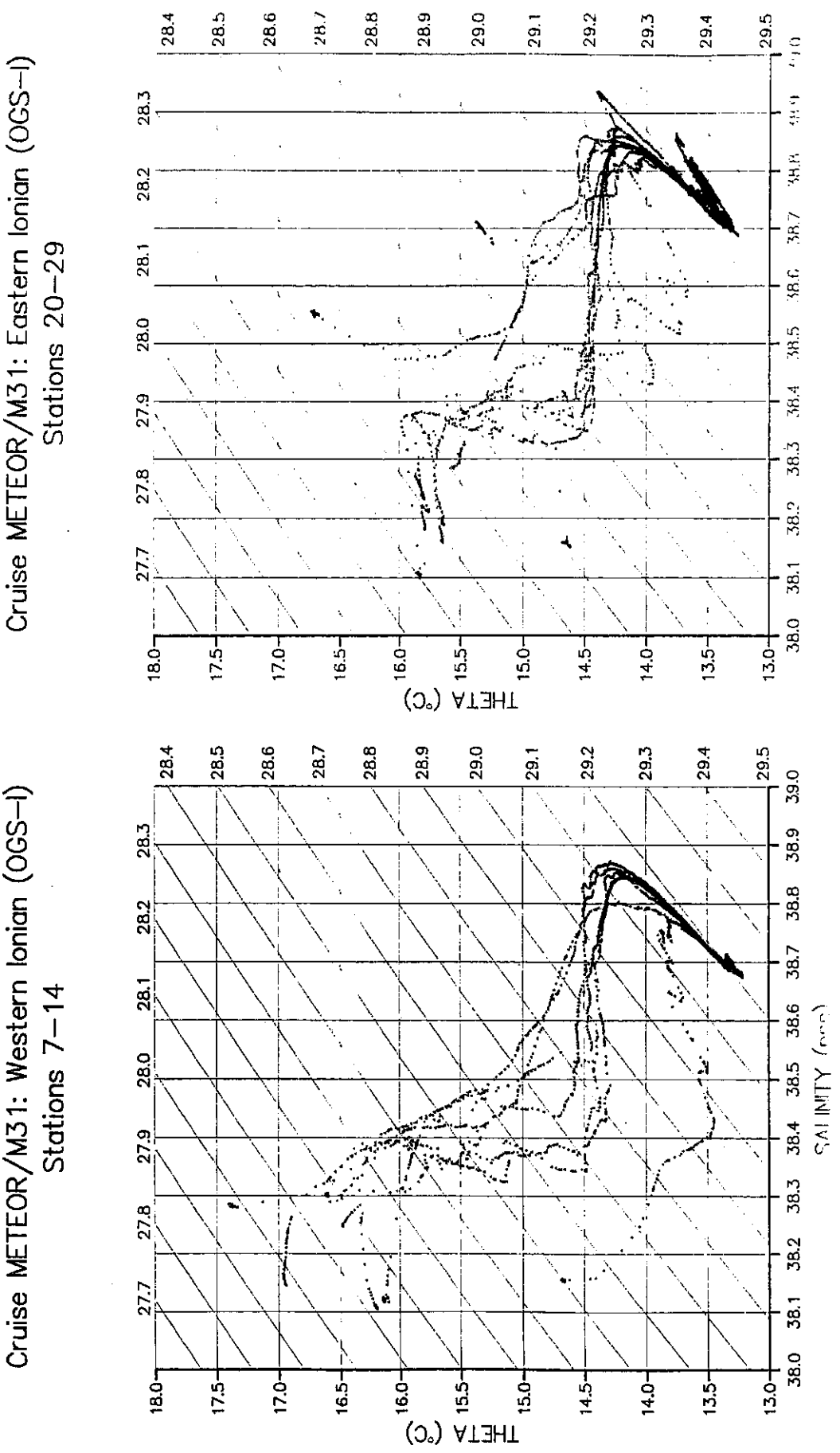

Fig. 10: Potential temperature and salinity relations for the Western part (left) and Eastern part (right) of the Ionian Sea.

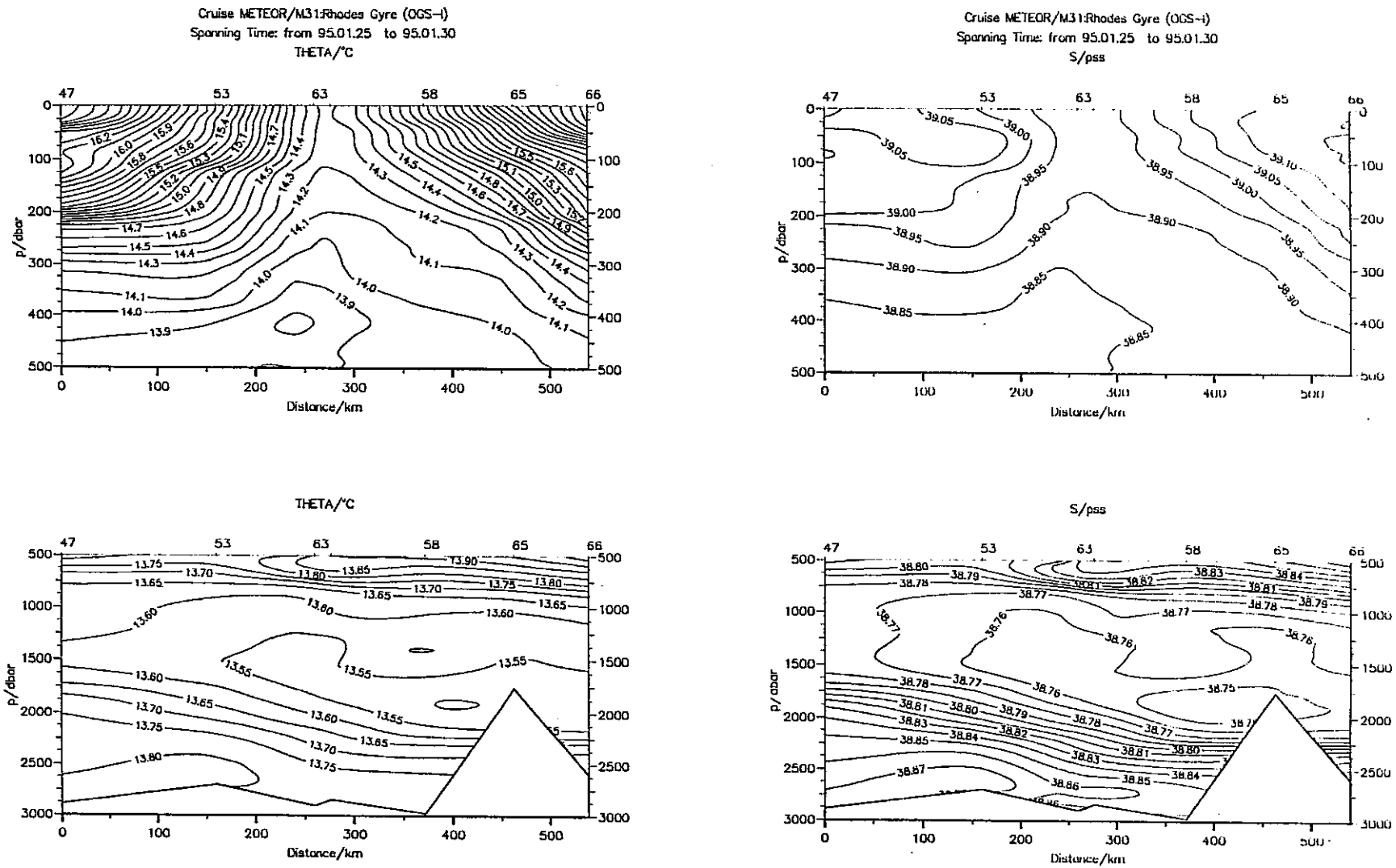

Fig. 11: Vertical sections of temperature (left) and salinity (right) for the transect in the Levantine basin across the Rhodes gyre.

5.1.3 Nutrient measurements

(D. Bregant, A. Luchetta, S. Cozzi)

One of the main objectives for the determination of dissolved oxygen, silicate, nitrate, phosphate and nitrite during the METEOR cruise M31/1 was to contribute to the knowledge of the general circulation of the Eastern Mediterranean Sea on basin scale, which is still inconclusive, and to improve the knowledge of some specific local features and processes as eddies, permanent gyres, deep water formation, LIW formation (MALANOTTE - RIZZOLI et al., 1988, SCHLITZER et al., 1991) that can be well characterized by their hydrochemistry. Another aim is to correlate the nutrient-availability in the surface layer of one of the most oligotrophic area of the world, and their advection from the intermediate layers, with phytoplankton population and new production.

Methods

During the cruise samples were collected for the analysis of dissolved oxygen and nutrients from each CTD cast. They were analyzed on board immediately after recovery of the rosette. Alltogether 2500 samples of each species, coming from 76 stations, were analyzed. At station 73 samples were collected for a test of nutrient intercalibration. These samples were immediately frozen and are going to be analyzed on land by six different laboratories involved in the POEM-BC program.

Dissolved oxygen was analyzed according to the Winkler method reported by GRASSHOF (1983), the end point was detected potentiometrically. Series of five replicates were performed all along the cruise for different depths and different concentration ranges. The standard deviation was less than 0.70 mmol/l. For example a standard deviation of ± 0.51 mmol/l resulted for a mean concentration of 198.5 mmol/l at 570 dbar (variation coefficient Cv = 0.25 %), ±0.42 mmol/l for mean value of 244.9 mmol/l (Cv = 0.17 %) and ± 0.60 mmol/l for 216.0 mmol/l.

Dissolved silicate, phosphate, nitrate and nitrite were analyzed by means of a Technicon II Autoanalyzer according to GRASSHOFF (1983). Replicates were run on different concentration values and the following results were obtained:

Tab. 4:

	Stand. Dev. [mmol/l]	Mean Conc. [mmol/l]	Cv [%]
Silicate	±0.05	6.75	0.75
	±0.04	1.05	3.84
Nitrate	±0.04	5.90	0.73
	±0.02	0.53	4.30
Phosphate	±0.003	0.11	3.12
Nitrite	±0.036	0.03	1.21

Results

Figure 12 shows vertical profiles of all analyzed species for station 64, in the Rhodes Gyre. This station appears to be the center of the gyre, characterized by a very homogeneous density from the surface to the bottom (3000 dbar). The top euphotic layers appears to be chararacterized by high concentrations of oxygen and nutrients, indicating a winter condition, with nutrients not yet consumed and quite homogeneous concentrations. Below 500 dbar we can observe a sharp nutricline leading to the maximum concentration values in a region extending down to 1000 dbar, below this range the nutrient concentrations decrease and reach a constant value from 1750 down to the bottom. The oxygen profile is in good anticorrelation with the nutrients, with a minimum region down to 1000 dbar, possibly reaching a little deeper than the corresponding nutrient layer, and a homogeneous layer of more oxygenated water from 2000 dbar to the bottom.

Comparing profiles from different basins in the Easterrn Mediterranean reveals important differences in oxygen content, expecially with regard to the deep waters. In particular the Cretan Sea (Figure 13) is characterized by waters which are very rich in oxygen over the whole water column compared to the Ionian Sea or the Levantine Basin. While the oxygen content in the minimum layer exceeds 210 mmol/l in the Cretan Sea, it is only about 190 mmol/l for the other two basins. Deep and Bottom Waters in the Cretan Sea have oxygen concentrations of 230 mmol/l compared to 210 mmol/l in the Ionian and Levantine Basin.

In a section through the southern Adriatic Sea a high correlation between oxygen and T, S distributions was observed indicating a dynamic feature. It was centered at station 17 and showed characteristics of a cyclonic circulation of this basin, exhibiting recirculation of modified Levantine Intermediate Water along the Italian coast. At station 17 the vertical oxygen profile is nearly constant from the surface to the bottom, in contrast to the stations nearby (Figure 14).

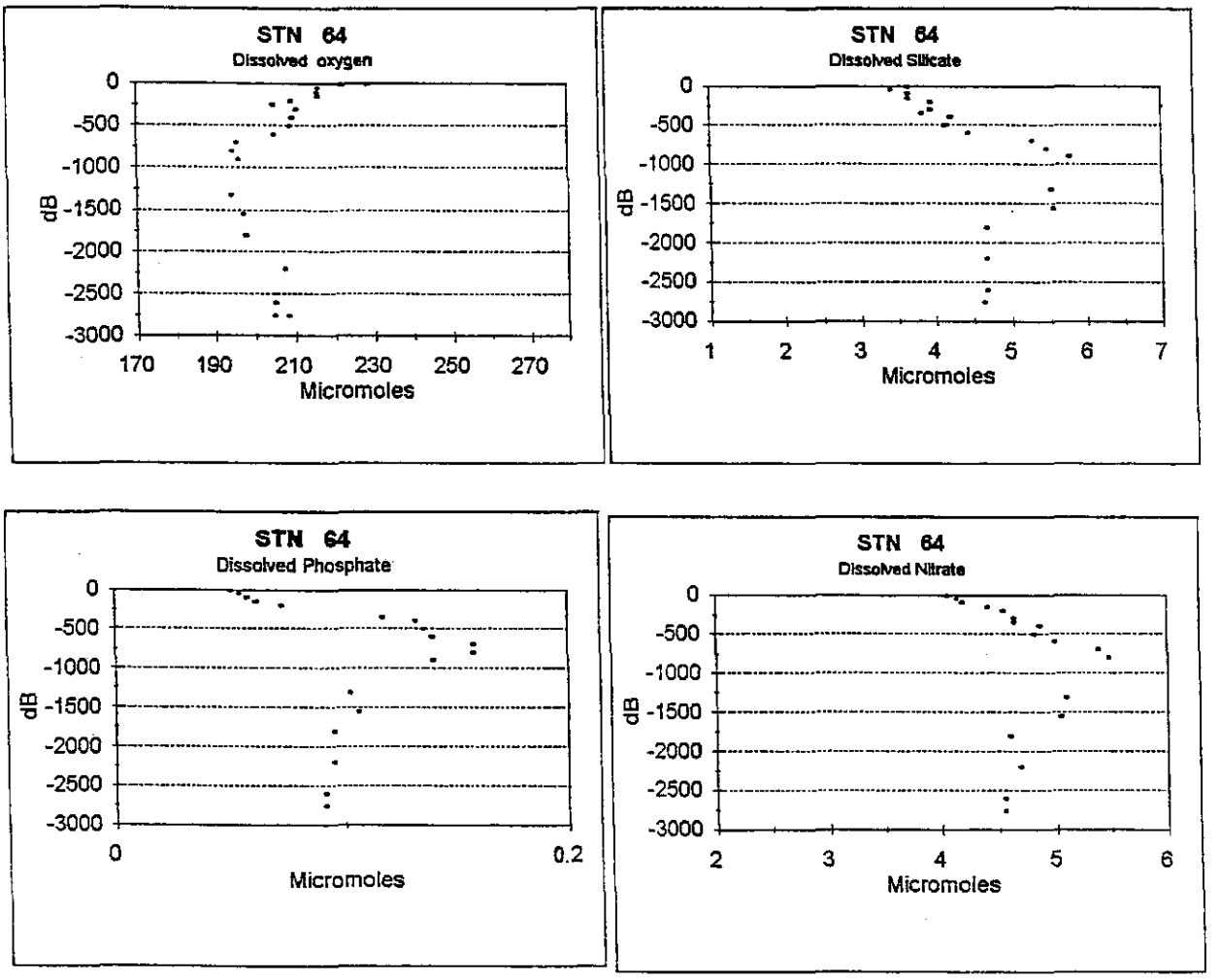

Fig. 12: Vertical profiles of oxygen (µmol/l), silicate (µmol/l), phosphate (µmol/l) and nitrate (µmol/l) for station 64.

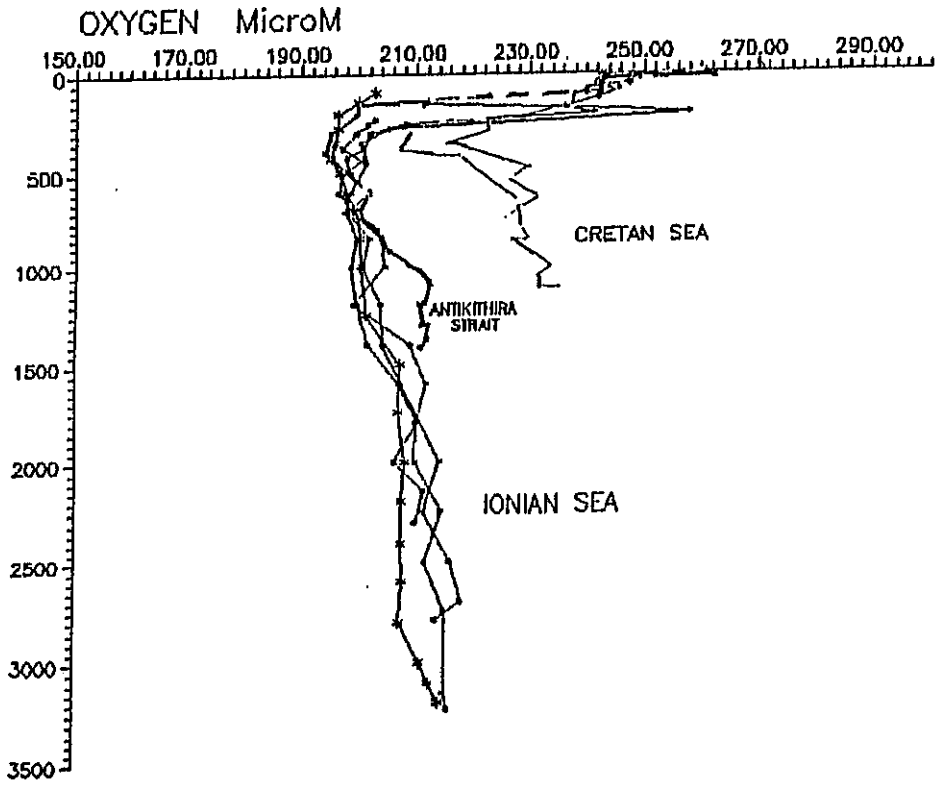

Fig. 13: Vertical profiles of oxygen (µmol/l) from three different regions within the Eastern Mediterranean.

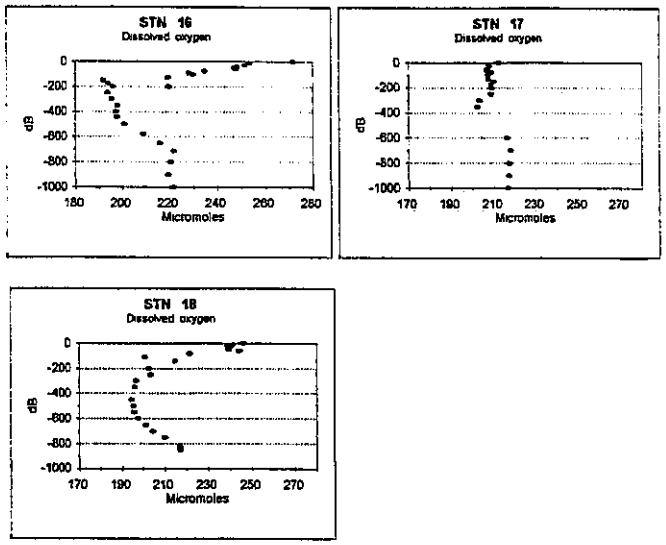

Fig. 14: Vertical profiles of oxygen (µmol/l) for three stations in the Ionian basin.

5.1.4 Levantine Intermediate Water Experiment and Ocean Prediction Research

(A.R. Robinson, H.G. Arango, W.G. Lesie, H.M. Hassan, A.M. Mahar and M. Candouna)

Research cruise M31/1 was used to obtain a comprehensive Eastern Mediterranean basin-wide data set of upper ocean temperature profiles with mesoscale resolution during winter. The data set was used to describe the synoptic mesoscale state, derive mesoscale statistics, compare it with the summer-time mesoscale data of August-September 1987, input the data to high resolution nowcasts and forecasts and input the data to dynamical studies of the mesoscale circulation and mesoscale processes.

The Levantine Intermediate Water (LIW) formation experiment (LIWEX-95) is part of POEM-BC (Physical, Biological and Chemical Oceanography of the Eastern Mediterranean) carrying out a comprehensive experiment on the preconditioning, formation and spreading of LIW. Five ships and eight institutions have been participating in the programm between January to April 1995. The Harvard group objectives were to define the state of stratification, mixing and preconditioning of the upper ocean in the Levantine Basin during January and early February 1995, to prepare analyses, nowcasts and forecasts and to transmit them to the RV BILIM (Turkey) to help to guide her LIW cruise which started on February 7, 1995.

The field estimation and ocean prediction research comprised real-time sea-tests of novel methods of nowcasting, forecasting and simulating real ocean multiscale synoptic fields. It involved nested regions of high resolution within a full basin synoptic estimate and melding of dynamics with various data types, including historical synoptic realisations, climatologies and direct data streams acquired at sea.

Data acquisition and presentation

Along the ship track of Figure 15, 503 XBTs were obtained (see 7.1.3) at the station positions indicated. Vertical sections were prepared within 30 minutes of data acquisition and made available for interpretation, together with the associated temperature profiles. A sample presentation is shown in Figure 16, an east-west section through the center of the Rhodes Gyre. Note the interesting, almost totally vertically mixed region and profiles. Together with a relevant CTD, this data indicates the presence of newly formed LIW to at least 200 m.

Analysis and interpretation

Both subjective and objective analyses were made of the XBT data, together with the CTD data. The subjective analyses were based upon features appearing in the sections, linked by horizontal isotherm mapping at 125 m and 200 m. The synoptic circulation features appearing in the Levantine Basin are shown in Figure 17. The objective analysis was carried out using a Gaussian correlation function with an e-folding length of 150 km and a zero crossing of 75 km. The rather large values were chosen to be consistent with the mapping pattern of Figure 15, which is of coarse resolution with regard to definition of the linked sub-basin scale features

which constitute the general circulation of the Easterrn Mediterranean. Temperature at 50 m and 125 m in the Levantine Basin are shown in Figure 18. The picture of the synoptic state of the general circulation of the Levantine Basin, obtained by subjective (Figure 17) and objective (Figure 18) analyses, are in excellent agreement.

Nowcasts, forecasts and simulations

Data was assimilated into a full Eastern Mediterranean domain at 25 km resolution and into a north-central Levantine Basin domain at 6.25 km resolution. The Harvard group brought aboard the RV METEOR two Sun Sparc-10 workstations in which to run the numerical models. One model day of the full basin required 1.25 hours of wall clock time and one model day of the north-central domain required 1.75 hours.

The approach to model initialization and data assimilation for nowcasting and forecasting was to first prepare a background circulation, corresponding to a wintertime situation and with synoptic resolution of sub-basin sacle features. Into this background circulation, the objectively analyzed METEOR data, with mesoscale resolution along a coarsely resolved sub-basin scale mapping pattern, was then melded via optimal interpolation. Temperature, 'salinity', and geostrophic velocity were assimilated with high weights along-track and horizontal weight distribution structered by the OA expected error maps. The salinity associated with XBTs was chosen via analog search of CTD temperature profile nearby in space or seasonal time. The associated CTD salinity profile was then assigned to the XBT. The background circulation was constructed from a basin-wide AXBT data set from December of 1991 (HORTON et al, 1994) and a CTD and XBT data set for the Sicily Straits and the western Ionian Sea from November of 1994 obtained by the SACLANT Undersea Research Centre with cooperation of the Harvard Group (WARN-VARNAS et al, AIS-94 Cruise Plan, 1994),

Figure 19 shows sample results from both the large and small domains after the RV METEOR data have been assimilated and dynamically adjusted. The consistency of Figure 19 with Figure 17 and 18 is noteworthy.

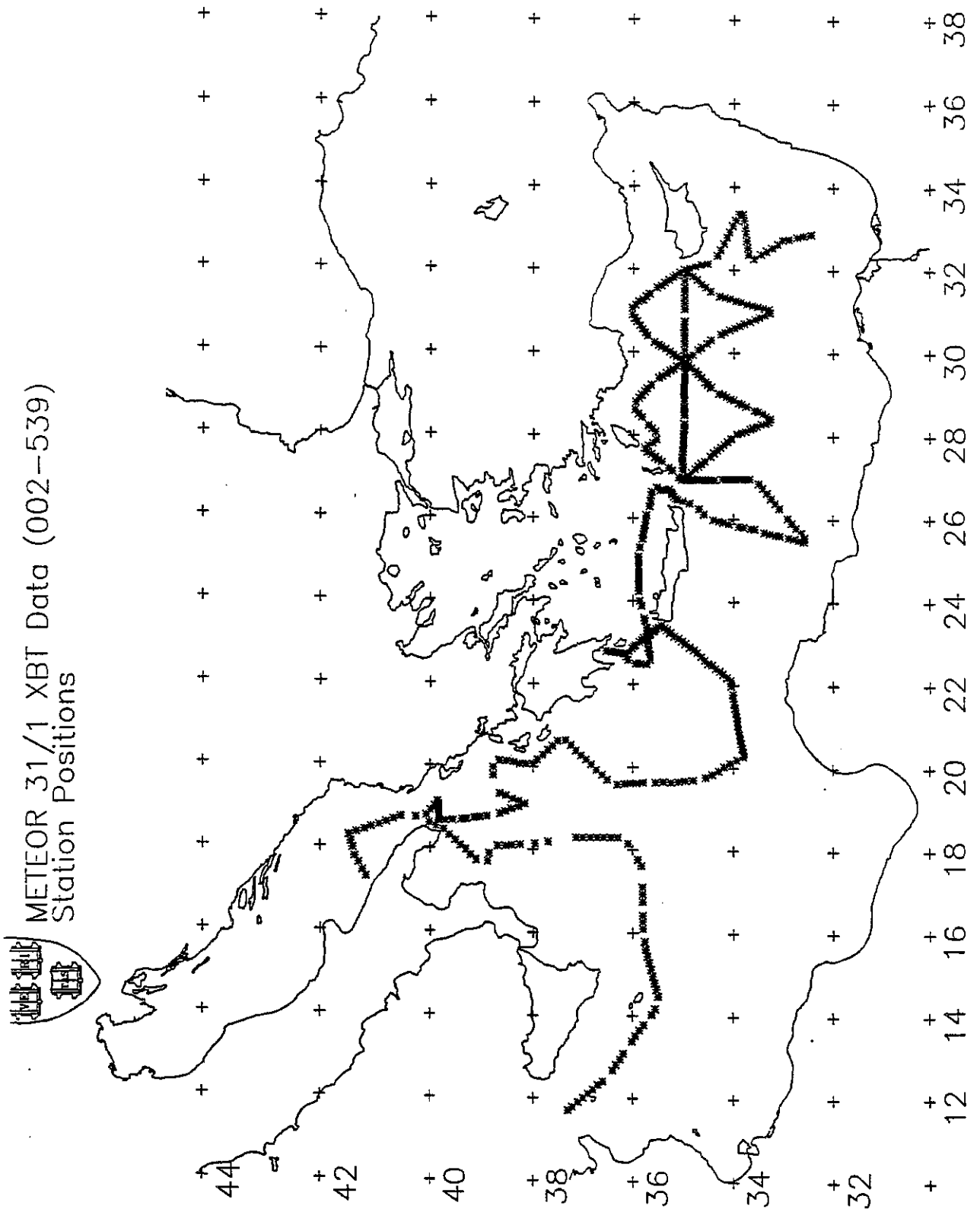

Fig. 15: XBT station position.

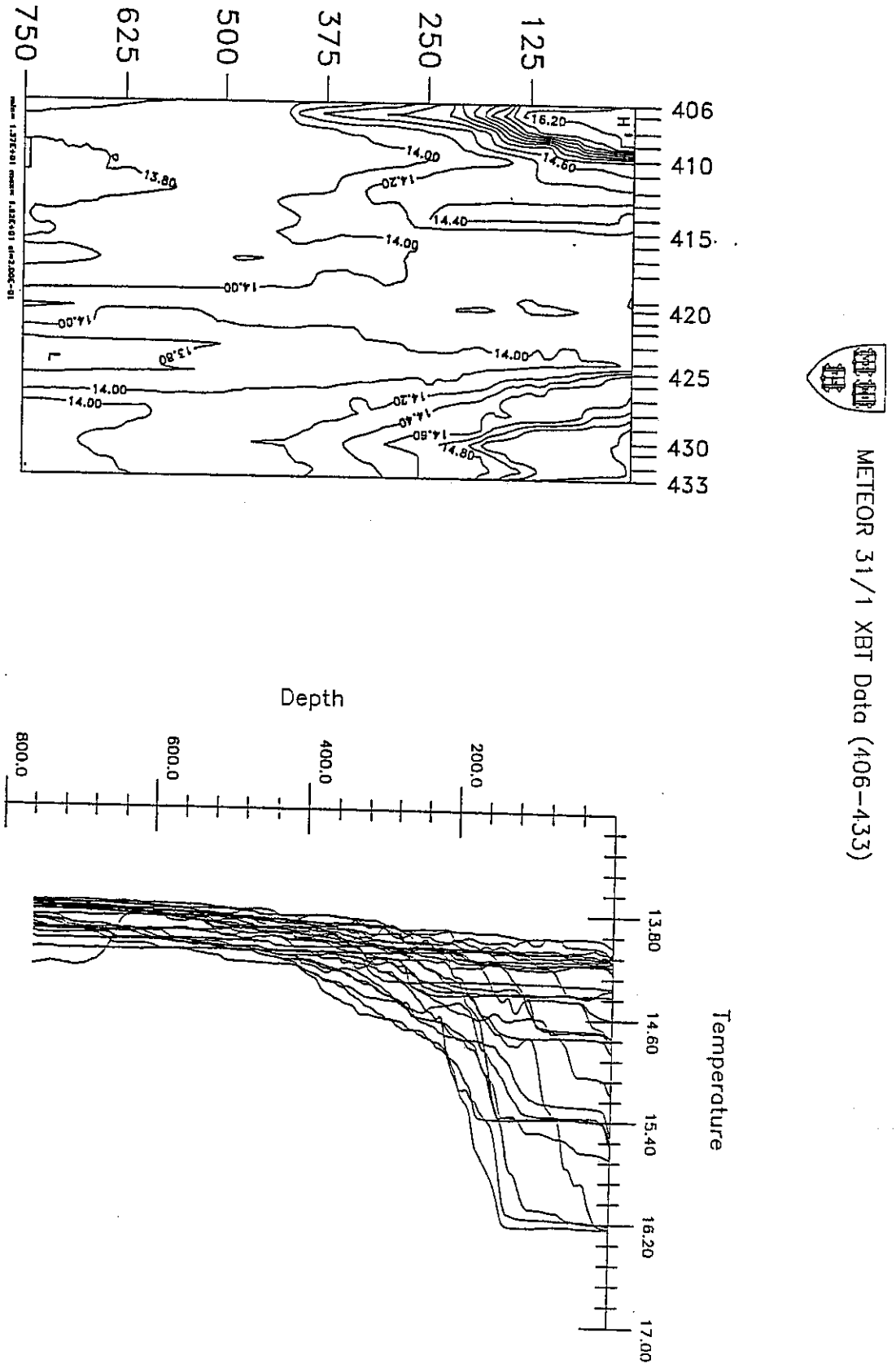

Fig. 16: Vertical temperature section (left) and temperature profiles (right) along 35° N between 27° E and 30° E.

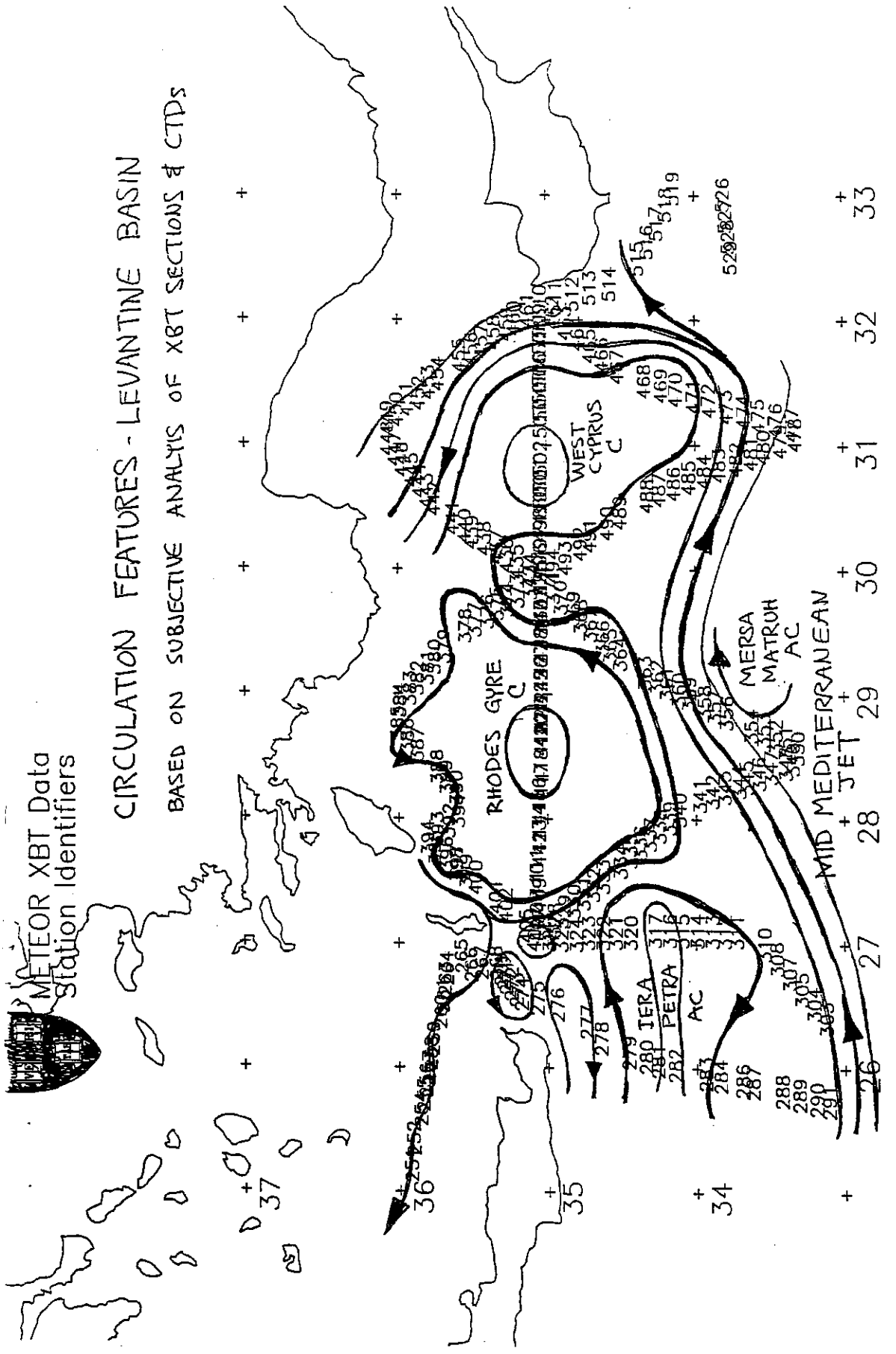

Fig. 17: Subjective analysis of circulation features in the Levantine Basin.

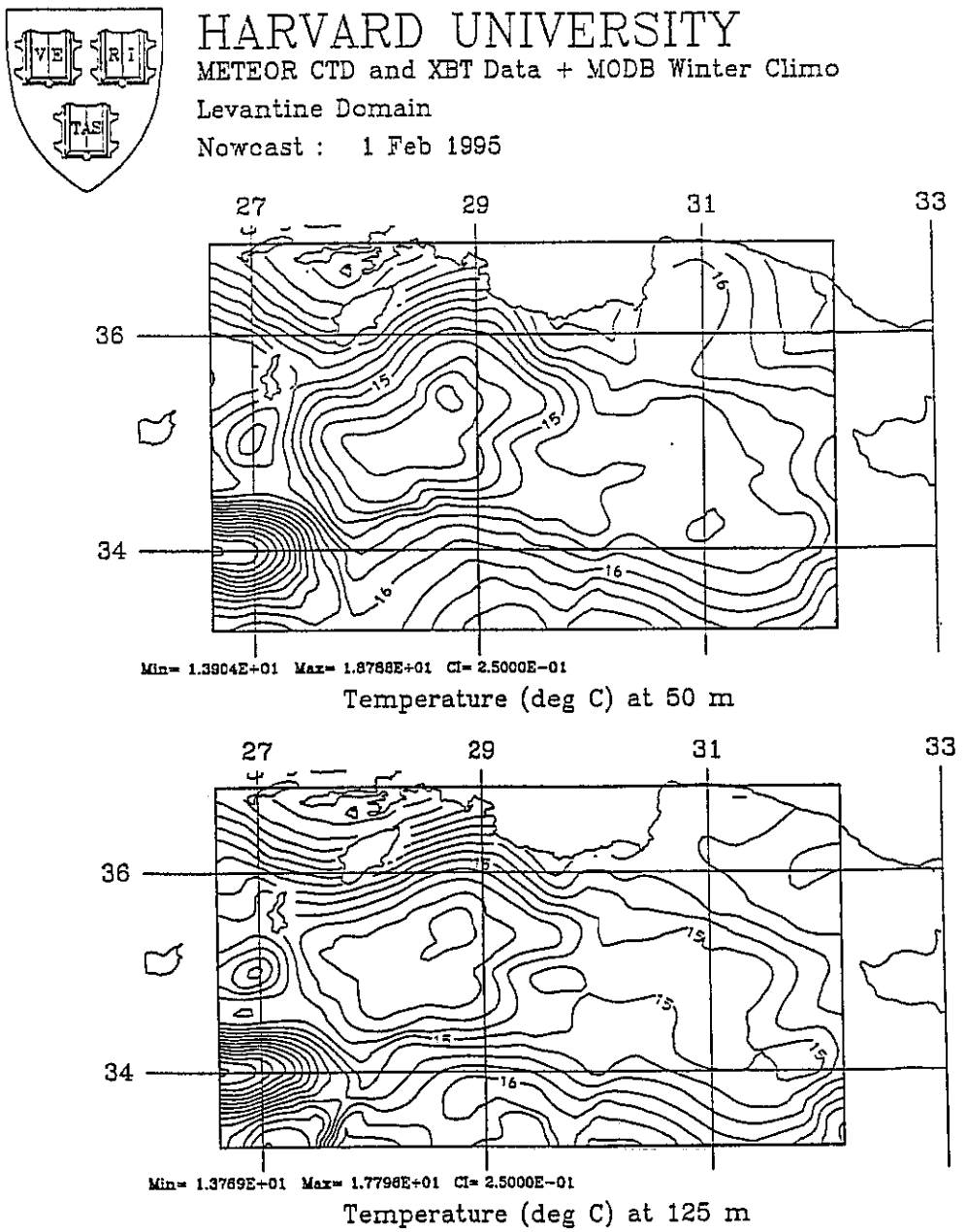

Fig. 18: Objective analysis of temperature at 50 m and 125 m.

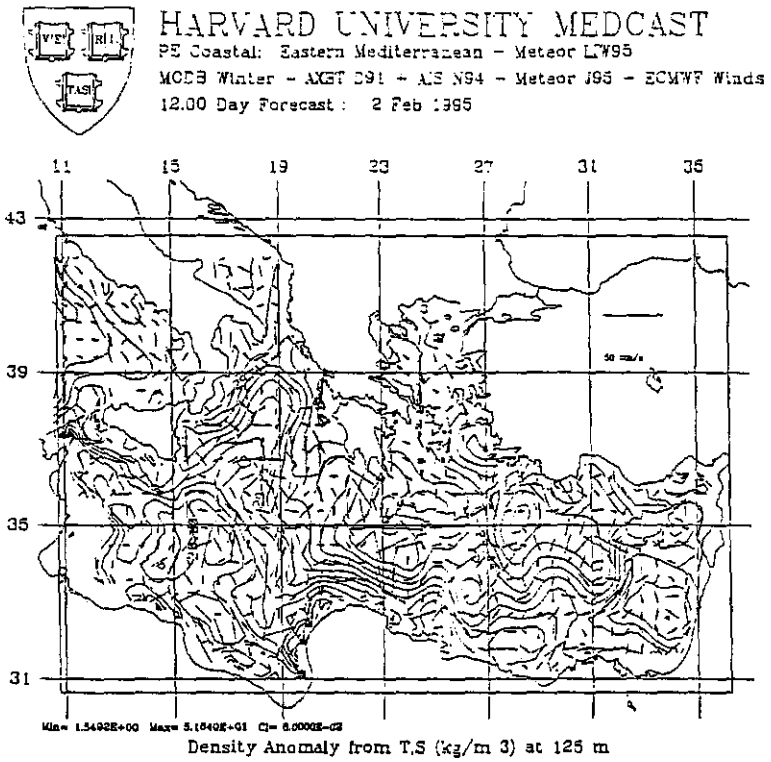

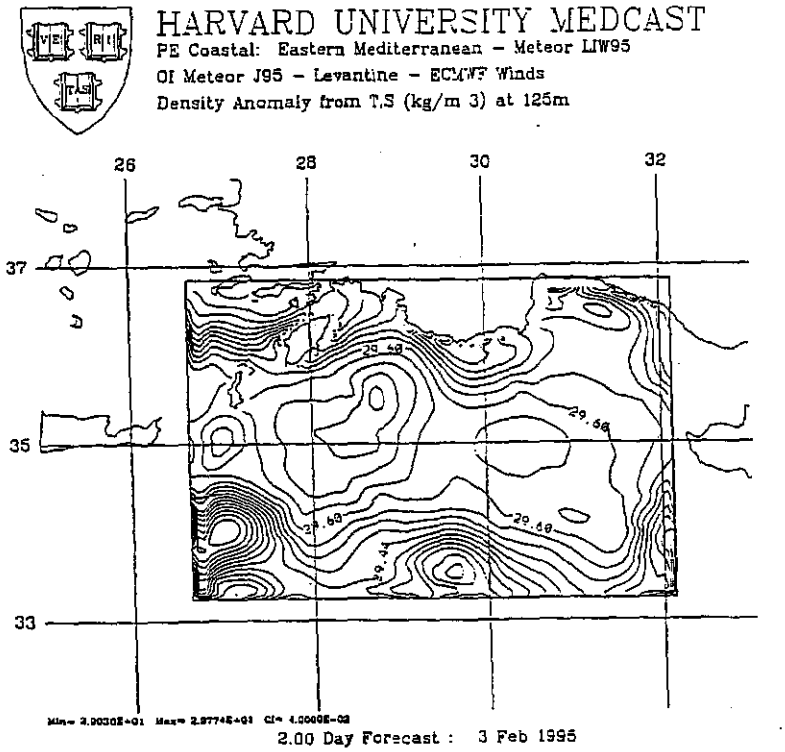

Fig. 19: Density anomaly and horizontal total velocity (vectors) at 125 m for forecast day 12 in the full Eastern Mediterranean domain (top) and density anomaly at 125 m in the northwest-central Levantine Basin domain.

5.1.5 Planktonic Ciliates

(H. auf dem Venne)

Microorganisms have been studied intensively since about 15 years in order to model carbon flows in planktonic ecosystems. It was realized that the classical paradigm of plankton research, a food chain leading from phytoplankton via consumers of different order (e.g. crustacea) to fish had to be extended by microbial components. A new model of the microbial food web, the so-salled microbial loop, was established. According to this concept dissolved organic carbon, mainly from exudation processes of phytoplankton is transferred into bacterial biomass which is then consumed by protozooplankton, namely nanoflagellates and ciliates. The latter are grazed upon by larger metazooplankton and thus comprise a link to the classical food chain mentioned above.

However, the picture of planktonic ciliates as being solely consumers of auto- and heterotrophic nanoplankton has changed in the last few years, when it turned out that at least sometimes large fractions of planktonic ciliates may harbour intact chloroplasts which produce photosynthetic products metabolically using the ciliate. These chloroplasts are taken up by the ciliate during feeding on algae, but whereas the algal cells are digested, their chloroplasts are kept functioning for days or weeks. This mixotrophic mode of nutrition (phagotrophic uptake of food particles and photosynthesis) observed mainly in Oligotrichs, seems to be obligate for at least some species. A member of a different order, the cosmopolitan *Mesodinium rubrum*, even has to be regarded as true phytoplankton organism, since it has apparently lost its cytostome and thus its ability to take up any particles. Its metabolic demands are covered by the photosynthetic poducts of an endosymbiotic alga, which is provided with nutrients and probably carbon dioxide from the ciliate. In mass accumulations this ciliate may cause non-toxic red tides and extremely high primary production rates.

In the Mediterranean Sea ciliates with chloroplasts (plastidic ciliates) were only studied in the coastal area of the Gulf of Lyon, where they accounted for approximately 40 % of all species occuring in the area. The investigations performed focussed on the determination of the total ciliate abundances and fractions of plastidic ciliates in different depths of open ocean waters. These data supplement those obtained previously during summer (METEOR cruise 25/2). Together with data on the species distribution, biomass and production of ciliates they will help to understand the importance of planktonic ciliates in the Mediterranean Sea.

On 14 stations in the western and eastern Mediterranean 5 to 7 water samples from the upper 200 m were inspected for total ciliate abundance and the fraction of plastidic specimens using epifluorescence microscopy. 125 to 250 ml of water were fixed with formalin (2 % final concentration), filtered onto 0.6 mm Nuclepore black filters and the organisms finally stained with fluorochrome DAPI (diamidino-phenylindole), which enables detection of ciliate outlines when used in high concentrations (2 mg/ml). Whole filters were counted using the DAPI-fluorescence caused by UV-excitation. Presence or absence of bright chlorophyll autofluorescence (switching to blue light excitation) of the ciliates was used to decide between

mixo- or heterotrophy. *Mesodinium rubrum* could be identified by its characteristic orange autofluorescence.

Additional samples were fixed for later laboratory analysis of ciliates species composition and biomass. Production rates of planktonic ciliates will also be estimated from samples fixed at the end of 24 h incubations of prescreened (200 mm) surface waters performed on board in a running seawater bath.

Preliminary results derived from epifluorescence microscopy show that the ciliate densities were highest in the Western Mediterranean, reaching values of up to 5000 cells/l in 20 m (station 2), whereas in the eastern Mediterranean total abundance usually did not exceed 1000 cells/ l. However, at two stations at the periphery and center of the Rhodes gyre cell densities in the upper 150 m were much higher, reaching up to 2400 cells/l, corresponding to $2.5x10^8$ cells/m^2 (Figure 20). At these stations the autotrophic *Mesodinium rubrum* also showed highest densities of up to 880 cells/l, at most other stations it was rarely observed in the samples (mostly < 100 cells/l). The ciliate communities were dominated by mixo-heterotrophic Oligotrichs. Haptorids, which could not always be clearly separated from heterotrophic Oligotrichs, apparently were more abundant than Tintinnids. Plastidic ciliates (*M. rubrum* and mixotrophic Oligotrichs) accounted for 20 % (average value for the upper 150 m) of total communities, their fractions generally decreased with depth. Total cell densities were comparable to summer values but did not show the pronounced deep maxima observed in summer.

It is concluded that plastidic ciliates may play an important role in terms of total ciliate biomass during the whole year. This is in contrast to temperate or higher latitudes, where seasonal variations of their relative abundances seem to be more pronounced.

Abbreviations:
M. Rubrum (autotr.): *Mesodinium rubrum* (autotrophic)
Oligotr. (mix.): mixotrophic Oligotrichs
misc. heterotr. cil.: miscellaneous heterotrophic ciliates

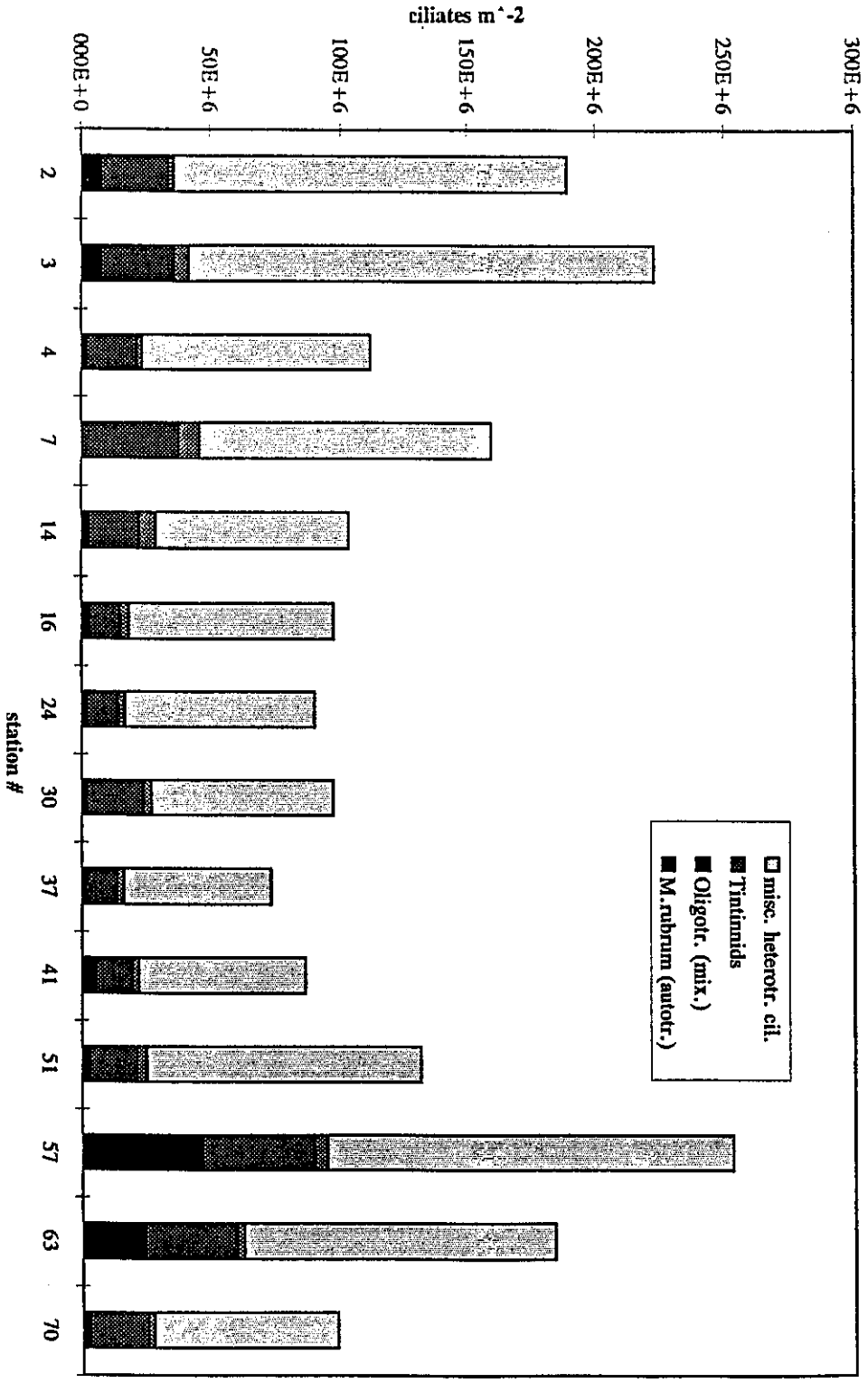

Fig. 20: Integrated (0-150 m) ciliate cell densities at different stations in the western (station 2 to 4) and eastern (others, incl. Adriatic) Mediterranean Sea.

5.1.6 Research of Marine Species in Ballast Water

(M. Dammer)

The Umweltbundesamt (environmental agency) at Berlin, has initiated a research project entitled 'Invasions of non-indigenous marine species into the North and Baltic Sea via ship's ballast water: investigations on the ecological threat'. For this project numerous ballast water samples have been taken from commercial ships entering the ports of Hamburg, Bremen and Bremerhaven. The samples were subjected to microscopical analysis to search for non-indigenous species.

During the cruise ballast water samples were obtained periodically between Brindisi and Port Said. The samples were taken with a hand pump and a hose through the sounding-pipe of the double-bottom tank 3. The tank was sampled daily, while during the first four days even 12-hour intervals have been used. Measurements of temperature, pH, oxygen, dissolved carbon and alkalinity have been performed on the samples. For each sample 30 liters have been filtered through a 10 micron plankton-net and the samples were preserved for biological analysis in Kiel and Hamburg.

This sampling will give information about the changes in the biological, chemical and physical environment in the ballast water tank while the ship was at sea, and about the time period over which potential invaders can survive.

5.1.7 p-Limitation Study of the Eastern Mediterranean

(T. Zohary and R.D. Robarts)

Biotic processes: Response of the microbial community to available P

In most of the world's oceans the planktonic microbial (bacteria and algae) populations were traditionally considered to be limited by the availability of nitrogen. More recently, it was demonstrated that in some of the nitrogen-rich, biomass-poor oceans, such as the Equatorial Pacific, algal production may be limited by iron. There is evidence that phosphorus may be as deficient as nitrogen in some oligotrophic central gyres, particularly in the Sargasso Sea (AMMERMAN et al., 1993). Recently, KROM et al. (1991) suggested that phosphorus is likely the limiting nutrient to planktonic microbial production in the Levantine Basin. This hypothesis was based on unusual nitrate to phosphate (N:P) molar ratios in the deep water and has not been experimentally tested.

The main objective of this study was to examine the hypothesis that phosphorus is the primary nutrient limiting algal and bacterial growth in the Eastern Mediterranean and to examine the spatial variability in the extent of P-limitation. We used a suite of complementary measurements, all related to the dynamics of phosphorus in the water, in order to arrive at conclusions regarding P-limitation. These included:

1. Ambient nutrient concentrations (N, P, Si)
2. Bacterial numbers and activity (thymidine incorporation into macromolecules)
3. Chlorophyll-a concentrations
4. Alkaline phosphatase activity (enzymatic activity for the conversion of organic phosphorus to inorganic phosphorus) - a strategy by algae and bacteria to gain phosphorus when inorganic P is in limiting concentrations.
5. ^{32}P turnover time - a measure of the rate at which inorganic phosphorus is removed from the water by the microbial community - as phosphorus becomes more plentiful the turnover time becomes longer.
6. Size fractionation of ^{32}P uptake - to determine the dominant group of organisms responsible for phosphorus cycling
7. Determination of the concentration of biologically available phosphorus - available phosphorus was calculated using ^{32}P uptake and Michaelis Menten enzymatic equations.
8. Nutrient enrichment bioassays - microcosms were set up and combinations of nitrogen, phosphorus, iron and EDTA were added - over a three day period changes in bacterial activity and numbers and chlorophyll-a were measured. These microcosms studies indicated the potential limiting nutrient to microbial growth.

The above analyses were done at selected stations and depths (usually the depth of maximum chlorophyll fluorescence in the water column) in the Ionian and Aegean Seas and the Levantine Basin. Data analysis is not complete yet, but preliminary indications are that phosphorus limitation of the planktonic microbial populations in the Eastern Mediterranean is widespread. However, we also found areas where phosphorus was abundant, such as near the core of the Rhodes Gyre and in the Aegean Sea (Figure 21, 22).

Abiotic processes: The effect of dust on phosphorus dynamics in the Levantine Basin

Several studies have shown that substantial quantities of dust are blown across the Mediterranean, particularly the central and eastern basins (GUERZONI et al. 1989). Dust from the Sahara Desert contains a high proportion of Fe oxides and poorly crystalline clay minerals both of which have a high affinity for PO_4^{-3}. KROM et al. (1991) suggested that this dust removes orthophosphate as it falls through the water column, particularly from the deeper layers where there is no competition by the biota and the PO_4^{-3} content is relatively high.

The objective was to test Krom et al.'s hypothesis empirically that Saharan Desert dust has a significant impact on phosphorus dynamics in the Levantine Basin of the Eastern Mediterranean. Water from the surface mixed layer and from beneath the nutricline were placed in a series of bottles to which measured amounts of fresh, aged or no dust were added. Phosphorus dynamics were measured over 16 hours using ^{32}P. Parallel experiments were carried out using particle-free seawater, whole seawater and water in which the biota was poisoned. Preliminary analysis of the data supports Krom et al.'s hypothesis.

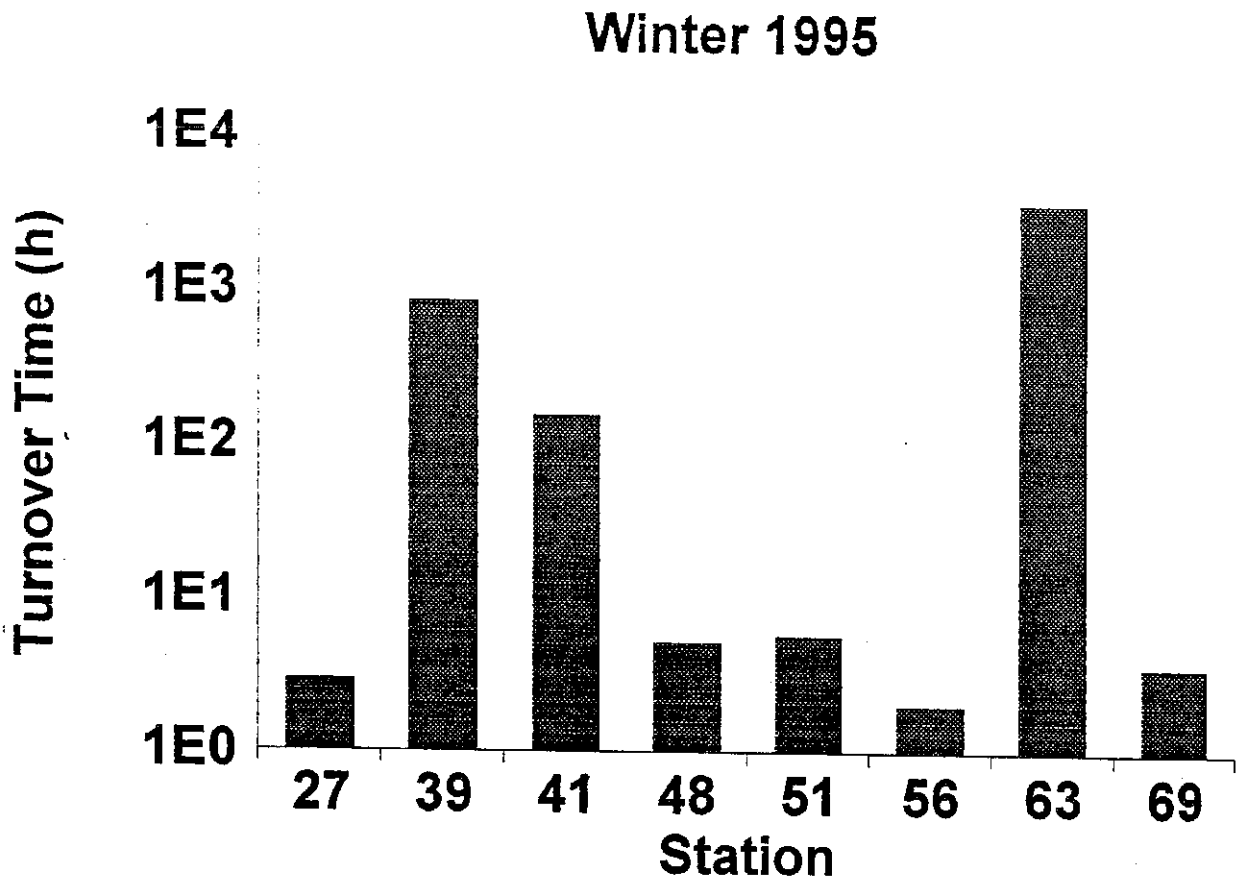

Fig. 21: Range of phosphorus turnover times by the plankton (algae and bacteria) in the eastern Mediterranean as measured by the rate of ^{32}P incorporation. Turnover times ranged from 3711 hours at station 63 in the Rhodes gyre core to 2 hours at station 56 in the Levantine Basin. Phosphorus turnover times of approximately <10 hours indicate that the plankton was P-deficient; longer turnover times suggest P-sufficiency.

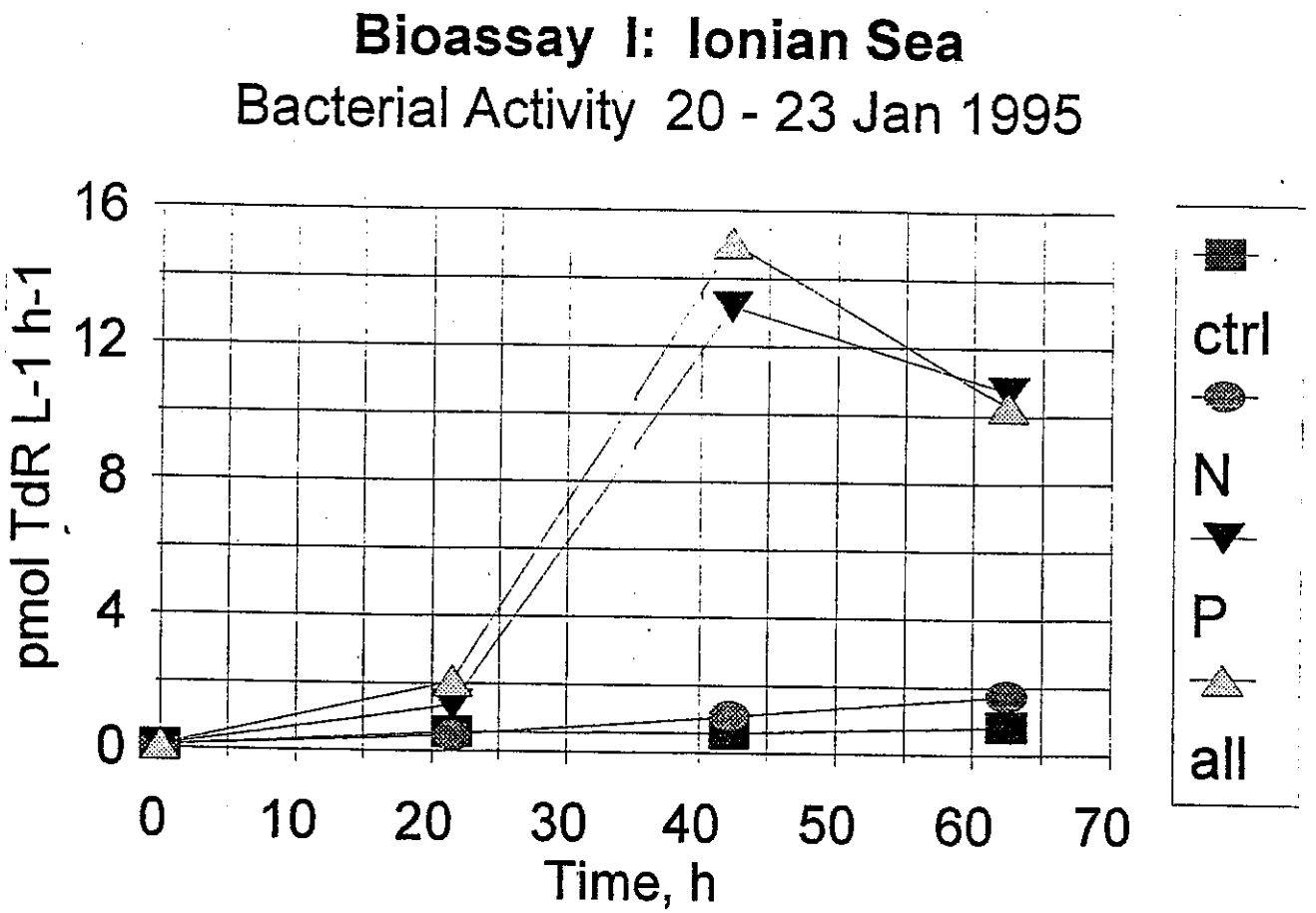

Fig. 22: An example of results from a nutrient enrichment bioassay conducted during the METEOR cruise. Twelve 2-litre bottles were filled with water from 50 m depth at station 27. Nutrients were added in four treatments: no nutrient addition (ctrl); addition of ammonia nitrogen, Fe and EDTA (N); addition of orthophosphate (P); and the addition of all the above (all). N:P were added at the molar ratios characteristic of the Levantine Basin deep water (20:1). Each point indicates the mean of three replicate treatments. The figure shows that the addition of phosphorus alone, or in combination with other nutrients, significantly stimulated bacterial activity as measured by the rate of thymidine incorporation into macromolecules. Phosphorus is indicated as the primary limiting nutrient to bacterial activity, which supports the phosphorus turnover data in Figure 21.

5.1.8 Winter Distributions of Carbon Parameters in the Eastern Mediterranean

(B. Avril, C. Copin-Montégut, D. Ruiz-Pino, F. Vidussi)

The principal goal of LPCM team in the METEOR 31/1 cruise is to obtain some data in the Eastern Mediterranean basin, allowing to state precisely the carbon budget in the Mediterranean Sea. In spite of the numerous studies dealing with the carbon cycle in the global ocean, the carbon budget in the eastern Mediterranean Sea has never been precisely assessed. This is probably due to the paucity of the reliable carbon data for the Mediterranean waters. In the Eastern Basin, the sole reliable values for alkalinity have been obtained at station GEOSECS 404 and the data on the organic carbon distributions are also very scarce. The multidisciplinary cruise is a great opportunity for us to understand the biogeochemical carbon cycle at the basin scale, simultaneously to the study of water masses, and especially deep water formation, supported by the POEM program. Therefore we should be able to document the numerous sources and sinks of the marine carbon cycle during this crucial period of the Mediterranean hydrology. To try to constraint the spatial variability of carbon during the wintertime, differents measurements were performed during the METEOR 31/1 cruise (see Table 5). The combination of the mentioned biogeochemical parameters with the hydrodynamical (CTD and ADCP) and the other biological data (nutrients, oxygen, metabolism activities, and standings stocks) will allow to more completely study the carbon cycle in the eastern basin.

Tab. 5: Parameters measured by the LPCM

Parameters	Sampling	Measured	Methods
Alkalinity	shallow and deep rosettes	on board	Potentiometric
pH	shallow and deep rosettes	on board	pHmeter
TCO_2	shallow and deep rosettes	on board	calculated*
DOC	shallow and deep rosettes	at the laboratory	HTCO**
Pigments	shallow rosette	at the laboratory	HPLC***
Cells size and abundance	shallow rosette	at the laboratory	Flux cytometry

* From Alkalinity and pH, using the salinities values provides by CTD data
** High Temperature Catalytic Oxidation
*** High Performance Liquid Chromatography

I. INORGANIC CARBON

CO_2 System in the Water Column

The four main processes that determine the CO_2 content in the water column are: gas exchange at the air-sea interface, vertical mixing and advection, biological activity of marine

organisms and chemistry of carbonate system. In order to evaluate the relative importance of these processes, during the METEOR 31/1 cruise, numerous measurements of pH and alkalinity were performed. The concentration of inorganic carbon (TCO_2) shall be deduced from these measurements.

Methods

The samples for pH and alkalinity measurements were collected throughout the water column using the bottles attached to a rosette (shallow and deep). The numbers of samples taken in each station are indicated in Table 6. About 1000 samples were analysed on board and about 200 will be analysed in the laboratory. The pH measurements were carried out with a combined glass electrode (Ross electrode, Orion 8102) and a Radiometer PHM 93 pHmeter. The analytical method for the alkalinity determination used during the cruise was for the first time proposed by PEREZ and FRAGA (1987) and then improved by COPIN-MONTÉGUT (1993). The standard deviation for a sample is about 0.003 units for the pH at 25° C and 1.5 µmol/kg for the alkalinity.

Tab. 6: Sampling for Alkalinity, and pH
Stations analysed on board: 1, 2, 3, 4, from 20-77 with following exceptions
Stations to be analysed at the laboratory: 5, 7, 8, 11, 14, 15, 16, 17,18
Stations not sampled: 6, 9, 10, 12, 13, 19, 22, 26, 33, 34, 75.

Data examples

The data presented are not definitive. They have to be corrected for pH shifts during the measurements.

The Figure 23 represents the provisional relationship obtained between alkalinity in µmol/kg and salinity measured in the Eastern Basin during the cruise. The regression line corresponds to the relationship between alkalinity and salinity in the Alboran Sea after COPIN-MONTÉGUT (1993). It can be observed a good agreement between the METEOR 31/1 data and the regression line obtained for the Western Basin (taking into account the 95 % confidence level). The specific alkalinity of Eastern Mediterranean waters is therefore higher than that of less saline Atlantic water.

The Figure 24 compares the profiles at Station 1 (Atlantic station, Figure 24a) to the profiles at the station 64 (Levantin Basin, Figure 24b).

Alkalinity profiles are correlated to the salinity profiles at both stations. The samples from the euphotic layer have lower TCO_2 content. This reflects the consumption of inorganic carbon by photosynthesis. The TCO_2 pattern is similar to that of nutrients and the pH

pattern to that of oxygen. As for Alkalinity, the TCO_2 values are higher in the Eastern Mediterranean than in the Atlantic one.

pCO_2 at the Sea Surface

The sea seawater pumped ahead of the ship (depth about 3 m) was directed continuously to a Turner Design fluorometer (model TD-10, continuous flow cell, blue lamp) for chlorophyll fluorescence measurements and to a home-made equilibration cell for the pCO_2 measurements (COPIN-MONTÉGUT, 1985). The partial pressure of CO_2 in an air sample equilibrated with the surface sea water was determined using a Licor gas analyser (model LI-6252). The signals of the various apparatus were recorded each minute.

During the METEOR 31/1 cruise (December 1994 - February 1995) these measurements were performed from time to time during the transit via Atlantic ocean and western Mediterranean sea, and quasi-permanently during the transit and stations in the eastern Mediterranean sea (a rough sea state prevents generally the measurement, as before Brindisi). The temporal diagram of the preliminary data is enclosed (Figure 25). Several corrections, including calibrations, are to be processed. The data set collected by the ship sensors, pre-processed and kindly provided by Brigit Klein will be very useful for these calibrations.

The preliminary results examination allows to think that this unique database is of good quality as the measurement process was quasi-optimal. This database is of great interest because of its high spatial resolution (about 0,33 km) and because only few data already exist.

The mesoscale view allows to focuse on frontal structures and gyres, and to determine the local marine sources of pCO_2 in the area, which appears to be generally a sink (as atmospheric pCO_2 is about 360 ppmv).

The diagram temperature - pCO_2 (not corrected for the difference between the measurement temperature and the in situ temperature) for the whole cruise exhibits the existence of various water masses with differents characteristics that will be considered after the hydrological data.

II. ORGANIC CARBON

The Particulate Organic Carbon and the Phytoplankton Biomass

Phytoplankton is the first level of the marine food web. Its main roles are via photosynthesis in the CO_2 fixation and the synthesis of organic carbon. The distribution and dynamics of the phytoplankton populations are thus to be investigated.

Samples were collected along vertical profiles for the investigation of phytoplankton biomass. For this goal different approachs will be used:
- Pigments analysis by HPLC (High Performance Liquid Chromatography)
- Flux Cytometry analysis of the size distribution and abundance of cells
- Particulate organic carbon and particulate organic nitrogen (POC and PON) analysis

Sampling Strategy for all Methods

At the stations, samples were collected from the rosette bottles at 12 differents depths of the surface layer (shallow rosette 0-200 m). Depths were chosen according to the features of chlorophyll fluorometry, temperature and salinity. The stations sampled are listed in Table 7.

Tab. 7:

	Pigments	POC and PON	Flux cytometry
Station Number	1-5, 7-11, 14-25, 27-63, 65-77	1-5, 7-11, 14-16, 19-25, 27, 28, 31, 33, 34, 36, 38, 40, 41, 43-45, 47, 49-52, 54, 57, 58, 61-63, 65, 68, 69, 71, 73, 74, 76	1-5, 7-11, 14-17, 19-21, 23-25, 27-34, 36, 38, 40, 41, 43, 44, 47, 49, 50, 51, 54, 55, 57, 58, 61, 62, 65, 69, 71, 73, 74, 76

Pigment analysis by HPLC

This method of phytoplankton analysis is based on the measurement of taxon-specific chlorophylls and carotenoids of the differents algal groups (Prochlorophytes, Cyanobacteria, Diatoms, Prymnesiophyceae, Chrysophyceae, Dinoflagellates and Chlorophyceae). This method permits to measure the concentration of particulate chlorophyll-a, index of phytoplankton biomass. The pigments signature reflets the gross taxonomic composition of natural algal population. The evaluation of the composition of the phytoplanktonic communities is essential to understand the dynamics of phytoplankton standing stocks and primary production.

Sampling Procedure

2 liters of sample were filtered throught 25-mm GF/F glass fiber filter and immediatly stored in liquid nitrogen.

Flux Cytometry Analysis

With this analysis it is possible to obtain measurements of cells abundance of differents planktonics groups with emphasis on the ultraphytoplankton.

Sampling Procedure

4.5 ml of sample were preserved with 0.5 ml of paraformaldehyde and stored in liquid nitrogen.

Total Biomass CHN Analysis

The CHN measures the carbon and nitrogen content of the particulate organic matter, that is composed by the living organisms and the detrital metabolic material.

Sampling Procedure

2 liters of sample were filtered throught 25-mm GF/F glass fiber filter immediatly dried at 40° C.

THE DISSOLVED ORGANIC CARBON

The DOC is the main organic form of carbon in the ocean and largely participate to the biological and geochemical cycle of carbon, as a metabolic exudation and assimilation product and as a main potential vector of export of carbon from surface photic zone to deep layers, i.e. as a sink vector of carbon.

The samples were collected within the shallow and/or deep rosettes of stations number: 5, 7, 8, 11, 16, 18, 25, 30, 35, 38, 48, 63 and 76. The samples were immediately poisoned with saturated mercuric chloride solution, and conserved until the end of the cruise in a cool (+4° C) and dark place. These preservation procedures are proven to be efficient againts the biological, thermal and photochemical degradations of samples. The further transportation will unfortunately not fulfill these preservation needs.

The measurement will be performed in the laboratory using a Shimadzu TOC-5000 analyser. The methodology used there (HTCO) is now widely recognized and recommended, for instance, by JGOFS program.

The DOC measurements will allow us the calculation of the vertical and horizontal fluxes, the determination of the more productive areas and of the exact role of DOC in the carbon cycle of the Mediterranean Sea, according to global change approaches.

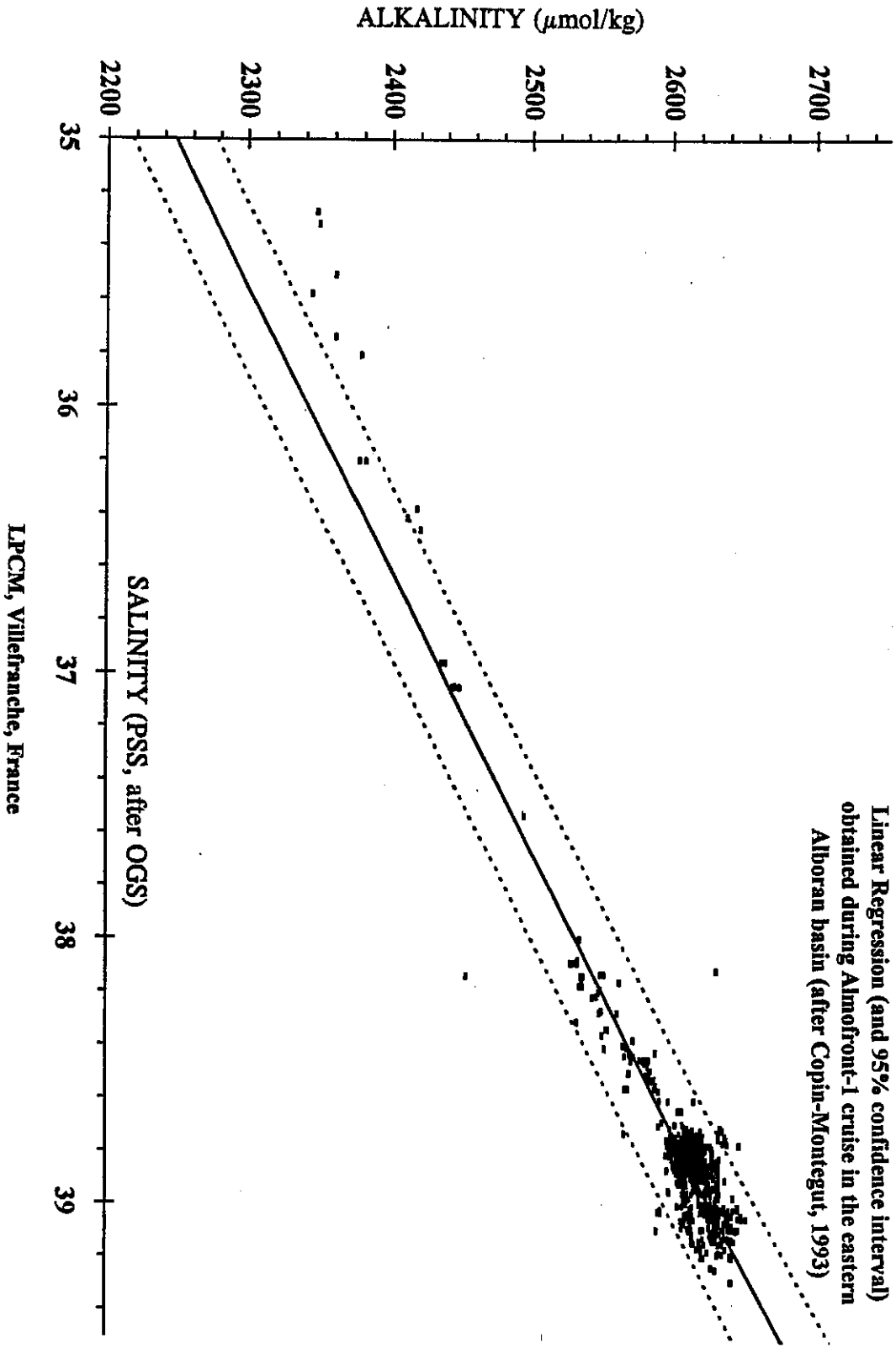

Fig. 23: Relationship between alkalinity and salinity as observed during M31/1. The regression line (heavy black line) has been derived by COPIN-MONTÉGUT, 1993 from data in the Alboran Sea.

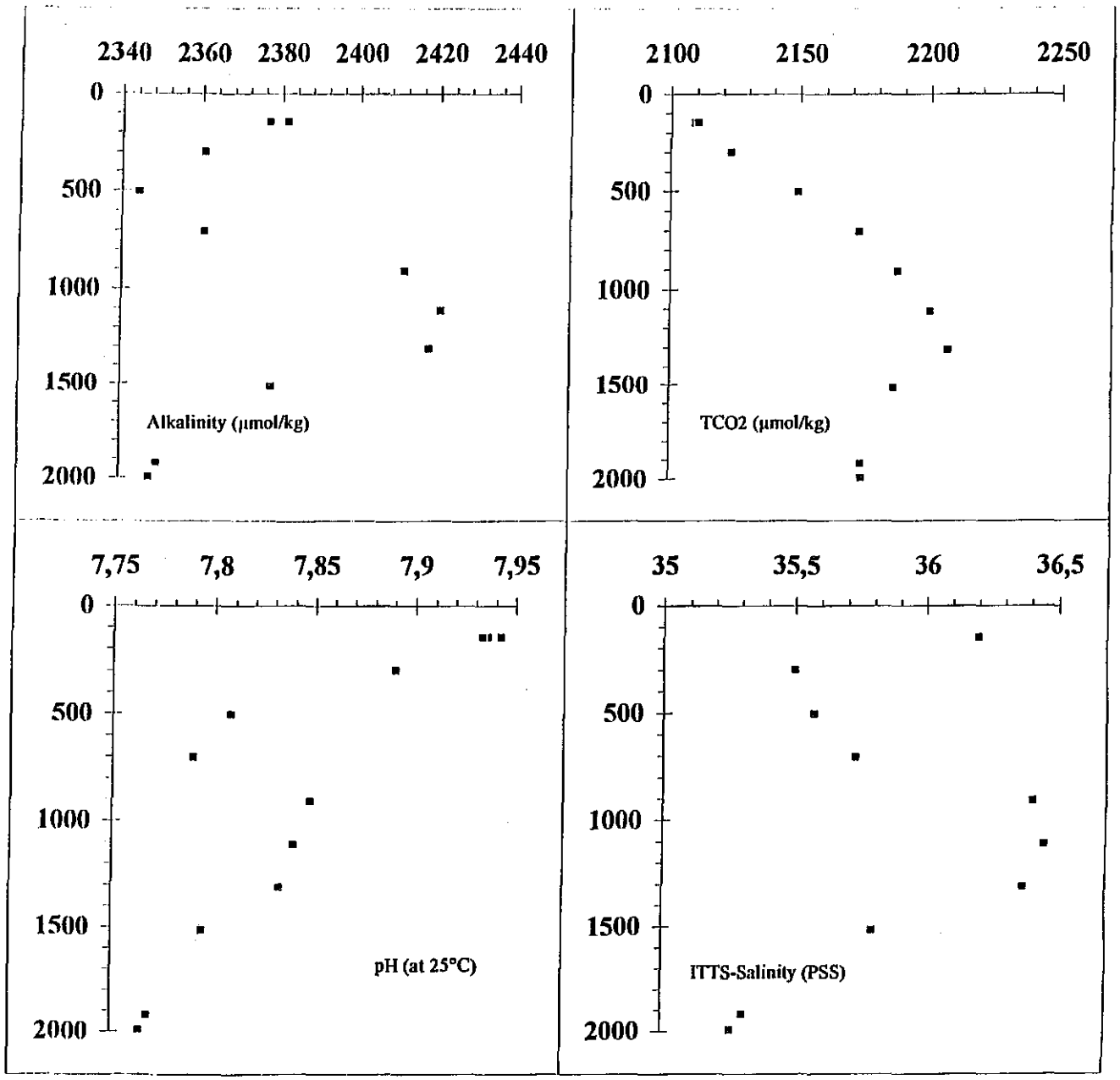

METEOR31_STATION01

Depth (m)	Alkalinity (µmol/kg)	TCO2 (µmol/kg)	pH at 25°C	Salinity (PSS)
150	2381,5	2109,3	7,9426	36,193
150	2377	2108,9	7,936	36,193
150	2376,8	2110,1	7,9334	36,193
300	2360,7	2123,2	7,8902	35,5
505	2344,2	2149	7,8075	35,571
707	2360,7	2172,4	7,7894	35,729
910	2411,3	2187,1	7,8481	36,405
1113	2420,6	2200	7,8396	36,45
1313	2417,7	2206,8	7,8328	36,371
1517	2378	2186	7,7945	35,798
1922	2349,3	2173,6	7,7681	35,311
1996	2347,6	2174,1	7,7641	35,265

Fig. 24: Vertical profiles of alkalinity (µmol/kg), TCO2 (µmol/kg), pH and salinity for station 1 (Figure 24a) and station 64 (Figure 24b).

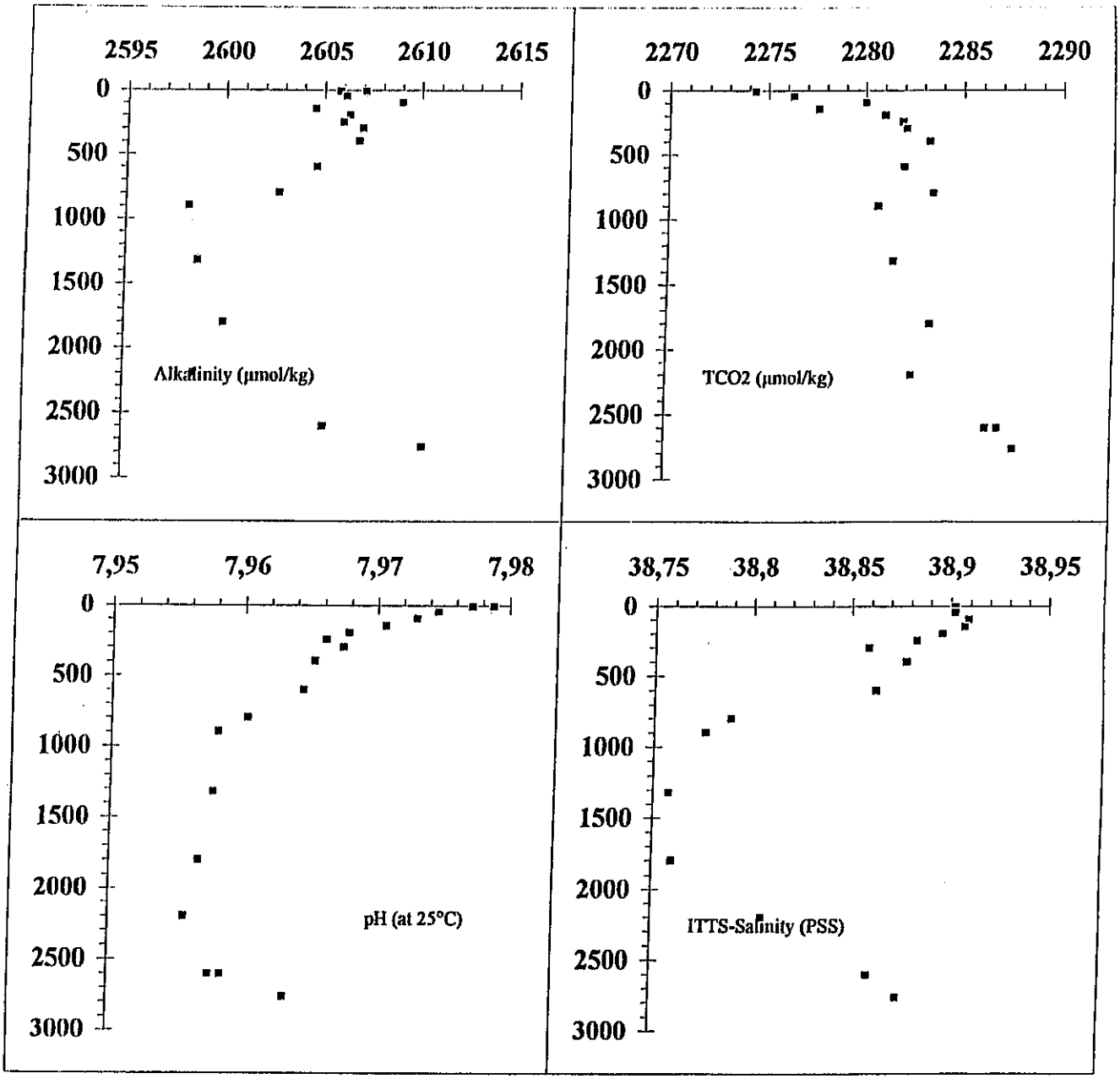

METEOR31_STATION64

Depth (m)	Alkalinity (µmol/kg)	TCO2 (µmol/kg)	pH at 25°C	Salinity (PSS)
10	2607,1	2274,4	7,9788	38,902
10	2605,8	2274,3	7,9772	38,902
50	2606,1	2276,3	7,9746	38,902
100	2609	2280	7,973	38,909
150	2604,6	2277,6	7,9706	38,907
200	2606,3	2281	7,9678	38,896
251	2606	2281,9	7,9661	38,883
301	2607	2282,1	7,9674	38,859
401	2606,8	2283,3	7,9653	38,878
601	2604,7	2282	7,9645	38,863
801	2602,8	2283,5	7,9603	38,789
901	2598,2	2280,7	7,9581	38,776
1322	2598,7	2281,5	7,9578	38,758
1803	2600,1	2283,4	7,9568	38,76
2203	2598,6	2282,5	7,9557	38,807
2604	2605,3	2286,3	7,9586	38,861
2604	2605,3	2286,9	7,9577	38,861
2765	2610,4	2287,7	7,9634	38,876

Fig. 24b:

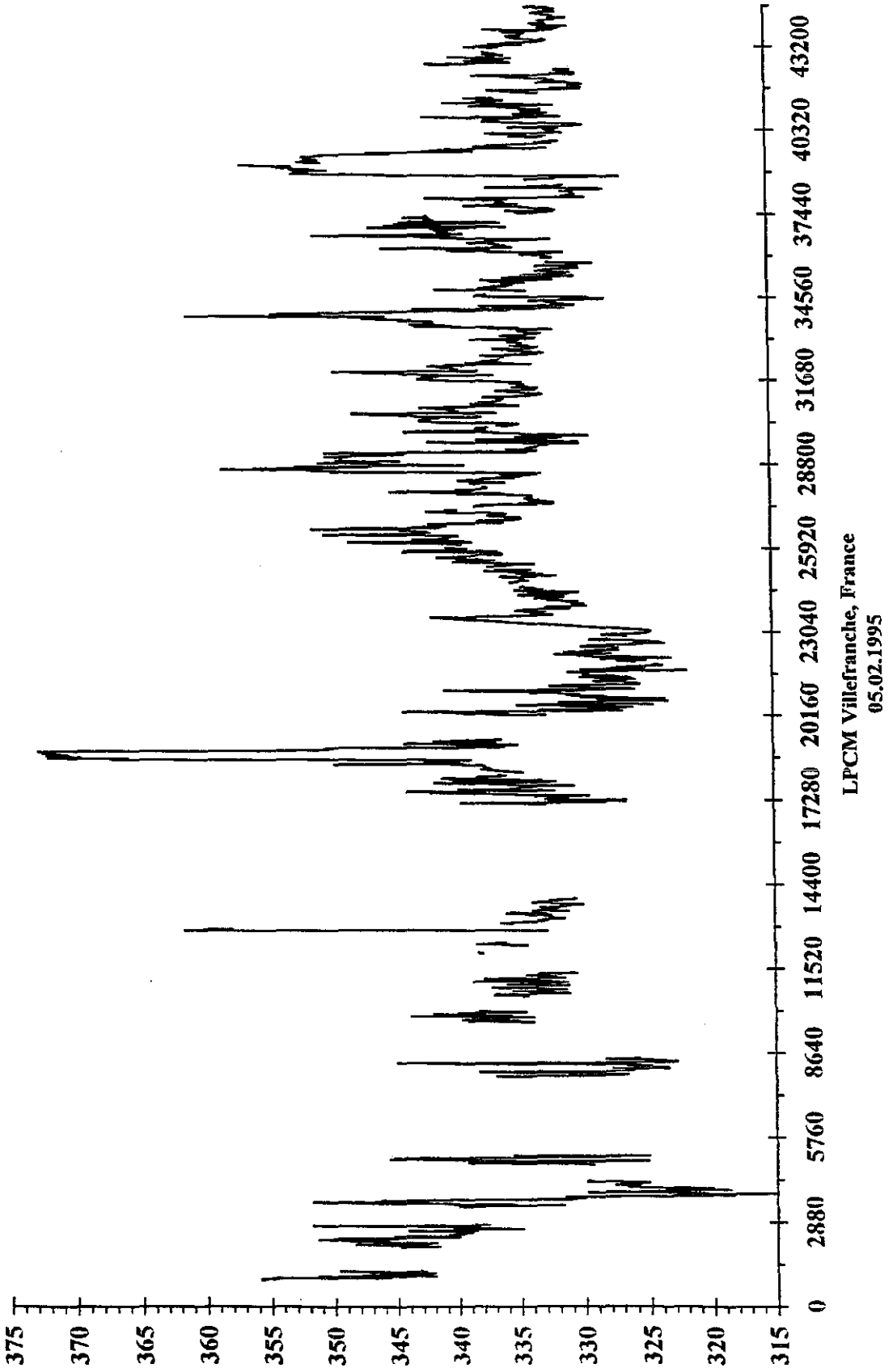

Fig. 25: Continuos recording of surface pCO2 during M31/1. Time is given in minutes since start of the cruise on the x-axis.

5.1.9 ADCP Measurements

(P. Drakopoulos)

Data acquision:

ADCP current data were continously collected during the cruise. For the first time, an Ashtech three dimensional direction finding system was employed, in order to acquire the most accurate navigation data possible. However, due to a malfunctioning of the Ashtech unit, actual recording of high-quality navigation data only started on January 18, 1995 at 13:00 UTC in the northwest Ionian Sea, after a replacement of the receiver had been received and calibrated along deck-side at Brindisi.

The following configuration was used during collection: The sampling interval amounted to 300s. This corresponds to a spatial resolution of 1.8 km at an average cruising speed of 12 knots. The depth resolution was 8 m with a range of 480 m. The ship's gyro compass was used for compensation of the ship's pitch, roll and heading.

Quality control:

In order to assess the quality of the navigational data, bottom tracking was enabled while cruising at low speed (~ 2-3 knots) over the shallow northeast end of Karpathos Strait. This procedure was carried out three times in both directions (Figure 26). A preliminary analysis of the results of this experiment indicated a bias of the gyro compass heading with respect to that obtained by the GPS system by about 0.5°. However, the scattering of the GPS data was found to be larger (standard deviation 15 cm/s). The flow structure in the strait (Figure 27) was found to be in good agreement with that indicated by the XBTs.

Further quality control and processing of the ADCP data (i.e. filtering of the short term variability and of possible tidal currents present in the straits) will be performed in cooperation with the University of Kiel.

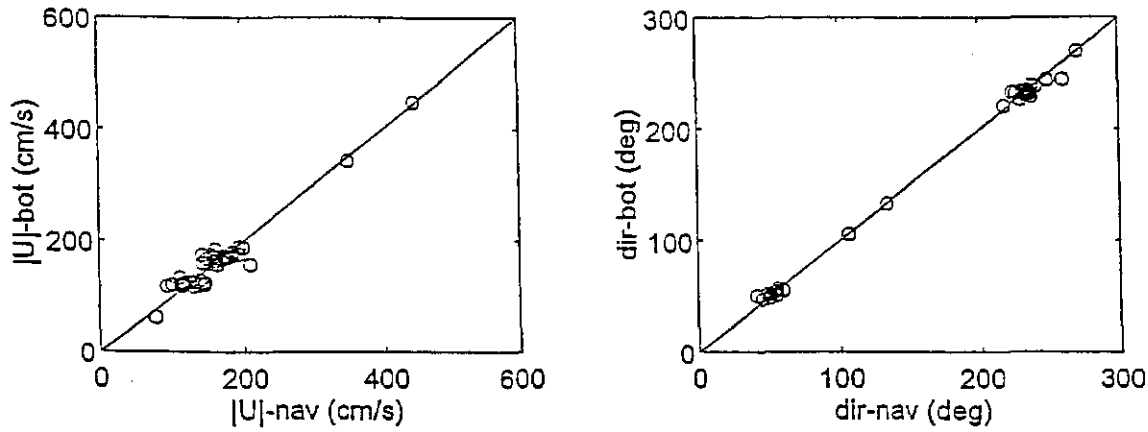

Fig. 26: Quality control of navigational data in the Karpathos Strait.

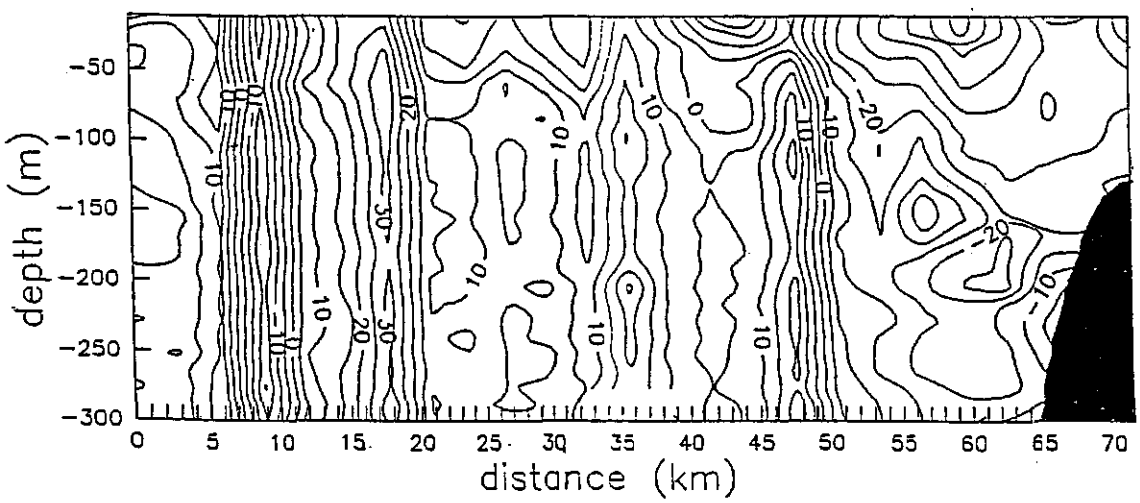

Fig. 27: Vertical section of velocity (cm/s) in Karpathos Strait.

5.1.10 Investigation of Phytoplankton Abundance

(A. Yilmaz)

The main purpose of this study was to investigate the phytoplankton abundancy in the upper pelagic waters of the Eastern Mediterranean. The deep chlorophyll-a (DCM) formation, maintainance, and spatial distribution is of special interest. Thus sea water samples were collected down to 200 m depth at selected stations (Table 8). Sampling depths were chosen according to in situ fluorometer output (Rosette, 0-200 m shallow cast). The sea water samples from each depth (ca. 2 L) were filtered on Whatman GF/F filter paper and kept frozen (-20° C). The analysis of chlorophyll-a and phaeopigments will be performed in the Institute's laboratories in Erdemli, using STRICKLAND and PARSONS (1972) fluorometric method. Sigma chlorophyll-a standard will be used for calibration purposes.

There is little data on the particulate organic matter (POM) concentration as an indicator of phytoplankton biomass in the Eastern Mediterranean. Further investigation is needed on how the ratios of C:N, C:P and N:P in POM deviate from normal Redfield ratios according to nutrient availability during winter mixing in the basin. For this purpose, sea water samples were collected from selected stations (Table 8) and sampling depths were arranged according to in-situ-fluorescence profiles. Approximatey 10 liters of sample was filtered through pre-combusted Whatman GF/F filter paper and the filters kept frozen (-20° C). The analysis of Particulate Organic Carbon (POC), Particulate Organic Nitrogen (PON) and Particulate Phosphorus (PP) will be performed in the Institute's laboratories. Prior to analysis filters for POC and PON are dried at low temperature (ca. 50° C), exposed to HCl fumes and then dried again. 20-25 mg of subsample are placed in a pre-cleaned tin capsules and combusted in Carlo Erba model CHN analyzer. Filters for PP analysis are combusted at 450-500° C for 3 hours and then extracted with 0.5 N of hot HCl (KARL et al., 1990). After adjusting the pH to 8 and the final volume to 20 mL, the concentration of phosphorus oxidized to inorganic form is determined colorimetrically.

Water samples for the Total Organic Carbon (TOC) analysis were collected only from four stations (Table 8) dealing with both the shallow and deep casts. 50 ml glass bottles were filled, 0.05 mL of 6N HCl was added for preservation, and the bottles were kept at +4° C (in the fridge). The analysis of TOC samples will be performed at Erdemli using a TOC-Analyzer.

Tab. 8: Stations occupied for the analysis of Chlorophyll-a (Chl-a), POC, PON, PP and TOC. * Intercomparison Station

Location	Station no.	Coordinates	Chl-a	POC,PON,PP	TOC
Ionian Sea	24	37° 25' N, 20° 45'E	yes	yes	no
Ionian Sea	27	35° 40'N, 19° 39'E	yes	yes	no
South of Crete	48	33° 28'N, 25° 43'E	yes	yes	yes
Southeast of Crete	54	34° 00'N, 28° 00'E	yes	no	no
Southeast of Crete	55	33° 12'N, 28° 24'E	yes	yes	yes
Rhodes Region	58	35° 36'N, 29° 20'E	yes	yes	no
Rhodes Region	63	35° 00'N, 28° 24'E	yes	yes	yes
Antalya Bay	66	36° 06'N, 31° 00'N	yes	yes	no
Southwest of Cyprus	69	34° 24'N, 31° 24'E	yes	yes	no
Southwest of Cyprus	73*	34° 25'N, 32° 12'E	yes	yes	yes

INTERCOMPARISON EXERCISE

IMS/METU organized an intercomparison exercise on some biochemical parameters during the cruise, largely in connection with LIWEX-95 0f POEM-BC. This exercise was performed at Station 73 near Cyprus (34°25' N/32°12' E) on February 2, 1995. The participating Institutes and the corresponding parameters are listed in Table 9. The details on the sampling procedure, preservation and transportation are enclosed in Table 9.

Tab. 9: Summary of intercomparison exercise on selected biogeochemical parameters, METEOR M31/1, January-February 1995, Eastern Mediterranean

Participating Institutions	Parameter
National Centre of Marine Research, Athens, Greece	Nutrients, Chloropyll-a
Istituto Sperimentale Tallasografico, Trieste, Italy	Nutrients
Institute of Marine Sciences Middle East Technical University, Erdemli, Turkey	Nutrients, Chloropyll-a, TOC, POC, (PON,PP)
Israel Oceanographic and Limnological Research Ltd, Tiberias, Israel	Chloropyll-a
Instituto di Biologia del Mare, Venezia, Italy	Nutrients, TOC
Stazione Zoologica 'A. Dohrn', Napoli, Italy	Chloropyll-a
Israel Oceanographic and Limnological Ltd, Haifa, Israel	Nutrients
Laboratoire de Physique et Chimie Marines, Villefranche sur Mer, France	Chloropyll-a, TOC, POC, (PON, PP)

Sampling, preservation and transportation has been handled as follows:

Nutrients:

- Sea water samples for nutrient analysis (Nitrate, nitrite, phosphate and silicate) were taken from various depths and were frozen (-20° C) immediately after collection.
- 25-30 mL HDPE bottles were used for sampling and these bottles were pre-cleaned with 10 % HCl, rinsed with distelled water and finally rinsed with the sampled sea water twice.
- The bottles should have been transported in dry ice.
- The time interval between sampling and analysis should not have exceeded 2 months.

Total chlorophyll-a:

- Sea water samples were collected from 5 m, 30 m, 50 m (fluorescence maximum) and 75 m and were filtered through GF/F filter papers and then immediately frozen (- 20° C).
- The filter papers should have been transported in dry ice.
- The time interval between sampling and analysis should not have exceeded 2 months.

POC:

- Sea water samples (ca.2-10 liters) were collected from 5 m, 30 m, 50 m (fluorescence maximum) and 75 m and were filtered through pre-combusted GF/F filter papers and then immediately frozen (- 20° C).
- The filter papers should have been transported in dry ice.
- The time interval between sampling and analysis should not have exceeded 2 months.

TOC:

- Sea water samples (50-100 mL) were collected from 50 m (fluorescence maximum) and 1000 m . Parallel sampling was done and samples were preserved using 6N HCl (0.05 mL/50 mL sample or saturated $HgCl_2$. Samples were kept cool (+4° C) until transportation.
- Samples should have been transported as cool as possible.
- The time interval between sampling and analysis should not have exceeded 2 months.

5.1.11 Geological Work

(D. Meischner, D. Fleitmann, T. Bukowski, J. Meyer)

The Adriatic Sea is the source of the East-Mediterranean Deep Water. Salt-enriched (>38 ‰) East Mediterranean Intermediate Water enters the Strait of Otranto. It surfaces and, centred by the Coriolis force, runs all along the Dinaric coast up to the Gulf of Trieste. On the northern

Adriatic shelf the water cools during long, cold winters. It returns as Adriatic Bottom Water along the eastern Italia coast, and leaves the Adriatic along the bottom of the Strait of Otranto.

The Adriatic Bottom Water spreads over vast areas in the eastern Mediterranean (WÜST 1961). Sediments in this region are known for their sapropelites that are deposited during phases of stagnant, anoxic bottom water (KULLENBERG, 1952).

The causes of such anoxic events are still controversial. Obvious coincidence of sapropelites with phases of high monsoon activity (ROSSIGNOL-STRICK, 1985) led to the conclusion that enforced runoff from the African continent via the river Nile and hence increased organic production and stable stratification may be the cause of oxygen depletion in bottom waters. However, VAN STRAATEN (1972) concluded that mild winters would have prevented the formation of cold, dense bottom water on the northern Adriatic shelf so that the Adriatic Bottom Water would no longer have replenished the Eastern Mediterranean Deep Water. MANGINI and SCHLOSSER (1986) calculated that warming of the Adriatic by 0.7° C or a decrease in salinity by 0.2 ‰ would already preclude the formation of Adriatic Deep Water. Anoxic phases in the southern Adriatic deep sea and in the Ionian Sea should then be coupled; the time of their beginning and their duration should be related to known climatic developments.

In order to test this hypothesis, long piston cores (>20 m) had been planned from the centre of the Ionian Sea, the Strait of Otranto, and from the South Adriatic Abyssal Plain. However, when a first core of 11.6 m had been taken on Station M31/1-12 in the Ionian Sea at 3.950 m water depth the wind gusted up to full storm (84 kn max.). Therefore, only one more station was possible in the South Adriatic at 1.139 m depth.

The core from the Ionian Sea (KL 12-1) lines up with a series of cores taken on METEOR cruise M 24 by Jörg Keller, Freiburg, but is only slightly longer than the older gravity cores. KL 12-1 contains a variegated series of hemipelagic clay intercalated with turbidites, volcanic ashes and sapropelites interspersed with ash. The age of the core is still undetermined.

The cores from the station in the South Adriatic have incidentially been taken in a fine-grained mass flow. The structure of the clayey sediment is dominated by densely spaced flow lamination, no primary bedding is preserved.

Tab. 10: Piston core recovery, Mediterranean

Station	Latitude N	Longitude E	Water depth(m)	Core No.	Barrel(m)	Core recovery(m)
12	36° 34,2′	18° 17,9′	3.950	KL 12-1	12	11,60
16	41° 30,2′	18° 17,5′	1.139	KL 16-1	12	11,50
16	41° 30,8′	18° 17,2′	1.139	KL 16-2	24	21,80

5.2 Preliminary Results of Leg M31/2

5.2.1 Physical Oceanography

5.2.1.1 CTD

(F. Wehner)

The hydrographical conditions in the Red Sea

During METEOR leg M31/2 (February 1995) several CTD-profiles were taken down to the bottom at geological and hydrographical stations. In addition, high resolution profiles (upper 300 m) have been measured for phytoplankton studies.

For CTD-measurements an EG&G Mark V-CTD was used, equipped with pressure-, temperature-, conductivity- and oxygen sensors and a backscattering fluorometer integrated in an 12*12 l rosette system of General Oceanic. For calibration of the CTD, reversing thermometers were used, and bottle samples were taken for salinity measurements with an Autosal-Salinometer (leg 31/2).

Temperature and Salinity:
The Red Sea represents a landlocked marine area and can therefore be regarded as a quasi-unperturbed system. Water exchange mainly depends on the relation between in- and outflow through the Strait of Bab el Mandeb, where high-salinity deep water leaves the Red Sea and becomes balanced by incoming (sub-)surface waters of the Gulf of Aden (POISSON et al., 1984; PAPAUD and POISSON, 1986). For selected profiles of the Red Sea, temperature and salinity is presented in Figure 28. At the stations 80-82 (Shaban Deep), 87/91 (Kebrit Deep) and 96 (Atlantis II Deep) the CTD-profiles were cut, because of hot brines. The graphs exhibit for both temperature and salinity a pronounced difference between the northern and the southern part of the Red Sea. The typical situation at the end of the winter is visible in the northern part (station 81 - station 84), south of the Gulf of Suez. Because of evaporation and cooling the water column is almost completely mixed by thermohaline convection (PATZERT, 1972). The vertical temperature and salinity gradients are weak, with differences of less than 2° C in temperature, and less than 0.5 psu for salinity over the total water column. High resolution profiles show that the thermocline reached down to 200 m. After an exponential decrease, the temperature remains nearly constant ($\Delta T \leq 0.02°$ C). Similar observations were made for salinity gradients.

A special situation was found at the stations 80 to 82. Water with a lower temperature but a higher salinity is intruding from the Gulf of Aqaba and stratifies itself into two layers in the upper 300 m. The depth of the first peak marks the pycnocline and the maximum of phytoplankton distribution (see Figure 29).

In the southern part of the Red Sea (Station 87 - Station 102) a stable stratification has been observed, during this intermonsoon season (February - May) (QASIM, 1982). There is a stable

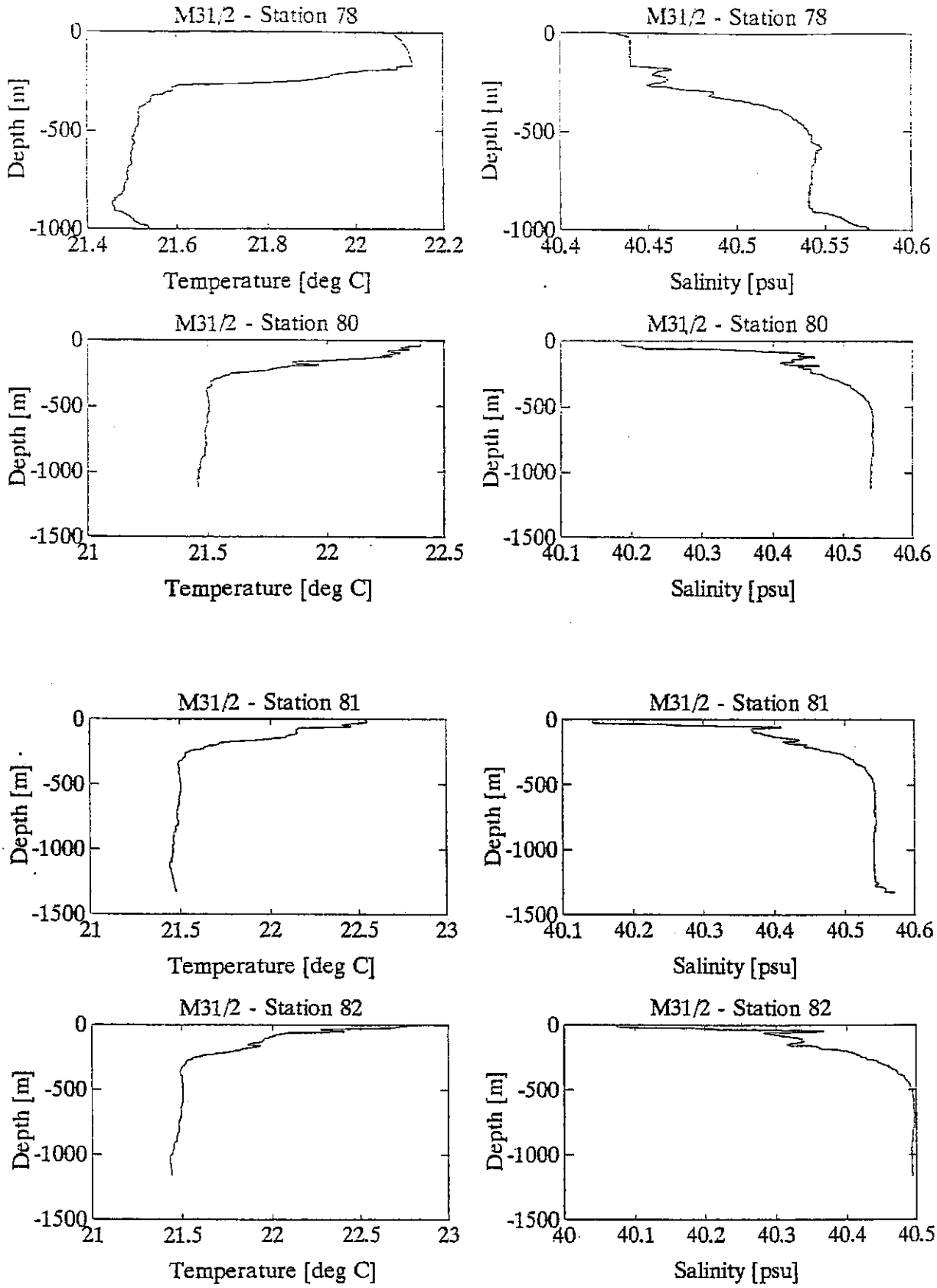

Fig. 28a: Temperature- and Salinity-Profiles during M31/2.

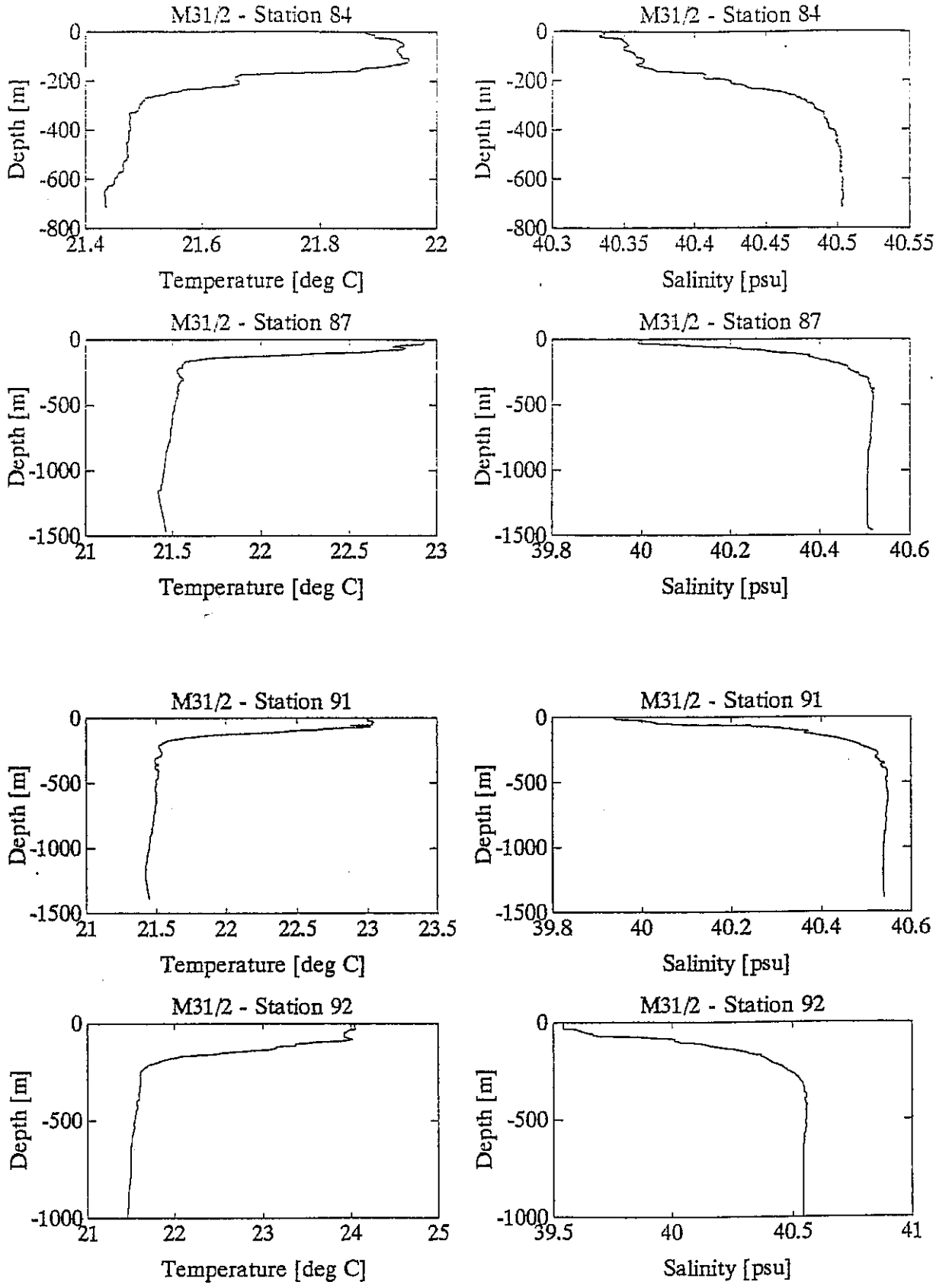

Fig. 28b: Temperature- and Salinity-Profiles during M31/2.

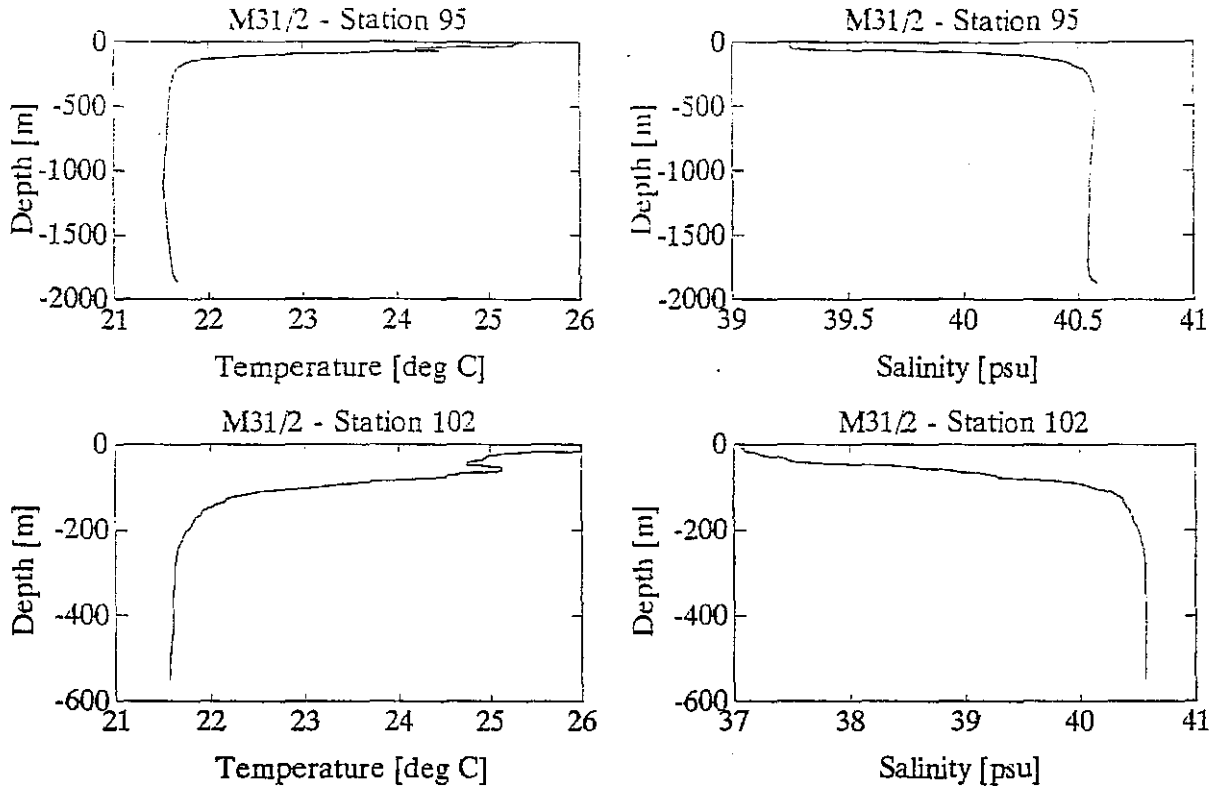

Fig. 28c: Temperature- and Salinity-Profiles during M31/2.

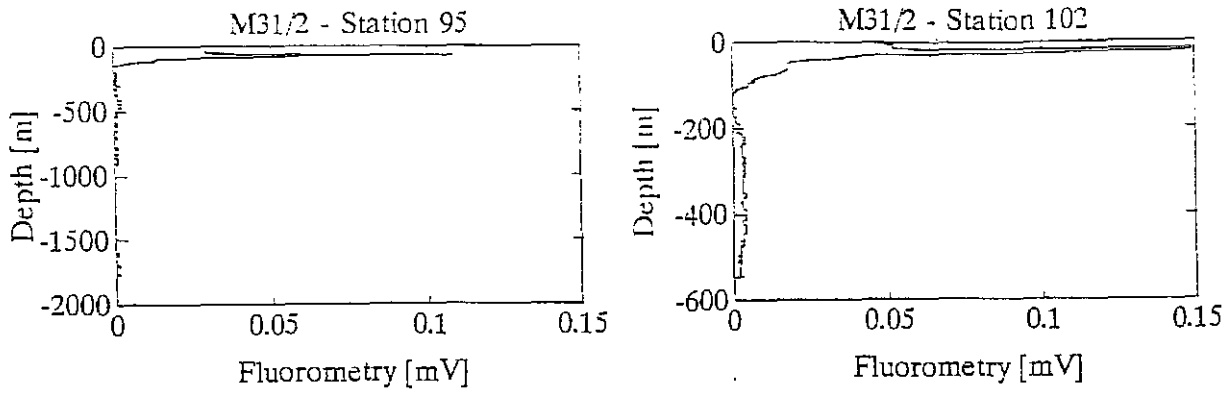

Fig. 29a: Flurometry-Profiles during M31/2.

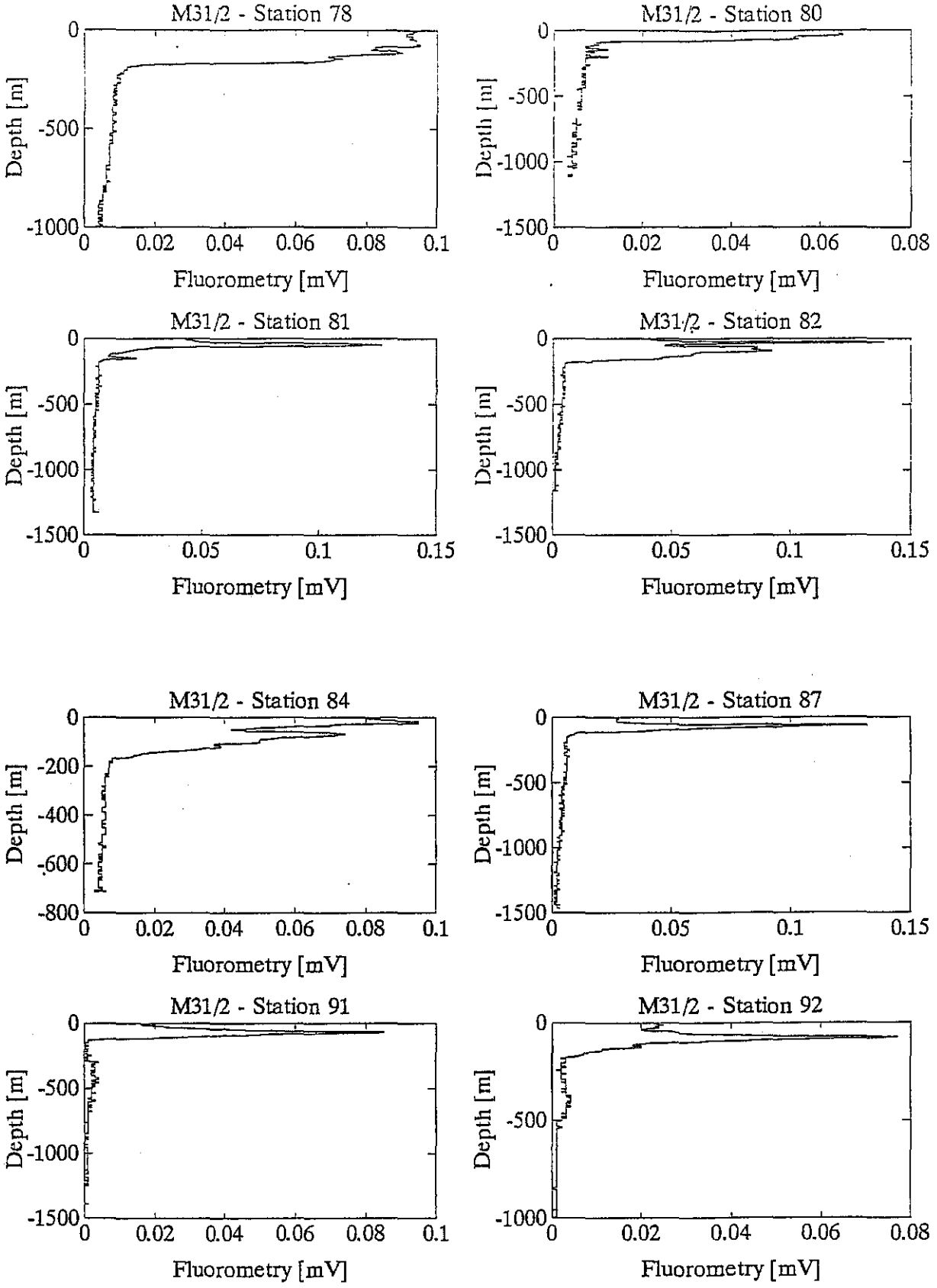

Fig. 29b: Flurometry-Profiles during M31/2.

and marked thermocline in all profiles, reaching down to a depth of 200 m (Station 87 - 92), or 125 m respectively (Station 96 / 102). The shallowing of the mixed layer is caused by increasing influence of incoming water from the Gulf of Aden. In deeper intervals of the water column the temperature remains nearly constant. An interesting observation concerns the temperature signal in the mixed layer, which has no corresponding signal in salinity. It represents the wind-driven surface inflow, accelerated by the end of NE-monsoon, from the Arabian Sea (Gulf of Aden) through the Bab el Mandeb Strait (BETHOUX, 1988).

5.2.1.2 Hydrography and Chemistry of Deeps filled with high-salinity Brines

(M. Hartmann)

Objectives of investigations

Main objectives during METEOR cruise 31/2 were to determine the hydrographic structure of several deeps in the northern and central Red Sea, which are filled with brines of high salinity and slightly to strongly increased temperatures, and to study changes since earlier investigations. Comparing temperatures, chemistry of major and trace elements, and depth position of the characteristic interfaces, we expected valuable hints as to the changing activities of the supply of solution, its mechanism and the nature of its sources. Suspended matter, especially from the transition zones, may help to understand the chemical processes taking place during mixing of brines and normal seawater.

Sampling and investigations on board ship:

At Shaban- and Kebrit Deep hydrographic profiling of the water column and sampling was performed at 12 locations using a rosette sampler equipped with 12 Niskin bottles (10 L) and a CTD-unit (NEIL-BROWN). The depth positions for profiles and hydrocast samples taken with this equipment should be correct within ± 1 m.

In the Atlantis II Deep profiling and sampling with this CTD-unit was only possible at one location (17011-1). This profile ended at the temperature zone of 32° C, the maximum temperature allowed for this device. The range of reliable values for salinities, however, ended at about 41 ‰ S.

Therefore another CTD (from ADM-Company), especially prepared to register the higher temperatures, was used for taking profiles through the high-temperature brine sections of Atlantis II- and Discovery Deep. As this device could not be combined with the rosette sampler, profiling and sampling in both deeps had to be done successively. At each location a CTD-lowering was followed by a hydrocast series (8 Niskin-bottles à 5 L) taken on hydro cable.

Unfortunately the temperature sensor was the only sensor of this CTD-device which registered values of good reliability up to the highest values found in the Atlantis II Deep. The conductivity-registration, however, ran out of range when the salinity exeeded 80 $^{o}/_{oo}$ S; reliable values probably ended at 45 to 50 $^{o}/_{oo}$ S. And the pressure registration for scaling the depth position of the equipment ended as soon as the temperature exceeded 40° C . So cable length and pinger - bottom distanaces were the only means for depth scaling within the high-temperature sections of both parts of th Atlantis II Deep.

When we later on tried to evaluate the data files on the harddisk of the CTD, it appeared that most profiles were stored incomplete and were partially illegible. The pressure values were totally out of range. And the profile from the Discovery Deep was missing. Therefore no depth-diagramms for temperature and - as far reliable - for salinity could be generated. The only possibility left was to display them against the data line number. The depth positions of the hydrocast samples taken in both deeps correspond to the cable lengths.

For the Atlantis II Deep samples, however, corrections based on the chlorinities were possible (s. below).

For chemical investigations on board ship and later, the following samples were taken from the Niskin bottles:

0,5 L for trace elements (samples were acidified with 0,5 ml HNO_3) and stored
0,1 L for chlorinity and other major components
0,1 L for pH-measurements on board ship
O_2 - titration of selected samples on board ship
fixing of H_2S by addition of Zn-acetate and storage for titration later (only selected samples).
filtration of selected samples through 0.45 µm Nuclepore-filters, especially from transition zones and near interfaces.
At the time of writing, the following data are available:
Chlorinities of all samples
H_2S results
some trace element results.

The pressure registrations (db-values) of the Neil-Brown-CTD were transformed according to SAUNDERS and FOFONOFF (1976) to meter values. The depths within the brines additionally were corrected for the higher densities (up to 1.2 g/ccm) in these sections. Depths from mappings with echosounding and hydrosweep respectively are corrected after MATTHEWS (1939). Depth-sections within the brines were corrected additionally for higher sound velocities (about 1810 m/sec) of the high salinity brines (HARTMANN, 1972, SCHOELL, 1974).

Results:

Shaban Deep:

This deep consists of four basins filled with high salinity brines (SW-, SE, NW, and NE-basin). While the southern parts were already known from former investigations (PUCHELT, 1984), the presence of brines in the northern basins was found first by the present METEOR-Expediton M31/2 in 1995. CTD-profiles were run in each of these basins in combination with water sampling. Figure 30 shows these 4 profiles, the chlorinities from samples are mentioned at the respective depth positions.

As may be seen from the profiles, the interface between normal seawater and brines is registered the same depth (1325 ± 0,5 m) for all basins. This value corresponds to the depth found during the SO29-Expedition in 1984 (STOFFERS et al., 1990).

Within both southern basins a second interface was found at a constant depth of 1459 m. In the SE-basin a third interface appears at 1520 m, just above bottom at the sample location. Equal values for chlorinity were measured in all basins (upper layer, 150,8 ‰ Cl) and probably in the intermediate layer (southern basins, only one sample 152,4 ‰ Cl). A clear difference concerning temperature may be seen between southern basins on the one hand (24,07° C in both basins) and the northern basins on the other hand (22,73° C in both basins). Further differences between northern and southern basins were measured for pH (5,7 and 6,2 respectively) and for several trace metals. Oxygen is missing and H_2S is absent as well in all brine sections.

The accordance of the interfaces as well as of the chlorinities in all 4 basins suggests free or subbottom connections. While the threshold depth from SE to SW-basin is about 35 m below the second interface and just near the brine-seawater boundary between the northern deeps, the northern and souterns parts of the Shaban Deep, however, are clearly separated by thresholds surmounting the brine - seawater interface by nearly 50 m, so that only subbottom connections can be responsible for the accordance of interface depth and chlorinity between northern and southern parts of the Shaban Deep.

Residues of filtered samples taken clearly below the brine - seawater interface showed grey colours suggesting the presence of metal sulfides, while those from the immediate interface were strongly orange-colored, evidently due to iron oxides precipitated during mixing processes of Fe-rich brine (about 7 and 14 mg Fe/L respectively in the southern and northern basins) with seawater.

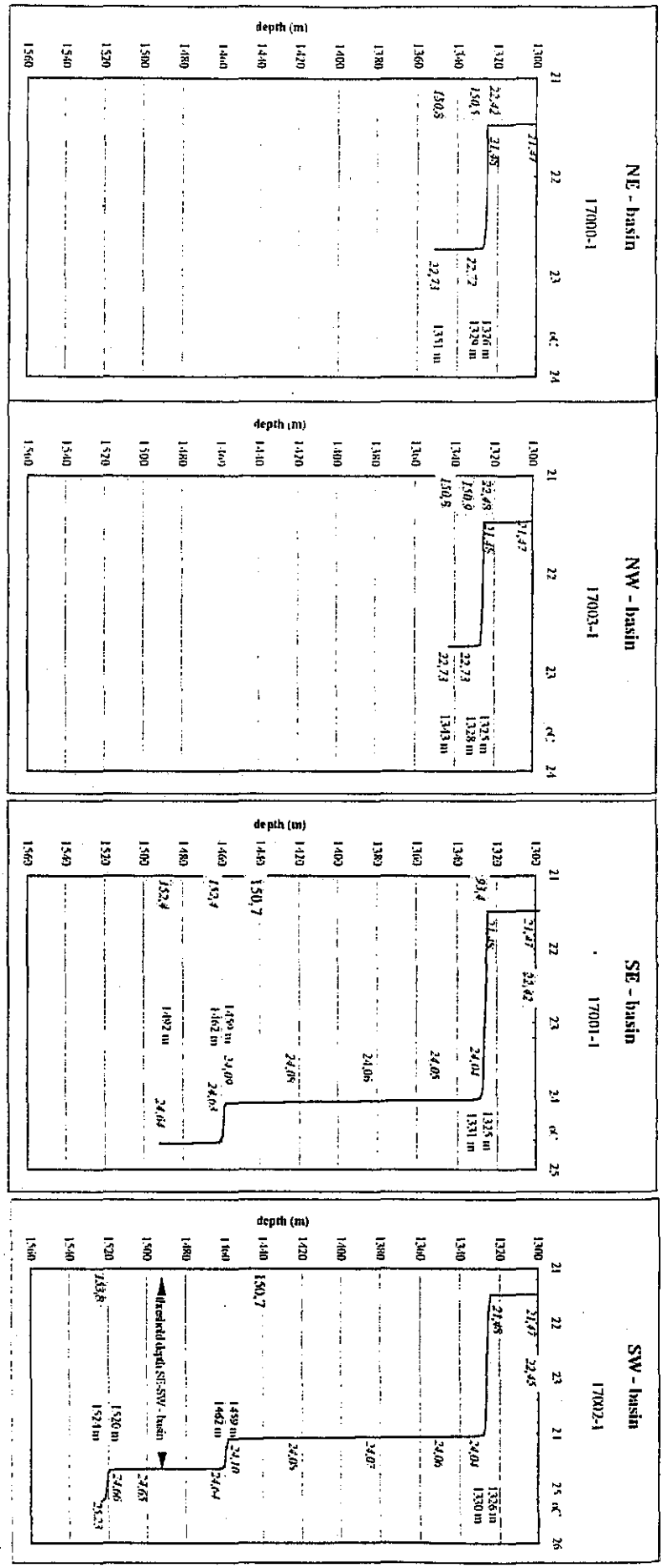

Fig. 30: Temperature profiles in the four Shaban Deeps.

Kebrit Deep:

Three hydrographic profiles were taken in the Kebrit Deep area. Only two of them sampled the high salinity brine. Figure 31 gives the profile at station 17006-1. The brine - seawater interface was the only boundary layer found in this deep. The temperature increase (from 21,46° C to 23,34° C) extending over nearly 7 m is less sharp than in the Shaban Deep.

Concerning chlorinity, however, this interface seems to be appreciably sharper. During a TV-grab lowering to this boundary it was clearly visible as a light-colored, narrow surge line running across the TV-monitor where the interface contacts the bottom, and small internal waves formed around the rope of the bottom weight crossing the brine surface. Therefore we presume a chlorinity interface of only centimeter to decimeter thickness. The begin of temperature increase was found at 1466 m waterdepth corresponding to the same depth already measured in 1972 (SCHOELL, 1974), and the temperature remained constant since that time. The samples from the salt brine strongly smelled of H_2S. Its concentration was found at 12 to 14 mg S/L.

The residues from deeper sections as well as above the interface found on Nuclepore filters (0.45 µm poresize) were scarce. One sample, however, taken only about 1 m below the boundary gave a strong black residue. Evidently it was very fine-grained to colloidal, as it was retained on the filter only partly. Probably this residue formed only after sampling and further grey suspension continued to form in the filtered solution. On contact with air, the colour changed from black to grey-olive hue, suggesting that the residue mainly consits of iron sulfides. They probably owe their formation to the mixing of Fe-rich solution on the one hand and H_2S -rich solution on the other hand captured in the same Niskin bottle from the immediate transition zone (at 1467 m waterdepth). While the Fe-concentration in two samples from this depth exceeded 1000 µg Fe/L, only less than 100 µg Fe/L were measured from the H_2S -rich deeper brine sections. A dynamic process of precipitation and resolution evidently takes place between O_2-containing seawater and strongly reducing brine. The presence of a strong enrichment of precipitation products at the immediate brine surface was confirmed by a clear shadow of the bottom weight rope visible on the interface during the TV-lowering.

Atlantis II Deep:

Two locations were investigated in the Atlantis II Deep. First the rosette sampler -CTD-combination was used in the SW basin (17011-1) in order to take a temperature/salinity profile of the transition zone from normal seawater down to the temperature level of 32° C, and sample this section. The resulting profile is given in Figure 32. An at first slight and then steeper and steeper increase of temperature and salinity may be seen. This profile mainly resembles those measured during former expeditions (SCHOELL, 1974). The level of 32° C was reached at 1996 m (corrected depth).

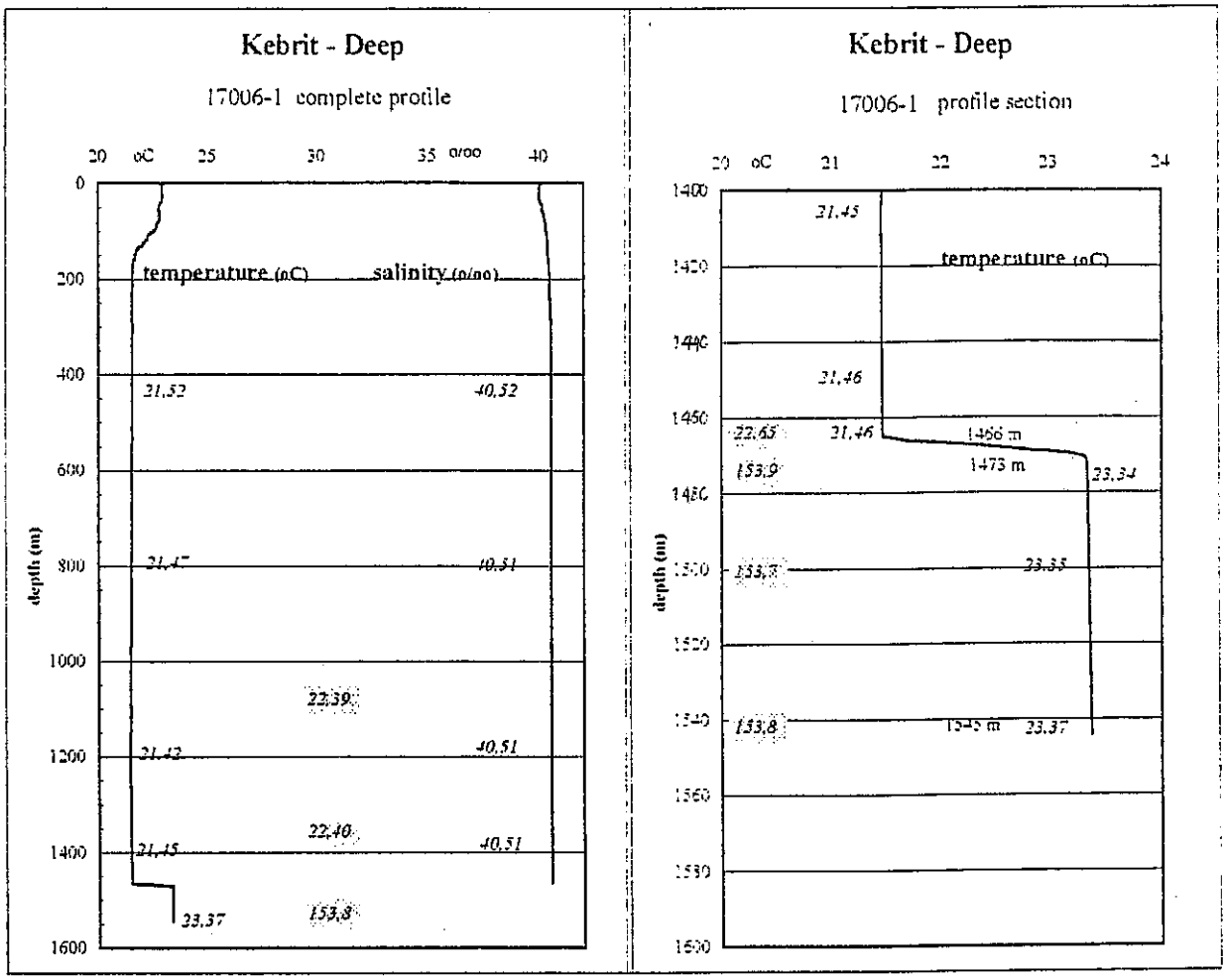

Fig. 31: Kebrit Deep, temperature and salinity profile.

Secondly a lowering of the ADM-CTD was carried out to register the temperature structure of the deeper sections of the Atlantis II Deep down to the bottom of the SW basin (17011-2). Due to the already mentioned loss of pressure registration when the temperature exceeded 40°C, only uncertain depth positions of interfaces were found. Only the cable length received from the winch could be used. Instead of depth profiles only the data line number of registrations could be used for the diagrams from this lowerings.

In Figure 33 the upper section between 24° C and 61° C of the CTD-lowering at this station is shown. This section was registered both as a lowering and a heaving profile. Figure 34 shows the deepest part of this profile down to near bottom depth. The maximum temperature of 71,70° C was measured just below the interface, while it remained constant at 71,64° C throughout the deeper parts of the lower brine.

The profile recieved from the N-basin (location 17013-1) is shown in the same manner (Figure 35). Starting at normal seawater temperatures of 21,6° C it extends down to the deepest brine. It shows a maxmimum temperature (70,38° C) just below the lower brine surface and ends in the deeper parts of this body at a temperature of 66° C. Reliable salinities ended at about 50 ‰ S.

The profiles from both parts of the Atlantis II Deep mainly resemble each other for the sections above the lower brine interface concerning temperature and - as far as reliable - salinity. Below this boundary, however, they clearly differ from each other. While the temperature below this level is mainly constant at 71.6° C in the SW-basin, it decreases after reaching a maximum of 70,38° C just below the boundary with increasing depth and ends at 66° C at the deepest point of the profile in the N-basin. This dissimilarity of both basins was already known from earlier investigations and may be explained by the narrow and shallow connection of both basins near their lower brine surface thus restricting the exchange of brine below this level.

The CTD-lowerings were followed by water sampling at both locations from the transition zone and from the high salinity sections of the profiles (stations 17011-3 and 17013-2 respectively). The unreliable depth positions from cable lenghts subsequently were corrected by relating the chlorinities (from sample titration) to those titrated from the rosette - CTD station 17011-1.

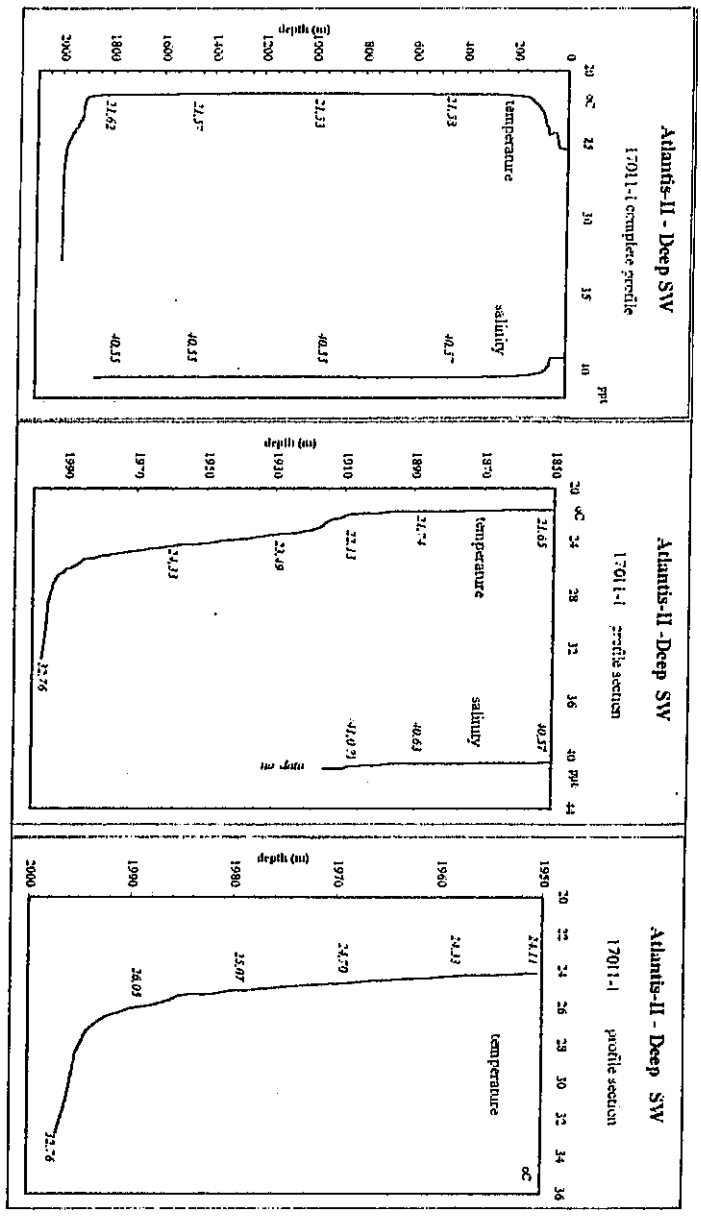

Fig. 32: Atlantis II Deep, SW-basin, temperature and salinity profile.

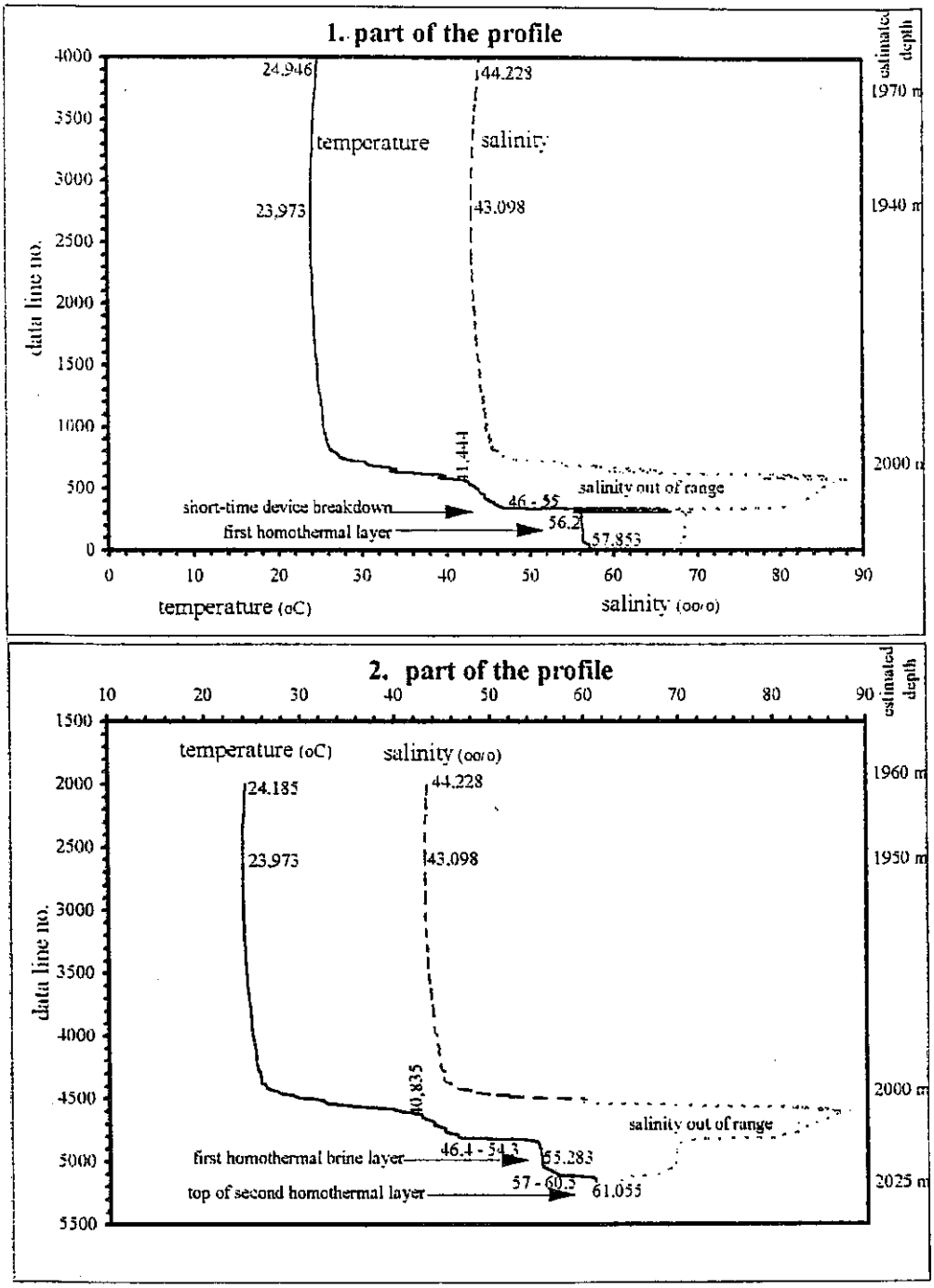

Fig. 33: Atlantis II Deep, SW-basin, CTD-profile 17011-2.

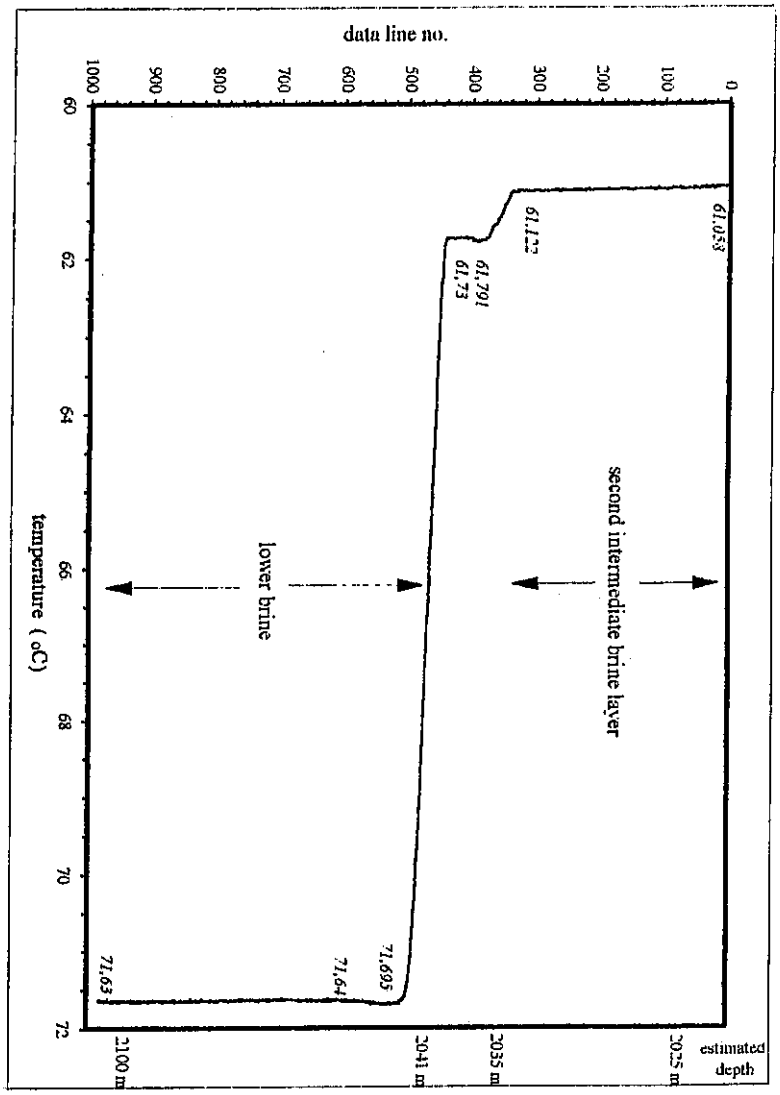

Fig. 34: Atlantis II Deep, SW-basin, CTD-profile 17011-2, lower section.

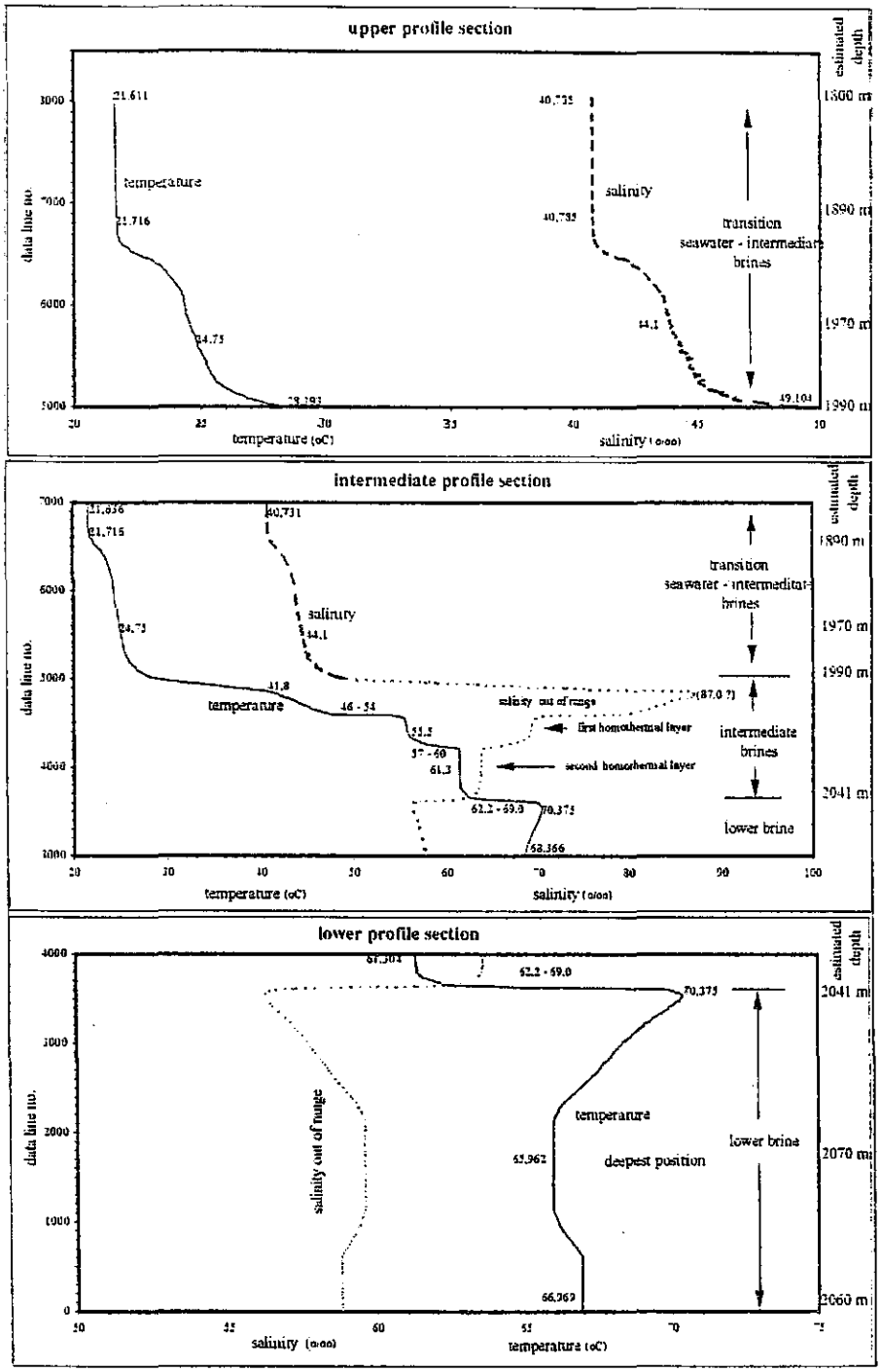

Fig. 35: Atlantis II Deep, N-basin, CTD-profile 170013-1 with ADM device.

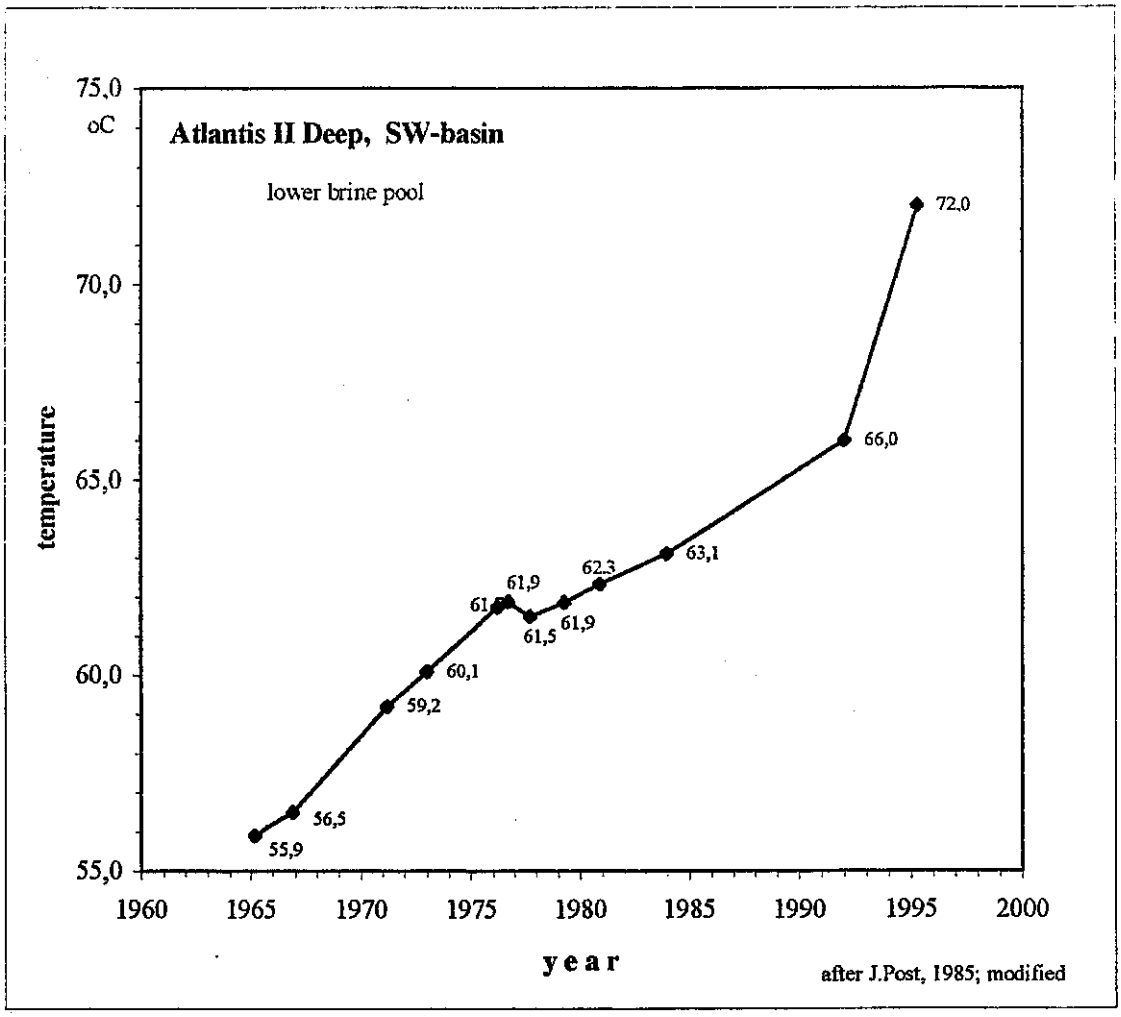

Fig. 36: Atlantis II Deep, temperature changes in the lower brine between 1965-1995.

This gave a depth for the lower brine upper boundary of 2041 ± 5 m, showing an ascent of this interface since 1977 (HARTMANN, 1980) of about 7 m. During this time the chlorinities of the lower brine changed slightly from 156,5 ‰ Cl to about 158,0 ‰ Cl; pH 5,7 ± 0.1 was measured in both parts of the Atlantis II Deep giving a value of pH 5,2 at insitu temperature. Oxygen is below detection limit, traces (0,5 mg O_2 /L) were found at the 32° C level.

Three striking differences are found for the Atlantis II Deep compared to former times:

1. The lower brine interface has risen by about 7 m during the last 15 to 20 years.
2. The temperature of the lowest brine section increased strongly, from 61° C to more than 70° C since 1977 (HARTMANN, 1980). ANSCHUTZ and BLANC (1995) already in 1992 registered a clearly increased temperature of 66° C. Figure 34 shows the rise of temperature since 1964. The exceptionallly steep gradient of nearly 1,7° C/year for the period after 1992 compared to that of former times (only about 0,5° C/year) demonstrates a strongly enhanced hydrothermal activity.
3. While only one homothermal section with a temperature near 50° C was found during former investigations, presently two such zones (55,3 and 61,0° C, each probably 10 to 20 m thick) exist. ANSCHUTZ and BLANC (1995) mentioned an additional third homothermal section of only small thickness.

Discovery Deep:

Due to the malfunction of the device no data file was stored from the CTD-recordings in the Discovery Deep (17014-1). During the lowering of the CTD at this location the upper surface of the homothermal lower brine was found at 2045 m from cable length. A temperature of 49,6° C was recorded at the top of this brine. Further down to the near bottom position (2226 m) the temperature slightly increased up to 50,8° C . In case the still uncertain depth position is correct this would mean a rise of the Discovery Deep brine interface of more than 10 m since 1977, and the temperature increased by 5 to 6° C since 1977 (44,7° C).

According to these findings the increase of hydrothermal activity now has extended from the nearby Atlantis II Deep to the Discovery Deep, which had shown mainly constant temperatures during former periods. Two samples gave slightly higher chlorinities of 154,6 ‰ Cl compared to 153,5 ‰ Cl in 1977. Oxygen was below detection limit and pH 6,45 (corrected) was measured in the high salinity brine.

5.2.1.3 Hydrothermal Methan in Red Sea Waters

(E. Faber and R. Botz)

During METEOR 31/2 - cruise water samples were taken from vertical profiles in the Shaban-, Kebrit- and Atlantis II Deeps using the common (10 l) Niskin bottles. Hydrographic parameters were recorded with a CTD (N. Brown, IfM Kiel). All brine samples and normal

Red Sea water have been degassed by the ultrasonic vacuum procedure described by SCHMITT et al. (1991). The CH_4 (C_{2+}) contents were determined by gaschromatography (Shimadzu GC-14A, wide bore quartz cappillary columnn, FID) directly after the gas was obtained. Evacuated glass vessels were used for gas transport to the stable isotope laboratory at the BGR in Hannover. For gas genetic interpretation measurement of the carbon- and, if possible, hydrogen isotope ratios of CH_4 (C_{2+}) are planned for the near future.

During METEOR 31/2 cruise the concentrations of light hydrocarbon gases were measured in the water column and brine bodies of the Red Sea. In particular the Shaban-, Kebrit-, Atlantis II- and Discovery Deeps were investigated to detect and sample hydrocarbon anomalies. Results of onboard analyses for CH_4 (C_1) and C_2H_6 (C_2) are given in Chapter 7.2.2. In general C_1 contents range from normal background values (<100 nl/l) in the water column (note a relative C_1 maximum which occurs in the surface near water) to extreme high concentrations (Figures 37-40) in the brines with a maximum of 22.58 ml/l in the Kebrit Deep at 1516 m water depth (Figure 38). The very high hydrocarbon contents of the brines are responsible for the extreme concentration differences between brine and overlying normal Red Sea water (note the sharp contrast between brine and overlying water bodies) and caused severe contaminations during sampling the upper water column. As a consequence the water column above the brine had to be sampled prior to brines itself. The contamination of the water column by hydrocarbons released from the brine during sampling can be recognized comparing hydrocarbon concentrations in Red Sea water measured at the same location before and after sampling of the brine (Figure 40). This is the reason why we developed a composite diagram (Figure 38d) showing concentration data based on separate casts on brine and sea water.

The various Deeps show remarkable differences in both the amounts of C_1 dissolved in the brines and the gas composition (Figures 37-40). The Kebrit Deep which contains extremely gas-rich brines up to some 130 ml total gas per liter fluid also exhibits the highest C_1 (C_2 and C_3) contents (7.2.2.). Two distinct brine layers are characteristic for the Atlantis II- and the Discovery Deeps. The upper brine layer contains C_1 up to some 123 ul/l and only little C_2 (< 100 nl/l and C_3 below detection limit). The lower brine, however, is characteristically enriched in C_2 and C_3 (Figure 40). These findings agree with the results of BURKE et al. (1980) who found similar concentrations of C_1 and higher hydrocarbons in brines and sediments of the Atlantis II Deep. The significant amounts of C_2 (and C_3) in the brines indicate a thermogenic origin of the hydrocarbons probably as a result of high heat fluxes causing thermal maturation of sedimentary organic matter within Miocene evaporitic sequences. The situation may be much more complex for C_1 occurring in hydrothermal systems. Its origin can be related to biogenic production by methanogens (upper brine in the Atlantis II Deep where higher hydrocarbons are largely missing) or it may also be of thermogenic origin but higher in temperature (or maturity) of the organic precursor or it may represent abiogenic reactions at high temperatures and pressure (mantle origin?). Considering hydrocarbon concentrations further complications are caused by secondary oxidation processes which may reduce their actual quantities in the water and sediments. Thus, concentration measurements alone are probably not indicative for the complex origin of C_1 in Red Sea brines (and sediments). Future

stable isotope analyses will shed light on the origin of hydrocarbons (C_1, C_2, C_3) and CO_2 dissolved in Red Sea fluids.

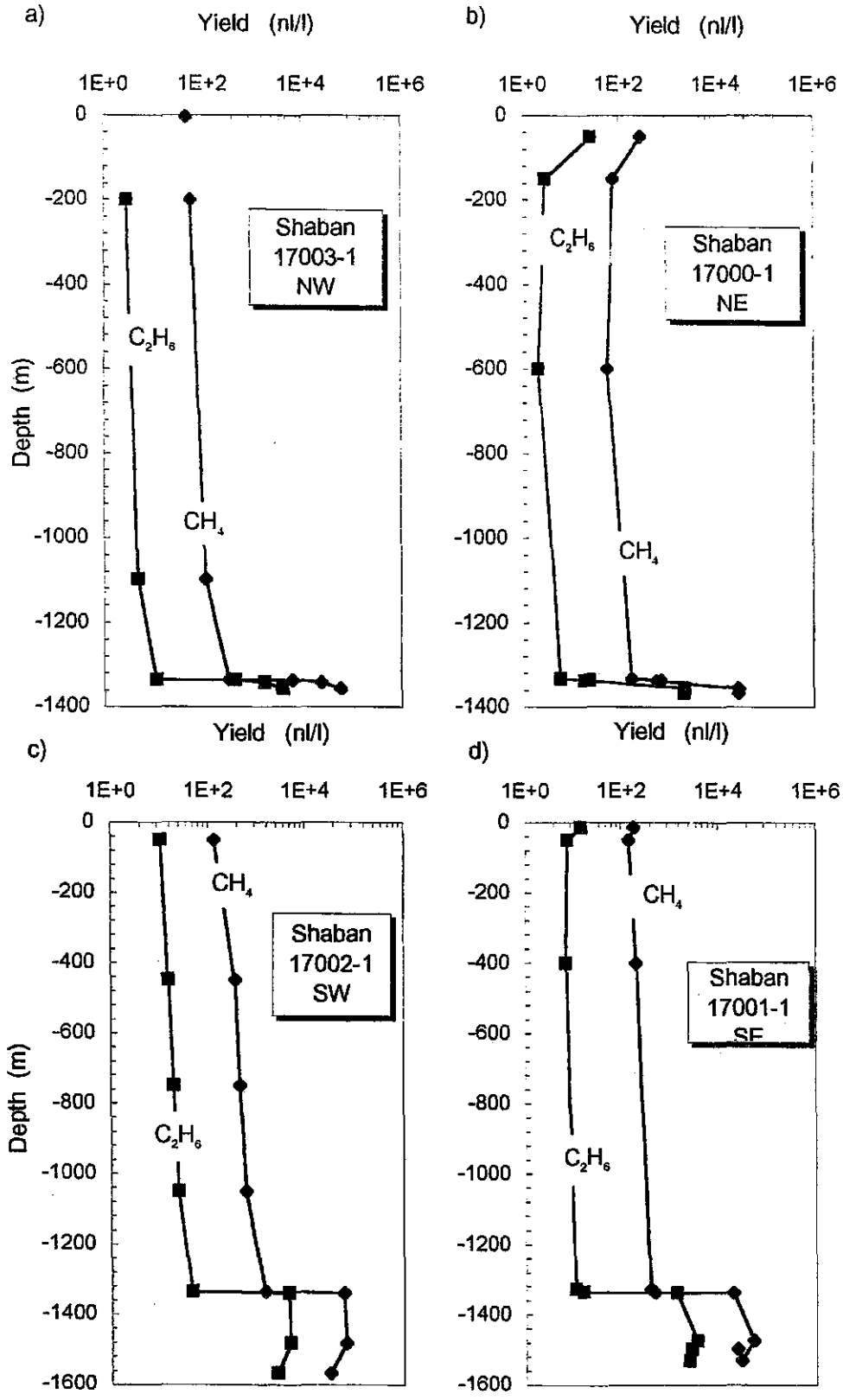

Fig. 37a-d: Gas concentrations in the Shaban Deep - water-column and brine pool.

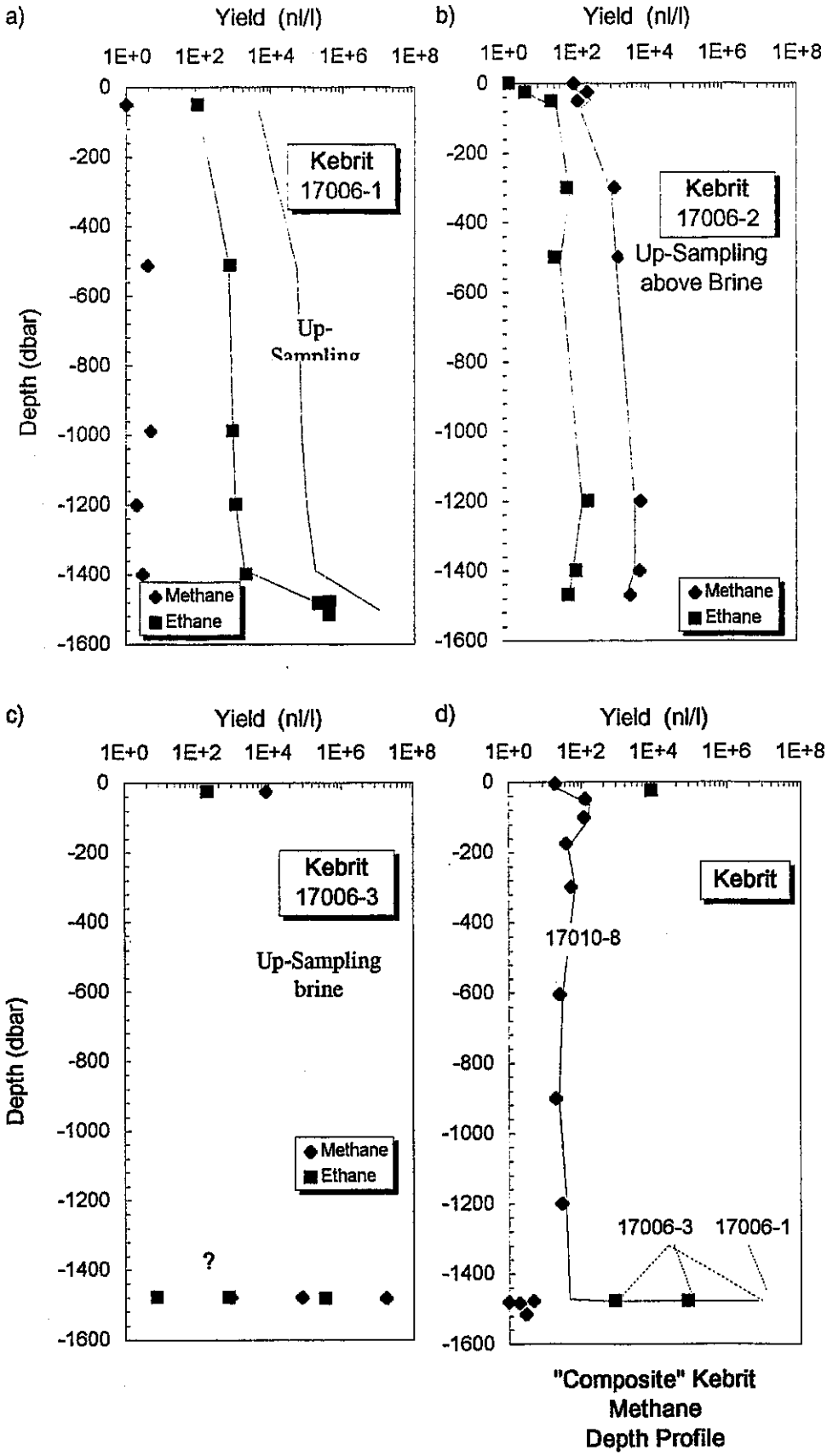

Fig. 38a-d: Gas concentrations in the Kebrit Deep; a), b) in the deep water-column; c) in the brine pool; d) based on separate sampling of water-column and brine pool.

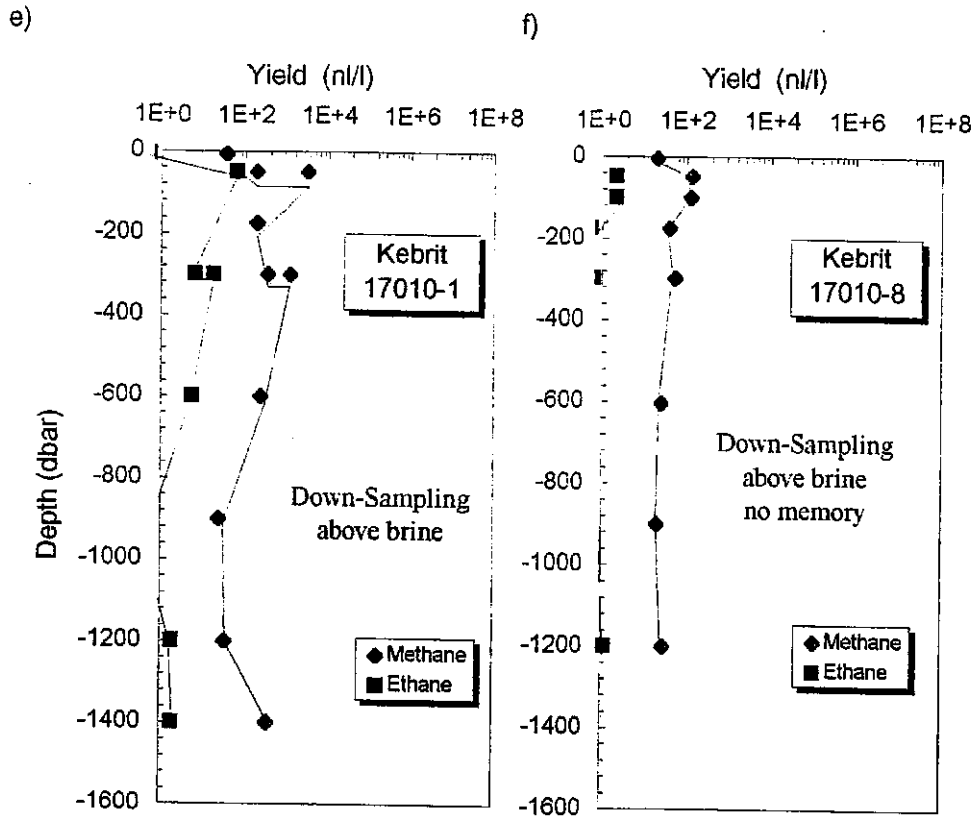

Fig. 39e,f: Gas concentrations in the Kebrit water-column; no brine sampling.

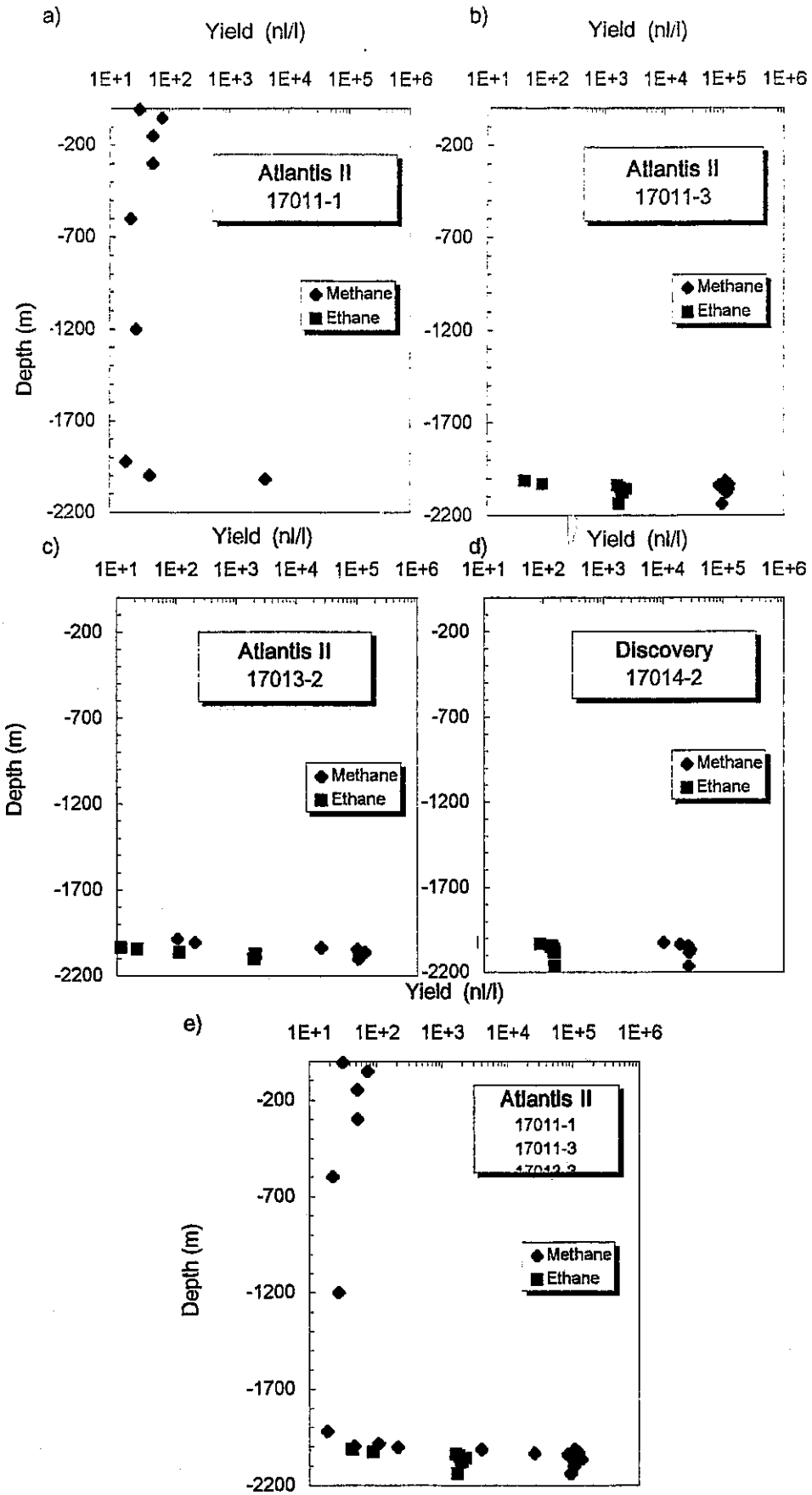

Fig. 40a-e: Gas concentrations in the Atlantis II Deep.

5.2.2 Planktology

5.2.2.1 Planktic Foraminifera

(Ch. Hemleben, Th. Mühlstrasser)

At most stations (7.2.3) 11 multiple opening/closing hauls comprising 55 plankton samples were taken at various depth. These samples will be washed and counted to be compared with core data on the north - south transect. Previously collected data revealed a distinct faunal gradient from the southern Red Sea, which is still influenced by the Golf of Aden water, to the highly saline area of the northern Red Sea (AURAS et al., 1989) and has been verified by our newly collected data set.

5.2.3 Benthic Biology and Actuopalaeontology

(W. Oschmann, J. Nebelsick, F. Wesselingh and W. Wranik)

During the METEOR cruise M31/2, a box-core program supplemented by multicorer and dredge samples was carried out in order to obtain bottom-sediment and shelly macrobenthic samples (7.2.4). This resulted in a north - south sampling transect below a depth range of 400 m. Additionally, three near shore to basin box-core transects have been taken off Sudan with two transects situated near Albington Atoll (~20° 50'N/ 37°30'E) and a third one off the Suakin-Archipelego (~19°00' N/ 38°30' E). Some Dredge-samples derived from small ocean basins of the central part and from the southern part of the Red Sea near the Bab al Mandeb (~15°20' N/ 41°40' E) were also included.

The boxcorer and multicorer samples were used to recover the benthic fauna, which was sieved immediately with sea water on board at two to three horizons (à 15 cm) according to the penetration depth. The live fauna as well as the hartparts of the surface layer were conserved in formalin. They will be separated later at the biology department of the University of Rostock. The species numbers of the living (biocoenosis) and the dead faunal assemblage (thanato- and taphocoenosis) of the samples will be compared. After sieving, the hartparts of the lower horizons were rinsed with freshwater, dried and carefully packed for transport in order to prevent artificial fragmentation.

Distribution and ecology of the benthic organisms:

Three major physiogeographic units occur in the Red Sea each with an distinctive faunal content (see also Table 11) The three main units are:

1) Carbonate Platform facies (~0-150 meters)
2) Slope and bathyal plain facies (~150-1700 meters)
3) Oceanic Basin (hydrothermal) facies (~1400-2000 meters).

1). A highly diverse malacofauna was observed in samples taken from the carbonate platform facies in the Red Sea and the Bab el Mandeb. These represent the diverse modes of ecological habits typical for shallow water environments of tropical seas.

2). The unusual eco-physical conditions prevailing in the Red Sea (oligotrophy; T>20° C throughout the water column; high salinity above 40 $^{o}/_{oo}$) are reflected in the faunal composition and distribution in the slope and bathyal plain environments, which according to our short and preliminary observations, are rather uniform. Representatives of tropical benthic molluscs, which normally are restricted to the surface layer of the tropical oceans (max. a few hundred meters), occur down to a depth of 1500 meters. The malacofauna contains carnivorous anomalodesmatan bivalves, various pectinids (e.g. *Propeamussium*) and a number of carnivorous gastropod groups. Anomalodesmata as second level consumers are unusually abundant among the bivalves. The small clypeasteroid sea-urchin *Echinocyamus* is common among the echinoderms.

3). Faunas from the marginal areas of the oceanic basins in the central Red Sea grabbed by dredges, box cores and TV-cores include a few lucinid species. This bivalves are comparatively large (up to 3.5 cm's) and associated with hydrothermal sulphidic deposits. Lucinids are common at many cold seeps and hydrothermal vent areas and well known as chemosymbionts, which have developed endosymbiotic relationships hosting H_2S oxidizing, chemosynthetic bacteria in their tissues. The autotrophic bacteria detoxify the poisonous H_2S, which otherwise would cause a complete cessation of pulmonary function of the bivalves and additionally provide carbohydrates as food source to them. The large size of the lucinids, compared to other deep sea molluscs, and their occurrence associated with sulfidic mineraliferous deposits favour a chemosymbiotic life habit in the Red Sea oceanic basins, too. A high level of endemism is indicated by the fact that other chemosymbiontic bivalves like *Calyptogena* and *Bathymodiolus* which are well known from the world oceans are missing. Occasionally some faunal elements from the bathyal plane facies occur. They very presumably date prior to the hydrothermal activity.

Diagenetic alterations of calcareous skeletal elements

Although the sediments recovered in the box cores and dredges are, geologically speaking, of a very young age, various skeletal alteration have been noticed in our material of both planktonic and benthic organisms. These alteration range from an opaque appearance of the originally transparent shells (e. g. of pteropods) to dark brown/blackish "impregnation", to lithification of the sediment fill, to internal moulds (steinkerns). Particularly below 400 meters, Steinkern-fossilisation of gastropods and bivalves is partially reached within the uppermost cm's of substrate. Selective precipitation and solution obviously takes place within periods of only some hundreds to a maximum of a few thousand years. The rapid loss of information occurring during early diagenesis may be comparable with marine settings occurring on the green-house earth during Jurrassic and Cretaceous times.

Evidence of sea floor lithification

Various dredge samples contained large slabs of lithified substrates consisting of a highly porous supported fabric of pteropods only partly filled by a muddy matrix. The slabs are very large and reach several dm in thickness. They are characterized by smooth to partly very rough surfaces, which occasionally are encrusted with serpulids proving that the slaps have been (partly) exposed at the substrate surface. Serpulids and their remnants are also found in pockets, which may be relicts of bioturbation. From the marginal areas of the oceanic basins very similar slabs were found, with, however, an impregnation by mineraliferous sulfids.

Biogeographical aspects

Some of the taxa dominating the benthic molluscan faunas below 150 meters in the Red Sea, like several *Cuspidaria*, *Cardiomya* and *Propeamussium* species, have not been observed in samples from the Gulf of Aden- Arabian Sea (see M31/3). Morphologically these taxa are very similar to species distributed throughout the Mediterranean such as *Propeamussium fenestratum* (Forbes), *Cuspidaria rostrata* (Spengler), *C. nitens* (Locard), *C. abbreviata* (Forbes) and *Cardiomya costellata* (Deshayes). Systematic-morphometric analysis is needed to investigate possible relationships.

It is also very conspicuous that protobranch bivalves (e. g. nuculids and nuculanids) as well as limopsids are extremely rare in the Red Sea. Particularly these bivalve groups represent a high percentage of the bathyal and abyssal benthic fauna in the world oceans.

The expected distribution of shallow water regular echinoids in the near shore sediments is observed with a dominance of the spines of *Eucidaris metularia* and *Echinometra mathaei*. The increasing importance of thin shelled infaunal spatangoids in deeper water fine-grained sediments is also observed. Surprising is the fact that the clypeasteroid genus *Echinocyamus* is found in all depths and most sediment types (except for the hydrothermal facies). This genus is also the most cosmopolitan echinoids found in the Red Sea.

Tab. 11: Summarized facies and faunal distribution of the major physiogeographic units of the Red Sea

ENVIRON-MENT	FACIES/ SEDIMENT.	DEPTH (m)	DOMINANT SHELLY MACROFAUNA	DIVERSITY AND PRESERVATION	DOMINATING BENTHIC MOLLUSCS
CARBONATE PLATFORM	reef-sands	2 - 10	algae, corals, echinoids, benthic molluscs, bryozoans, crustacea, worm-tubes;	diversity: high density: high preservation: fragmentation: high abrasion mod. encrustation: high solution: low	**bivalves**: Arcidae, Glycymeridae, Lucinidae, Carditidae, Veneridae, **gastropods**: Conidae, Trochidae, Vermetidae
	Hetero-stegina sands	50 - 100	algae, large foraminifera, benthic molluscs, echinoids, worm-tubes;	diversity: high density: mod. preservation: fragmentation: high abrasion low encrustation: mod. solution: low	**bivalves**: Nuculidae, Arcidae, Veneridae, **gastropods**: Terebridae, Turridae, Cypraeidae, Turritellidae, Nassaridae
	reef-debris	50 - 150	algal and coral fragments, molluscs, bryozoans, echinoids, worm-tubes	diversity: high density: high preservation: fragmentation: low abrasion low encrustation: mod. solution: low	**bivalves**: Arcidae, Chamaidae, Lucinidae, Carditidae, Veneridae, **gastropods**: Terebridae, Nassaridae, Naticidae
	echinoid-ooze	50 - 150	echinoids, benthic and planktonic molluscs	diversity: high density: mod. preservation: fragmentation: low abrasion low encrustation: low solution: low	**scaphopods**; **bivalves**: Nuculidae, Lucinidae, Veneridae, **gastropods**: Nassaridae, Turridae, Pyramidellidae

ENVIRON-MENT	FACIES/ SEDIMENT.	DEPTH (m)	DOMINANT SHELLED MACROFAUNA	DIVERSITY AND PRESERVATION	DOMINATING BENTHIC MOLLUSCS
S L A N O P D E	Cuspidaria ooze	150 - 1400	benthic and planktonic molluscs, fish otoliths	diversity: high density: mod. preservation: fragmentation: low abrasion low encrustation: low solution: mod.	**bivalves**: Anomalodesmata, Pro-peamussidae, **gastropods**: Turridae, Trochidae pteropods, heteropods
D P E L E A P I N S	"sea-mount" carbonate sands	300 - 500	benthic and planktonic molluscs, echinoids, bryozoans	diversity: mod. density: mod. preservation: fragmentation: low abrasion low encrustation: low solution: low	**scaphopods**; **bivalves**: Veneridae, Cardidae, Anomalodesmata, **gastropods**: Nassaridae, Naticidae
B A S I N S	brine pool sulphid - rich muds	1400 - 2000	benthic and planktonic molluscs, crustacea, fish otoliths, brachiopods	diversity: low density: low preservation: fragmentation: low abrasion low encrustation: low solution: high	**bivalves**: Lucinidae, Corbula, Anomalodesmata, **gastropods**: Risoidae. pteropods, heteropods

5.2.4 Marine Geoscience

5.2.4.1 Export of Shallow Water Carbonates

(P. Emmerman, J. Reijmer and T. Brachert)

During METEOR cruise 31/2 Parasound measurements were used to locate sediment sampling positions. The ships safety regulations, however, did set limits to the distance between the reef itself and the locations of our coring sites, but it did not hamper to acquire an excellent set of piston cores. Two types of sampling devices were used, Kastenlot-cores and gravity cores. The length of the Kastenlot-cores and gravity cores varied between 6 m or 9 m. For both sampling methods a weight of 1,200 kg was used. The devices were lowered with a speed of 1 m/s. At about 30-50 m above the sediment surface the lowering was stopped, allowing the apparatus to stabilise itself in the water column and to stop its swinging back and forth. When the device hang quietly it was lowered with an increasing speed up to 1 m/s in order to achieve maximum penetration into the sediment. The drop in tension on the cable made it possible to check if everything had functioned as it should during the coring procedure. With a speed of 1 m/s the core was taken back to the water surface. On board the sediments of the Kastenlot-cores were described, photographed and sampled. Every 10 cm a 30 cm^3 sample was taken. The samples will be used for a large variety of laboratory analyses like (1) grain-size analysis, (2) geochemical analyses i.e. X-ray diffraction and total organic carbon, (3) quantitative component analyses (4) stratigraphical oriented analyses like biostratigraphy, oxygen and carbon isotope analysis and (5) dating techniques (^{14}C-AMS and U/Th-TIMS). Smear slides were taken at characteristic intervals in the cores and described on board. The piston cores were cut into 1 m pieces. Description and sampling of these cores was done after the cruise at GEOMAR in Kiel, Germany.

Two areas were investigated situated off the coast of Sudan, namely the Abington Reef and the Sanganeb Atoll. Seven Kastenlot-cores ranging in length from 6 m to 9 m and 2 piston-cores of 6 m length were taken at waterdepths ranging from 498 m to 810 m. The sediments recovered consist mainly of greenish-gray nanno-ooze with planktonic foraminifera and pteropods as main coarse grained components. The strongly bioturbated carbonate oozes are intercalated with black-dark gray, pteropod-rich sapropel horizons. In some of the cores sandy intercalations are present. They contain large amounts of sandy shallow water-derived bioclastic reef detritus. In the cores that are situated at greatest distance from the reefs, the sandy intervals are finer grained and mostly present as a kind of relict structures in the strongly bioturbated sediments. Bioturbation has destroyed most of the primary sedimentary structures.

A phenomenon observed in all cores that needs special attention is the 60 cm to 70 cm thick interval consisting mainly of carbonate crusts. This interval was found in the upper 1 m to 2 m of all cores taken. The crust is mostly succeeded upcore by a maximum 7 cm thick pteropod-rich sapropel layer that represents the Holocene-Pleistocene boundary (Brachert, pers. com.). The carbonate crust layer consists mainly of aragonite and high-Mg calcite, and is described in literature as being deposited during the Last Glacial Maximum (BRACHERT subm., and MILLIMAN et al., 1969).

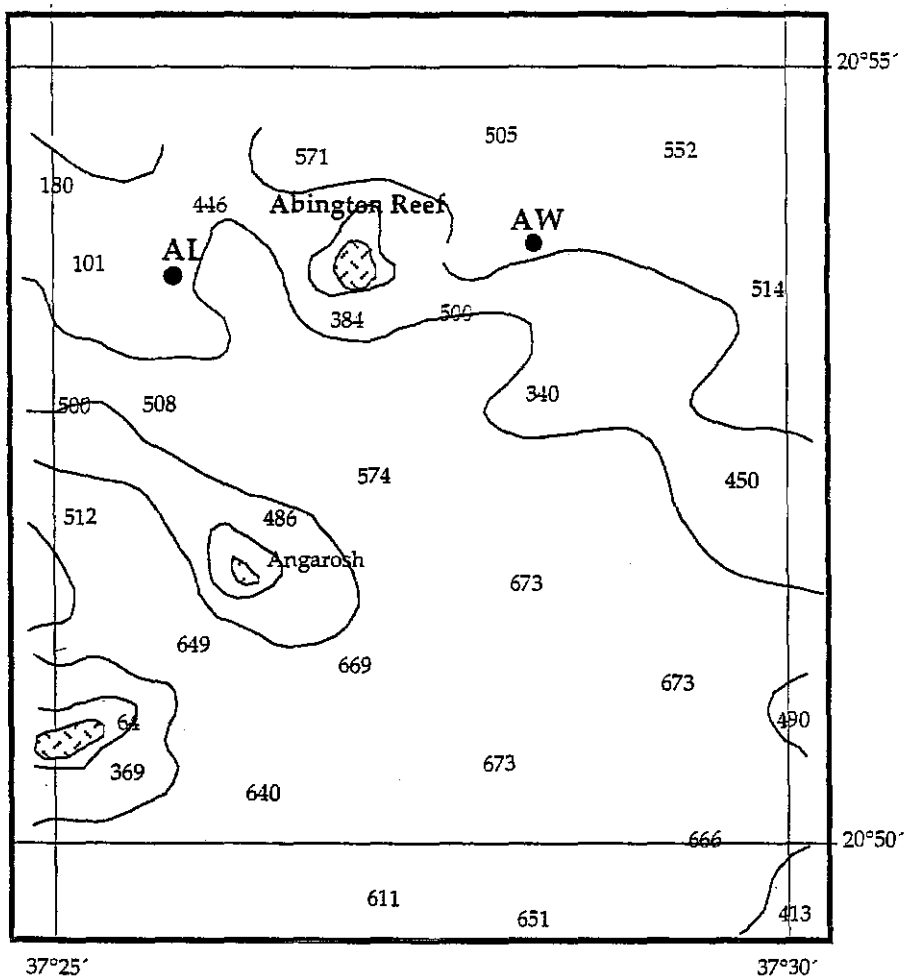

Fig. 42a: Coring sites near Abington Reef (working area 1). Numbers show water depth in metres.

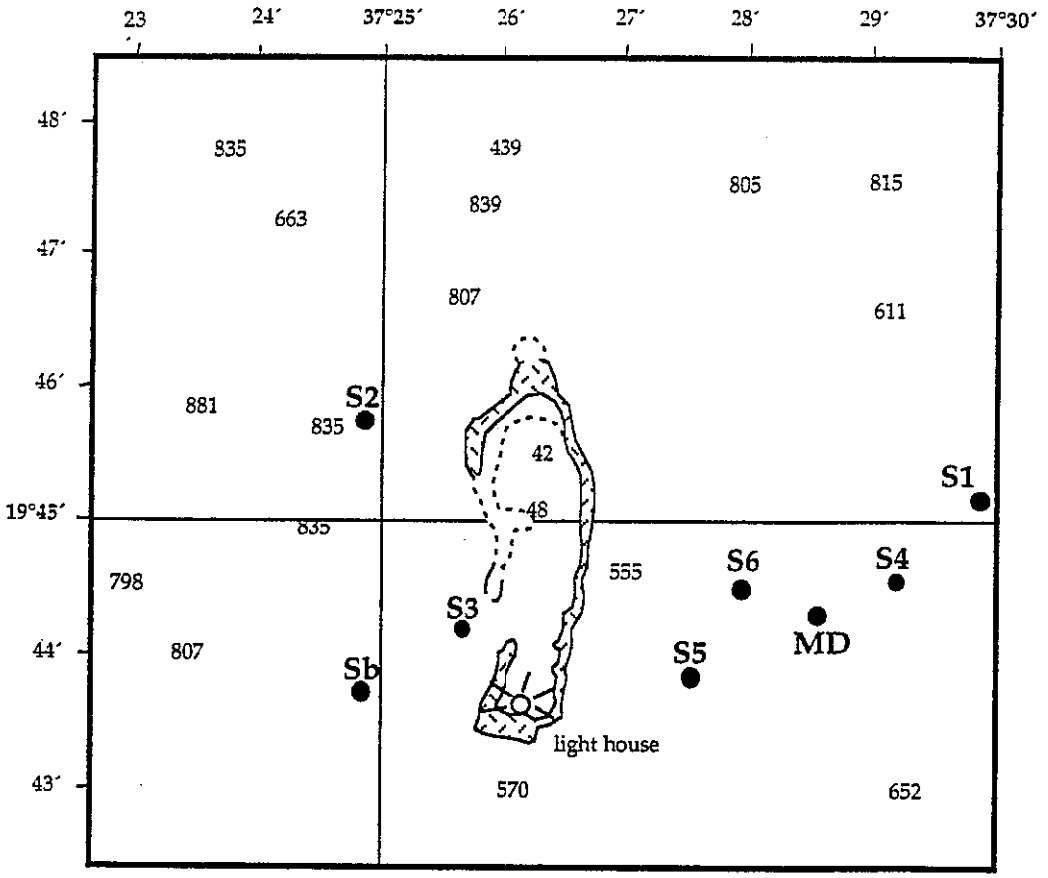

Fig. 42b: Coring sites near Sanganeb Atoll (working area 2). Numbers show water depth in metres.

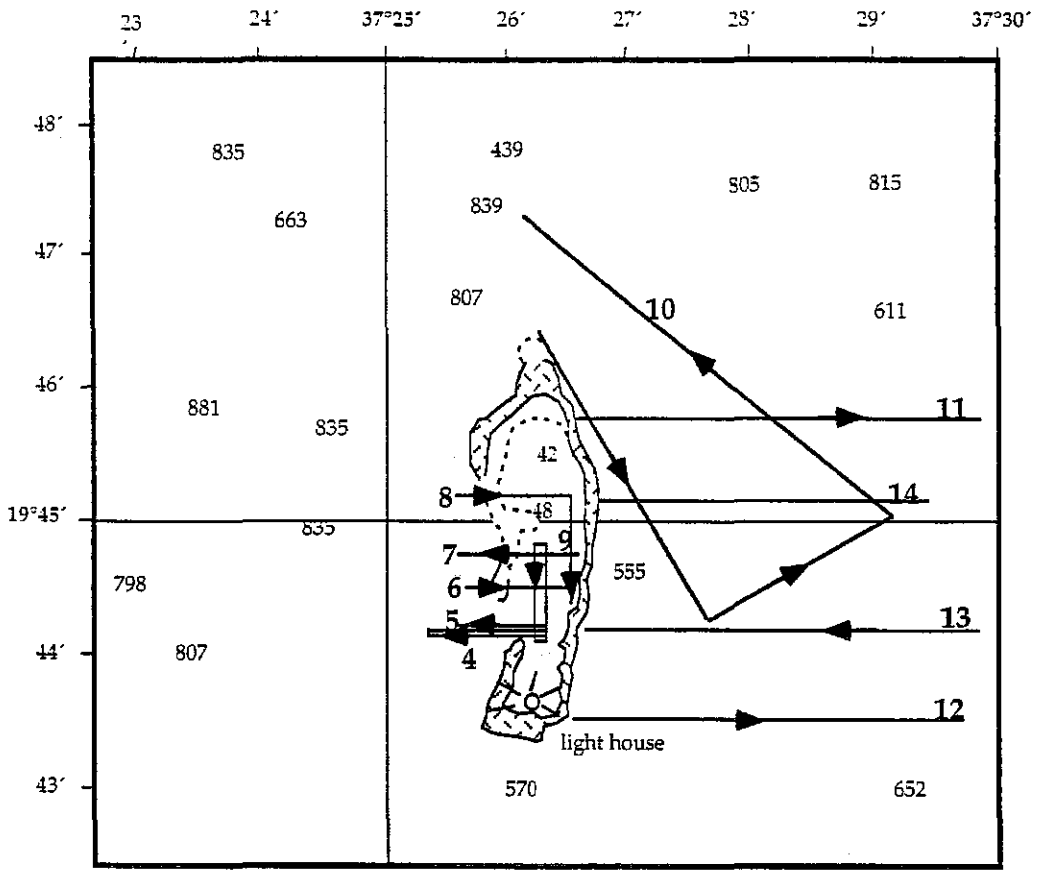

Fig. 42c: Track chart of the 3.5 kHz-profiles at Sanganeb Atoll. Numbers show water depth in metres.

The Abington Reef (Station no. 94 and no. 96)

In the Abington Reef area two cores were taken after Parasound reconnaissance. One at the leeward side of the reef and the other on the windward side. Both positions were situated about one nautical mile (nm) from the reef edge. The cores were taken at waterdepths of 498 m (leeward) and 517 m (windward) (Figure 42a).

The cores were positioned in two channels near the reef. The original plan was to sample at the toe-of-slope of the reef, but this could not be done because of safety regulations of the ship. The cores recovered didn't contain coarse-grained reef input. The reason for the lack of coarse-grained reef detritus might be the relative small size of the productive area of the reef itself resulting in a relatively small amount of material that can be exported. Another cause might be that the reef detritus is transported relatively far away from the platform due to strong bottom currents. Other factors influencing the lack of coarse debris in our cores might be the existing bottom topography. The entire western coast of the Red Sea is strongly tectonically influenced and mainly shows a horst and graben structure (MAKRIS and RIHM, 1991; GASPERINI et al. subm.). Perhaps the exported material is funnelled into one of the pre-existing deep channels which have their origin in this tectonic setting. See also Figure 42b, Figure 42c and Figure 43 that display a similar structure near Sanganeb Atoll.

Despite the lack of coarse-grained material the cores taken near the Abington Reef will form an excellent dataset for comparison with the cores taken near the Sanganeb Atoll especially for the fine-grained aragonite input cycles. Do these datasets display the same type of sedimentation input pattern? Using calcite-aragonite ratios downcore we will test the principle of "highstand shedding" in both settings (DROXLER et al., 1983; DROXLER and SCHLAGER, 1985; SCHLAGER et al., 1994).

M31/2-94-AL (Position: 20°53.670 N; 037°25.740 E)
This Kastenlot-core was taken at a waterdepth of 498 m. It is situated at a slight elavation at the edge of a channel positioned about 1 nm SW of Abington Reef (Figure 42a). In total 5.30 m of fine grained, light gray-greenish carbonate sediment were recovered (Figure 44). The upper 0.67 cm of the core were lost. The lithology and smear slide descriptions show the following picture. The sediments in this core consist of nanno-ooze with mainly planktonic forminifera and pteropods. In addition, varying amounts of bioclasts, biogenes and terrigenous material could be observed. In the matrix aragonite needles and silt-sized detritus of various origin can be found. Pteropod-rich sapropel layers occur at various levels within the nanno-ooze.

The coarse-grained components are mainly bioclasts. A detailed analysis of the components will be made in due time in order to detect the number of reef-derived components. In some parts of the core the terrigenous input, mostly quartz grains and feldspars, increases to 10 % of the coarse fraction. The planktonic foraminifera found are mainly *Globigerinoides* and individuals of *Orbulina universa*. The percentage of foraminifera varies between 0 and 10 %.

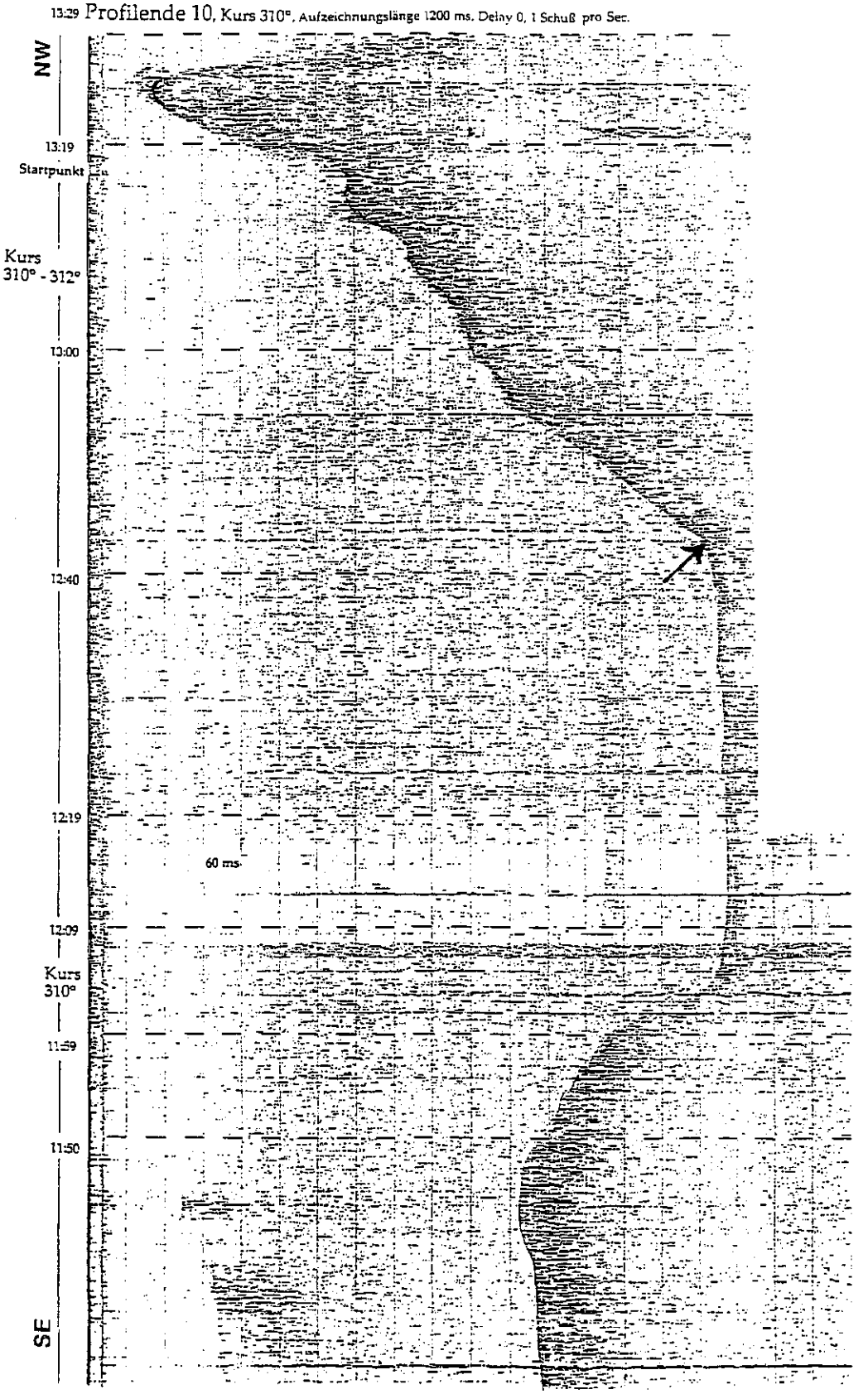

Fig. 43: Profile no. 10: A SE-NW 3,5 kHz- profile situated on the channel east of the Sanganeb Atoll. The arrow points at the sedimentary onlap of the channel infill towards the atolls base.

A relative small amount, max. 5 %, are components of biogenic origin like sponge spicules and Ascidia. The finely laminated sapropel layers are characterised by the large abundance of pteropods (*Creseis sp.*). Especially the layer between 0.96 and 0.99 mbsf is of great interest. It is located at the top of a very prominent layer, between 0.99 and 1.68 mbsf that consists of carbonate crusts. Most of the time the crusts are broken up into small chip-like fragments. This fragmentation possibly results from the coring procedure. This horizon, called the "hard layer" in the following text, can be found throughout almost the entire Red Sea and is mainly made up of high-magnesium calcite and aragonite and was deposited during the Last Glacial Maximum (LOCKE and THUNELL, 1988, p. 179-180). The origin of these carbonate crusts is still a matter of debate. Some authors describe them as being chemically precipitated (MILLIMAN 1974; LOCKE and THUNELL, 1988; BRACHERT subm.) while others prefer the diagenetic origin (STOFFERS et al., 1990).

Most of the primary sediment structures i.e. layering, are totally disturbed by bioturbation. Coarse material is mostly encountered in the bioturbation tubes that reach vertical lenghts between 2.5 cm to 10 cm. The sediment filling in the burrows is characterised by up to 2 mm large bioclasts, fragments of gastropods, oysters and sea-urchins. Through detailed analysis of the cores we expect to detect the existence of the layers containing reefal material. The presence of such material in the bioturbation tubes could show that shallow-water input occurred during certain periods of time.

M31/2-96-AW (Position: 20°53.825 N; 037°28.341 E)

The first try (Station no. 94 KL 1) to obtain a Kastenlot-core at the windward side of the Abington Reef was unsuccessful. This was due to the fact that the core catcher failed to close. Due to the tight time schedule of the scientific program the coring was not repeated immediately afterwards, because another part of the program (Station no. 95) had to be completed first. The second try (Station no. 96) was situated 1 nm from the eastern side of the Abington Reef. It was located at the distal edge of a deep at a waterdepth of 513 m (Figure 42a).

The Kastenlot-core reached a length of 5.75 m out of 6.0 m (Figure 44). Unfortunately, the top 0.25 m of sediment were lost. The characteristic "hard layer" is, thus, found at 0.25 mbsf which means that the upper probably Holocene part of the sedimentary column is missing. Reason for this might be that the coring device penetrated too deep into the sediment. Just like in Kastenlot-core M31/2-94-AL the sediment consists mainly of light greenish-gray nanno-ooze with planktonic foraminifera, pteropods and varying percentages of silt to sand-sized bioclasts and terrigenous input. Once again bioturbation has removed most of the primary sedimentary structures. However, one can still observe that the percentage of coarse material is higher in comparison with the leeward core.

The matrix is composed of nanno-ooze, in this case a mixture of coccoliths and in some parts aragonite needles. The variety of components that is found in this core is more or less the same as that observed in the leeward core. In addition, 1 mm to 3 mm large peloids occur, made up of micrite and in some parts recrystallized into secondary sparite/microsparite. Other different

components encountered are 0.2 mm to 0.3 mm large monocrystalline clasts with sharp edges. The fossil content of this core is very similar to the leeward M31/2-94-AL core. Planktonic foraminifera and pteropods are the main biota within this group. Pollen were also observed in the core, showing that some wind-blown component is present in the sedimentary record.

Unfortunately the sediments in the "hard layer" interval, between 0.0 and 0.65 mbsf, are totally disturbed due to the coring procedure meaning that the crusts are broken up into cm-sized small chips. The hard crusts are separated from each other by soft layers consisting of pteropod-rich carbonate ooze with varying percentages of carbonate clasts and bioclasts (fine sand to silt fraction).

Site 2: Sanganeb Atoll (Station no. 99)

The main targets of our research program during RV METEOR cruise 31/2 were the surroundings of the Sanganeb Atoll. Based on earlier investigations by members of our research group, including 3.5 khz-seismic survey (Figure 42c and Figure 43) and piston-core MD 921022 (RV MARION DUFRESNE 1992) we selected two transects, one on the leeward (western) and one on the windward (eastern) side of the atoll. Waterdepths at the different core locations varied between 694 m and 810 m (Figure 42b). The first two sites (S1 and Sb) were chosen without Parasound support, because the equipment was out of function. At all other sites we used the Parasound recordings to find the most ideal coring positions.

The main objectives of our studies at Sanganeb Atoll were the investigation of turbidite shallow water sheddings and their dependence on sealevel changes. On the leeward side two 6 m Kastenlot-cores (S2 and S3) were taken in the channel running parallel to the atoll, S2 in a local depression, S3 directly at the toe-of-slope (Figure 42b). The other cores were taken in the channel at the windward side of the atoll (Figure 42b, 42c and 43): S1 is situated at the channel's distal eastern margin, S4 at the channel's centre and S5, S6 directly at the toe-of-slope. The latter two are situated closer to the atoll than core MD 921022 (Figure 42b). Gravity-cores S5 and S6 were cut in 1 m pieces and stored for later studies and sampling at GEOMAR in Kiel. The Kastenlot-cores were opened directly on board of RV METEOR, described and sampled just like the cores from Abington Reef (see above).

The first analysis shows that the sediments from the cores taken at the toe-of-slope are coarser grained and contain more reef input in comparison with the more distally situated ones. The distal cores are similar to the cores taken near Abington Reef and consist predominantly of foraminifera- and pteropod-rich, greenish-gray nanno-ooze. Higher percentages of sandy intercalations are partly present containing shallow-water biota and bioclasts. These components are enriched in the bioturbation burrows. Bioclastic sand layers and water-rich sapropels are characteristically interbedded in the oozy sediments. The characteristic Red Sea "hard layer" was also found in the cores surrounding Sanganeb. This time it consisted of lithified crustal fragments mixed with "soft layers" of skeletal sands and carbonate ooze. In the

following text a short lithologic description of the individual cores is given (core profiles: see Figure 44).

M31/2-99-S1 (Position: 19°45.150 N; 037°24.704 E)
This Kastenlot-core was taken at the distal NE-edge of the channel at the seaward side of Sanganeb Atoll at a water-depth of 771 m. The distance between the RV METEOR and the lighthouse on the southern edge of the atoll was 3.54 nm when the coring device touched the bottom (Figure 42b). The recovery was 4.93 m. The upper/lower part of the core was lost, washed away, during sampling.

The sediment predominantly consists of greenish-gray periplatform ooze rich in planktonic foraminifera, different pteropod species (*Creseis* sp., *Limacina* sp. and *Clio* sp.), and bioclasts (numerous pteropod fragments and other skeletal grains). On top of the "hard layer" (0.5-1.20 mbsf) the pteropod-rich sapropelitic layer was found again. The crust is broken once again into chip-like fragments (mm to cm sized flattened pebbles) which are mixed with unlithified ooze layers. Most sedimentary structures are disturbed by bioturbation resulting in a mottled texture with distinct burrows.

M31/2-99-Sb (Position: 19°43.789 N; 037°24.704 E)
This core was taken from the centre of the channel 1.75 nm west of lighthouse Sanganeb, at 810 m waterdepth (Figure 42b). The Kastenlot-core itself was bent during coring (probably at the "hard layer"). For that reason the recovery is just 75 cm. The sediment is of planktonic foraminifera- and pteropod-bearing carbonate ooze.

M31/2-99-S2 (Position: 19°45.894 N; 037°24.797 E)
This core was taken at a local depression in the channel 1.38 nm west of lighthouse Sanganeb. Waterdepth was 810 m at this site (Figure 42b). The recovery of this core is 4.60 m. The sediment composition is similar to that of S1. From 2.15 mbsf downwards dark, water-rich, 2-cm thick sapropels are intercalated irregularly with the carbonate ooze. Surrounding sediments are worked into the sapropels by bioturbation. Due to bioturbation both sediments are reworked resulting in blurred sedimentary boundaries. From 4.0 mbsf downcore bivalve shells were abundant.

M31/2-99-S3 (Position: 19°44.321 N; 037°29.143 E)
This core was located directly of the atolls western toe-of-slope. Distance to Sanganeb lighthouse was 1.37 nm. Waterdepth was 757 m (Figure 42b). Core recovery was 4.47 m. The sediments of this core consist of sandy layers of reef detritus intercalated with the periplatform ooze and the "hard layer". The sapropel usually found on top of the "hard layer" is missing in this core. Instead a mm-laminated fine-sand is present. The "hard layer" itself (0.11-1.20 mbsf) is intercalated with coarse, sometimes graded turbidites (see Figure 45) consisting of bioclastic reef detritus (coral, hydrozoan, bryozoan and algal-fragments). The base of the "hard layer" (1.16-1.20 mbsf) is marked by a lithified skeletal-sand. This skeletal grainstone is broken into mm- to cm-sized chips partially mixed with "normal" crustal fragments.

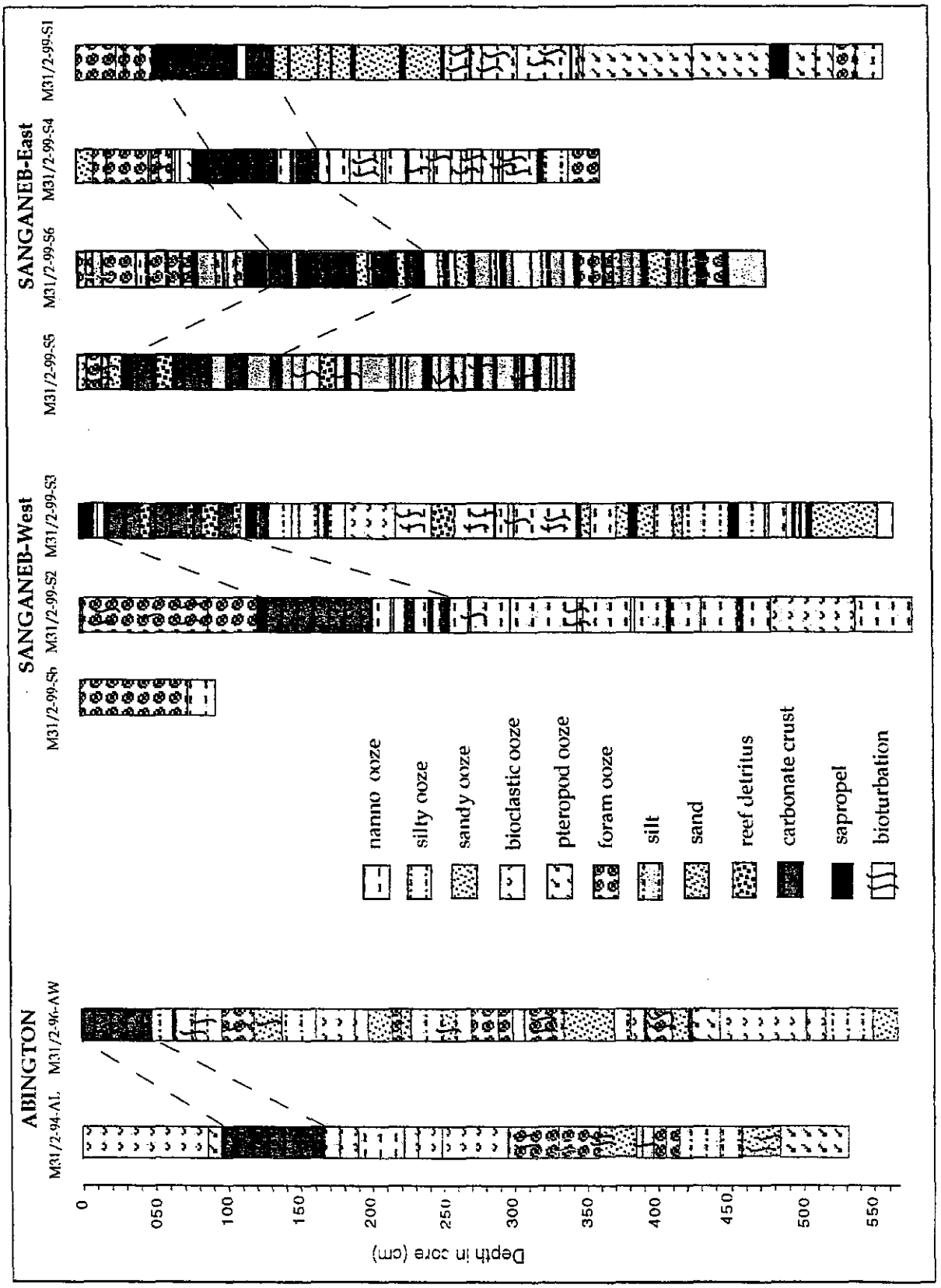

Fig. 44: Core lithology Abington Reef and Sanganeb Atoll.

The sediment below the "hard layer" consists of greenish-gray, silty to fine-sandy carbonate ooze alternating with (a) cm-thick lithified layers, (b) sapropels and (c) turbidite layers (like above; Figure 45).

Remarkable is a 5 cm thick, light white-greyish layer of very well-sorted silt and fine-sand at 3.27 mbsf. A bivalve of the genus *Caspidaria* has been identified in this layer. Most of the primary sedimentary structures have been destroyed by bioturbation which led locally to distinct dark-light colour bending. Many burrows are stuffed with coarser sediment (skeletal grains, pteropods) in comparison with the surrounding matrix. Some burrows have been identified as traces of the genus *Chondrites*.

M31/2-99-S4 (Position: 19°44.614 N; 037°29.143 E)
This core was taken from the centre of the channel east of the Sanganeb Atoll at a distance of 2.76 nm and at a waterdepth of 762 m (Figure 42b). This 9 m Kastenlot-core was bent during coring resulting in the low sediment recovery of 3.20 m. The sediment composition is similar to that found in core S1 and S2. The sapropel on top of the "hard layer" is not laminated in S4. The pteropod species *Clio pyramidata* is very abundant in the oozy sediments and the "hard layer".

M31/2-99-S5 (Position: 19°43.910 N; 037°27.626 E)
and S6 (Position: 19°44.566 N; 037°27.968 E)
At these positions gravity-cores instead of Kastenlot-cores were taken primary because of low sediment recovery of the Kastenlot-cores and secondary because of shortening of the working time resulting from changes in the ship's time schedule. The piston-cores were taken from the toe-of-slope at about 1.2 and 1.8 nm. east of lighthouse Sanganeb at 694 m and 744 m waterdepth respectively (Figure 42b). The plastic liners of these cores were cut in 1m tubes and stored. They were opened, described and sampled at GEOMAR in Kiel after the cruise.

M31/2-99-S5
The recovery of this 6 m piston core was 3.40 m. The sediment above the "hard layer" is of open marine character, consisting of greenish-gray, strongly bioturbated, foraminifera-rich, pteropod-bearing nanno-ooze with some bioclastic input. The sapropel layer on top of the crust is developed like in cores S1, S2 and S4. The "hard layer" reaches from 0.37 to 1.40 mbsf and consists of mixed layers of lithified crust (broken into chips by coring) and unlithified coarse skeletal sands. The skeletal grains of both sediments consist of reef derived shallow water components, like coral-, algae- and bryozoan fragments and benthic foraminifera. The sandy layers (soft and hard) are mixed with slightly sandy to silty ooze. The sediments below the "hard layer" are rich in bioclastic and reef derived components. Layers of coarse skeletal sands are intercalated in the strongly bioturbated sandy (bioclasts-, foraminifera- and pteropod-bearing) nanno-ooze.

M31/2-99-S6
The sediment recovery of this core was 477 cm. The sediment composition of S6 is similar to S5. The sediments in S6 are slightly finer grained. In the upper nanno-ooze interval that ranges

from 0 to 1.26 mbsf a distinct layer (0.83-0.96 mbsf) consisting of inverse graded, coarse skeletal sands was observed. The "hard layer" is equally developed like the one found in core S5. It reaches from 1.26 to 2.40 mbsf. Below the "hard layer" a zone consisting of sandy ooze and partially graded skeletal sands was found (2.40-2.95 mbsf). The deeper parts of the core are made up of green-greyish, fine-sandy to silty nanno-ooze, with varying percentages of bioclasts and planktonic components (foraminifera are dominant). Sapropel layers are often intercalated in the strongly bioturbated sediments.

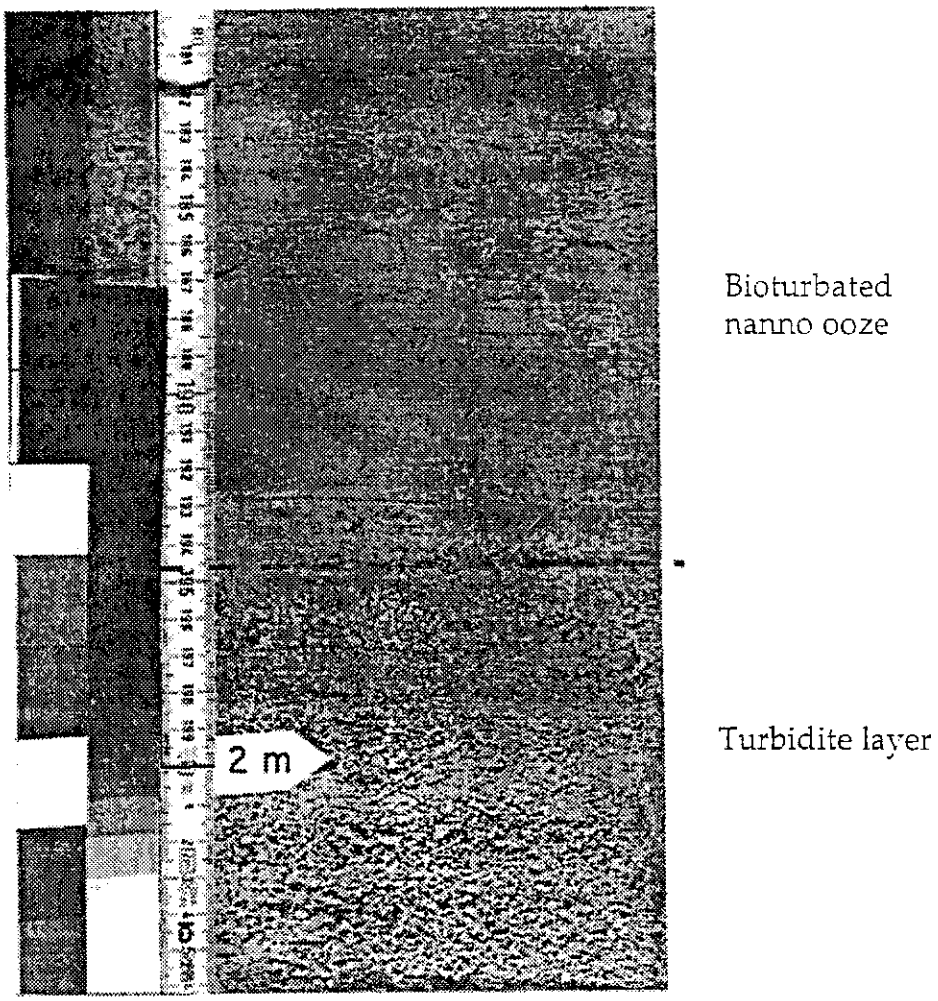

Fig. 45: Image of a turbidite layer in core M31/2-99-S3.

5.2.4.2 Hydrothermal Activity and Volcanic Activity in the Northern Red Sea

(P. Stoffers, M. Fey, W. Plüger, H. Puchelt, J. Scholten)

The distribution and occurrence of hydrothermal activity in the Shaban and in the Kebrit Deep was investigated during METEOR 31/2 cruise by means of sediment coring, GTV observations and dredging.

Sediments

In the Shaban Deep sediments were sampled in the four basins using 6 to 8 m long kasten cores and 12 m long piston cores (Figure 46-47). An attemp of sampling surface sediments by means of giant grab corer failed because the sediments were too soft and liquid.

Two kasten cores (17005-1, 17003-2) were positioned in the NW-basin, one core (17000-3) in the NE-basin, four cores (17001-2, 17004-1, PC 17008-1; PC 17009-3) in the SE-basin and one core (17002-2) in the SW-basin. At some stations (17001-2,17003-2, 17005-1,17004-1, PC17008-1) very stiff sediment layers and/or basaltic basement prevented the kasten and picton corer from penetrating deeper into the sediment column.

All kasten cores were opened on-board METEOR. Immediately after the cores were opened, sediments were sampled for pore water extraction using N_2 filled 50 ml Falcon tubes. The tubes were centrifugated and the pore water was filtered (0,2 µm nuclepore filters) in a N_2 filled chamber. The remaining solution was acified and stored in pre-cleaned 10ml containers. Photos were taken from all cores and a core description was done based on Munsell Color Chart. Sediment cores were sampled in 10 cm intervals using 10 ccm syringes. Extra samples were taken from hydrothermal layers, organic rich layers and diagenetic hard layers.

Generally the sediments in the Shaban Deep consist of olive gray mud with distinct layering. These layers vary in their composition according to the carbonate and biogene silica content. Organic rich layers sometimes containing thin calcareous hard layers occur in cores from the SW- and SE-basin. These layers are probably of diagenetic origin. Very stiff sediments with petroleum odor were observed in core PC17008-1 (550 cm to base). Indications of fluids, which may have penetrated the sediments, can be observed in core 17001-2. Here, small veins occur which vertically cross the sediments.

Although all cores were retrieved from a relatively small area in the Shaban Deep and sediment stations were sometimes situated not more than a few miles from each other, a stratigraphic correlation between the cores based on characteristic sediment sequences was not possible. For instance, the four cores retrieved from the SE-Basin show only in their upper parts similar sediment sequences of laminated diatomacous mud. Further similarities in deeper core section were not observed.

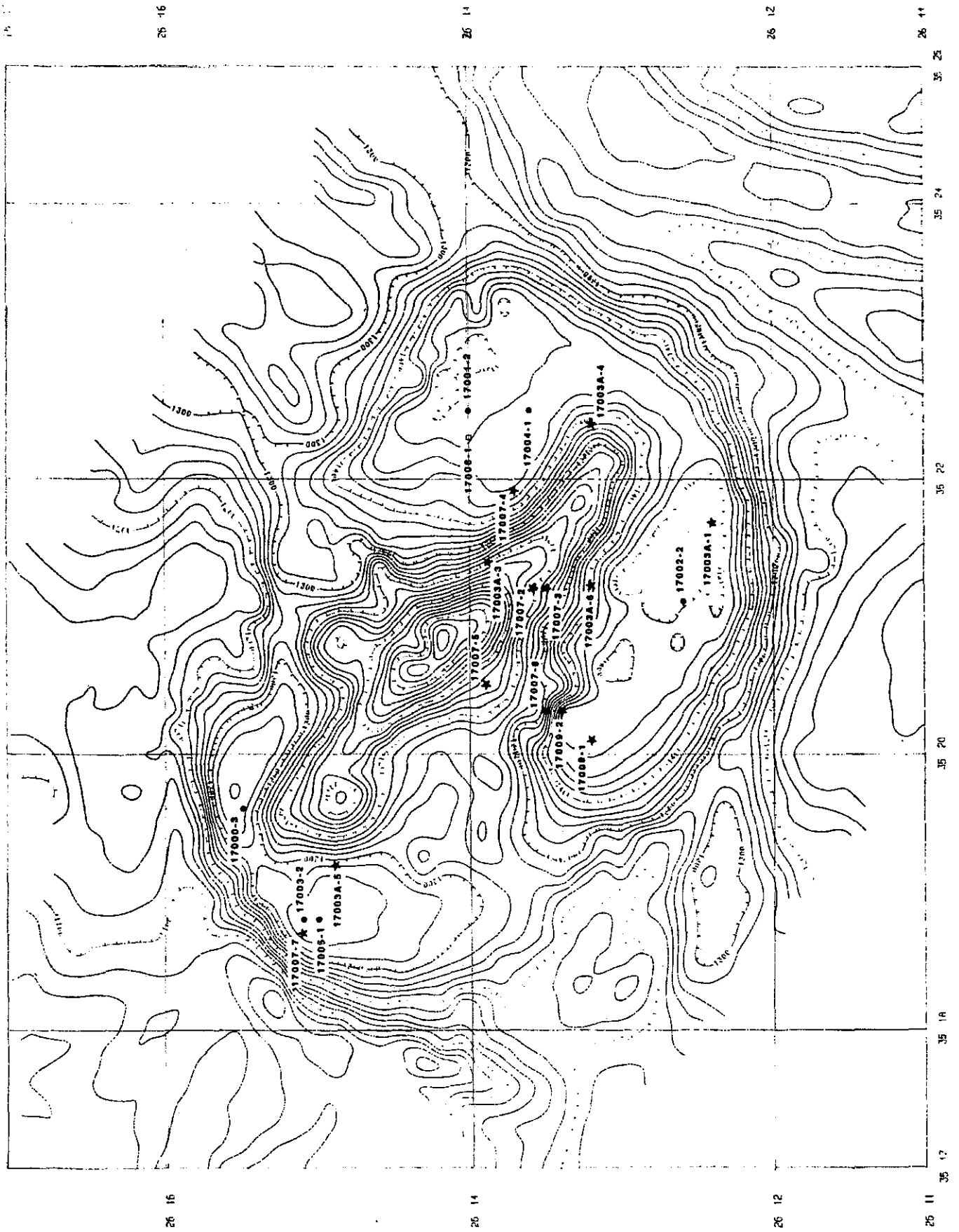

Fig. 46: Bathymetry of the Shaban Deep; filled dots: locations of kasten corer; open squares: locations of piston-corer; asterisks: locations of dredge stations (first bottom contact).

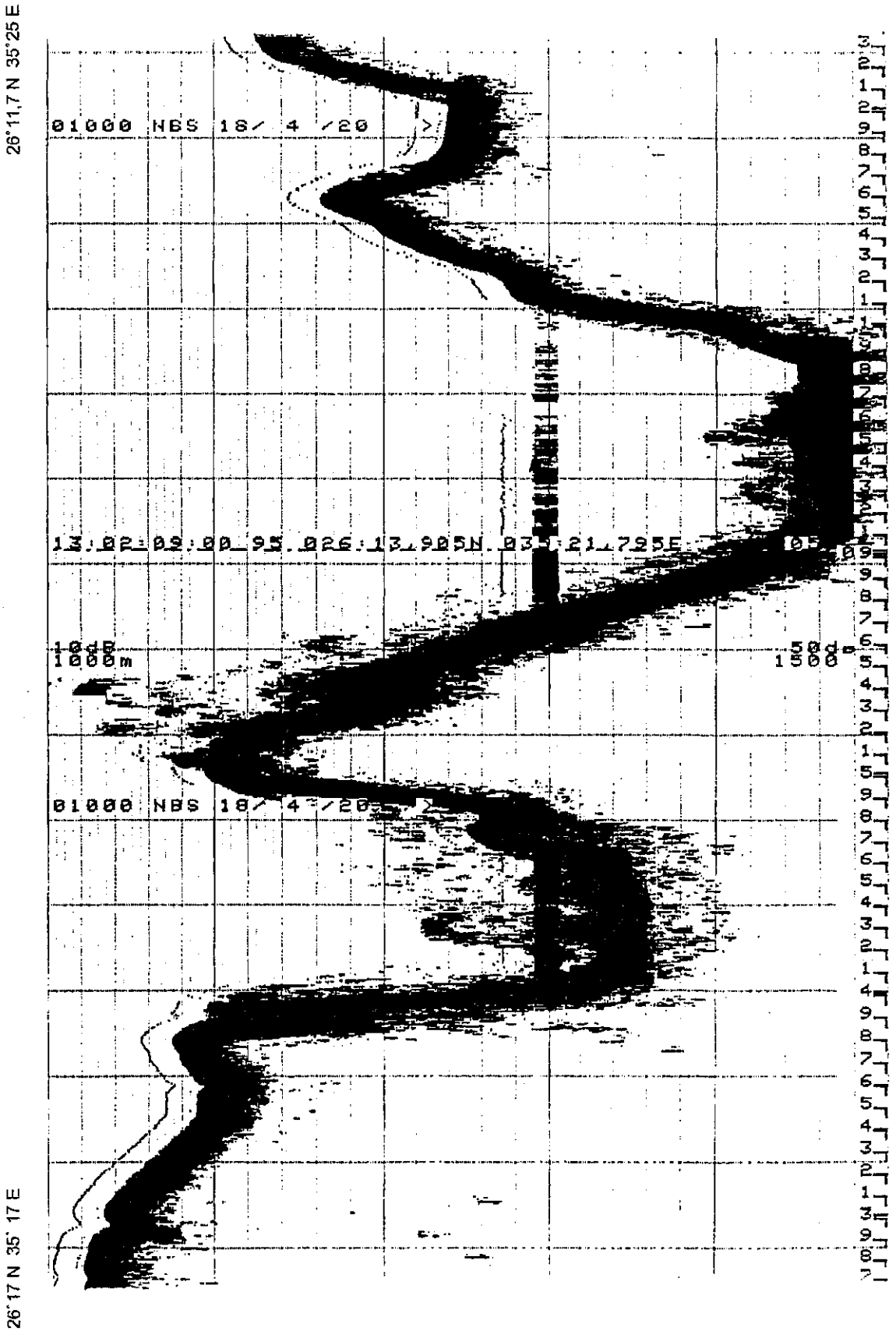

Fig. 47: 3,5 khz profile across the NE- and SE-basin of the Shaban Deep; the horizontal reflector indicates the surface of the brine pool.

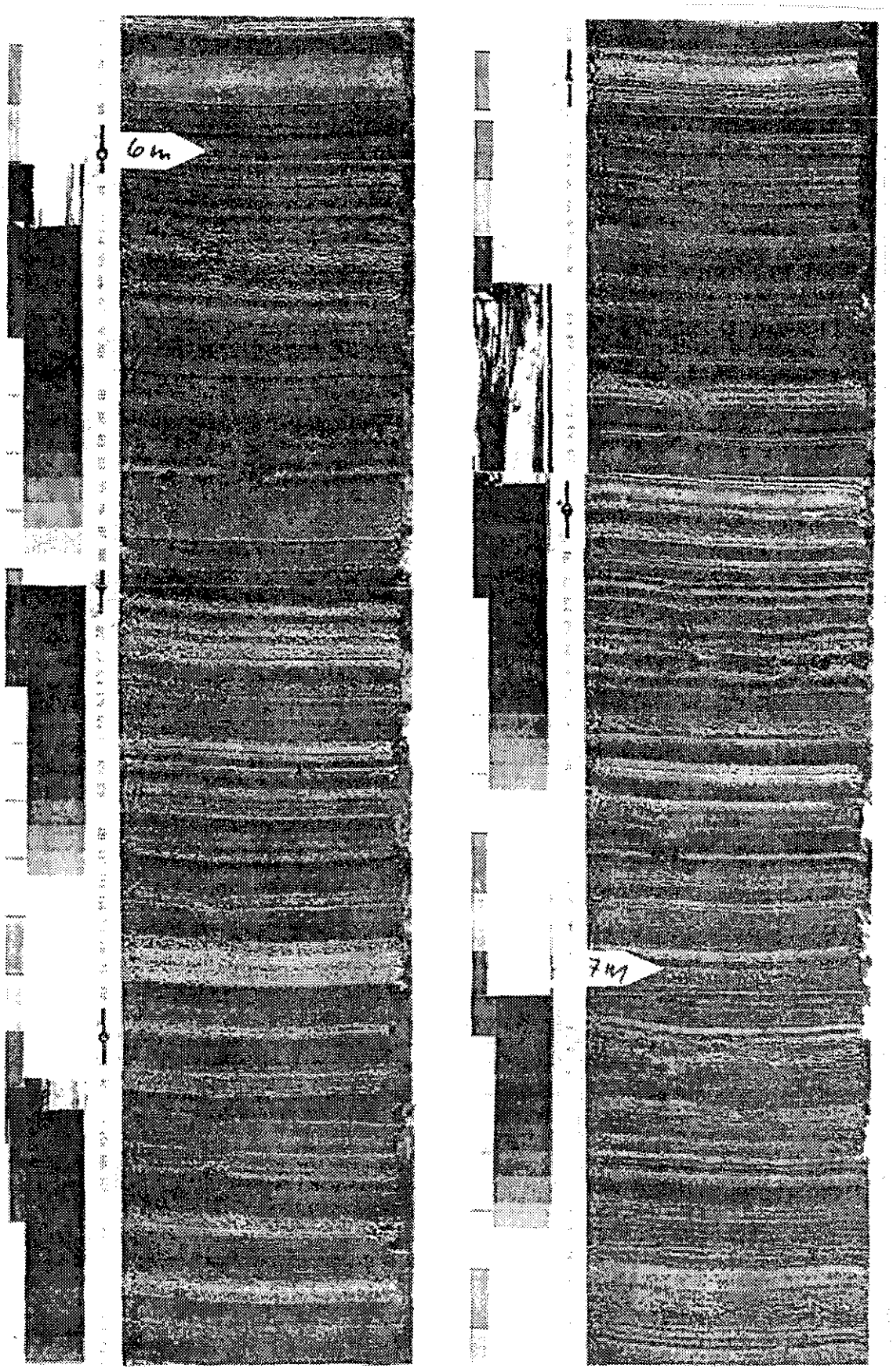

Fig. 48: Image of core 17002-2 (594-717cm) showing laminations of diatom oozes and organic rich oozes.

This is partly due to turbidites, which occur frequently in these sediments. In addition sediment stratigraphy in core PC 17009-3 was destroyed by coring.

Core 17002-2 from the SW-basin is believed to be the core where sedimention in the Shaban Deep is best preserved (Figure 48). The very fine layering of diatom oozes and calcareous oozes will allow detailed investigations of the sedimentation and climate history of the northern Red Sea.

Indications of hydrothermal activity in the Shaban Deep could only be detected in two cores from the NW- (17000-3) and NE-basin (17005-1). They consist of limonitic layers in core 17000-3 (480-490 cm) whereas in core 17005-1 a red staining of the sediments can be observed at the base of the core.

In the Kebrit Deep two sediment cores were retrieved (Figure 49). One core (17006-5) was positioned in the center, the other (17010-2) at the rim of the Deep. Very soft and liquid surface sediment were sampled from the deep basin with a giant boxcorer (17006-4).

From about 190 cm to the base of core 17006-5 sediments were very homogeneous consisting of calcareous ooze. In contrast the composition of the upper part of the core is very variable, and fine laminations of calcareous oozes can be observed. The changes of the sediment facies between the lower and the upper parts of the core is believed to be due to formation of the brine pool in the Kebrit Deep. The brine will allow an anoxic environment to develop in the basin. Thus, sediments will be deposited having a more grayish-green color. More detailed investigations of the sediment composition and pore water analyses will reveal the timing and extend of brine formation in the Kebrit Deep. The only indications of hydrothermal mineralisations occur between 110-125 cm in this core. In the view of the widespread occurences of massive sulfides in the Kebrit Deep (see below) it is quite surprising that so little indications of hydrothermal activity are preserved in this sediment core.

According to the yellowish sediment color hydrothermal sediments are deposited in core 17010-2 which was positioned in the area of massive sulfide occurrences.Similiarly to core 17006-5 it is composed of a more homogeneous sediment section in its lower part and more variable in the upper. Gas bubbles and gas inclusions are common features in this core.

The hydrothermal sediments occurring in the Atlantis II Deep are much more concentrated compared to other basins in the Red Sea. One core (17015-2) was positioned in the W-basin of the Deep and recovered beautifully coloured sediments. According to the lithostratigraphic zones previously described from the Atlantis II Deep (BÄCKER and RICHTER, 1973), the sediments can be devided in to an upper amorphous and sulfidic facies (0-326 cm) followed by a thick central oxidic zone (326-842 cm). The lower part is again composed of a sulfidic facies (Figure 50).

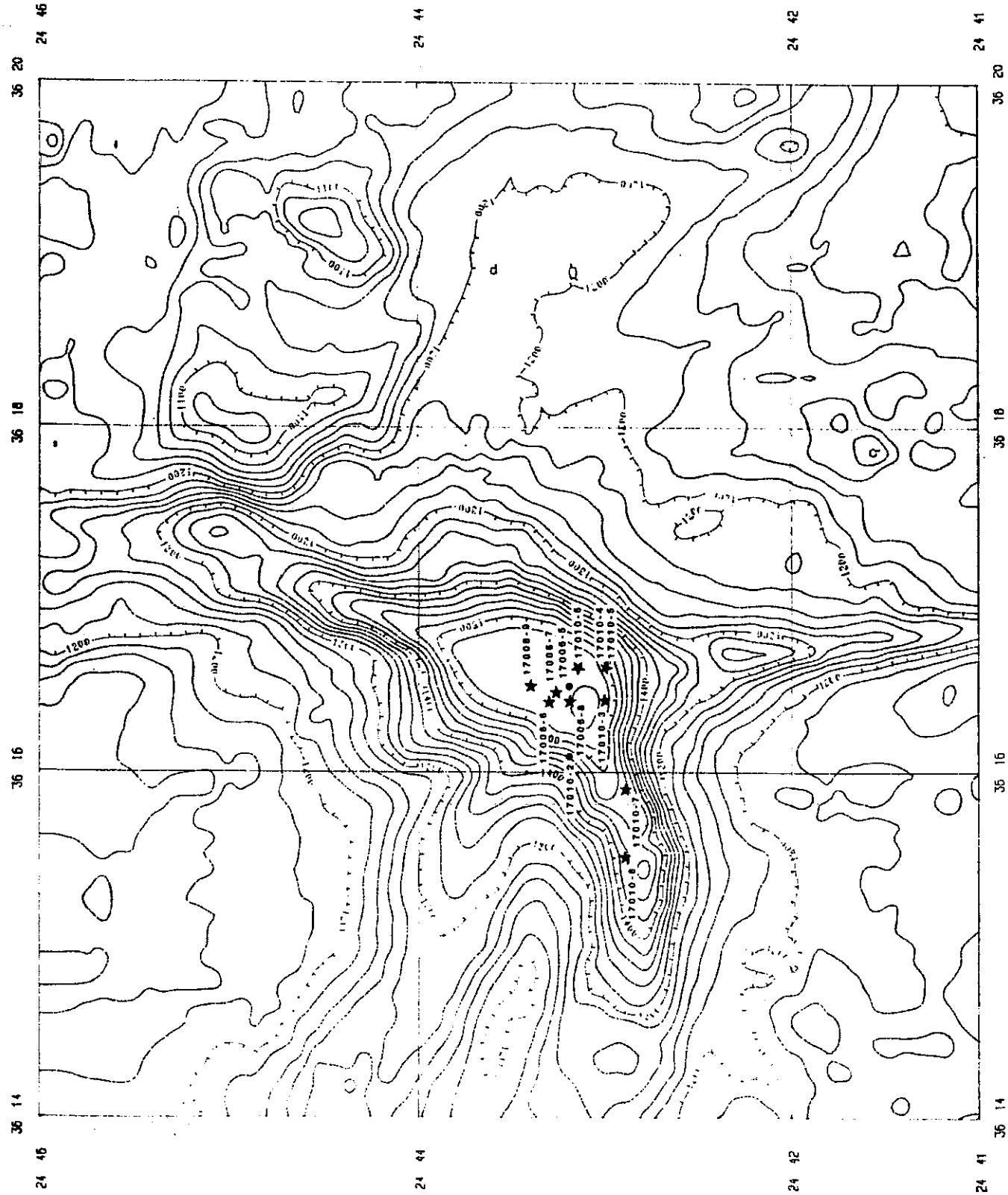

Fig. 49: Bathymetry of the Kebrit Deep; filled dots: locations of kasten corer; asterisks: locations of dredge stations (first bottom contact).

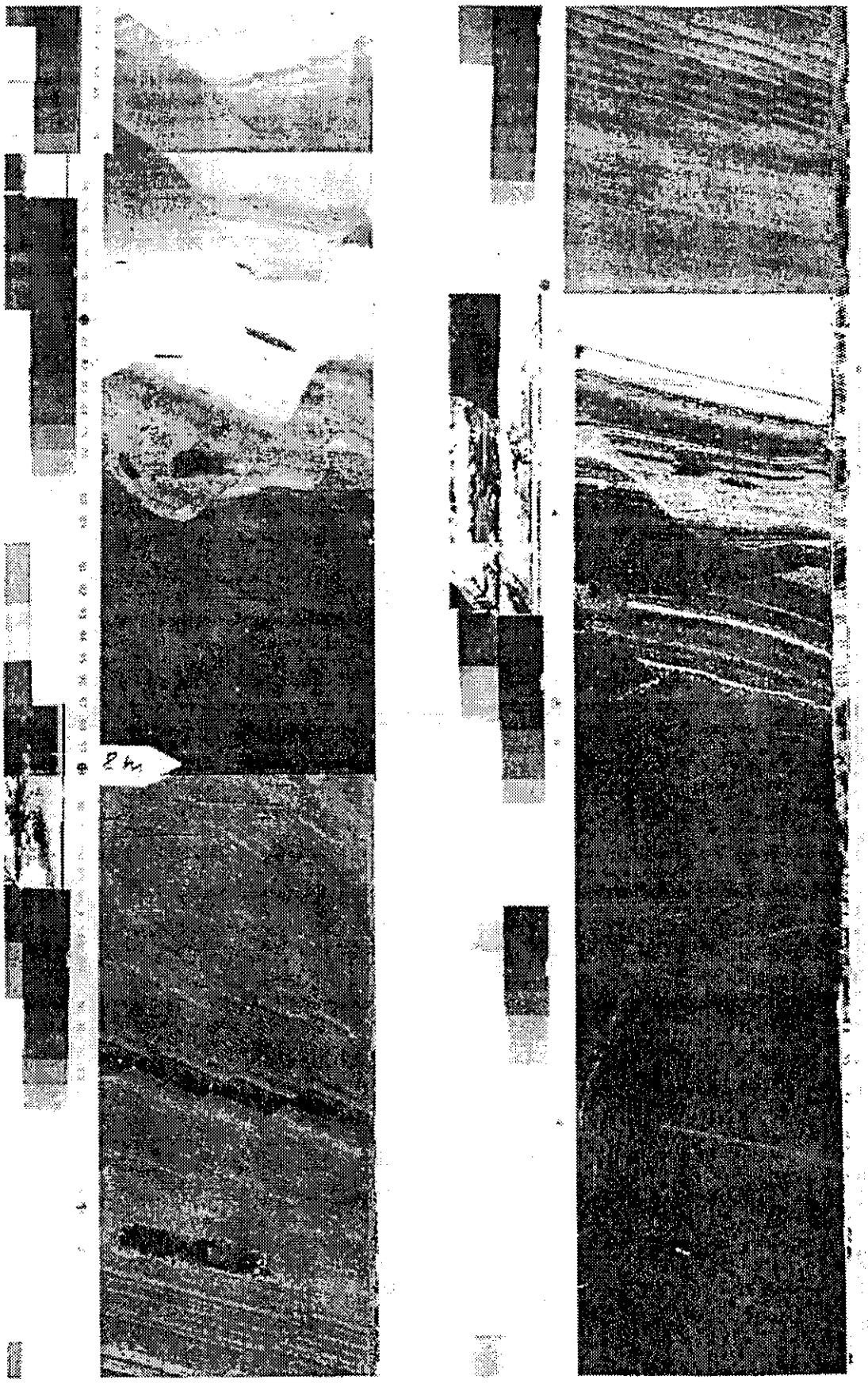

Fig. 50: Image of core 17015-2 (765-890 cm) showing the transition of the central oxidic facies (red colours) to the sulfidic facies.

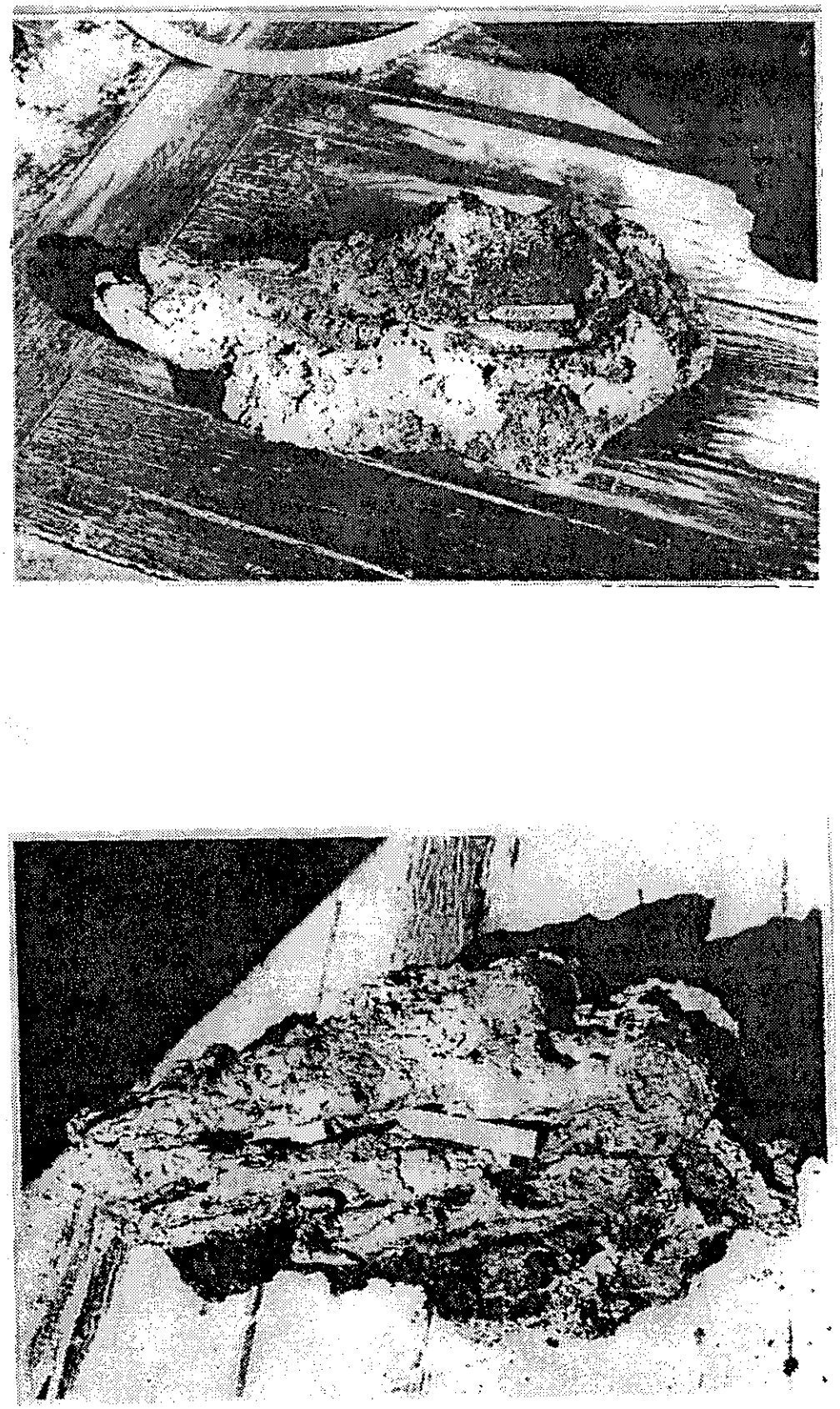

Fig. 51: Image of massive sulfides (Station 17006-7; length of marker is 10 cm).

Massive Sulfides

During SONNE 29 cruise (1984) massive sulfides were found in the Kebrit Deep. Their distribution was investigated in detail during METEOR 31/2. Intensive dredging at the eastern and the western flanks of the basin recovered more than 200 kg of porous and scoriaceous massive sulfides (Figure 51). It turned out that the sulfides only occur above the brine pool at the western side of the basin in a narrow zone (about 30 width). They stick out of the sediments like isolated chimneys or lie on the sediments as plates. Sometimes the sulfides form veins surrounded by (stiff) sediments. In mineralogical terms they consist mainly of pyrite and sphalerite and were partly soaked with an oil-like substance. Apart from sulfides, carbonate crusts and fist-sized gypsum crystals were dredged from the Kebrit Deep. Only one dredge from the Shaban Deep (17009-1) recovered massive sulfides. These sulfides were found within a sediment matrix forming veins comparable to the deposits observed in the Kebrit Deep. They consist mainly of pyrite.

Volcanic Rocks

Volcanic rocks, all originating from the Shaban Deep, Red Sea (Figure 42), were recovered during the course of stations 91, 88, 92 und 102 of the METEOR cruise 31/2 (7.2.4). Most rock samples are comparatively small (< 5 cm in diameter). Sample M31/2-81 DR-1-3 and D-1-4 consist of sheet flow lava with more than 10 cm length. Sample M31/2-88 PC, recovered by a piston corer, constitutes a glass-breccia cemented by a fine-grained glassy matrix. The volcanic rocks are mostly vesicular. Vesicle contents average at 10 vol.- % but occasionally are much higher (M31/2-88 GTV and D-2). As a result of rapid cooling of lava at the contact with seawater, glassy rims of up to 15 mm thickness (M31/2-81 DR-1-4, M31/2-88 DR-2) have been developed at pillow fragments. Most samples display glass in the groundmass.

Most Shaban Deep volcanics, with the exception of M31/2-88 DR-3, contain phenocrysts up to 10 mm in size, of plagioclase, olivine and sometimes clinopyroxene. The glass-breccia (M31/2-88 PC) is virtually unaltered. Most other samples are more or less palagonitized. Palagonite is seen as a red alteration product (3 mm thickness) affecting the outer part of the glassy rim. Besides palagonite, carbonate mineralizations fill vesicles (M31/2-88-DR-2). Sample M31/2-81-DR-1-1 is a porous volcanic rock displaying abundant smectitic crusts of various colours. M31/2-88-GTV is covered by a manganese crust up to 4 mm thick. Most samples show palagonite rims, covered by a biogenic carbonate "hard ground" on which *serpulidae* have settled (M31/2-88-DR-3). Incrustation of foraminiferal marl is seen only on M31/2-88 DR-3.

Red Sea Pos.: 26°15.5N 35°19.6E

Core No.: 17000-3 Corelength: 558cm Waterdepth: 1290m

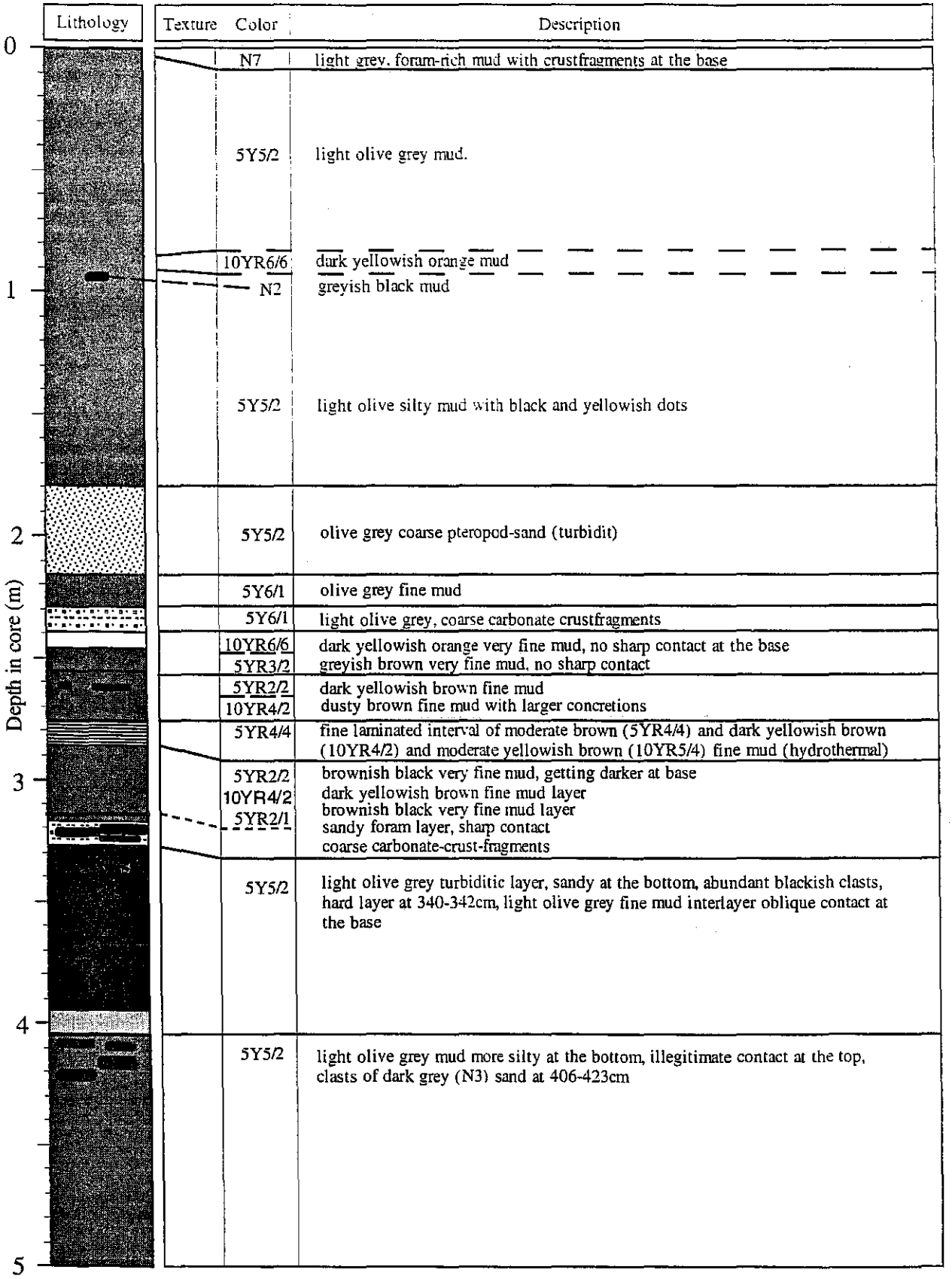

Fig. 52a: Core 17000-3: core description.

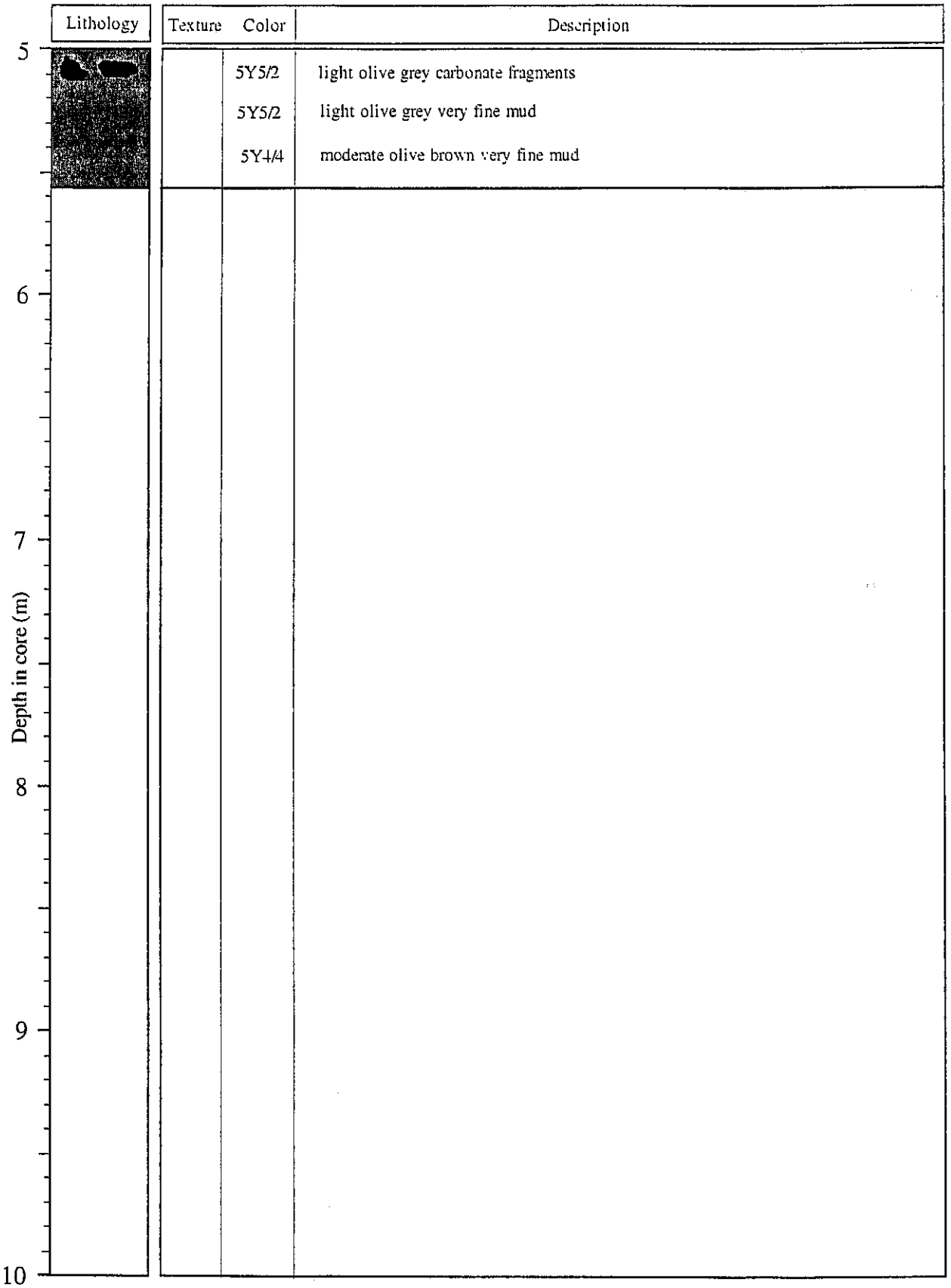
Lithology
Texture
Color
Description
5Y5/2
light olive grey carbonate fragments
5Y5/2
light olive grey very fine mud
5Y4/4
moderate olive brown very fine mud
Depth in core (m)
5
6
7
8
9
10

Red Sea Shaban Deep SE-Basin Pos.: 26°12,6N 35°21,1E

Core No.: 17001-2 Corelength: 560cm Waterdepth : 1354m

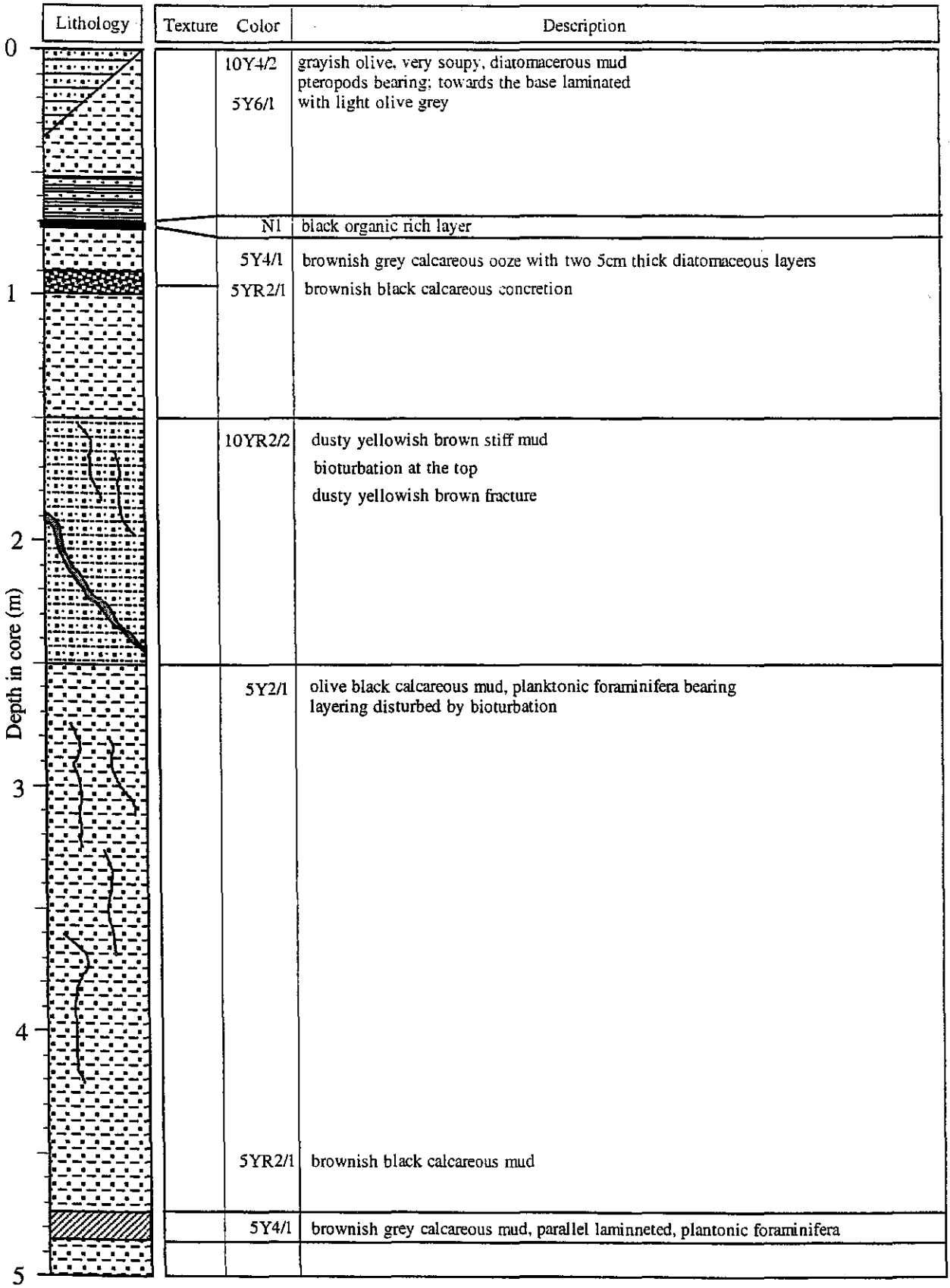

Fig. 52b: Core 17001-2: core description.

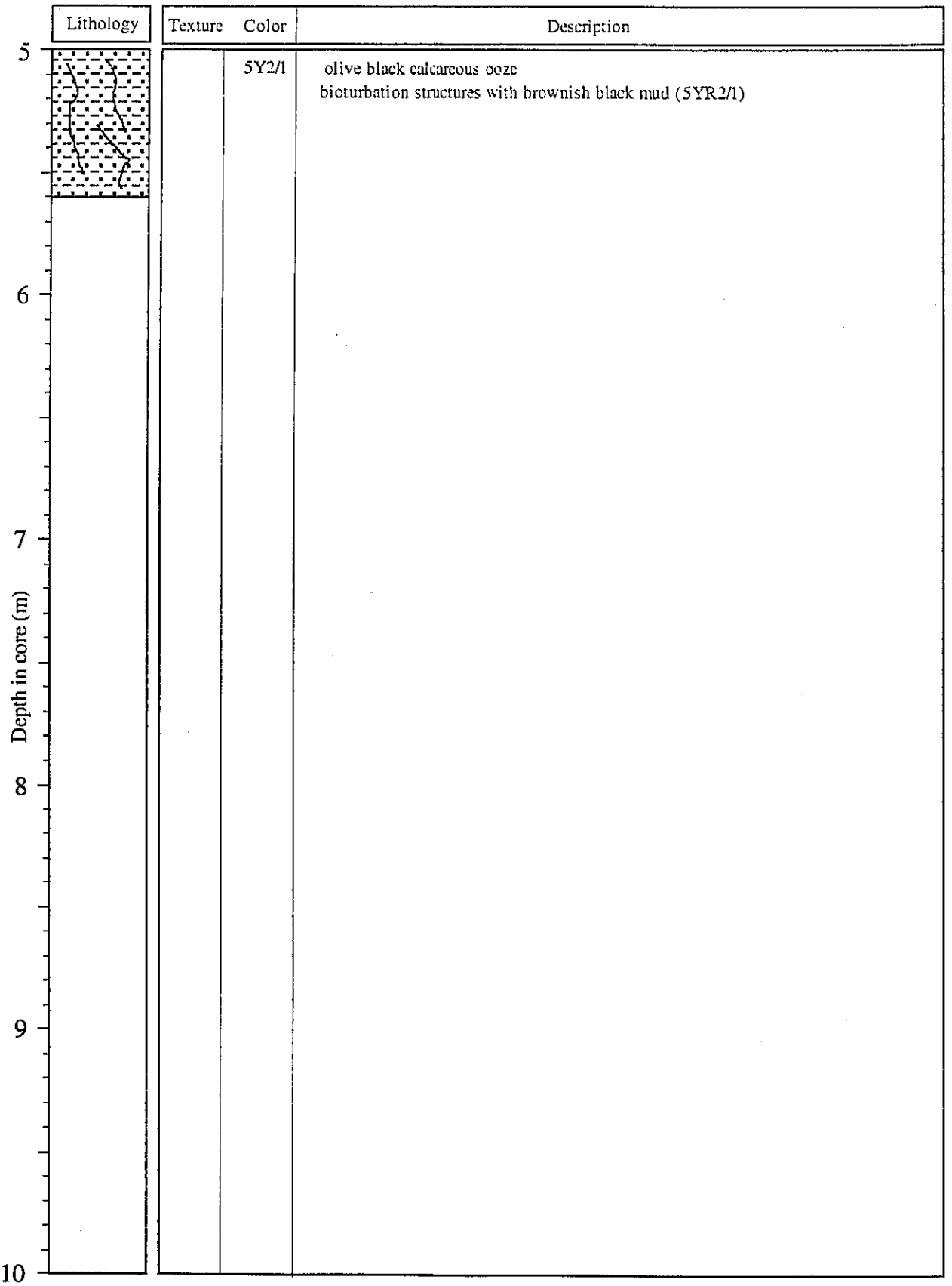
Lithology
Texture
Color
Description
5Y2/1
olive black calcareous ooze
bioturbation structures with brownish black mud (5YR2/1)
Depth in core (m)
5
6
7
8
9
10

Red Sea Shaban-Deep SW-Basin Pos.: 26°12,6N 35°21,1E

Core No.:17002-2 Corelength :851cm Waterdepth : 1549m

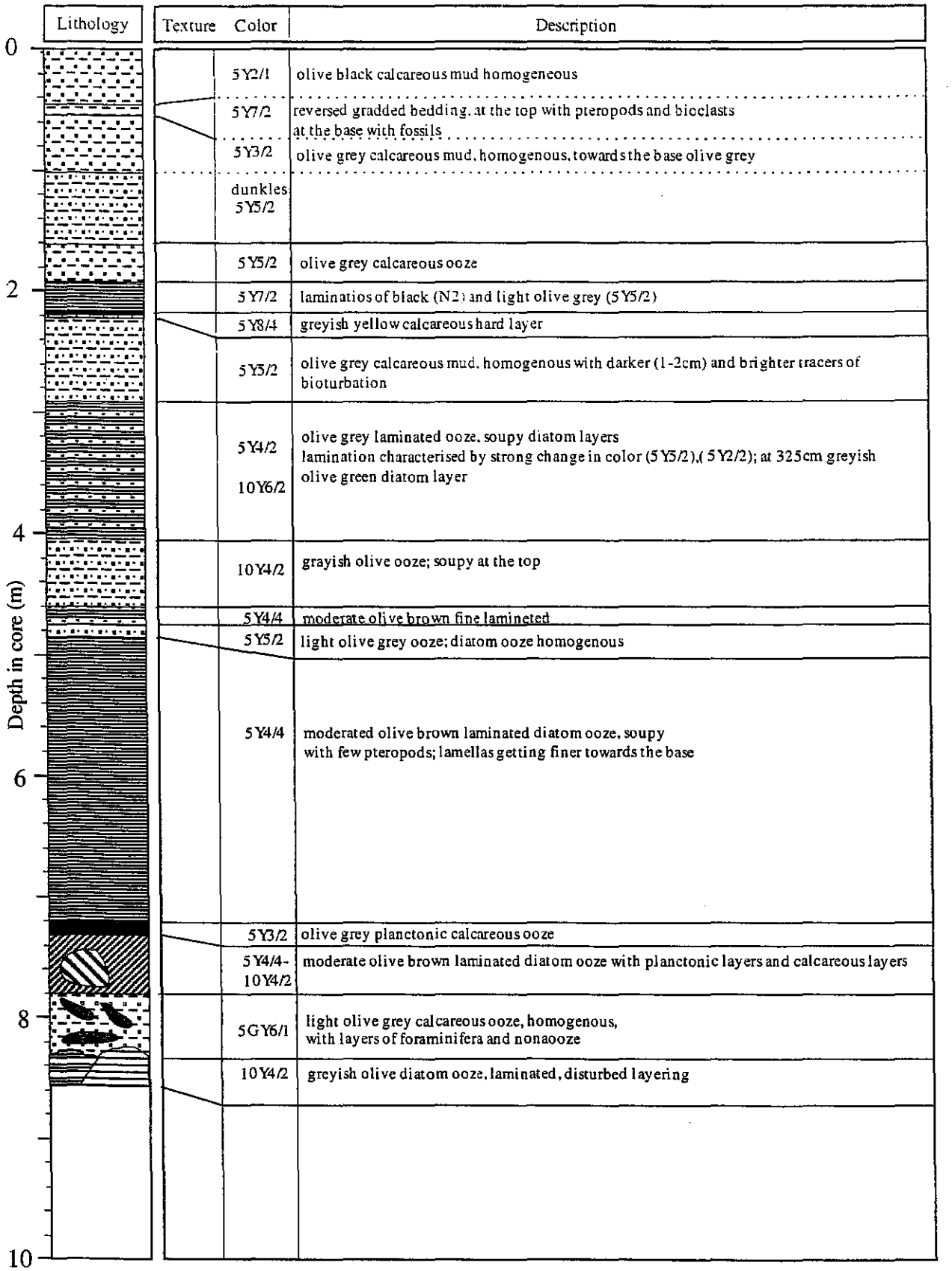

Fig. 52c: Core 17002-3: core description.

Red Sea Shaban-Deep NW-Basin Pos. : 26°15,1N 35°18,8E

Core No.: 17003-2 Corelength: 298cm Waterdepth: 1362m

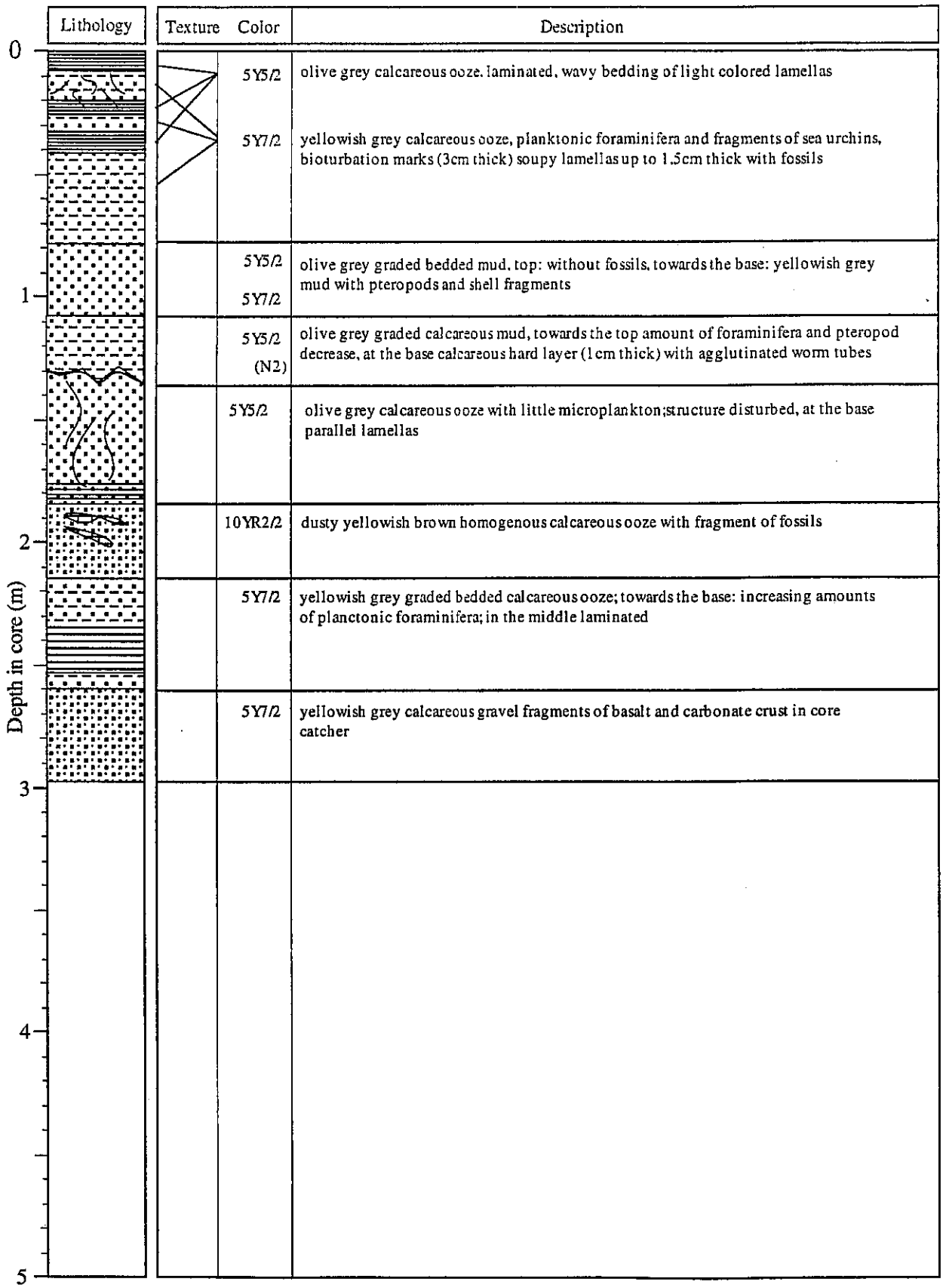

Fig. 52d: Core 17003-2: core description.

Red Sea Shaban-Deep SE-Basin Pos. :26°13,6N 35°22,5E

Core No.: 17004-1 Corelength: 200cm Waterdepth: 1447m

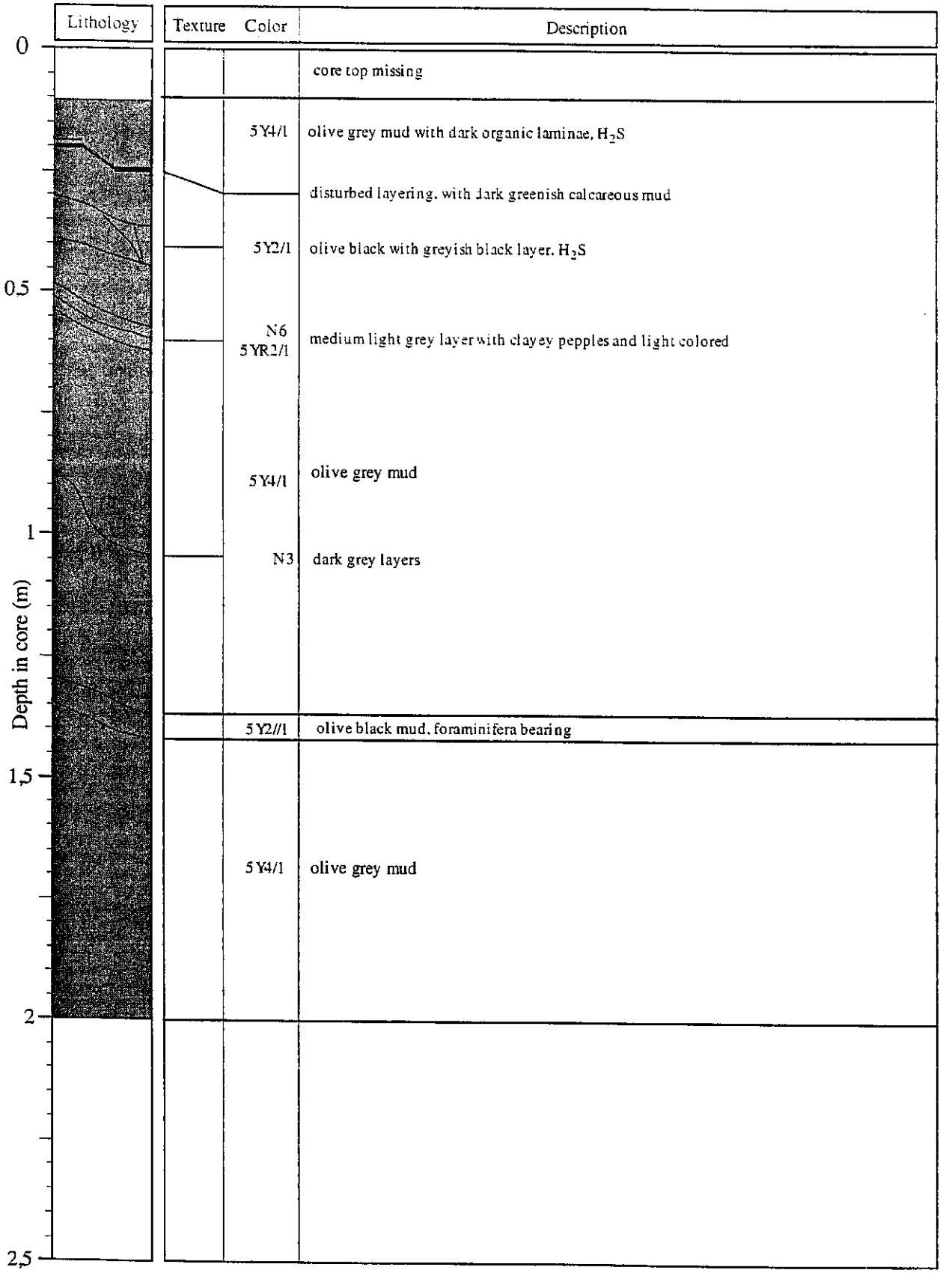

Fig. 52e: Core 17004-1: core description.

Red Sea Shaban Deep NW-Basin Pos. : 25°15N 35°18,8E

Core No.: 17005-1 Corelength: 200cm Waterdepth : 1390m

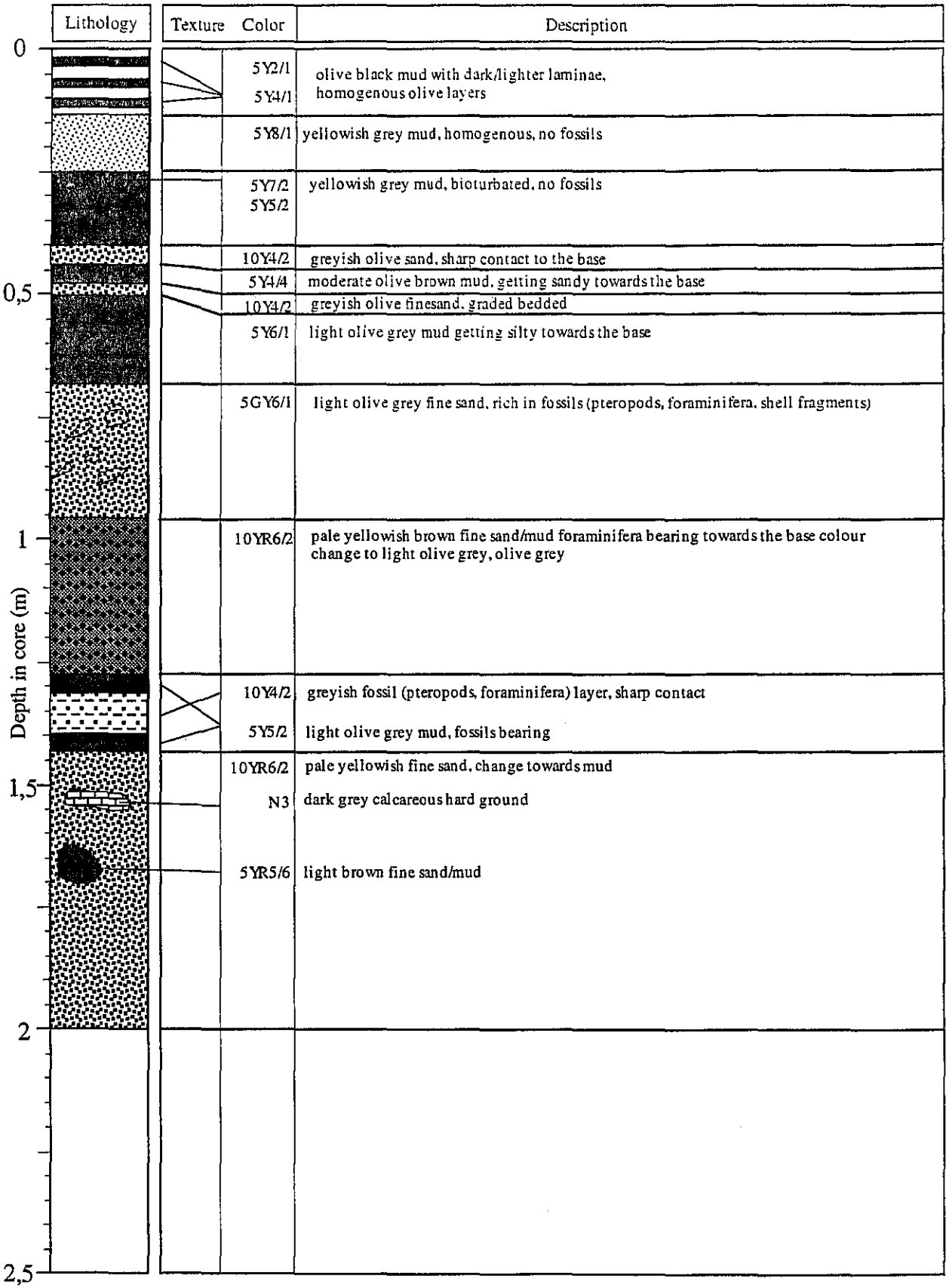

Fig. 52f: Core 17005-1: core description.

Red Sea Kebrit-Deep Pos. : 24°43,2N 36°16,5E

Core No.: 17006-5 Corelength: 1000cm Waterdepth : 1567m

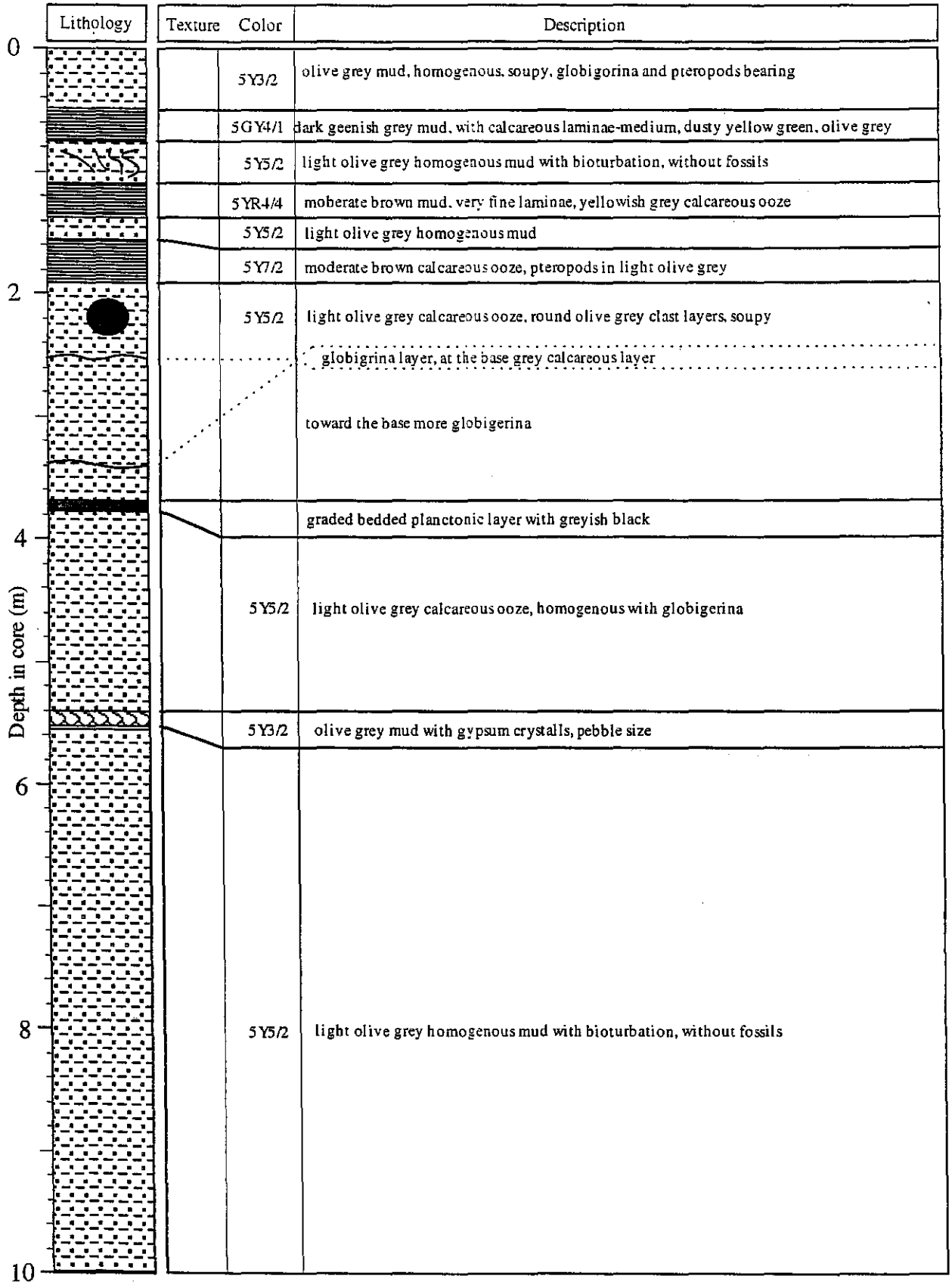

Fig. 52g: Core 17006-5: core description

Red Sea Pos.: 26°14.0N 35°22.3E

Core No.: 17008-1 Corelength: 578 cm Waterdepth: 1441m

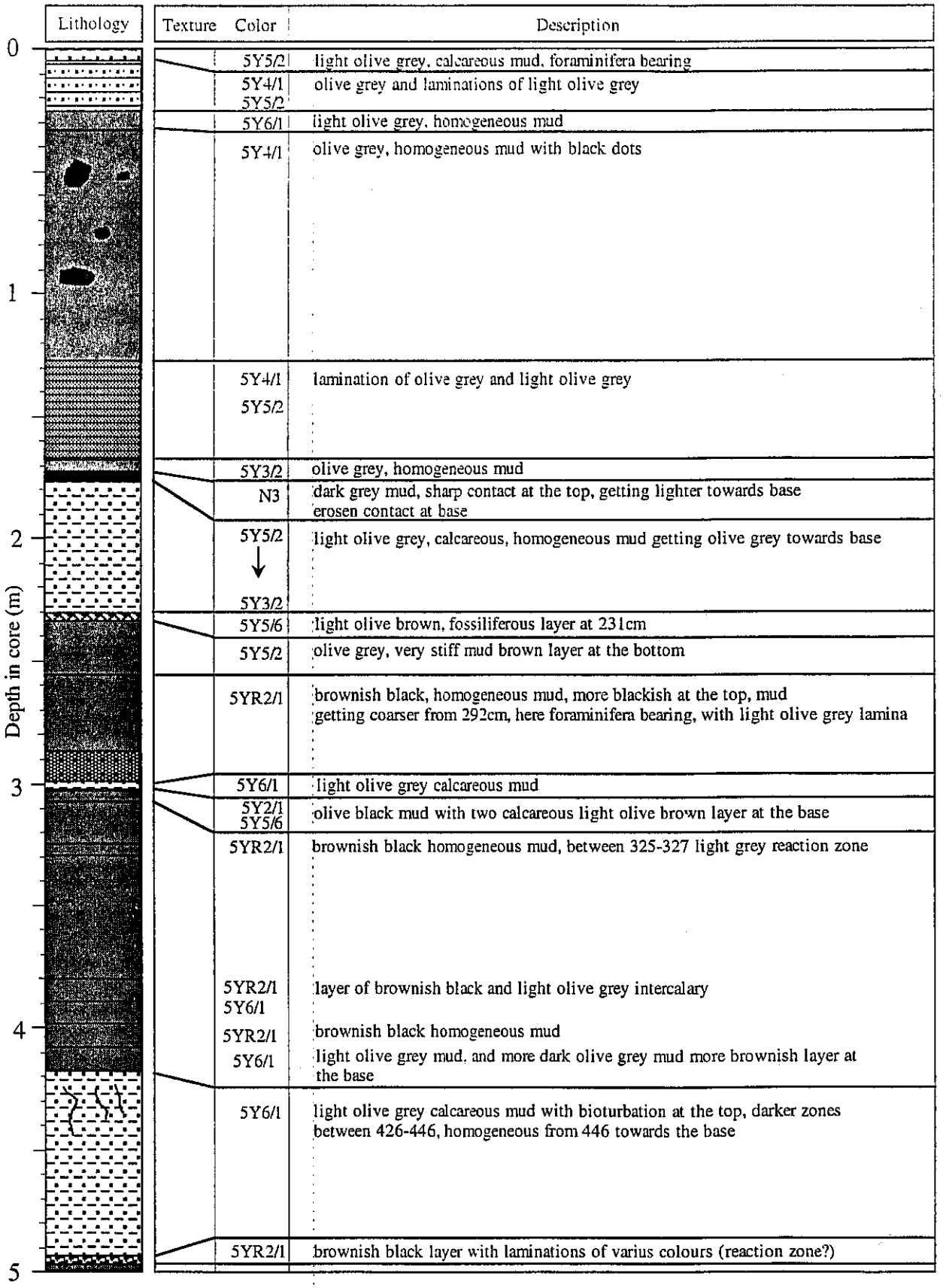

Fig. 52h: Core 17008-1: core description.

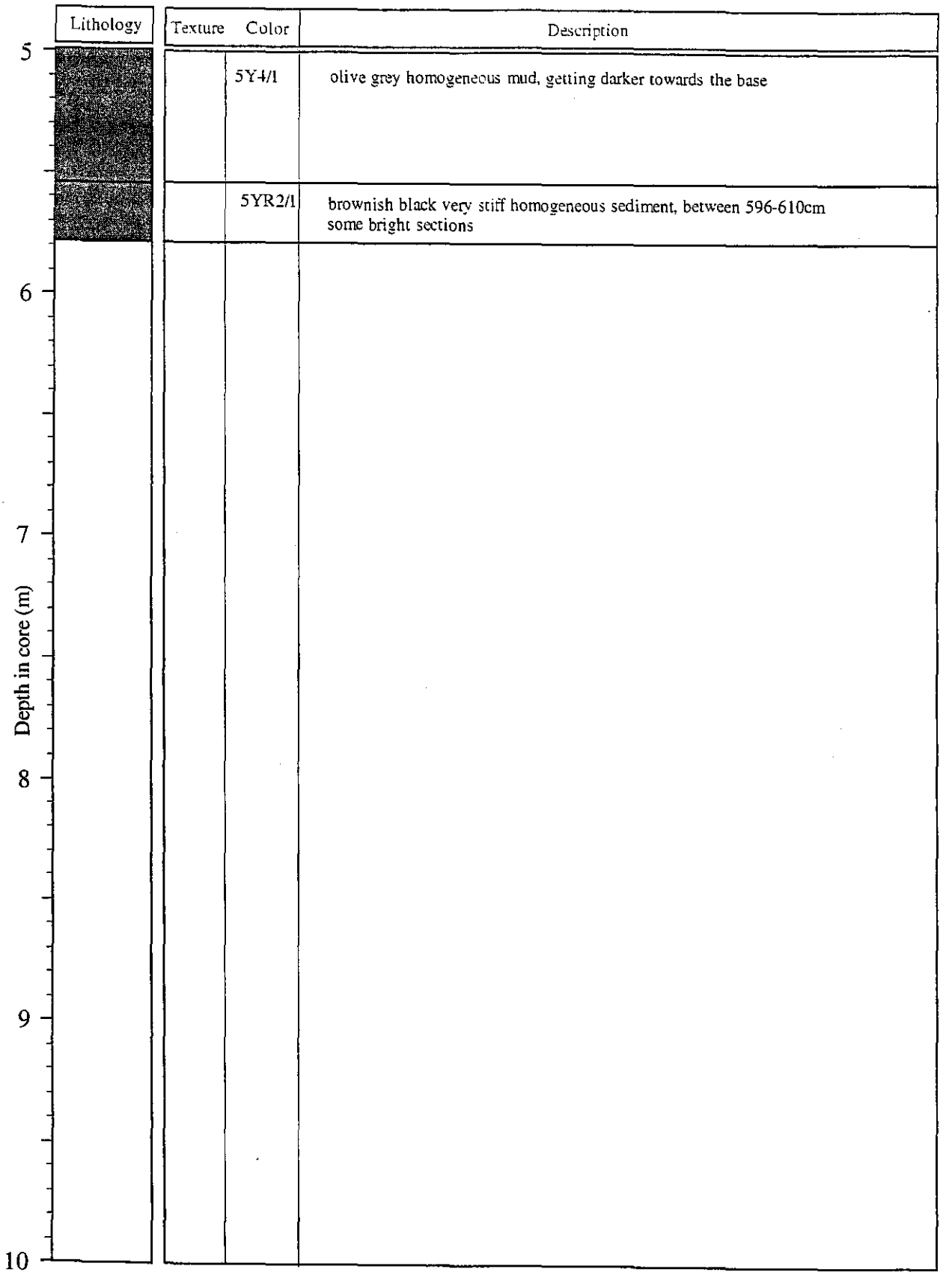
Lithology
Texture
Color
Description
5
6
7
8
9
10
Depth in core (m)
5Y4/1
olive grey homogeneous mud, getting darker towards the base
5YR2/1
brownish black very stiff homogeneous sediment, between 596-610cm
some bright sections

Red Sea Shaban-Deep Pos.: 26°13,9N 35°22,7E

Core No.: 17009-3 Corelength: 1100cm Waterdepth: 1474m

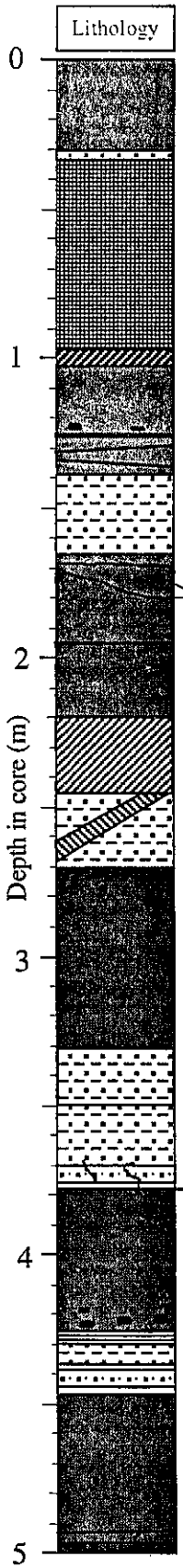

Texture	Color	Description
	5Y5/2 5Y4/4 5Y5/2	light olive grey, homogeneous mud with few black dots moderate olive brown, homogeneous mud light olive grey, homogeneous, fine grained mud, getting coarser towards the base
	5Y5/2	coarse grained calcareous mud, turbiditive
	5Y4/1 5Y6/1	laminations of olive grey and light olive grey mud, with black strippes
	5Y4/1 10Y4/2	olive grey, homogeneous mud, discordant layer at top at 104-105cm greyish olive clay, from 110cm increase amounts of black material
	5Y1/1	olive black layer, with coars material at bottom and top
	5Y4/1	olive grey mud with black layers at 129cm and 131cm, disturbed layering between 130cm and 136cm
	5Y6/1 5Y5/2	olive grey calcareous mud, getting light olive grey towards the base
	5Y4/4	moderate olive grey mud with dark layer at the top
	5Y2/1 5Y4/1 5Y6/1	olive black sapropele layer, no sharp contact at the base olive grey mud light olive grey with darker layer at the top, mud getting coarse grained towards the base, black dots at the base
	5Y4/1	olive grey mud, at the base coarse grained
	5Y2/1 10Y4/2	disturbed layering of sediments: laminations of 5Y2/1 olive black with 10Y4/2 greyish olive, between laminations 5Y6/1 calcareous rich mud coarser grained olive grey 5Y4/1 mud
	5Y4/1	olive grey, homogeneous mud
	5Y6/1	light olive grey, coarser grained, foraminifera bearing, calcareous mud
	5Y6/1	olive grey calcareous mud with olive layer at 358cm more olive layer, towards the base bioturbatic layering
	5Y4/1	olive grey homjogeneous mud with dark dots towards the base
	5Y4/1	fine laminations of olive grey and olive grey (5Y3/2) organic rich mud
	5Y4/1	olive grey coarse grained calcareous ooze, foraminifera and pteropods bearing olive grey layer at the base laminations of 5Y4/1 olive gray and light olive gray (5Y6/1)
	5Y2/1	olive black organic rich mud with fine laminations of olive grey and light olive grey
	5Y4/1	olive grey homogeneous mud (with black structures at 490-500cm), getting slightly darker towards the base, light grey laminations at 556-557cm

Fig. 52i: Core 17009-3: core description.

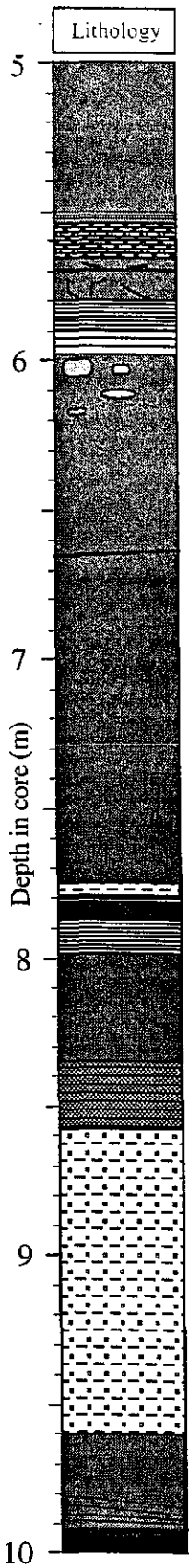

Texture	Color	Description
	5Y4/1	olive grey homogeneous mud(with black structures at 490-500cm), getting slightly darker towards the base, light grey laminations at 556-557cm
	5Y5/2	light olive grey coarse grained mud with foraminifera and pteropods, with olive grey laminations
	5Y5/2	light olive grey homogeneous mud, boiturbated at the base
	5Y4/1	layers of olive grey and moderate olive brown (5Y4/4) bioturbatic
	5Y4/1	fine laminations of olive grey (5Y4/1), dark olive and light olive grey
	5Y4/4 5Y5/2	moderate olive brown light olive grey mud with olive grey laminations
	5Y4/1	olive grey mud, between 598-620cm dark olive grey dots (bioturbative), from 620cm homogeneous, at 665cm dark lamina, getting more coarse grained at the base
		coarse grained calcareous ooze, foraminifera and pteropods bearing, with calconic fragments
	5Y4/1	olive grey with dark olive gray laminations, at 783-787cm olive grey diatomous mud
	5Y5/2	light olive grey, changing toward olive grey (5Y4/1), homogeneous mud layering of olive grey muds with variations composition, several diatomatic layers
	5Y5/2	light olive grey calcareous mud with olive grey dots
	5Y4/1	olive grey mud, homogeneous
		layering of olive grey muds from 994cm with fine olive black laminae
	5Y2/1	olive black mud, organic rich
	5R2/6	very dark red mud, stiff and fine grained

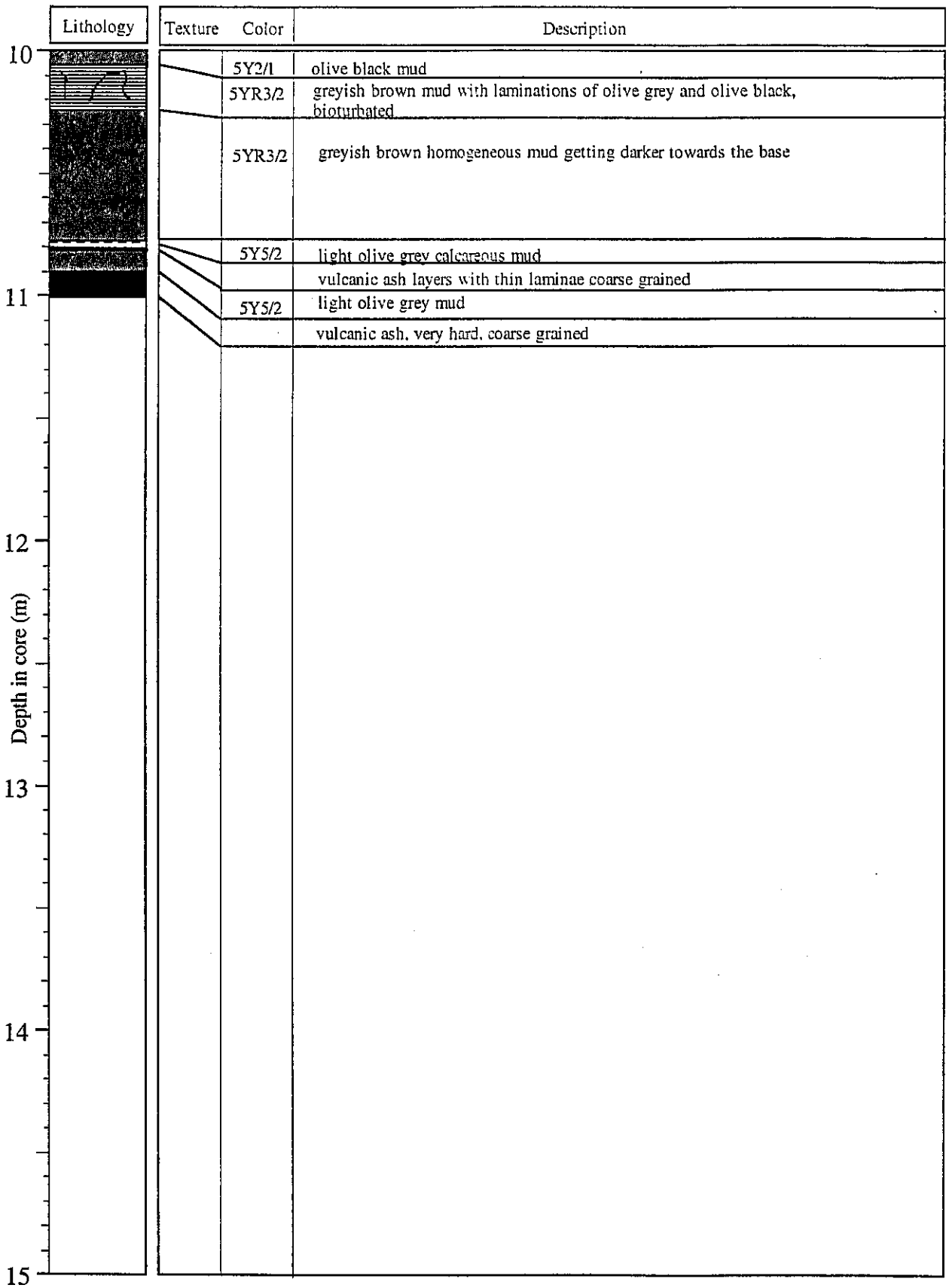
Lithology
Texture
Color
Description
10
11
12
13
14
15
Depth in core (m)
5Y2/1
olive black mud
5YR3/2
greyish brown mud with laminations of olive grey and olive black, bioturbated
5YR3/2
greyish brown homogeneous mud getting darker towards the base
5Y5/2
light olive grey calcareous mud
vulcanic ash layers with thin laminae coarse grained
5Y5/2
light olive grey mud
vulcanic ash, very hard, coarse grained

Red Sea Kebrit-Deep Pos. : 24°43,2N 36°16,1E

Core No.: 17010-2 Corelength: 1004cm Waterdepth :1474m

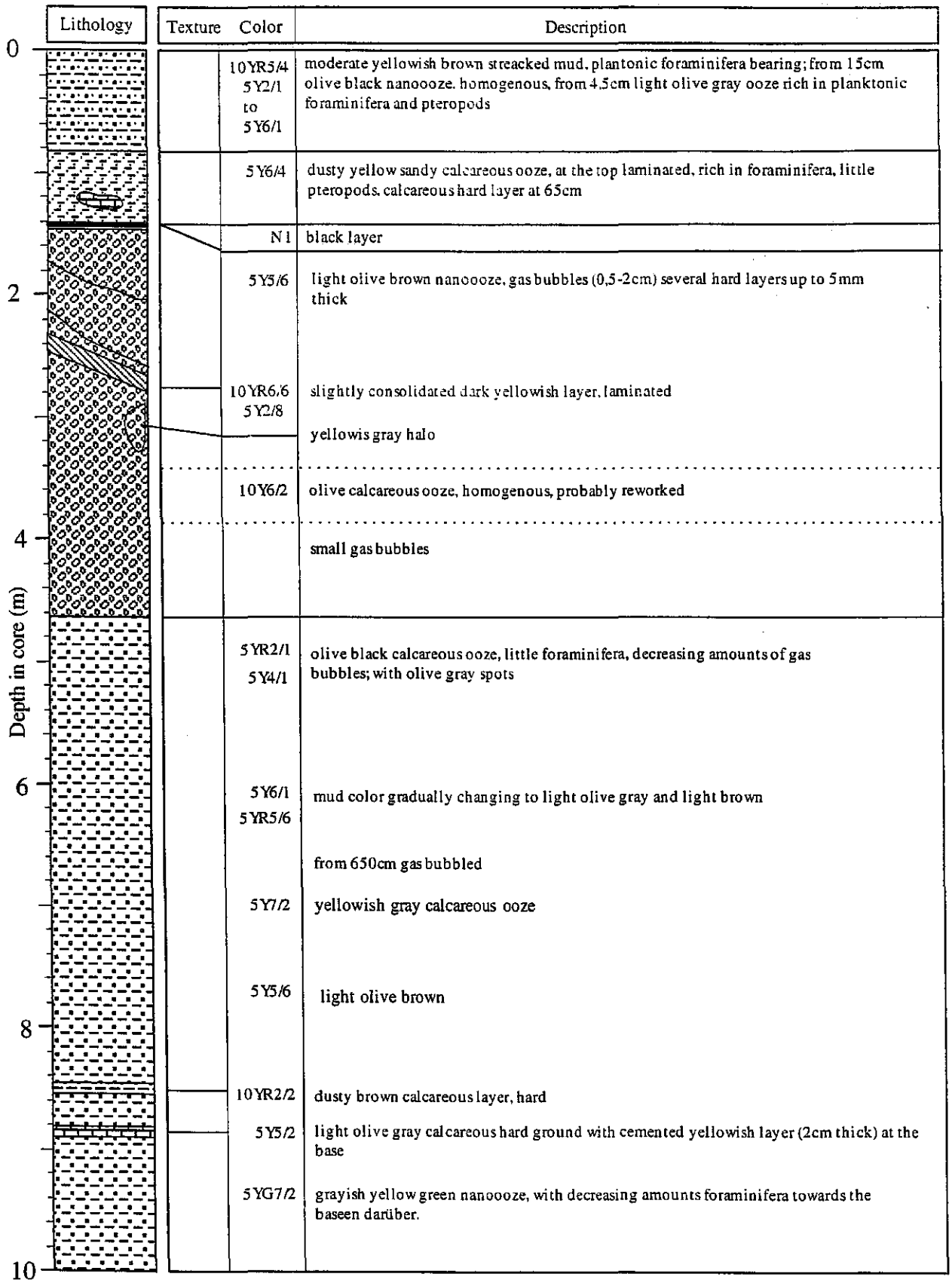

Fig. 52j: Core 17010-2: core description.

Red Sea Atlantis II-Deep Pos. : 21°21,96N 38°04,11E

Core No.: 17015-2 Corelength: 1120cm : Waterdepth :2138m

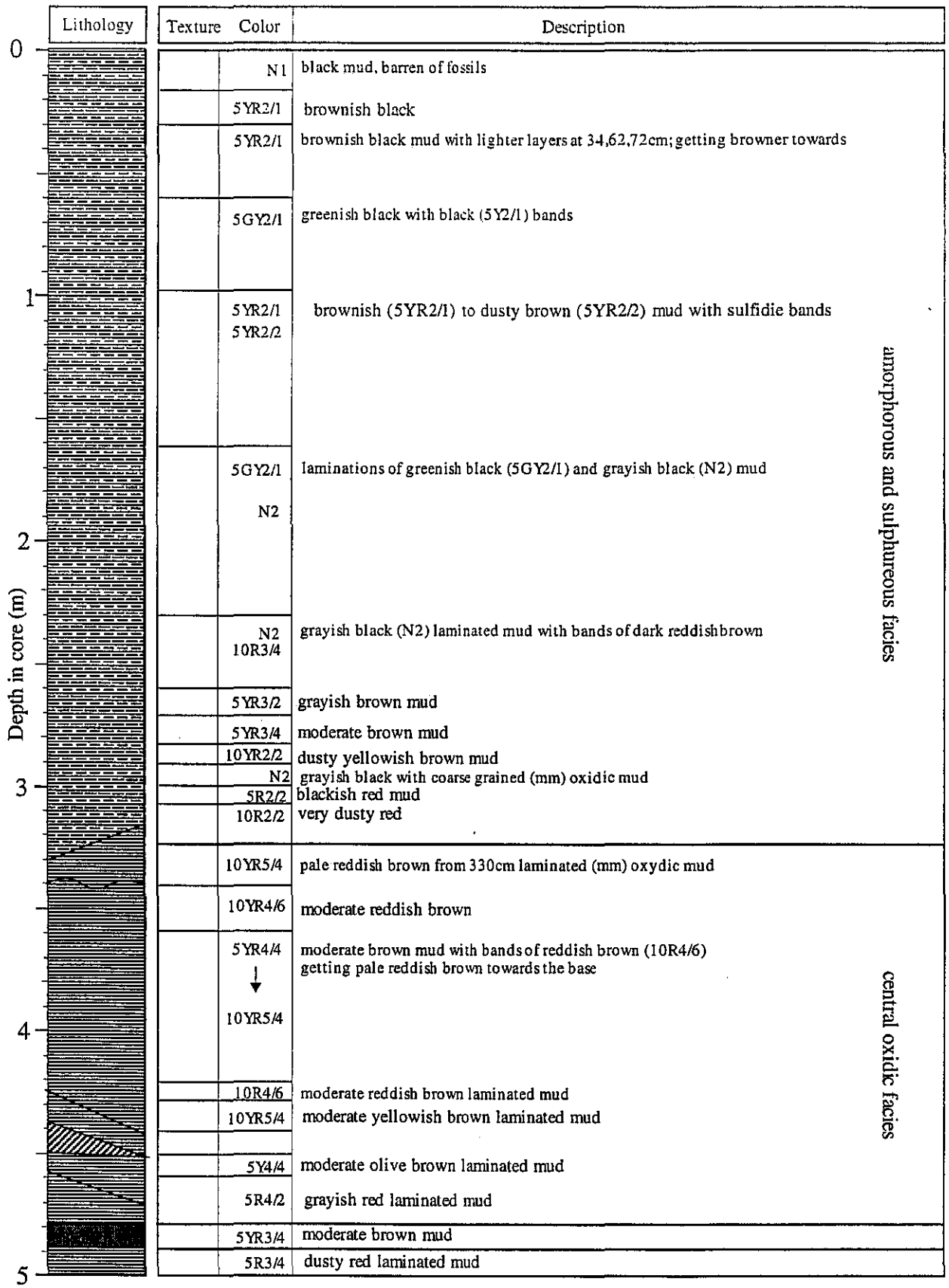

Fig. 52k: Core 17015-2: core description.

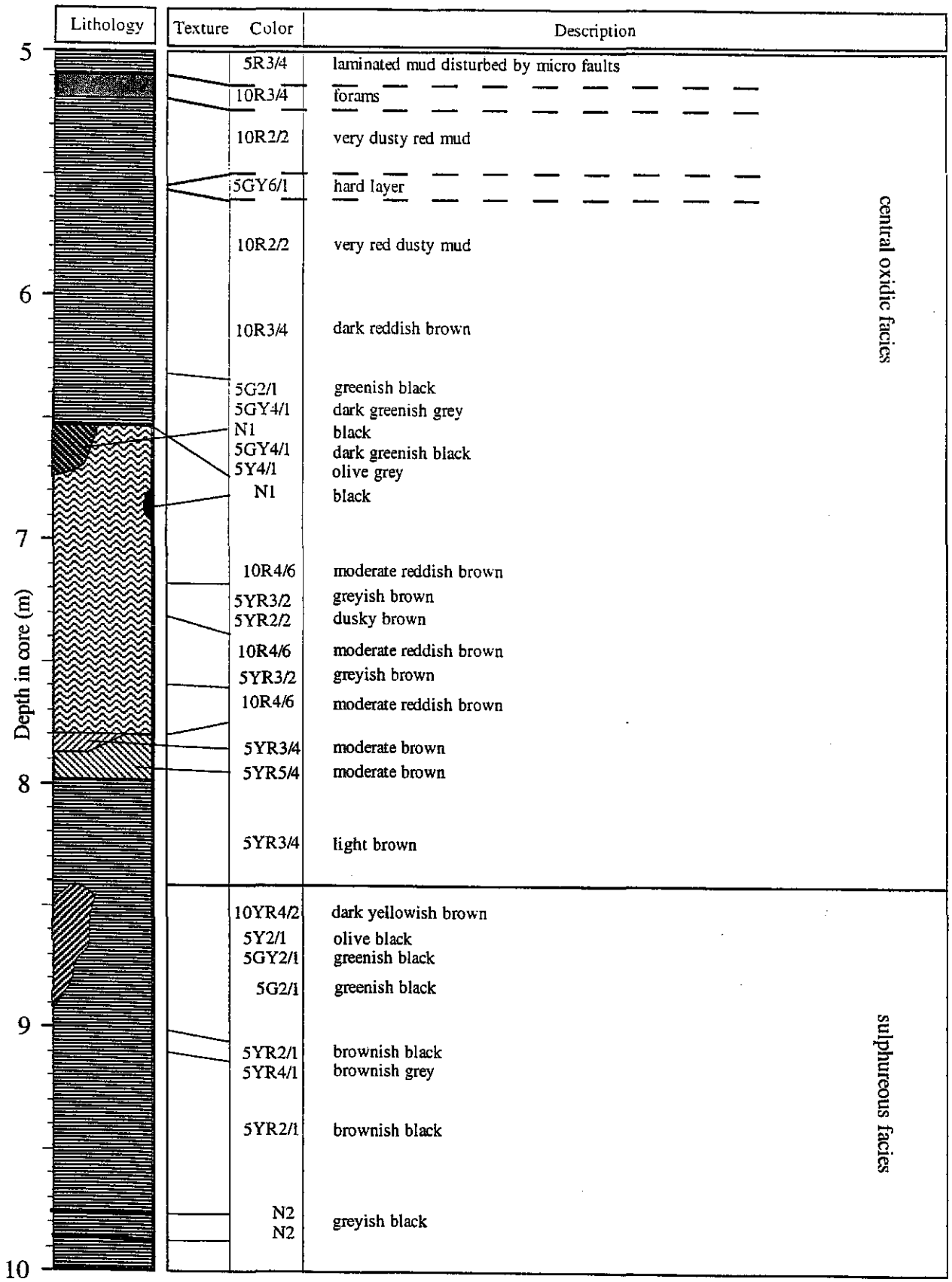
Lithology
Texture
Color
Description
Depth in core (m)
5
6
7
8
9
10
5R3/4 laminated mud disturbed by micro faults
10R3/4 forams
10R2/2 very dusty red mud
5GY6/1 hard layer
10R2/2 very red dusty mud
10R3/4 dark reddish brown
5G2/1 greenish black
5GY4/1 dark greenish grey
N1 black
5GY4/1 dark greenish black
5Y4/1 olive grey
N1 black
10R4/6 moderate reddish brown
5YR3/2 greyish brown
5YR2/2 dusky brown
10R4/6 moderate reddish brown
5YR3/2 greyish brown
10R4/6 moderate reddish brown
5YR3/4 moderate brown
5YR5/4 moderate brown
5YR3/4 light brown
central oxidic facies
10YR4/2 dark yellowish brown
5Y2/1 olive black
5GY2/1 greenish black
5G2/1 greenish black
5YR2/1 brownish black
5YR4/1 brownish grey
5YR2/1 brownish black
N2 greyish black
N2
sulphureous facies

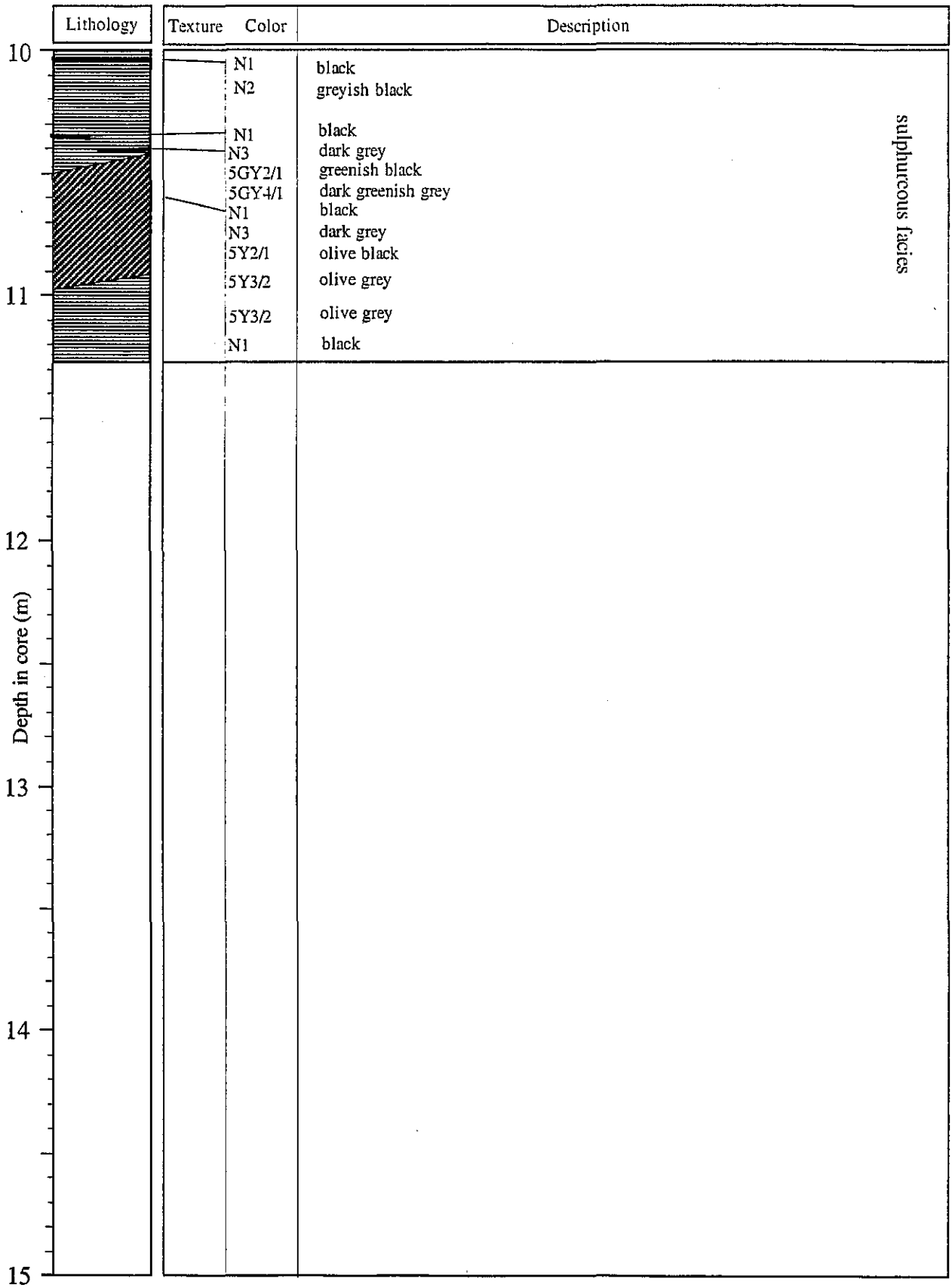
Lithology
Texture
Color
Description
10
11
12
13
14
15
Depth in core (m)
N1
black
N2
greyish black
N1
black
N3
dark grey
5GY2/1
greenish black
5GY4/1
dark greenish grey
N1
black
N3
dark grey
5Y2/1
olive black
5Y3/2
olive grey
5Y3/2
olive grey
N1
black
sulphurcous facies

5.2.4.3 Paleoceanography and Monsoonal History of the Red Sea
(Ch. Hemleben)

Sediment Sampling

Along the north-south transect through the Red Sea multicorer, boxcorer, gravity corer and piston corers were used at 11 stations to retrieve deep sea sediments. For details see the station list (7.2.1).

Multicorer (G. Schmiedl, F. Wesselingh)

A multicorer was used at 9 stations to recover undisturbed surface sediments and overlying bottom water for paleontological and geochemical studies. The multicorer was equipped with 8 larg tubes of 7 cm and 4 small tubes with inner diameter of 6 cm. At 8 sites all sediment cores recovered were of very good quality, at station 84 (MC362) the core recovery was low (11 cm) and the surfaces of 3 cores were disturbed, which was probably due to a pteropod crust just below the sediment surface. In total, penetration depths reached from 11 to 35 cm (26 cm on average).

At each multicorer station the overlying bottom water was sampled for stable isotope measurements. To avoid ongoing biological fractionation, samples for carbon istotope measurement were immediately poisoned with 1 ml of concentrated $HgCl_2$ solution.

From the sediment surface the following samples were taken:
- 1 large core: intervals 0-0.5 cm, 0.5-1 cm and 1-5 cm in centimeter slices were stained with Rose Bengal methanol for the investigation of recent benthic foraminifera. From the 5th cm downward one core was sampled in centimeter slices (unstained) for downcore isotopic and faunal analyses.
- 2 large cores: the uppermost sediment cm was stained with Rose Bengal methanol as additional samples for the study of Recent benthic foraminifera.
- 1 large core: the uppermost 0-0.5 cm was sampled for sedimentological studies such as grain size distribution, carbonate and organic carbon measurements.
- all other cores were sampled for macropaleontological studies.

Piston Coring (T. Bukowski, D. Fleitmann, Ch. Hemleben, J. Meyer, T. Mühlstrasser, G. Schmiedl, S. Weldeab)

Two formats of the Göttingen piston corer were used to recover long sediment cores:

(i) 1.5 to dead weight, 12 m barrels, 120 mm dia.
(ii) 3.5 to dead weight, 24 m barrels, 200 mm dia.

Both instruments are routinely used with aluminium barrels, 5 mm wall thickness, without liners. After recovery, the barrels are cut into pieces of 2.5 or 3.0 m length and stored away for later opening. No cooling was applied.

During the cruise the auxiliary winch developed problems so that the weight of the larger corer had to be reduced by 0.5 ton, (from sta. 102 onward) and higher free fall to be applied as a compensation (12 m instead of 6 m). This resulted in a slighly reduced core lengths.

The performance of both corers has been highly satisfactory. The small corer yielded an average of 11.00 m or 94 % recovery, the large corer 19.2 m or 82 % recovery (including an attempt on an indurated basaltic ash layer on Station 80-2).

A trigger corer of 150 kg dead weight, 2 m barrel, 90 mm dia. was used to core the uppermost 0.5 -1 m of uncemented, Holocene sediment on top of the ubiquitous carbonate crust of isotopic stage 2.

Two of the piston cores have been opened, documented and sampled for physical properties, foraminifera and pteropoda, and for geochemical analyses (total carbonate and stable isotopes $^{18}O/^{16}O$ and $^{13}C/^{12}C$):

Core KL 85-2 from the northern Red Sea reaches back to late isotopic stage 11. It is remarkable for increased sedimentation rates, an unusually high water content in sediments of isotopic stages 4 to 2, and a missing hard layer charaterizing normally stage 2.

Core KL 102-2 from the southern Red Sea is undisturbed to about 18 m core depth only, the rest of the core was highly deformed during extraction when the split piston did not separate. Stage 2 and all previous glacial sediments contain a rather well preserved planktic foraminiferal fauna.

Tab. 12: Core list of METEOR cruise 31/2

Red Sea

Station	Latitude	Longitude	Water depth	Core	Barrel (m)	GPI Tü No.	Core recovery
78	27° 41,25N	34° 35,9E	1018 m	KL 78-1	12	KL 16	11,65 m
78	27° 41,13N	34° 35,76E	1018 m	KL 78-2	24	KL 17	18,76 m
80	26° 16,690N	35° 20,837E	1112 m	KL 80-1	12	KL 18	11,35 m
80	26° 16,839N	35° 21,124E	1107m	KL 80-2	24	KL 19	10,16 m
82	26° 17,459N	35° 21,472E	1141 m	KL 82-1	12	KL 20	11,76 m
82	26° 17,477N	35° 21,451E	1149 m	KL 82-2	24	KL 21	22,30 m
85	25° 44,598N	35° 04,391E	690 m	KL 85-1	12	KL 22	11,60 m
85	25° 44,887N	35° 03,287E	702 m	KL 85-2	24	KL 23	22,10 m
88	26° 14,1N	35° 22,4E	1470 m	KL 88-1	12	KL 24	7,0 m

Station	Latitude	Longitude	Water depth	Core	Barrel (m)	GPI Tü No.	Core recovery
88	26° 13,9N	35° 22,7E	1445 m	KL 88-2	12	KL 25	11,0 m
90	24° 45,610N	36° 13,812E	1175 m	KL 90-1	12	KL 26	11,65 m
90	24° 45,605N	36° 13,744E	1172 m	KL 90-2	24	KL 27	16,0 m
92	23° 18,6N	36° 42,8E	998 m	KL 92-1	12	KL 28	11,60 m
92	23° 18,6N	36° 42,9E	996 m	KL 92-2	24	KL 29	20,50 m
101	17° 22,0N	40° 00,6E	474 m	KL 101-1	12	KL 30	11,60 m
102	15° 33,0N	41° 41,4E	582 m	KL 102-1	24	KL 31	20,0 m
102	15° 33,4N	41° 40,5E	598 m	KL 102-2	24	KL 32	23,58 m

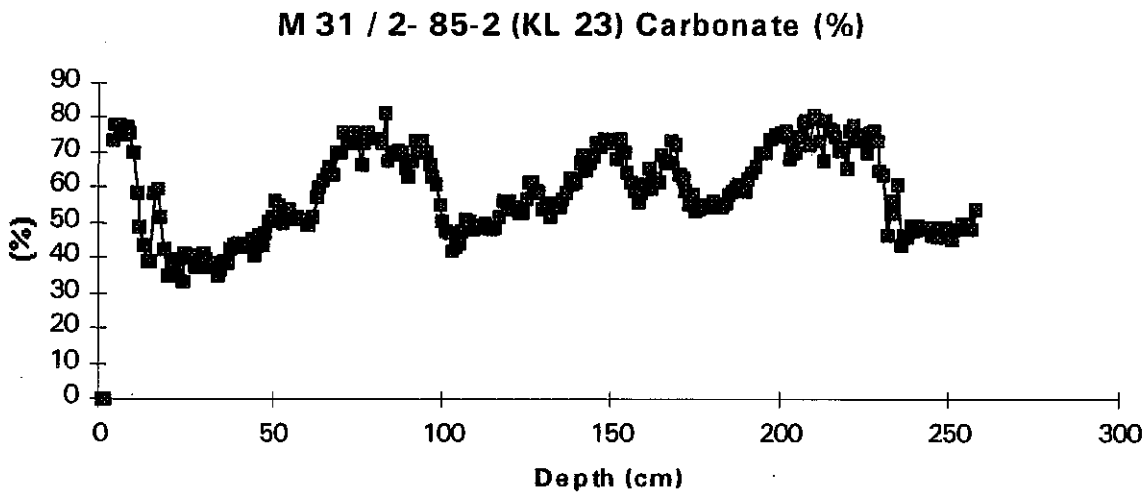

Fig. 53: Total carbonate content in core KL 85-2. Deepest sediment in core is late isotopic stage 11.

Benthic Foraminifera (G. Schmiedl)

Surrounded by continents the Red Sea is largely isolated from the global ocean circulation. The exchange of water masses with the Indian Ocean is restricted to the narrow and shallow sea way of Bab el Mandeb at the southern tip of the Red Sea. As a consequence of this isolation the Red Sea exhibits extreme hydrographic conditions. One of the most characteristic features are extraordinary high salinities that are measured in both surface and deep water masses (PICKARD and EMERY, 1990). Consequently, the benthic foraminiferal faunas of the Red Sea include a large number of endemic species, which were documented in the taxonomic work of HOTTINGER et al. (1993). However, compared to the adjacent ocean environments, in the Red Sea only a few studies concentrated on the ecology and paleoecology of benthic foraminifera (e.g. SCHERBACHER, 1994) although recent investigations demonstrated that

benthic foraminifera are useful tools for paleoceanographic studies in the Red Sea (ALMOGI-LABIN et al., in press).

During M31/2 a number of high quality surface sediment samples were collected for down-core studies of living (stained) benthic foraminifera and stable isotope measurements of their tests. The analysis of the ecological network between benthic foraminiferal faunas and sedimentological, geochemical and oceanographic parameters, will serve as a basis for paleoceanographic interpretations of fossil assemblages from long sediment cores. First results from recovered sediment cores indicate that the species composition changes dramatically through time. Recent sediments represent interglacial conditions and are usually dominated by epibenthic living foraminifera, e.g. different species of the genus *Cibicides*, *Cibicidoides* and *Discorbinella.* In contrast, core sections that are supposed to represent glacial conditions include a high number of infaunal living foraminifera, like *Bulimina marginata* and *Rectuvigerina* sp.. These species are well known from environments that are characterized by high organic carbon flux rates and low oxygen bottom and pore water conditions (e.g. SCHMIEDL 1995). This preliminary result is in accordance with HEMLEBEN et al. (1996) and ALMOGI-LABIN et al. (1996) who carried out stable isotope and micropaleontological studies on cores from the central Red Sea. They showed that the glacial sea level drop coincided with a strong salinity increase and reduction of deep water formation resulting in an oxygen decrease in deep and bottom water masses.

5.3 Preliminary Results of Leg M31/3

5.3.1 Physical Oceanography

5.3.1.1 CTD

(F. Wehner)

The hydrographical conditions in the Gulf of Aden and western Arabian Sea during March 1995

For the CTD-measurements an EG&G Mark V-CTD was used, equipped with pressure-, temperature-, conductivity- and oxygen sensors and a backscattering fluorometer integrated in a 12*12 l rosette system of General Oceanic. For calibration of the CTD-instrument reversing thermometers were used, and bottle samples were taken for salinity measurements with an Autosal-Salinometer Oxygen was measured by titration after Winkler.

Gulf of Aden and the western Arabian Sea

Temperature and Salinity

During leg 3 (March) a weak NE-monsoon dominated the calm weather conditions. All profiles show a clearly marked thermocline located in the upper 200 m (temperature drops

from about 26° C at the surface to 15° C), followed by a monotonous decrease in greater depths (Figure 54). A significant mixed layer with uniform temperature is not present. The results are in agreement with the previous studies, e.g. of WYRTKI (1971), COLBURN (1975) and BROCK et al. (1992). The pycnocline is located in nearly the same depth as the thermocline (verified by the fluorometry measurements). The upper 50 m is characterized by Arabian Sea Surface Water (ASSW), which originates in the central and northern Arabian Sea under conditions of annual excess of evaporation over precipitation. This water mass partly sinks to about 75 m (BROCK et al., 1992), building a shallow salinity maximum (see Station 111 - 114). The low salinity water overlying this maximum may have originated in the Bay of Bengal, and is brought by a strong branch of the NE-monsoon current into the western Arabian Sea (DIETRICH et al., 1975; WYRTKI, 1973). In the 50 to 500 m depth interval, the North Indian High-Salinity Intermediate Water (NIIW) were recognized by means of T-S-characteristics (Figure 54).

In contrast to the results of BROCK et al. (1992), the salinity maxima of deep Red Sea (RSDW) and Persian Gulf outflow waters (PGOW) can clearly be distinguished. Especially profiles of the eastern stations (Station 109 - 113) show the Persian Gulf Water, entering the Arabian Sea from the Strait of Hormuz and flowing southward along the coast of Oman, at a water depth of ca. 300 m. In the more southern stations (Station 105 - 108, 114 -116), the RSDW dominates in the deeper part of the water column. It enters the Arabian Sea through the Strait of Bab el Mandeb in two tongues (because of an overflow over two different sills) at a depth of about 800 m, forming a strong salinity maximum, which can be traced in almost the entire northern Indian Ocean (WYRTKI, 1971).

Strong signals in salinity are combined with relatively weak signals in temperature. Only for stations 105, 107, 114 and 116 peaks in temperature are recognizable, which point to the presence of RSDW and/or PGOW. A comparison of several CTD-stations (northern vs. southern profiles) may lead to the conclusion, that the main outflow of deeper saline water from the Gulf of Aden is located near the continental slope, as a recirculating boundary current, that is effected by the NE-monsoon. In contrast to the southern section (Station 105 - 111), we find a steady mixing of the high salinity cores with the surrounding waters, and a slow but constant deepening of the thermocline. The RSDW signal remains present in all northern profiles (station 112 - 116). In agreement with previous investigations at the most easterly CTD stations (station 110, 111) "literature-standard" conditions were recorded for the Arabian Sea. In this area, the vertical mixing of surface water with high saline RSDW and the PGOW results in a thick, high-salinity layer (NIIW), which extends to great depth (downward fluxes of salt, $S > 35.0$ psu at 1500 m). With regard to the T-S relation (Figure 54), the Deep-Water consists of a mixture of Indonesian Intermediate Water (IIW) and Antarctic Intermediate Water (AIW).

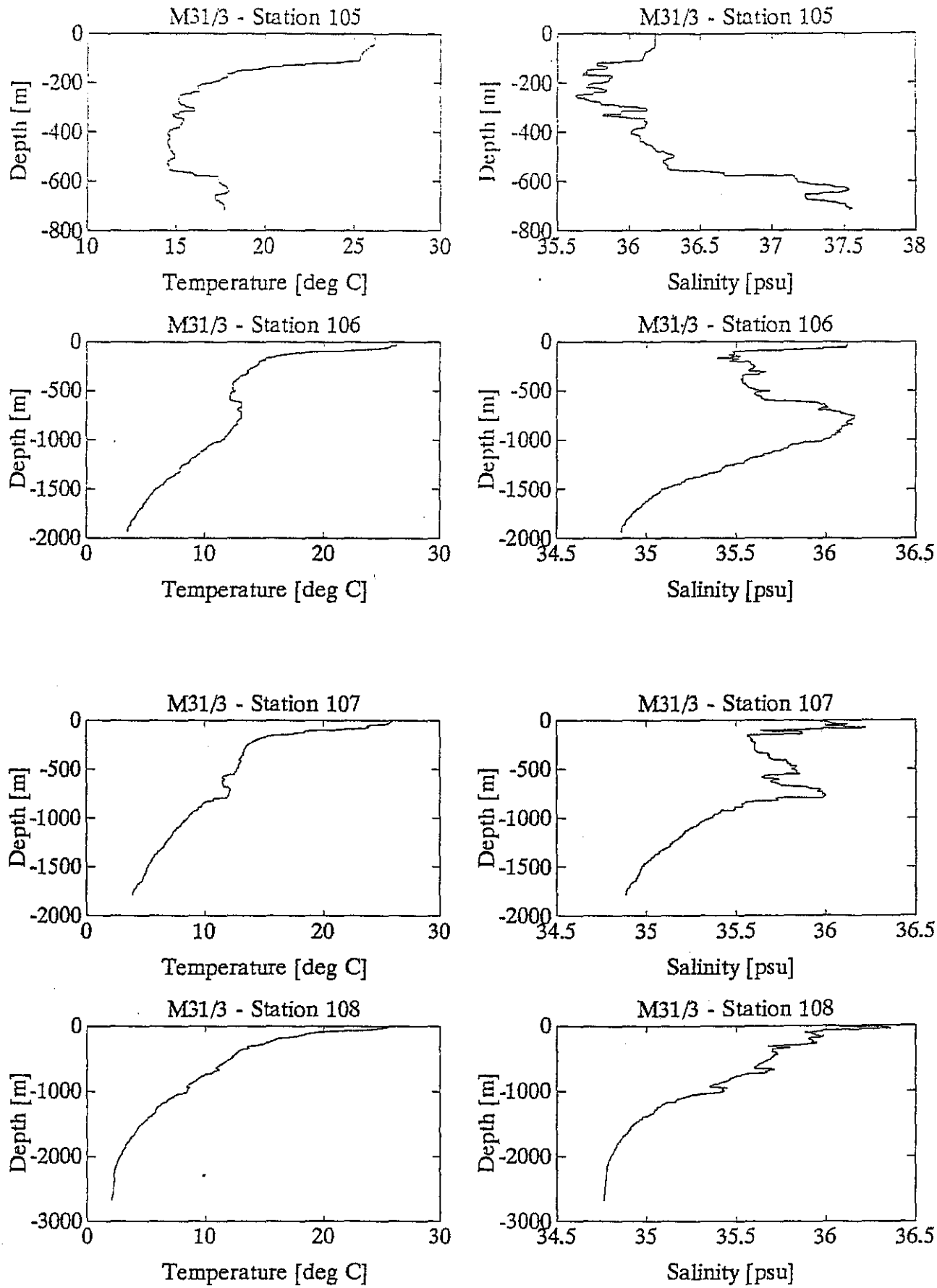

Fig. 54: Temperature- and salinity profiles during M31/3.

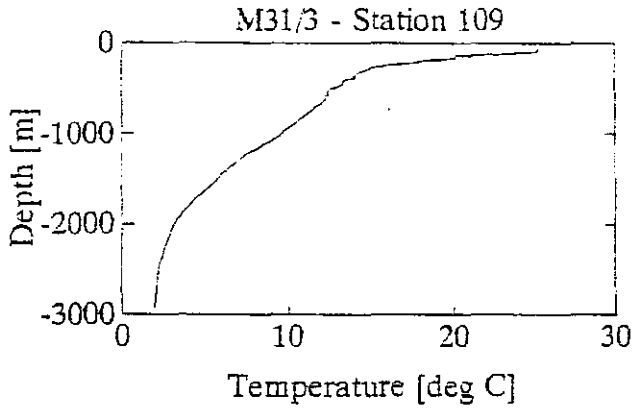
M31/3 - Station 109
Depth [m]
0
-1000
-2000
-3000
0
10
20
30
Temperature [deg C]

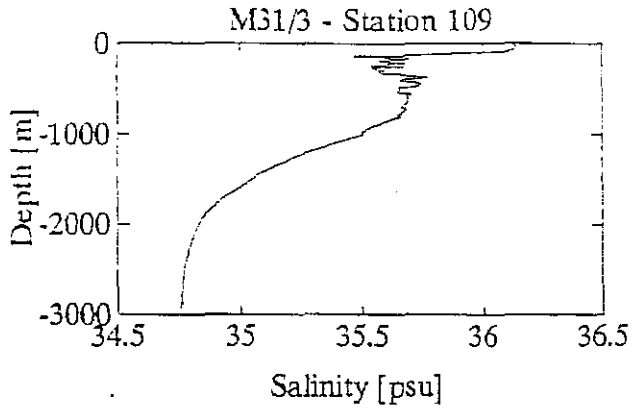
M31/3 - Station 109
Depth [m]
0
-1000
-2000
-3000
34.5
35
35.5
36
36.5
Salinity [psu]

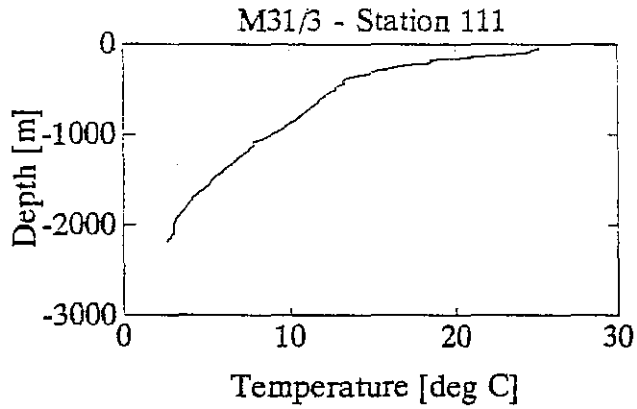
M31/3 - Station 111
Depth [m]
0
-1000
-2000
-3000
0
10
20
30
Temperature [deg C]

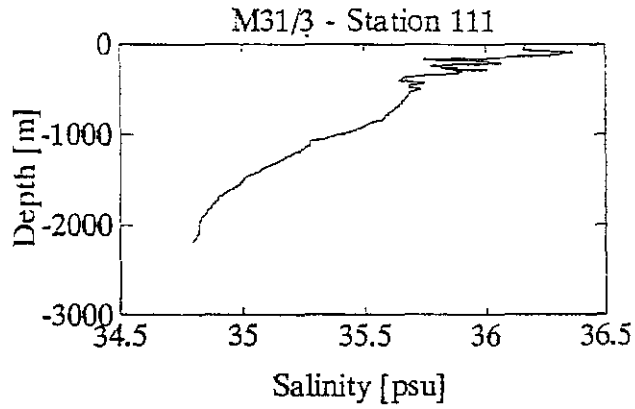
M31/3 - Station 111
Depth [m]
0
-1000
-2000
-3000
34.5
35
35.5
36
36.5
Salinity [psu]

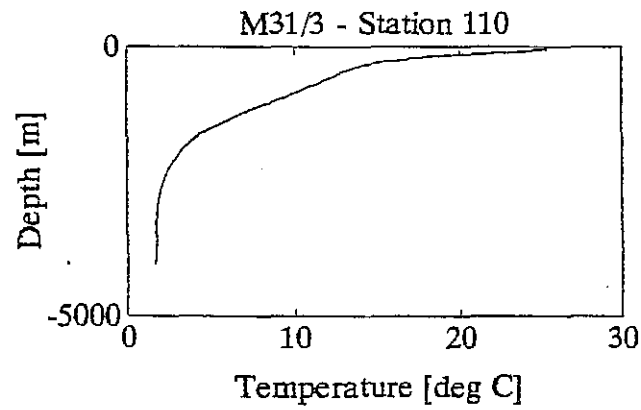
M31/3 - Station 110
Depth [m]
0
-5000
0
10
20
30
Temperature [deg C]

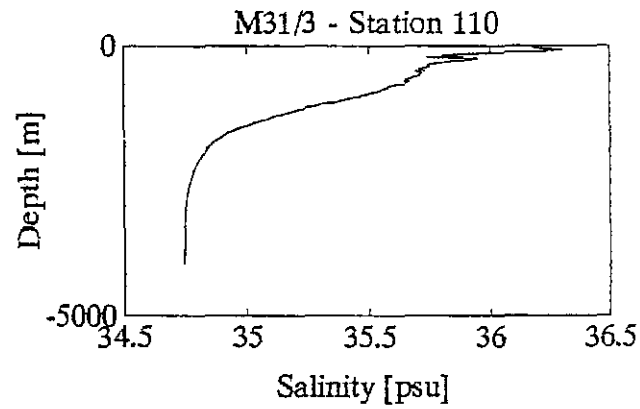
M31/3 - Station 110
Depth [m]
0
-5000
34.5
35
35.5
36
36.5
Salinity [psu]

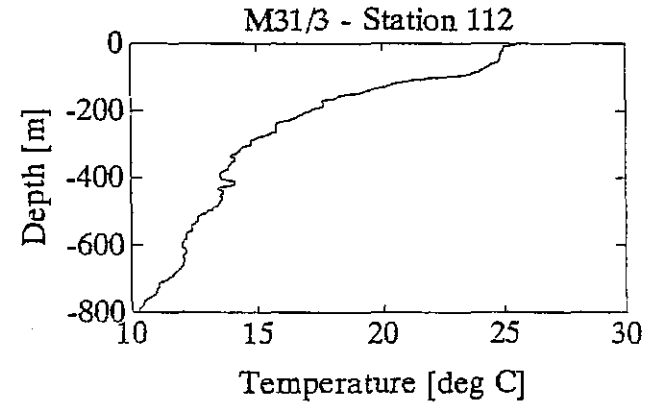
M31/3 - Station 112
Depth [m]
0
-200
-400
-600
-800
10
15
20
25
30
Temperature [deg C]

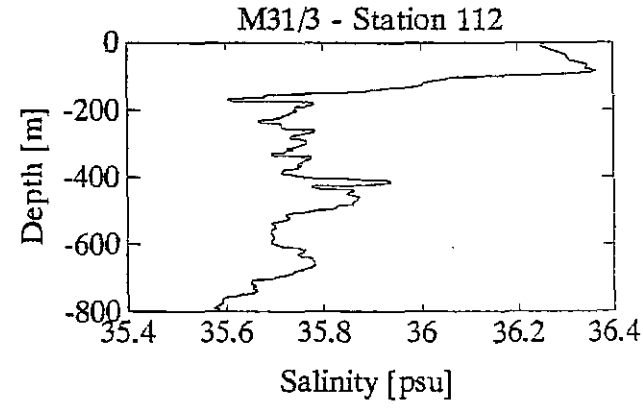
M31/3 - Station 112
Depth [m]
0
-200
-400
-600
-800
35.4
35.6
35.8
36
36.2
36.4
Salinity [psu]

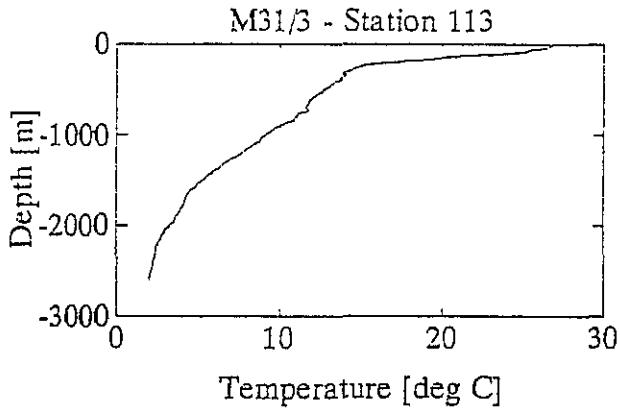
M31/3 - Station 113
Depth [m]
0
-1000
-2000
-3000
0
10
20
30
Temperature [deg C]

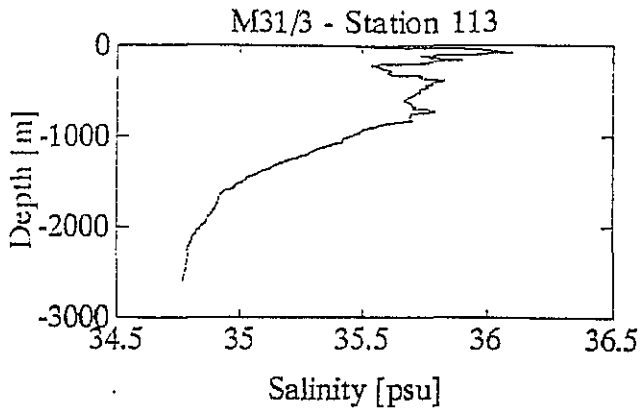
M31/3 - Station 113
Depth [m]
0
-1000
-2000
-3000
34.5
35
35.5
36
36.5
Salinity [psu]

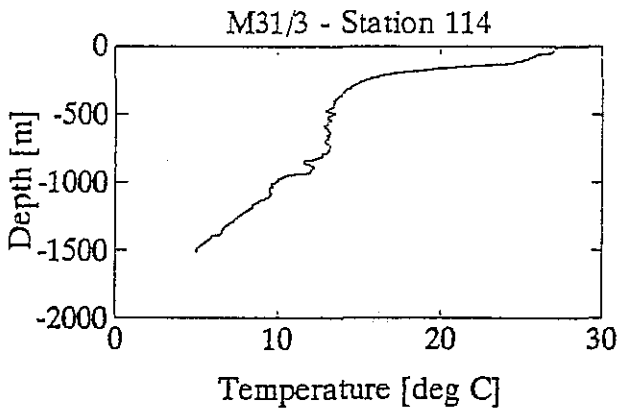
M31/3 - Station 114
Depth [m]
0
-500
-1000
-1500
-2000
0
10
20
30
Temperature [deg C]

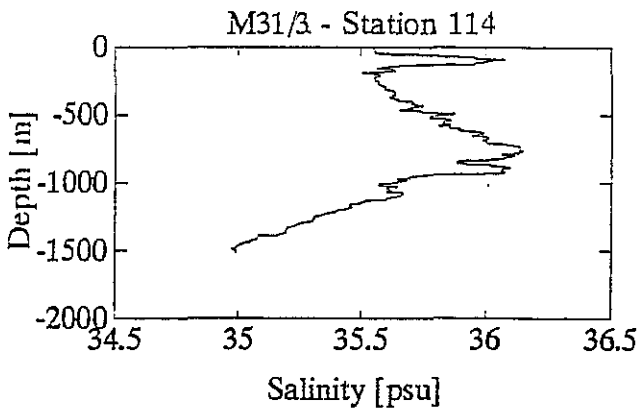
M31/3 - Station 114
Depth [m]
0
-500
-1000
-1500
-2000
34.5
35
35.5
36
36.5
Salinity [psu]

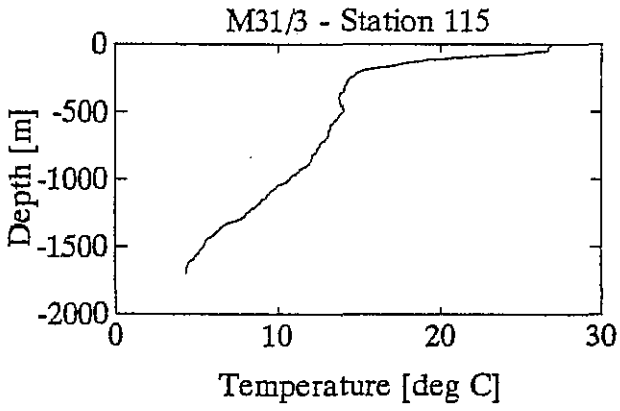
M31/3 - Station 115
Depth [m]
0
-500
-1000
-1500
-2000
0
10
20
30
Temperature [deg C]

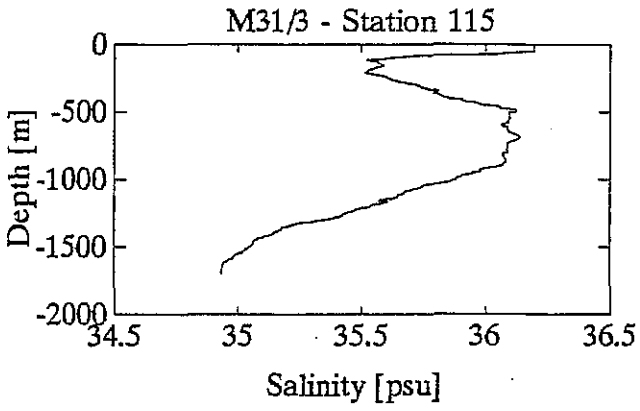
M31/3 - Station 115
Depth [m]
0
-500
-1000
-1500
-2000
34.5
35
35.5
36
36.5
Salinity [psu]

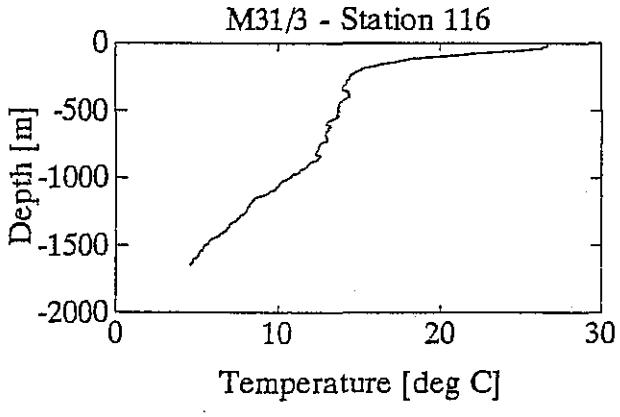
M31/3 - Station 116
Depth [m]
0
-500
-1000
-1500
-2000
0
10
20
30
Temperature [deg C]

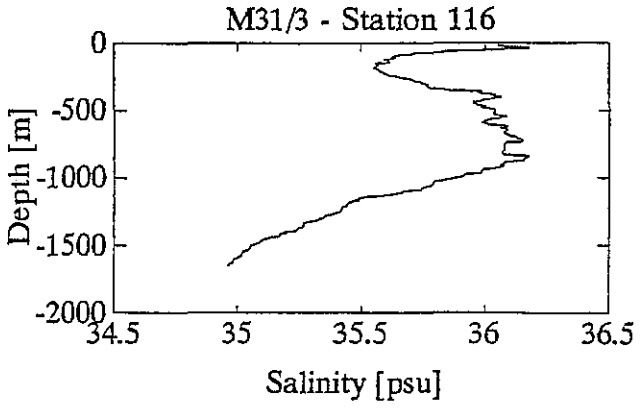
M31/3 - Station 116
Depth [m]
0
-500
-1000
-1500
-2000
34.5
35
35.5
36
36.5
Salinity [psu]

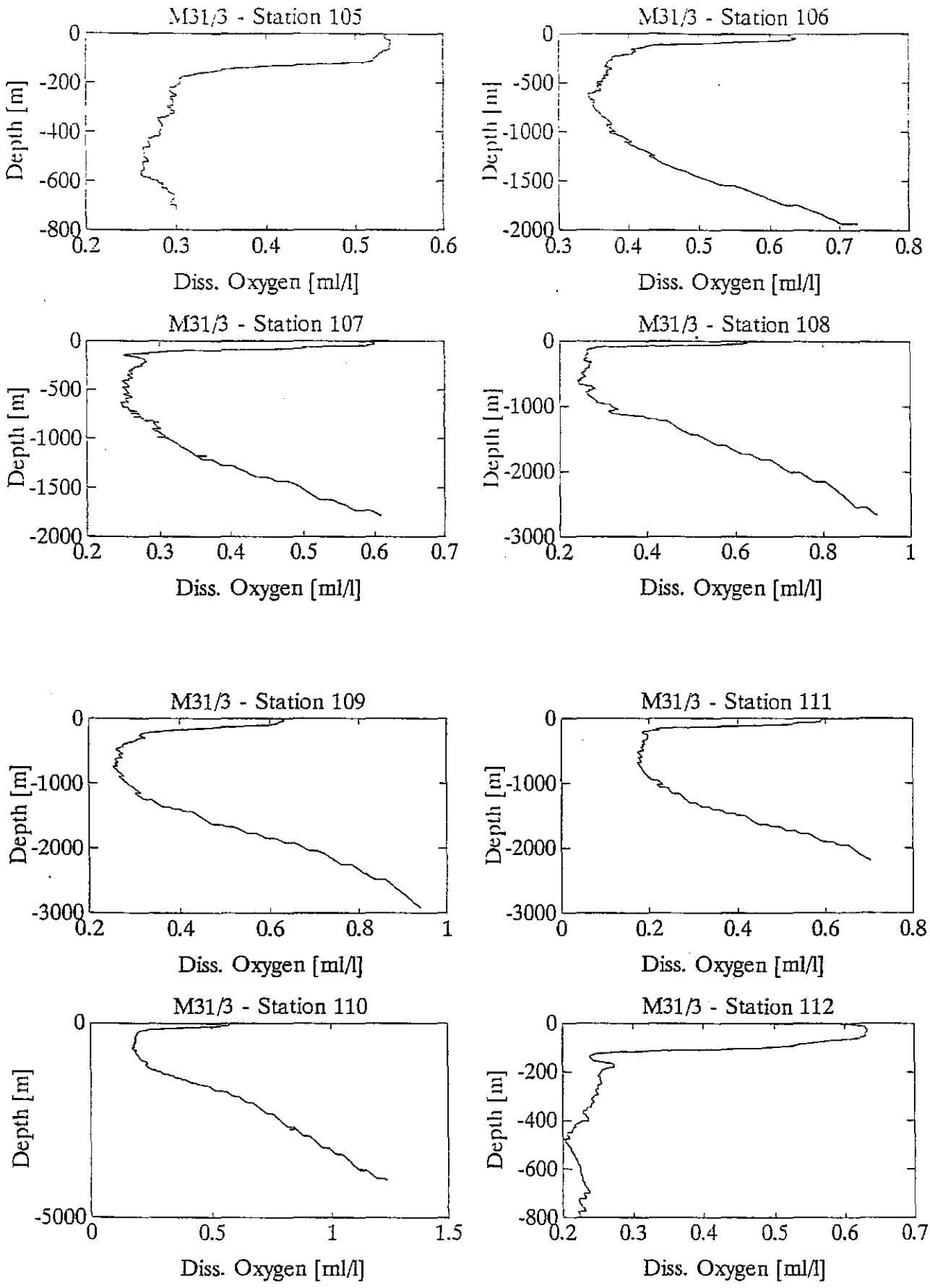

Fig. 55: Oxygen profiles during M31/3.

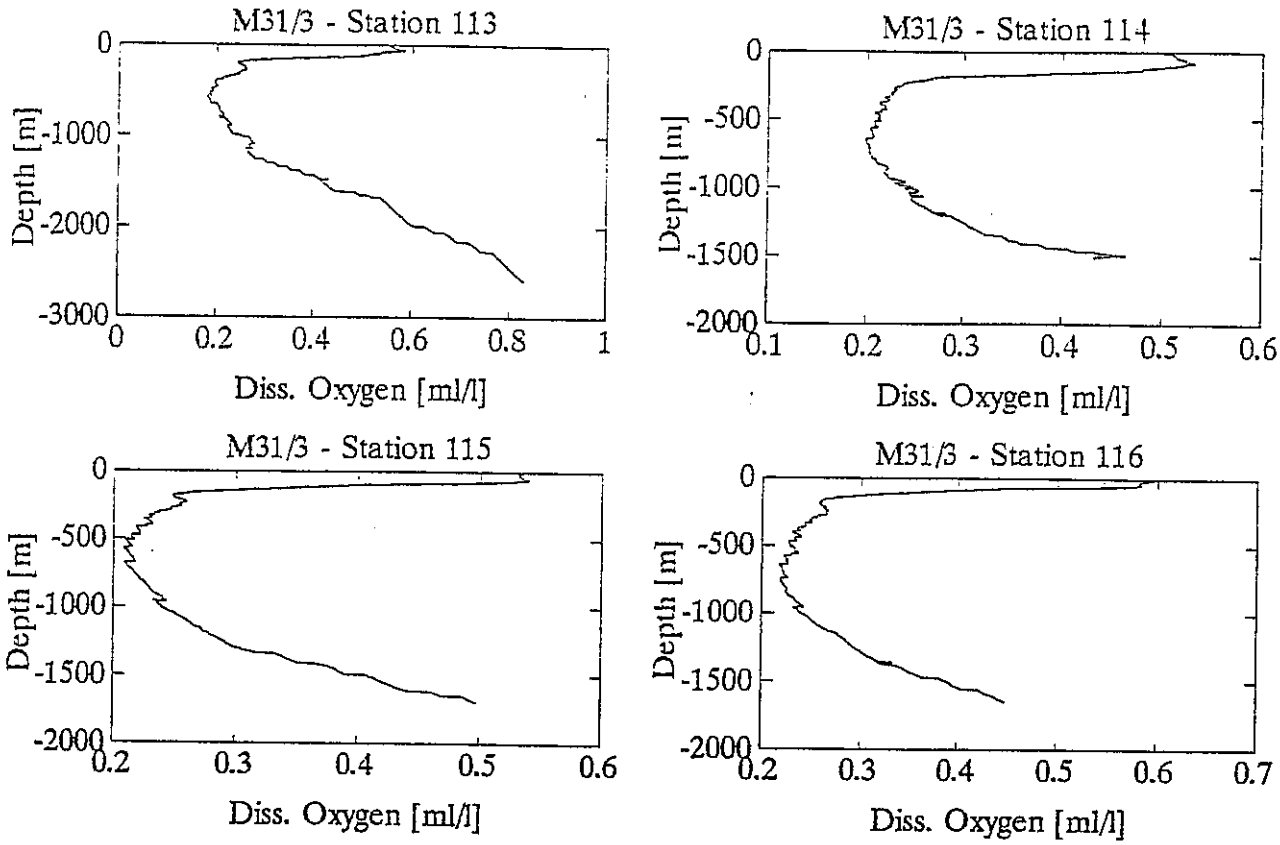

Fig. 55: Oxygen profiles during M31/3.

Oxygen

The oxygen conditions in the Arabian Sea and the Gulf of Aden are directly connected to the depth interval between ca. 200 m and 1500 m depth (mainly NIIW). Isolation and stagnation of the North Indian High-Salinity Intermediate Water, combined with a lack of horizontal advection and high biological productivity, causes a very low content of dissolved oxygen (O_2 <1.0 ml/l) over a large part of the water column. The input of RSDW (O_2 ~ 0.5 ml/l) (GRASSHOFF, 1969) enhances the O_2-Minimum. The profiles (Figure 55) show that the beginning of the oxygen-depleted zone is identical with the depth of the thermo- and pycnocline (150-200 m). The oxygen content decreases with a sharp drop until an oxygen-minimum is reached at a depth of about 700 m. Below 1000 m, oxygen increases again as a result of the influence of IIW and AIW, dominating the Deep-Water of the water column in this region.

5.3.1.2 Water samples

To get up-to-date information about the hydrographic conditions at all stations, a GO 7 (general oceanic) rosette, equipped with a CTD profiler, was used during the cruise M31/3. This CTD was equipped with sensors for presssure, conductivity, temperature and oxygen. At the stations listed in Table 13, water samples were taken for the determination of stable carbon and oxygen isotope ratios of sea water. For the carbon isotopes, water was filled carefully, to avoid contamination with air into brown glass bottles, poissioned with 1 ml saturated $HgCl_2$ solution and afterwards closed airtight with melted paraffin. The oxygen isotope sample were filled into bottles in the same manner, but were not poisoned.

Tab. 13: List of sea water samples for stable carbon and oxygen isotope analysis

ROS	bottle											
GeoB #	no. 1	2	3	4	5	6	7	8	9	10	11	12
	sample	depth	(m)									
3002-2	700	500	300	200	150	120	100	80	50	35	20	2
3003-1	1950	1650	1300	900	700	500	300	200	100	50	20	2
3004-3	2	1800	1500	1000	580	500	300	200	160	100	810	35
3005-4	2700	2000	1500	1300	1000	900	650	350	100	50	25	2
3006-1	3000	2500	2000	1600	1300	1000	700	500	300	100	20	2
3008-4	2210	1500	1300	1000	700	500	300	250	100	40	20	3
3009-1	4078	3000	2000	1500	1300	1000	700	500	80	60	40	20
3010-1	800	600	450	350	300	250	200	150	100	64	35	2,5
3011-4	2607	2000	1300	800	500	200	150	100	60	40	20	4
3012-3	1517	1199	750	600	300	200	150	120	100	80	60	2
3013-3	1700	1200	800	600	400	300	200	150	100	80	55	4

The stable isotope measurements will be conducted in the mass spectrometry lab. at Bremen University. The sea-water isotope values are needed for direct comparison with those from calcitic shells of foraminifera caught in plankton nets. Moreover ^{13}C values of seawater dissolved inorganic carbon will be compared with nutrient measurements (University of Hamburg) from the same sample depths in order to evaluate whether the KROOPNICK (1985) relationship is valid also in upwelling regions.

5.3.2 Chemical Oceanography

5.3.2.1 Preliminary Results Concerning the CO_2 System of the Western Arabian Sea and the Gulf of Aden

(A. Hupe, R. Lendt, K. Pegler)

M31/3 in March 1995 was the first of three cruises (M32/4 June/July and M33/1 September/October 1995) where the Institute of Biogeochemistry and Marine Chemistry (IfBM Hamburg) carried out measurements of three parameters describing the CO_2 system in the Arabian Sea. The leg took place in the western Arabian Sea and the Gulf of Aden at the end of the NE-monsoon. Particle fluxes are controlled by monsoons: They cause higher fluxes during the NE and SW monsoons and lower fluxes during the intermonsoon periods (e.g. HAAKE et al., 1993). The objectives of the CO_2 group at the IfBM are to quantify the monsoon-forced variations within the "biological CO_2 pump" in the mixed layer (ML) which controls the exchange of CO_2 through the air-sea interface ("chemical pump"). Consequently, the enormous variability of the particle flux should also influence the CO_2 chemistry in the Arabian Sea, because destruction of organic matter as well as dissolution of carbonate minerals contribute to both, the total dissolved inorganic carbon (TC) and the total alkalinity (TA).

During M31/3, 194 discrete seawater samples were collected at 18 CTD stations with a multiple seawater sampler (12 x 10 dm^3 Niskin bottles). Along surface transects, 73 underway samples (uw) from ca. 7 m water depth were taken by the continual seawater pump system of the IfBM. Due to problems of the air freight carrier the scientific equipment had not been shipped to Djibouti in time. Therefore all TA and TC samples had to be poisoned and stored. Until now, only a small amount of the stored samples have been analyzed. pH cannot be measured, because it is impossible to preserve such samples. TA is measured using a potentiometric titration method (e.g. DICKSON, 1981; DOE, 1994, ALMGREN et al., 1983). TC is analyzed with a coulometric detector (UIC Mod. 5011 carbon dioxide coulometer) combined with a CO_2 extraction unit (ROBINSON and WILLIAMS, 1991; DOE, 1994). The results will be used to calculate the partial pressure of carbon dioxide (pCO_2) in seawater. The pCO_2 gradient between the sea surface and the atmosphere provide information whether the survey area is a potential sink or source for atmospheric CO_2 during M31/3. The computation of pCO_2 will start soon.

The TC and TA data discussed in this report are preliminary results. TA was evaluated by a granplot program not considering nutrient concentrations (provided by K. WALLMANN and coworkers, GEOMAR Kiel) and the electrode slope factor. Instead of the measured salinity (S) a uniform S of 35 psu has been used.

By definition, TC and TA change proportionally to salinity (e.g. BROECKER and PENG, 1982). To eliminate the salt effect on TC and TA, these parameters are normalized to a constant S of 35 psu (abbreviation: TCn, TAn).

Vertical profiles of TCn and TAn at various CTD stations are summarized in Figure 56a, b. The following stations were occupied:

Location	CTD-Station	Latitude	Longitude
Gulf of Aden	105	12°47'N	44°37'E
Gulf of Aden	106	13°29'N	50°18'E
	107	14°36'N	52°55'E
	109	15°50'N	57°00'E
WAST	110#3	16°03'N	60°16'E

Generally, the TCn profiles show similar patterns (Figure 56a). Starting with low concentrations in the ML (1925-1940 µmol/kg), TCn increases by at least 200 µmol/kg down to 150 m due to decomposition of organic matter. This is accompanied by a significant decrease in oxygen content (data provided by M. MOLIS, IfM Kiel). TCn rises moderately at the top of the oxygen minimum zone (150-500 m) and increases sharply below 500 m down to 2000 m depth with concentrations of 2340 µmol/kg, except station 105. This position, located in the Gulf of Aden, is strongly influenced by outflowing Red Sea Water (RSW) characterized by lower TCn concentrations (KUMAR et al., 1992). Due to the lack of data between 100 and 500 m at station 109, and 110#3, Figure 56a shows untypical TCn profiles in these depth. One would expect a similar distribution as at station 106 and 107.

In contrast, TAn does not depict a significant gradient in the upper 500 m (2300-2330 µeq/kg; Figure 56), because it is less affected by biological processes than TCn. According to ANDERSON and DYRSSEN (1994) the marked increase of TAn below 700 m suggests dissolution of calcium carbonate. At station 105, a TAn minimum of 2250 µeq/kg is clearly depicted at 693 m depth. This water is strongly influenced by RSW depleted in TAn and TCn: RSW looses carbon because calcifying phytoplankton and expanding coral reefs form calcium carbonate (ANDERSON and DYRSSEN, 1994).

The TCn concentrations (Figure 56a) are low in the ML due to primary production limited by nutrient availability. Presumably, nutrients are remineralized by zooplankton and bacteria within the ML and are consumed by phytoplankton again (regenerating communities; e.g. SMETACEK, 1991). Possibly, dissolved atmospheric CO_2 in the ML can be mixed down to the thermocline and is substituted by CO_2 of the thermocline which is balanced by nutrients. According to CHIPMAN et al. (1993) and TAYLOR and STEPHENS (1993), diurnal variations in the ML depth can support this CO_2 exchange. These processes can keep the TCn concentration low over a longer period.

A distinct regional trend is seen in Figure 56a. The TCn gradient in the upper 200 m rises from the Gulf of Aden (stations 105, 106) towards the western Arabian Sea (station 107). In the latter region higher primary production in the ML causes an enhanced vertical particle flux. Subsequently, respiration of organic matter within the upper thermocline is amplified and contributes to the TCn.

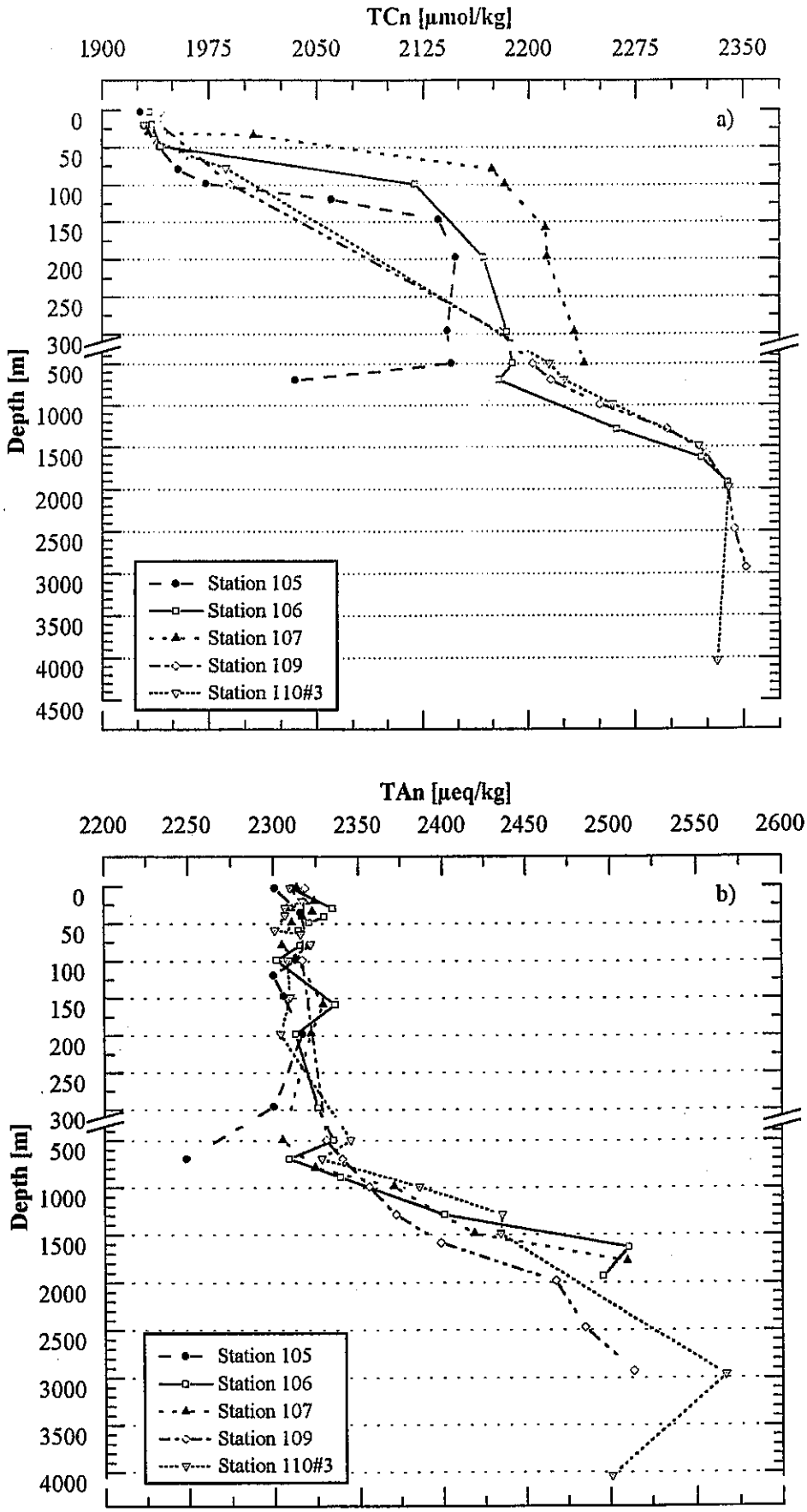

Fig. 56: Vertical profiles of TCn (a) and TAn (b) at various CTD stations during M31/3.

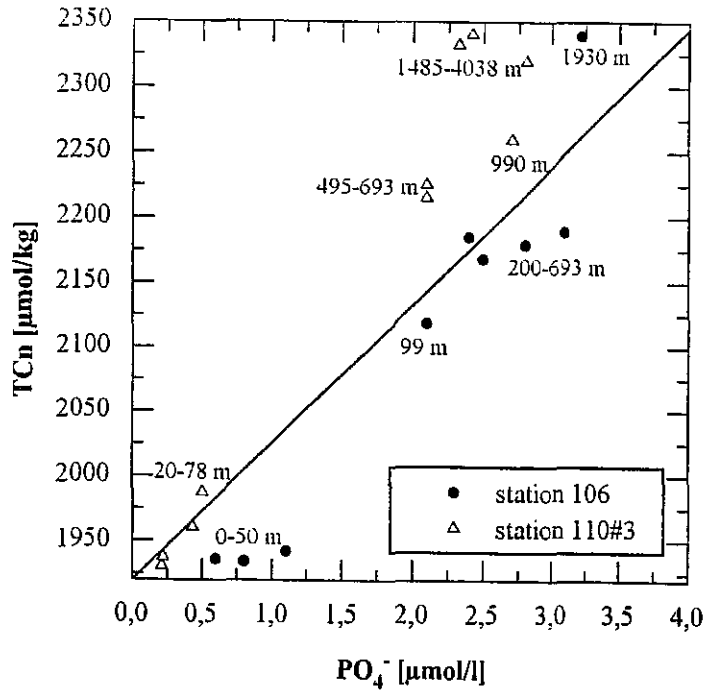

Fig. 57: TCn plotted against the phosphate concentration (data provided by K.Wallmann, GEOMAR Kiel) for stations 106 and 110#3. The straight line represents an ideal slope of 106:1.

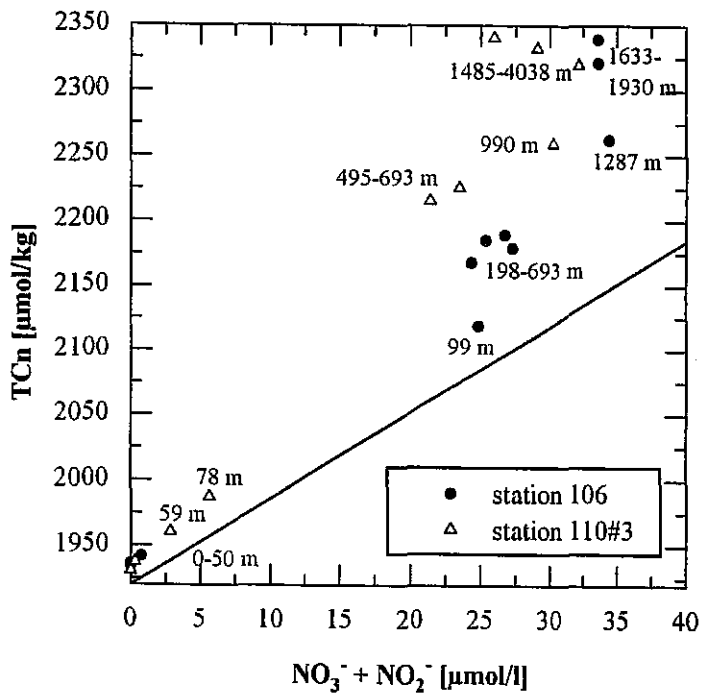

Fig. 58: TCn plotted against the concentration of nitrate + nitrite (data provided by K.Wallmann, GEOMAR Kiel) for stations 106 and 110#3. The straight line represents an ideal slope of 106:1.

In Figure 57 and Figure 58 TCn is plotted versus phosphate and nitrate concentrations, respectively. The ideal Redfield ratio of C:P = 106:1 nearly holds for depths above 1000 m. For the deep water the ratio is higher because of an increased TCn due to calcium carbonate dissolution. The theoretical Redfield slope of C:N = 106:16 does not fit the data because NO_3^- is consumed by denitrification processes above 1000 m (see e.g. ANDERSON and DYRSSEN, 1994). Figure 58 depicts that the denitrification in the oxygen minimum zone is amplified in the western Arabian Sea (station 110#3) than in the Gulf of Aden (station 106).

5.3.2.2. C_1 - C_4 hydrocarbons in the Gulf of Aden and the Arabian Sea (JGOFS)

(N. Delling, R. Seifert, W. Michaelis)

Introduction

Light aliphatic hydrocarbons are atmospheric trace gases which contribute significantly to the greenhouse effect. The increasing concentration of these greenhouse gases and their strong influence on the tropospheric and stratospheric chemistry call for endeavours to understand the processes that control these components.

The surface water of the ocean is regarded as a natural source for atmospheric hydrocarbons and usually supersaturated with respect to atmospheric hydrocarbons (LAMONTAGNE et al., 1974; BROOKS et al., 1981; CONRAD and SEILER, 1988; PLASS et al., 1992; PLASS-DÜLMER et al., 1993; 1995; SEIFERT et al., 1996). This supersaturation is due to biological *in situ* production in the upper water column of < 500 m depth (LAMONTAGNE et al., 1973; SCRANTON and BREWER, 1977; TRAGANZA et al., 1979; BURKE et al., 1983; OWENS et al., 1991). Presently, neither the processes responsible for the production and/or destruction of hydrocarbons in the ocean nor the quantities of the hydrocarbon fluxes between ocean and atmosphere are known satisfactorily.

The most abundant hydrocarbons in the surface water of the ocean are methane and ethene. Estimations of the methane flux from the ocean into the atmosphere range from 0,2 to 5 $\mu g\ m^{-2}\ h^{-1}$ (CONRAD and SEILER, 1988; KHALIL and RASMUSSEN, 1983; BANGE et al., 1994), but this flux can be exceeded several times in regions with high biological productivity (OWENS et al., 1991).

The major goals of our investigations during leg M31/3 were a) to determine the concentrations of C_1-C_4 hydrocarbons and their spatial and temporal distributions in the upper water column and b) to determine the fluxes of C_1-C_4 hydrocarbons into the atmosphere.

Samples and methods

In total 159 samples were taken at 11 locations along a transect from 12°17.1′ N, 45°37.3′ E to 16°13.2′ N, 60°16.9′ E between 0 and 2000 m water depth. Sampling was performed by a

rosette sampler, equipped with 12 Niskin bottles (volume: 10 L) and associated to a multiprobe system recording pressure, conductivity, temperature, and oxygen. Water samples for dissolved light hydrocarbon analyses were filled in 600 ml gastight glass bottles and stored at 4° C until analysis. All analyses were performed within ten hours after sampling.

A stripping-trapping technique of SWINNERTON and LINNENBOM (1967) was modified and used for hydrocarbon analyses (LADAGE et al., 1991). Dissolved light hydrocarbons in seawater were detected by a modified gaschromatograph (CARLO ERBA, GC 6000), equipped with a FID (flame ionisation detector).

500 ml of the seawater sample are transferred from the storage bottle into a 700 ml glass cylinder. Methane and its higher homologues (C_2 - C_4) are purged with precleaned helium and the extracted light hydrocarbons are selectively trapped at -80° C. After purging 35 minutes the traps are switched into the GC carrier gas circuit and heated to 80° C, thus releasing the light hydrocarbons. The isolated methane and its higher homologues are quantified by using a FID. The signal is recorded by a computer equipped with integration software (CHROMSTAR, BRUKER).

For the calibration of the system discreet volumes of standard (LINDE Prüfgas) are injected into the stripping unit, so that sample and standard undergo the same analytical procedure.
The detection limit of dissolved light hydrocarbons in seawater was 0.05 nL/L. The precision of the method is ± 5 % within the concentration range of 0.5-1000 nL/L and ±20% within the concentration range of 0.05 - 0.5 nL/L. Water samples for the calculation of fluxes across the seawater-atmosphere interface were taken in the upper 5 m of the surface layer.

Results

The hydrocarbons methane, ethane, ethene, propane, propene, butane and butene in the upper 2000 m of the water column of the Gulf of Aden and the Arabian Sea have been measured. The concentrations of methane in the upper 1000 m of the water column are summarised in Figure 59.

The surface water methane concentrations generally ranged between 48 and 77 nL/L down to about 50 m depth. Enhanced methane concentrations were observed in the water column of 80 to 150 m depth with varying concentrations (Figure 59). While some stations showed a clear maximum, most pronounced in case of station 110 reaching 158.4 nL/L, only slightly elevated concentrations were found at other stations. One additional maximum was found at station 105 at about 700 m depth. Generally the methane concentration decreased with increasing depth below 200 m to less than 30 nL/L below 800 m (except stations 105 and 115). The surface water concentrations of methane were supersaturated with respect to the atmosphere. Methane saturation in surface waters varied between 113 and 175 % with an average of 134 %.

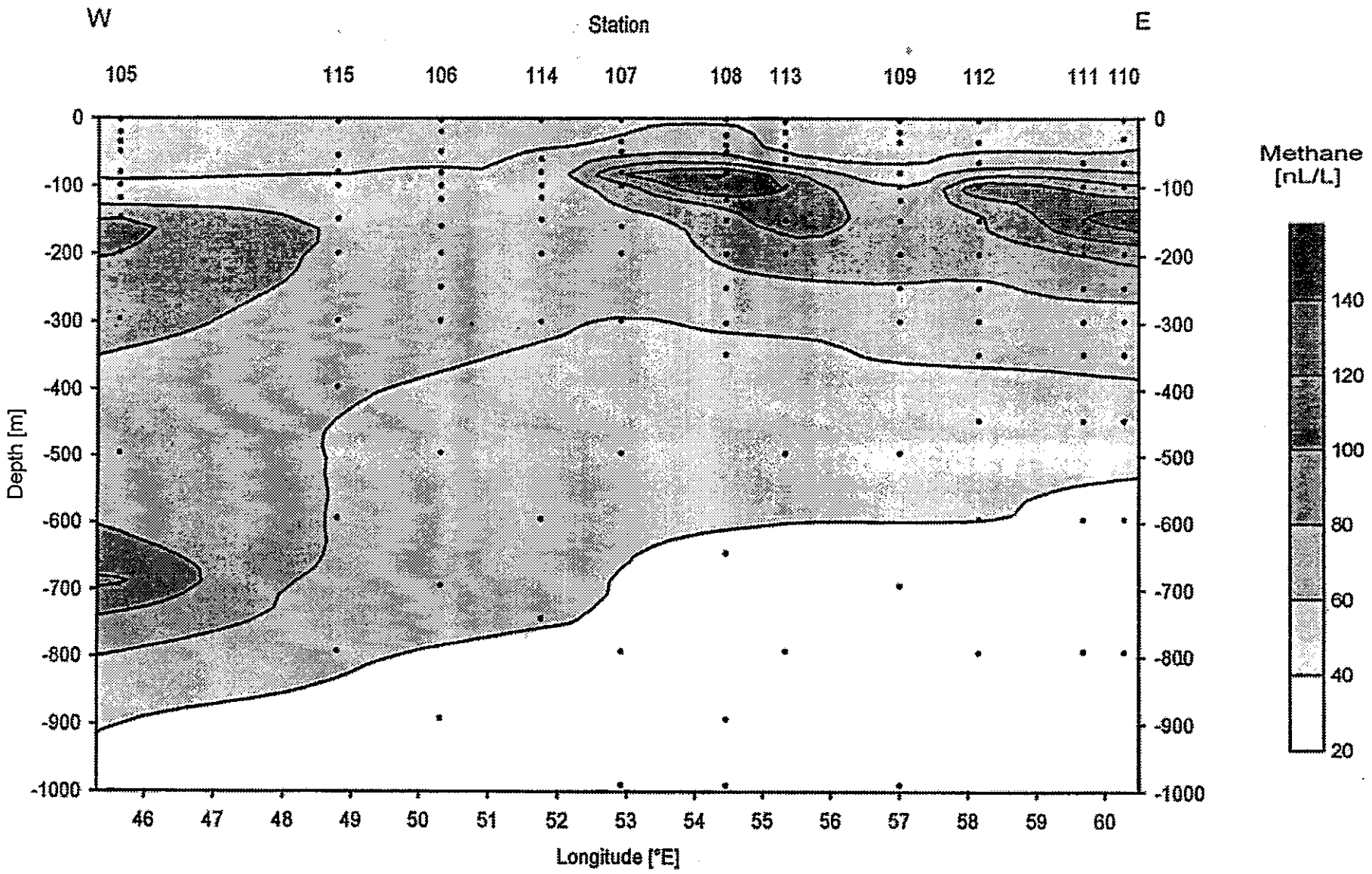
W
Station
E
105
115
106
114
107
108
113
109
112
111
110
0
-100
-200
-300
-400
-500
-600
-700
-800
-900
-1000
Depth [m]
46
47
48
49
50
51
52
53
54
55
56
57
58
59
60
Longitude [°E]
Methane
[nL/L]
140
120
100
80
60
40
20

Methane fluxes from ocean to atmosphere were calculated applying the relationship given by LISS and MERLIVAT (1986) corrected according to the Schmidt numbers of methane and carbon dioxide as given by LAMBERT and SCHMIDT (1993) and an atmospheric methane concentration of 1.751 ppmv. This value was calculated from a concentration of 1.710 ppmv in 1992 assuming an annual increase of 0.8 % (KHALIL and RASMUSSEN, 1986; THOMAS et al., 1989; LELIEVELD et al., 1993; DLUGOKENCKY et al., 1994). Air pressure, wind speed, water temperature and salinity were measured at each station. The resulting flux of methane into the atmosphere varies between the stations from 0.04 to 1.77 $\mu g\ m^{-2}\ h^{-1}$ (Figure 60).

Dissolved ethene could be observed at all stations; selected concentration profiles are depicted in Figure 61. Ethene concentrations in the upper 100 m of the water column varied between 1.25 and 8.03 nL/L. No maxima was found below 100 m depth except for station 106, where a weak maximum was observed at 120 m depth. Generally, the concentrations decreased with increasing depth below 100 m depth.

Discussion

Methane production in oxygenated sea water is still a subject of discussion. As all known methanogenic bacteria are strict anaerobes, various pathways of methane production coupled to anoxic microenvironments occurring in fecal pellets, digestion tracts of higher organisms, dead cells, or organic aggregates have been emphasised.

The occurrence and the variability of the methane maxima, observed in the upper 200 m of the water column, will have to be further interpreted consulting the biological and hydrographical parameters measured simultaneously. This will include results from other JGOFS campaigns conducted in the Arabian Sea and take into account seasonal and regional variations. The deeper maximum detected at station 105 at 700 m depth results from local hydrothermal activity in the Gulf of Aden (JEAN-BAPTISTE et al., 1990). Methane concentrations less than 30 nL/L below 800 m depth are thought to be largely the result of microbial oxidation (OWENS et al., 1991).

Our calculated methane fluxes from the seawater into the atmosphere are in the range of the world-wide investigations of the oceans, estimated on an average of about 1 $\mu g\ m^{-2}\ h^{-1}$ by BANGE et al. (1994). The reasons for the low fluxes in the eastern part of the studied area are mainly the very low wind speeds during our investigation.

Ethene concentrations of the investigated surface waters were supersaturated with respect to the atmosphere. This indicates, that the studied area of the Gulf of Aden and the Arabian Sea must be considered as a source for atmospheric ethene. The ethene concentration maxima in the upper 100 m of the water column may be caused by biological production. However, the source of ethene in ocean surface waters is far from unequivocally known. Biological ethene production is known from higher plants, bacteria and fungi (LYNCH and HARPER, 1974;

PRIMROSE and DILWORTH, 1976; PRIMROSE, 1977; MANSOURI and BUNCH, 1989; NAGAHAMA et al., 1991). For aquatic environments Brooks and Sackett (1973) suggested that ethene is associated with primary productivity. LAMONTAGNE et al. (1974) assume variations of ethene concentrations in the pacific to be the result of biological activity. Additionally, ethene production by photochemical reactions is discussed (RATTE et al., 1993).

Distinct informations on the processes controlling ethene concentrations may arise from the analysis of biological and hydrographical data collected during our investigation.

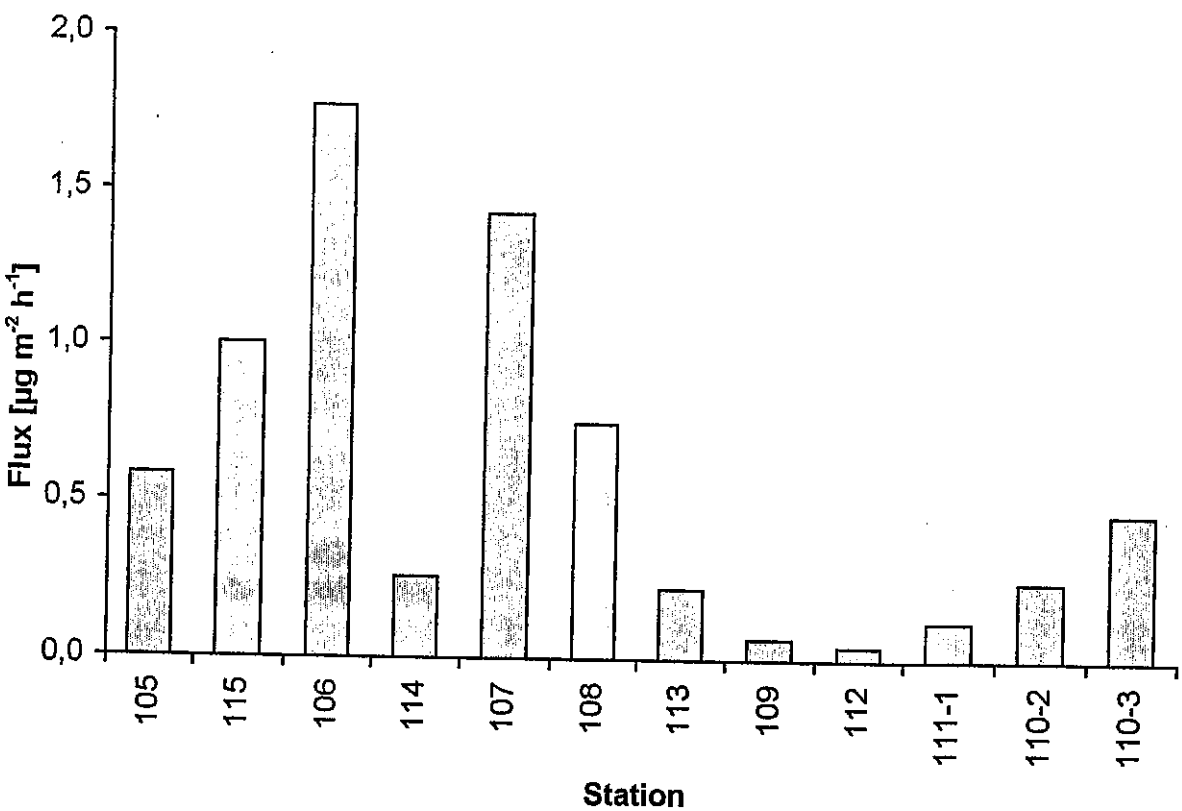

Fig. 60: Flux of methan from seawater into the athmosphere.

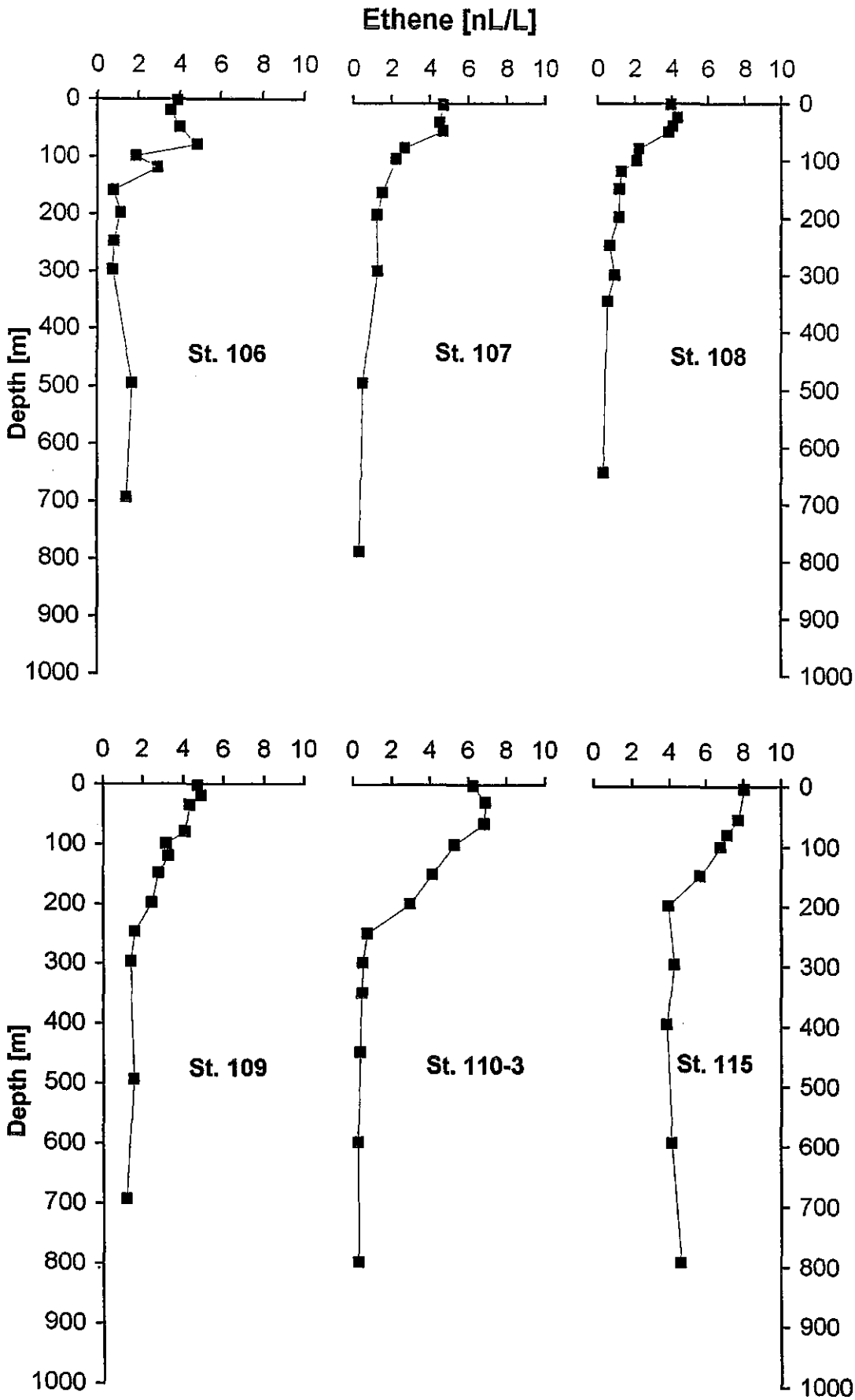

Fig. 61: Vertical distribution of dissolved ethene.

5.3.3 Biological Oceanography

5.3.3.1 Planktology

5.3.3.1.1 Planktological Activities

(W. Koeve)

The work carried out by the plankton group from IfM-Kiel concentrated on the characterization of the vertical oxygen distribution and the vertical and lateral patterns of particulate biogenic matter. This activity was part of the German contribution to the Arabian Sea Process Study of JGOFS. Since the respective German programm was still in ist very initial phase during early 1995, the research reported here was planned and carried out as part of the planktological North Atlantic JGOFS project at IfM-Kiel. Laboratory based analysis of data and interpretation of results, however, will be carried out as part of the respective Arabian Sea Project.

During the cruise 19 profiles were sampled for oxygen measurements (Winkler technique). Usually one shallow (about 300 m) and one deep CTD-cast were performed to allow a detailed characterization of the vertical O_2-distribution.

Samples for the analysis of particulate biogenic matter were taken from both the CTD-casts and from the continous pumping system that enabled sampling of the surface during cruising between CTD-stations. A total of 126 stations have been sampled with this device. Water samples were subdevided for respective particle concentration (filtration) for measurements of chlorophyll-a, phytoplankton pigments (HPLC), particulate organic carbon and nitrogen (POC/N) and biogenic silicium (Bsi). All filteres were stored at -40° C for latter shore based analysis. Logistic problems at the final port of M31/3 prevented a rapid and well controlled transport of scientific samples to Germany. During latter handling of samples at the port of Muscat, samples have been shipped to Germany without cooling. Therefore we expect that particularly results of chlorophyll-a and HPLC measurements will be less reliable.

5.3.3.1.2 Coccolithophorids

(A. Zeltner)

Material and Methods

Nannoplankton samples were collected on 11 sampling stations. To investigate Coccolithophores water sample hauls were employed at the water depth of 20, 40, 60, 80, 100, 200, 300, 500, 700, 1000, 1500, 2000, and 2500 m.

Hydrographical measurements were recorded using a CTD.

Aboard, 1,75 L of the phytoplankton samples were passed through Nucleoporefilters (47 mm diameter, 0.45 µm pore size) by means of a vacuum pump. Filters were air-dried and stored in plastic petri-dishes.

Species were taxonominally identified and the number of specimens was counted using an electron microscope. To determine the particular phytoplankton standing stock, coccospheres, single coccoliths, diatoms, dinoflagellates and silicoflagellates were counted using a magnification factor of 2000. At minimum 345 screens were counted.

Coccolithophore standing crop and diversity

The particulate standing stock > 0.45 µm of algae in the Arabian See (12° N/44° E to 16° N /60° E) is largely constituted by coccolithophorids, pennate and centric diatoms, dinoflagellates, and silicoflagellates.

In the top 20 m, the coccolithophore standing crop varied from 30 to 144 $x10^3$cells l^{-1} (Table 14).

A subsurface maximum in coccolithophorid cell densities was observed at 40 m depth, where the standing crop ranges from 45 to 178 $x10^3$ cells l^{-1}. At 60 m depth the cell densities with at maximum 139 $x10^3$ cells l^{-1} are decreased. In 80 m and 100 m a coccolithophore standing crop of 30 and 38 $x10^3$ cells l^{-1}, respectively, was recorded.

Decreases in cells in the upper 60 m are not associated with changes in species diversity (expressed as numbers of species).

Tab. 14: Distribution pattern of coccolithophorids (x1000 cells/l)

Stations											
Depth [m]	105	116	115	106	114	107	108	113	109	111-1	110-4
20		#			46	79	96	41	30	132	144
40		97			61	134	178	45	155	140	127
60						139	128		113	43	60
80							19			24	30
100							7		38	8	31
200							3				

Community structure

Seventyeight coccolithophore taxa have been recognized in the present study (see species list). In the upper 80 m *Emiliania huxleyi, Gephyrocapsa oceanica, Oolithotus antillarum, Calcidiscus leptoporus* are frequent to dominant, followed by less frequent species

Calciosolenia murrayi, *Umbilicosphaera sibogae* var. *foliosa*, *Michaelsarsia adriaticus*, *Algirosphaera robusta*, *Calciopappus rigidus* and *Umbilicosphaera sibogae* var. *sibogae*. *E. huxleyi* and *G. oceanica* predominated the floral assemblage in the most samples, but single species were sometimes more abundant.

The species composition in the top 20 m yields up to thirtythree species. In 40 and 60 m depth level the species diversity decreases around twenty species. Coccolithophorid floral assemblage studied at 100 m depth yielded a total of twelve species, which is dominated by *G. oceanica* and *C. leptoporus*.

The increase in abundances and diversity of coccolithophorids may be due to a well defined thermocline (GUPTHA, 1995). Small amounts of holococcolithophorids confirm oligotrophic conditions. High cell densities are often associated with increasing fluorescence. No relationship was found between the total standing crop values, and temperature or salinity.

Species list of M 31/3:
Division: HAPTOPHYTA Cavalier-Smith, 1986
Class: PRYMNESIOPHYCEAE Hibberd, 1976
Subclass: PRYMNESIOPHYCIDAE Cavalier-Smith, 1986, orth. mut. Jordan et Green
Order: PRYMNESIALES (Fritsch) Papenfuss, 1955

Family: NOELAERHABDACEAE Jerkovic, 1970

Emiliania Hay et Mohler in Hay *et al.*, 1967
E. huxleyi (Lohmann) Hay et Mohler in Hay *et al.*, 1967 var. *huxleyi*
Gephyrocapsa Kamptner, 1943
G. oceanica Kamptner, 1943
G.? sp. type A, Kleijne 1991
G. sp.
Reticulofenestra Hay *et al.* emend. Gallagher, 1989
R. punctata (Okada et McIntyre) Jordan et Young, 1990

Family: CALCIOSOLENIACEAE Kamptner, 1937

Anaplosolenia Deflandre, 1952
A. brasiliensis (Lohmann) Deflandre, 1952
Calciosolenia Gran, 1912
C. murrayi Gran, 1912

Family: COCCOLITHACEAE Poche, 1913

Calcidiscus Kamptner, 1950

C. leptoporus (Murray et Blackmann) Loeblich Jr et Tappan, 1978
Oolithotus Reinhardt in Cohen et Reinhardt, 1968
O. antillarum (Cohen) Reinhardt in Cohen et Reinhardt, 1968
Umbilicosphaera Lohmann, 1902
U. hulburtiana Gaarder, 1970
U. sibogae var. *foliosa* (Kamptner) Okada et McIntyre, 1977
U. sibogae (Weber-Van Bosse) Gaarder, 1970 var. *sibogae*

Family: HELICOSPHAERACEAE Black emend. Jafar et Martini, 1975

Helicosphaera Kamptner, 1954
H. carteri (Wallich) Kamptner, 1954 var. *carteri*

Family: PAPPOSPHAERACEAE Jordan et Young, 1990

Pappomonas Manton et Oates, 1975
P. sp.
Papposphaera Tangen, 1972
P. lepida Tangen, 1972
P. sagittifera Manton, Sutherland& Mc Cully, 1976

Family: RHABDOSPHAERACEAE Haeckel, 1884

Acanthoica Lohmann ex Lohmann, 1913
A. quattrospina Lohmann, 1903
A. maxima Heimdal, 1981
Algirosphaera Schlauder emend. R.E. Norris, 1984
A. robusta (Lohmann) R.E. Norris, 1984
Anacanthoica Deflandre, 1952
A. cidaris (Schlauder) Kleijne, 1992
A. sp. type A Kleijne, 1992
Cyrtosphaera Kleijne, 1992
C. aculeata (Kamptner) Kleijne, 1992
Discosphaera Haeckel, 1894
D. tubifera (Murray et Blackman) Ostenfeld, 1900
Rhabdosphaera Haeckel, 1894
R. clavigera Murray et Blackmann, 1898 var. *clavigera*
R. xiphos (Deflandre et Fert) R.E. Norris, 1984

Family: SYRACOSPHAERACEAE (Lohmann) Lemmermann, 1903

Alisphaera Heimdal emend. Jordan et Chamberlain, 1993
A. unicornis Okada et McIntyre, 1977
Calciopappus Gaarder et Ramsfjell emend. Manton et Oates, 1983
C. rigidus Heimdal in Heimdal et Gaarder, 1981
Canistrolithus Jordan et Chamberlain, 1993
C. valliformis Jordan et Chamberlain, 1993
Coronosphaera Gaarder in Gaarder et Heimdal, 1977
C. mediterranea (Lohmann) Gaarder in Gaarder et Heimdal, 1977
Gaarderia Kleijne, 1993
G. corolla (Lecal) Kleijne, 1993
Michaelsarsia Gran emend. Manton *et al.*, 1984
M. adriaticus (Schiller) Manton *et al.*, 1984
M. elegans Gran emend. Manton *et al.*, 1984
Ophiaster Gran emend. Manton et Oates, 1983
O. hydroideus (Lohmann) Lohmann emend. Manton et Oates, 1983
Syracosphaera Lohmann, 1902
S. anthos (Lohmann) Janin, 1987
S. dilatata Jordan *et al.*, 1993
S. epigrosa Okada et McIntyre, 1977
S. epigrosa sp. II cf. *S. epigrosa*
S. exigua Okada et McIntyre, 1977
S. halldalii Gaarder ex Jordan et Green, sp. nov.
S. lamina Lecal-Schlauder, 1951
S. marginaporata Knappertsbusch, 1993, orthog. emend.
S. nodosa Kamptner, 1941
S. orbiculus Okada et McIntyre, 1977
S. ossa Loeblich Jr et Tappan, 1968
S. pirus Halldal et Markali, 1955
S. prolongata Gran ex Lohmann, 1913
S. pulchra Lohmann, 1902
S. sp. A. Broken
S. sp. type B Kleijne, 1993
S. sp. type C Kleijne, 1993
S. sp. type F Kleijne, 1993
S. sp. type I Kleijne, 1993
S. sp.

Umbellosphaera Paasche in Markali et Paasche, 1955
U. irregularis Paasche in Markali et Paasche, 1955
U. tenuis (Kamptner) Paasche in Markali et Paasche, 1955 type I

Family: CALYPTROSPHAERACEAE Boudreaux et Hay, 1969

Calyptrolithina Heimdal, 1982
C. divergens var. *tuberosa* (Heimdal) Jordan *et al.*, 1993
Calyptrolithophora Heimdal in Heimdal et Gaarder, 1980
C. hasleana (Gaarder) Heimdal et Gaarder, 1980
Calyptrosphaera Lohmann, 1902
C. oblonga Lohmann, 1902
Corisphaera Kamptner, 1937
C. gracilis Kamptner, 1937
C. strigilis Gaarder, 1962
C. sp.
Poricalyptra Kleijne, 1991
P. magnaghii (Borsetti et Cati) Kleijne, 1991
P. sp.
Poritectolithus Kleijne, 1991
P. tyronus Kleijne, 1991
Syracolithus (Kamptner) Deflandre, 1952
S. catilliferus (Kamptner) Deflandre, 1952
S. confusus Kleijne, 1991
S. sp. 1
S. sp. 2
Zygosphaera Kamptner emend. Heimdal, 1982
Z. amoena Kamptner, 1937
Z. hellenica Kamptner, 1937

GENERA INCERTAE SEDIS

Florisphaera Okada et Honjo, 1973
F. profunda Okada et Honjo, 1973, var. *elongata* Okada et McIntyre, 1980
F. profunda Okada et Honjo, 1973, var. *profunda*
Polycrater Manton et Oates, 1980
P. galapagensis Manton et Oates, 1980
Thorosphaera flabellata Halldall et Markali, 1955

UNDETERMINED SPECIES

"Heterococcolithophorid" sp. 1

"Holococcolithophorid" sp. 1
"Holococcolithophorid" sp. 2
"Holococcolithophorid" sp. 3

5.3.3.1.3 Planktic Foraminifera

(B. Hiller)

Calcareous zooplankton

Planktic Foraminifera

The large-scale spatial distribution of planktic foraminifera in surface waters of the Indian Ocean was first described by BÉ and TOLDERLUND (1971) and BÉ and HUTSON (1977). These investigations serve as the basis for the high resolution description of the temporal and spatial distribution of the living fauna and of the flux of planktic foraminiferal tests, including the Arabian Sea.

First counts (out of 140 samples; see 7.3.2) of planktic foraminifera from station 108 (14°59,3' N/54°23,7' E) and station 111 (16°10,1' N/59°45,9' E) revealed only small differences in the species assemblage and in the abundance of foraminifera (Figure 62). In the upper 100 m of the water column an average of 150 to 180 specimens / m^3 (station 108 and 111) are recorded. The most abundant species at both stations are *Globigerinoides sacculifer* (about 20 % relative abundance), *G. ruber* (white) and *Globigerinita glutinata. Globigerinoides ruber* is more abundant at station 108 (28 %) than at station 111 (12 %). With 26 % at station 108 and 38 % at station 111, *Globigerinita glutinata* is the most frequent species. *Globigerinoides tenella* and *Globigerina bulloides* occur with about 5 % at station 108. At station 111, in the upper 60 m of the water column all species are more frequent than in 60 to 100 m water depth (Figure 63). In contrast to station 111, at station 108 this difference between the surface water and the deeper water column (below 60 m) is less distinct. Single species such as *G. glutinata* and *G. sacculifer* show a continuous decrease in number of specimens with increasing water depth.

In the centre of the of seasonal upwelling off the Arabian Peninsula (station 108) and adjacent to the upwelling centre (station 111), the composition of the planktic foraminiferal fauna was similar, on March, 8 to 12, 1995. Therefore, we conclude that the upwelling at this time was waning or perhaps over. At the upwelling centre (station 108) low abundances but high faunal representation of *G. sacculifer* and *G. ruber* (white), which prefer a higher temperature than *G. glutinata*, record relatively high water temperature and a low production of calcareous plankton. Weak upwelling at station 108 can be suspected from enhanced faunal representation of *G.bulloides*, and from low stratification in the upper water column. In contrast, at station 111 a distinct decrease of planktic foraminiferal abundance below 60 m water depth displays good stratification of the upper ocean. Surface temperature and salinity at station 108 and 111 (CTD recorded) show an even hydrography, whereas fluorescence at station 108 is much higher than at station 111.

Pteropods

Like planktic foraminifera, pteropods are present with similar abundances and with a similar species composition at station 108 and 111. The number of pteropod specimens decreases from 180 to 275 specimens per m^3 in the upper 60 m of the water column to 10 to 84 specimen per m^3 in 60 to 100 m water depth (Figure 64). With 95 to 99 % of the fauna *Limacina* dominates the pteropod assemblage. *Limacina inflata*, which is a characteristic upwelling species (ALMOGI-LABIN 1982), is the most frequent species at both stations. With 1,5 and 5 specimens per m^3 (station 108 and 111) at both stations *Creseis* is present only in the upper 60 m of the water column. *Clio convexa* is present at station 111, below 40 m water depth. *Diacria* was registered at station 108 in the upper 40 m of the water column.

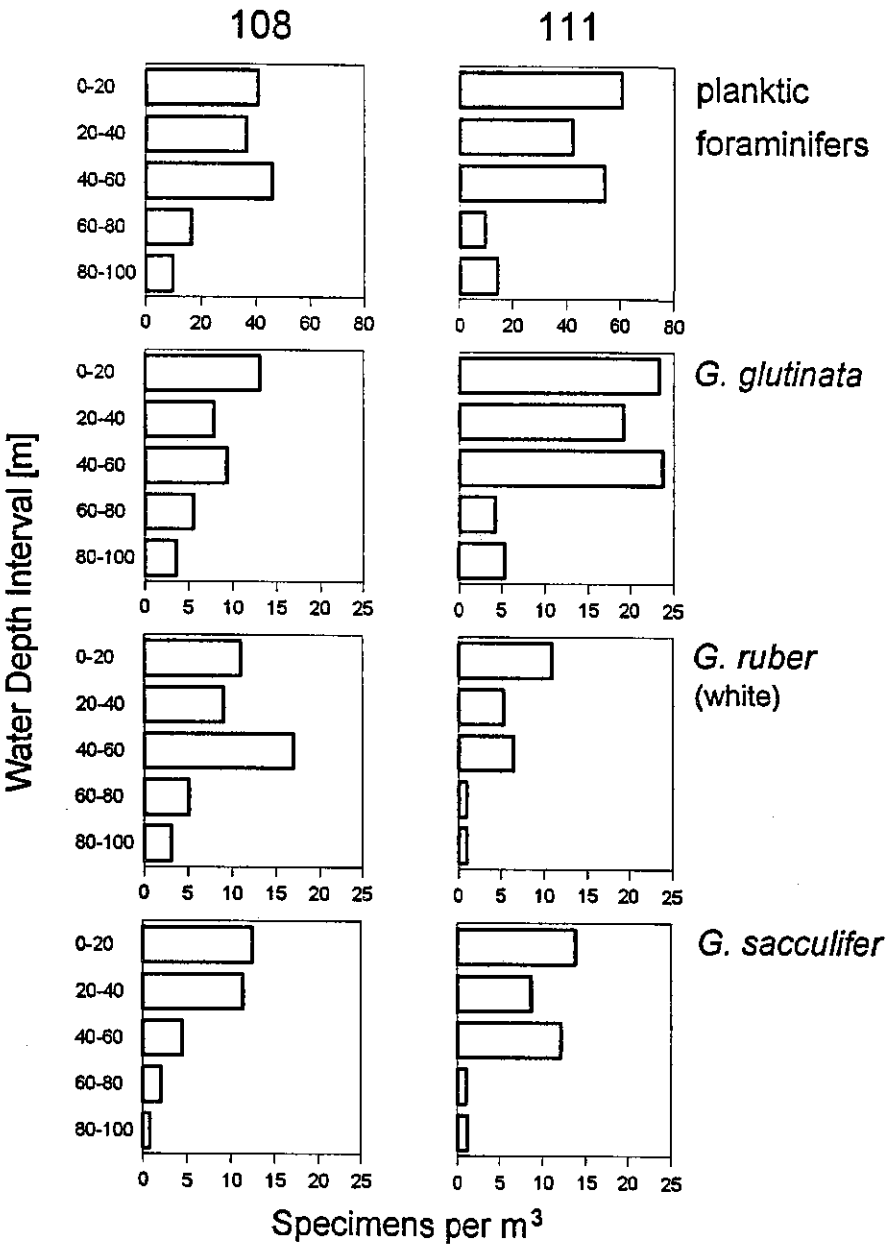

Fig. 62: Relative species distribution at station 108 and 111 in 0 to 100 m water depth. (n = average number of specimens per m^3).

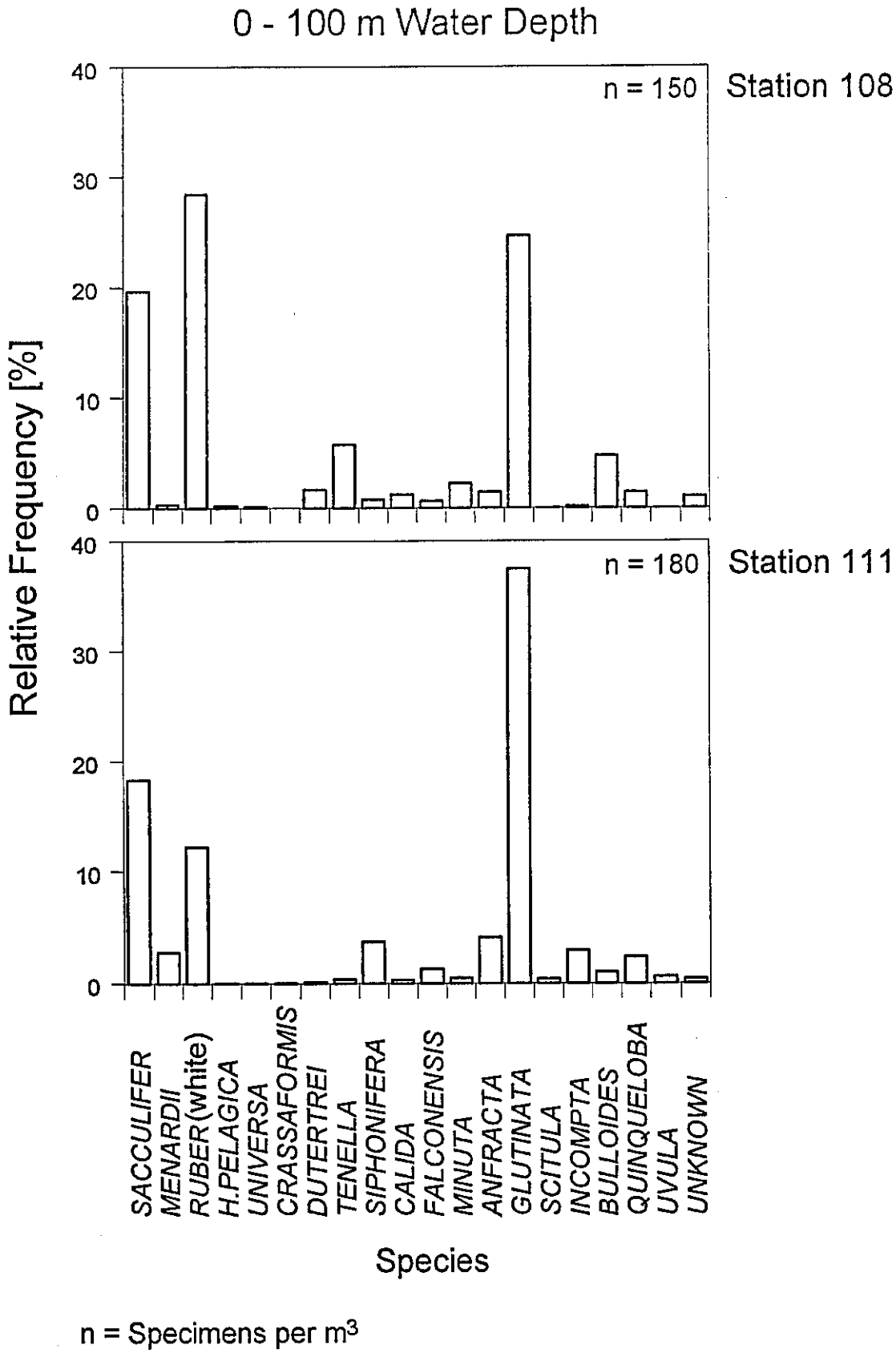

Fig. 63: Frequency of planktic foraminifera and of the three most abundant planktic foraminiferal species, between the ocean surface and 100 m water depth.

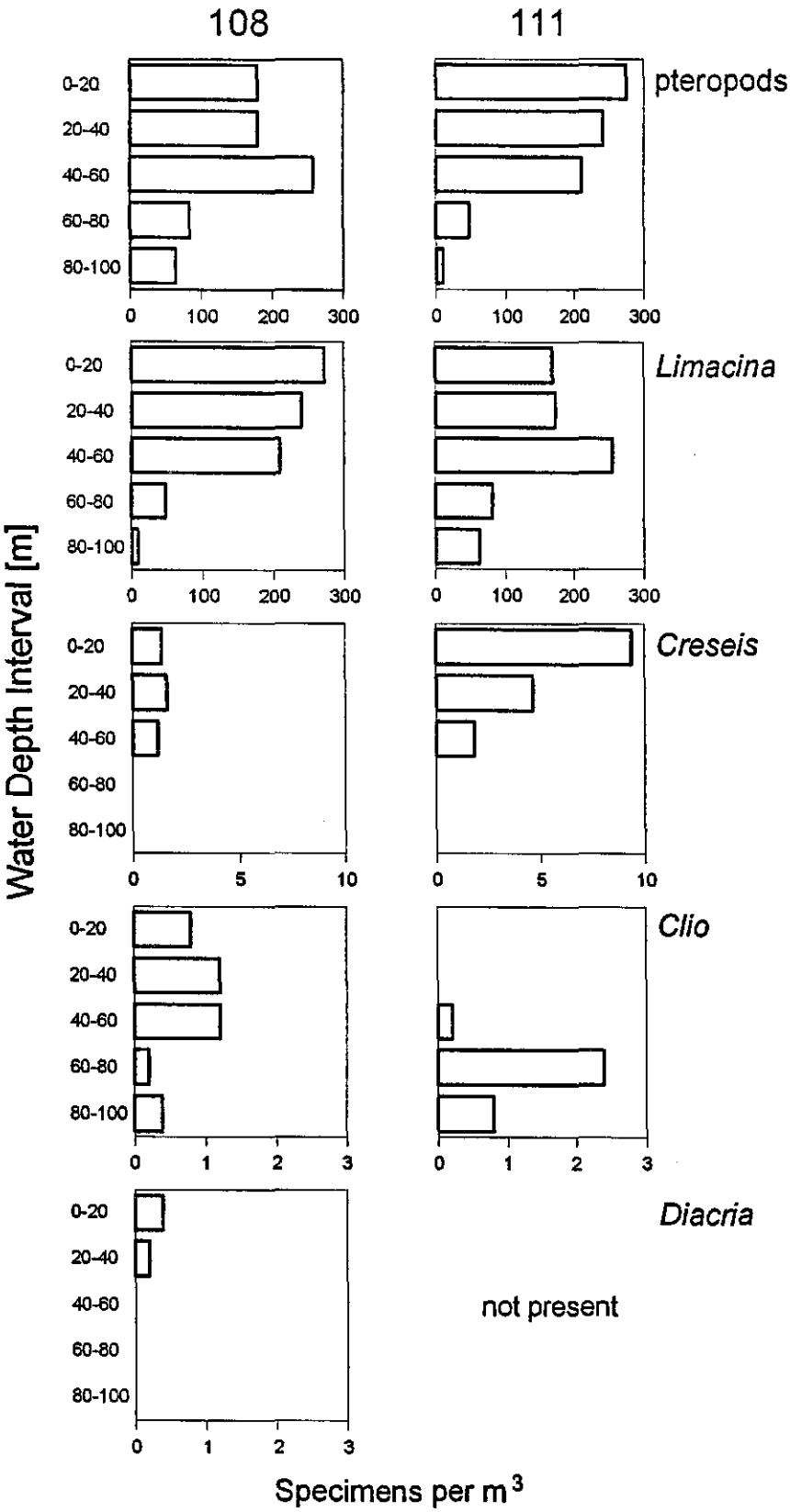

Fig. 64: Frequency of pteropods (bulk fauna) and of single genera, between the ocean surface and 100 m water depth.

5.3.3.1.4 Plankton Samples

Marine plankton from surface waters was sampled during the whole cruise (see 7.3.3). We used the shipboard installed clean sea-water pumpsystem to filter about 2000 to 5000 l each day, mostly during daylight. The amount of water filtered, depended on the plankton mass caught in the net. The sea-water was pumped through a net with a mesh size of 10 microns. When the water flow was stopped by the material closing the net openings, the plankton was washed into plastic bottles and the sampling was continued with the cleaned net. For each day the wet plankton samples were concentrated into one bottle and frozen at -20° C.

The plankton material will be investigated for the bulk composition of the biogenic detritus in order to obtain the ratios between opal, organic carbon and carbonate produced by near surface water plankton communities. In particular, the marine organic material will be investigated in more detail. It is planned to determine the stable isotopes and single organic compounds which can be related to specific phytoplankton organisms. This type of data is needed to compare the marine plankton production in the surface waters of different high productivity systems with fluxes of biogenic particles caught in sediment traps or found in the surface sediments beneath these high productive areas.

5.3.3.2 Benthos Biology

5.3.3.2.1 Benthosbiology

(U. Witte, G. Graf, J.S. Berg)

A multicorer (MUC), a boxcorer (BC) and a photo sledge (PS) were employed on six stations, where the following parameters were analysed:

- determination of sediment oxygen demand (SOD) and the depth of oxygen penetration (MUC);
- measurements of bioturbation (depth-profiles of chlorophyll-a-equivalents and decay constants; ^{210}Pb-profiles; shipboard incubation experiments with luminophores and bromide) (MUC);
- size-spectrum and abundance of the macrofaunal organisms and biogenic surface structures (BC);
- quantitative analysis of epifaunal densities by bottom photography (PS).

Station #108 was used as a test station, whereas the main study-site, the WAST-station, was sampled four times (#110-1 to #110-4). While steaming back to Djibouti, station #112 was sampled.

For the deep-sea plain (WAST; waterdepth approximately 4040 m) first results show a relatively high sediment oxygen demand of 1.28 ±0.8 mmol O_2 $m^{-2}d^{-1}$ (mean of 6 measurements) and a considerably low depth of oxygen penetration (about 11 mm sediment depth, see Figure 65). The sediment oxygen demand of station #112 was in the same range (1,39 ±0.12 mmol O_2 $m^{-2}d^{-1}$; n=3).

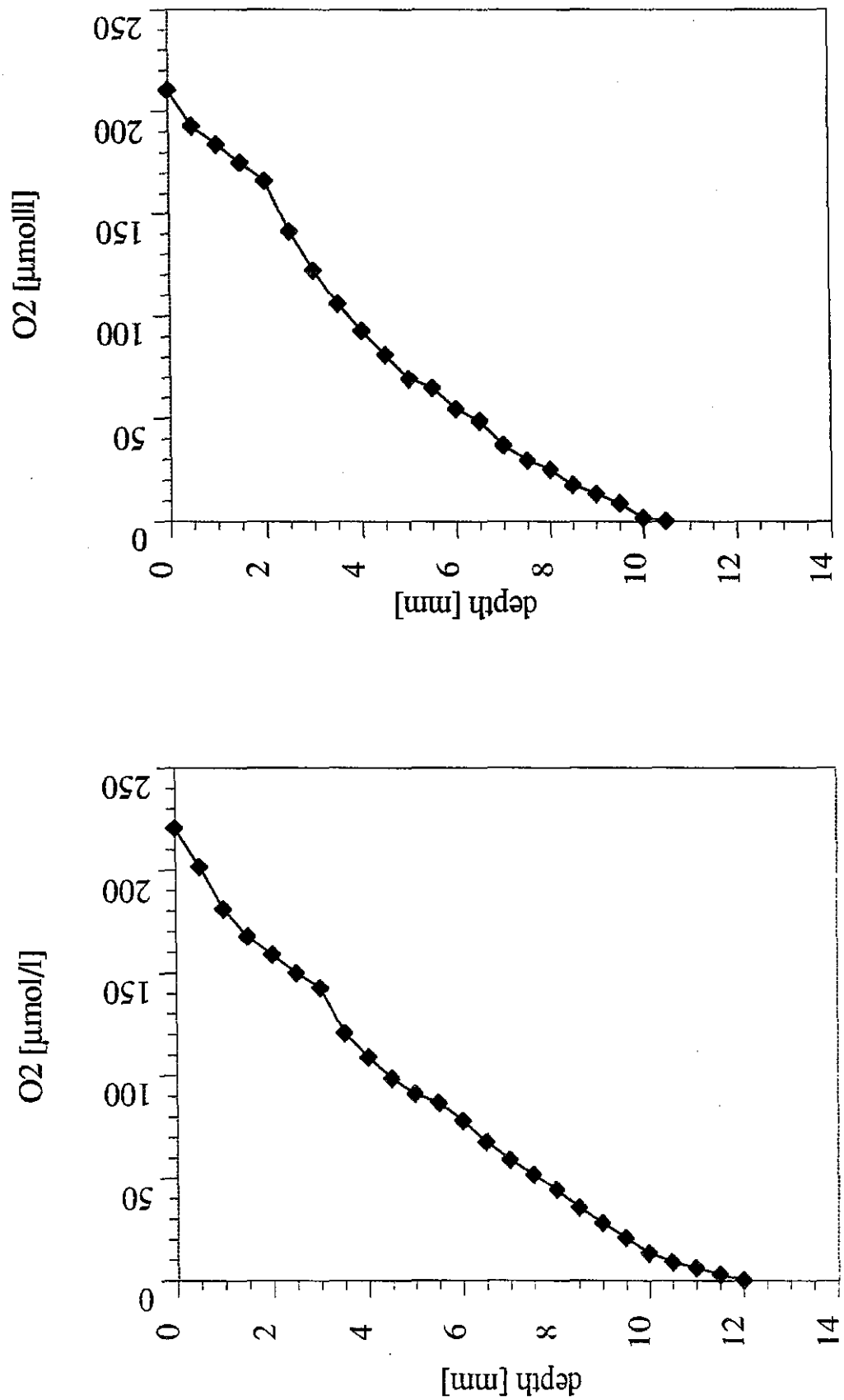

Fig. 65: Oxygen profiles at WAST showing a considerably low oxygen penetration.

Between the fluffy surface layer and the reddish-brown sediment underneath, a network of Xenophyophores was found. Foraminiferans of the genus *Bathysiphon* (Kitazato, pers com.) were common, too.

The vertical parts of macrofaunal burrow-structures reached down to a depth of about 20 cm. The upper 10 cm of the sediment were heavily penetrated by horizontal burrows. In sediment depths of up to 30 cm, nest-like assamblages of pellet-like structures were frequently observed. The surrounding sediment was firmer than on other locations at the same sediment depth. The bottom photographs showed that brittle-stars, occurring in a density of 28 ind/100 m^{-2} to be the most common group of larger epifauna. Now and then, single specimens of large, sponge-like xenophyophores were found. These xenophyophores, a new species named (*Reticulammina arabica*) (description not published yet),were also found on stations 108 and 112 being most abundant at the latter.

5.3.3.2.2 Standing Stock and Activity of Small Benthic Size Classes in the Northwestern Arabian Sea

(O. Pfannkuche and A. Kähler)

Research objective was a first evaluation of the numerical abundance, biomass and metabolic activity of small benthic size classes ranging from 2 µm - 500 µm in cross diameter, namely bacteria, nano- and meiofauna. These groups represent the main decomposers in deep-sea sediments. About 80 % of deep sea biological benthic carbon consumption is channeled through this benthic size classes (PFANNKUCHE, 1993), with bacteria clearly dominating (LOCHTE, 1993). This study was designed as a prestudy for future detailled investigations of benthic biogeochemical fluxes of carbon which were planned for METEOR cruise M33/1.

Sediment samples with a multicorer (BARNETT et al., 1984) were taken at stations 108, 109, 110, 112. Randomly selected multiple corer tubes were subsampled with small piston corers of 1.1 cm or 3,46 cm cross diameter. Three replicates for each parameter were taken from one multiple corer cast. Sediment samples were analysed in 1cm intervals down to 10 cm depth and in 2 cm intervals to a maximum of 30 cm depth. Samples for the following benthic groups and biochemical sediment analyses were taken (measurements marked with an asterisk were carried out in the ship's laboratory):

<u>Numerical abundance and biomass of organisms</u>
- bacteria
- nanofauna
- meiofauna (<500 µm)

<u>Biochemical sediment analyses</u>
Measurements of biomass
- adenylates (ATP+ADP+AMP)
- DNA

- phospolipids (bacteria)

Measurements of metabolic activity

- electron transport system activity (ETS, respirative poptential)*
- ATP
- hydrolysis rates of fluorescein diacetate (activity of bacterial exoenzymes)*

Measurements of plant pigments

- chlorophyll-a and pheopigments (fluorimetric)
- pigments (HPLC)

other measurements

- C_{org}, N_{org}, water content, porosity
- proteins*

The export fluxes of organic matter from the upper mixed layer into the deep Arabian Sea are coupled to the activity of the monsoons. At station 110 a distinct annual maximum of sedimentation (trap results from 3000 m water depth) was recorded by HAAKE et al. (1993) during the SW-monsoon (August - September) whereas during the NE-monsoon (December-February) only a slight increase was registered. In contrast to station 110 situated at the farest distance from the Arabian coast in NW- Arabian Basin (water depth -4000 m) the other station are shallower (2330 m-3150 m). Station 108 lies in the vicinity of a seamount while station 112 is located at the bottom of the continental slope. It appears likely that both stations are greatly influenced by these geomorphological structures in terms of the local sedimentation regimes.

Sampling was performed during the decline of the NE-monsoon. It was hypothesized that phytoplankton material produced in the peak period of the NE-monsoon (December - mid of February) had already settled on the seafloor before our sampling campaign. This hypothesis could be confirmed by the finding of phytodetrital layers ("fluff" *sensu* BILLETT et al., 1983) on top of many sediment cores. Even at the most oceanic station 110 the fluff layer of brownish colour reached a maximum thickness of 2 cm.

The measurement of particulate proteins represents like the determination of C_{org} and N_{org} a measure for both biomass and refractive organic matter thus it can be used as an indicator of benthic productivity. Protein contents (after one hydrolysis, Figure 66) were highest at station 108 and 112 followed by stations 109 and 110. At all station protein values increased with increasing sediment depth reaching maximum values between 5-8 cm depth and remained on a relative costant level until 25-30 cm sediment depth. The high protein values in deeper sediment layers indicate that a substantial part of sedimented organic matter is not consumed instantly by organisms like in the open NE-Atlantic (PFANNKUCHE, 1993). Station 112 exhibits significant changes between 10-15 cm sediment depth where a layer of coarse sand was found.

At all stations ETS activity (Figure 67) was significantly higher in the top centimetre, the area where the bulk of aerobic biological carbon consumption takes place. Below 1cm ETS activity

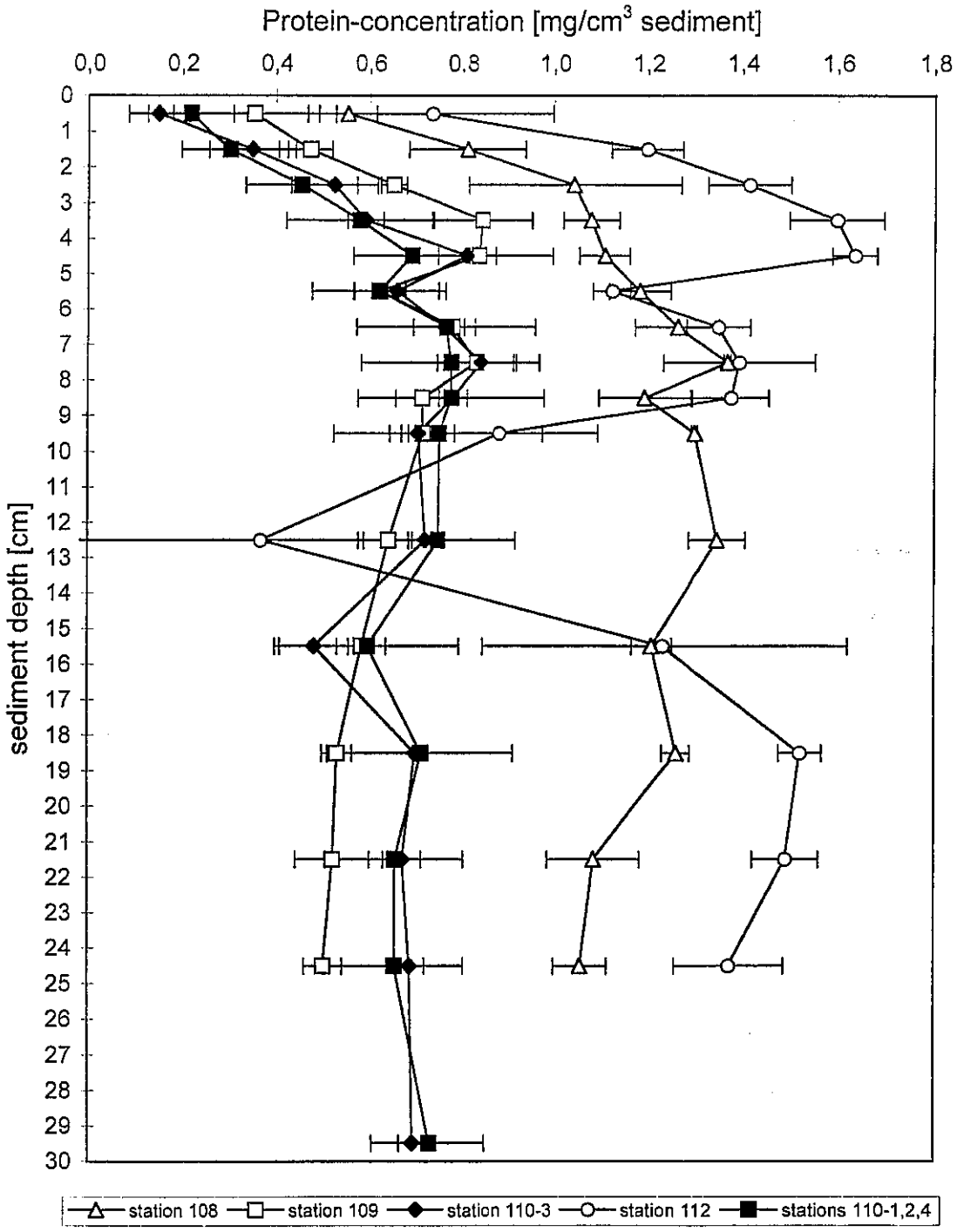

Fig. 66: Concentrations of proteins (1. hydrolysis) in the top 25-30 cm of the sediment. The horizontal lines give the confidence limits at the 95 % probability level.

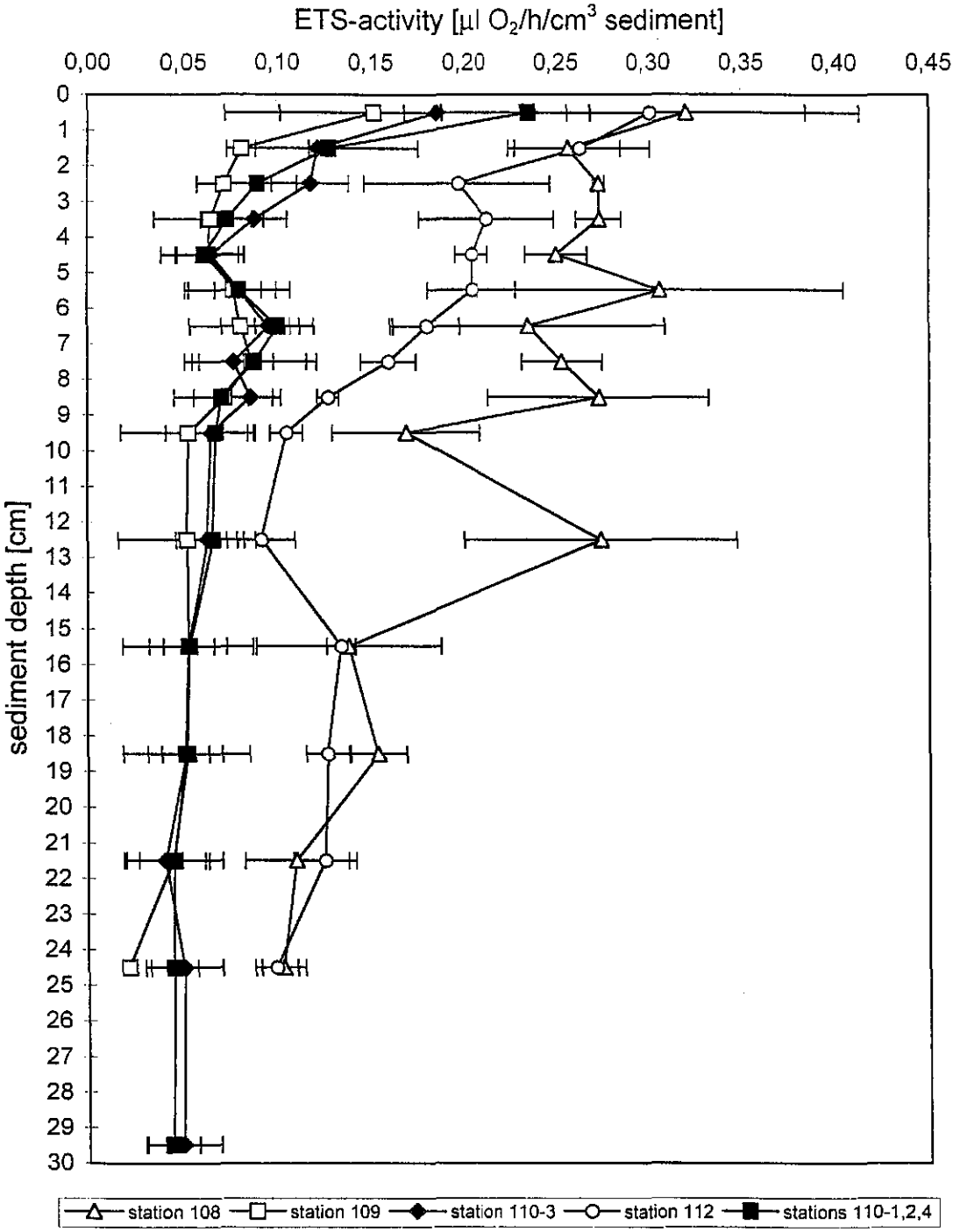

Fig. 67: Potential respirative activity measured (ETS-method) in the top 25-30 cm of the sediment. The horizontal lines give the confidence limits at the 95 % probability level.

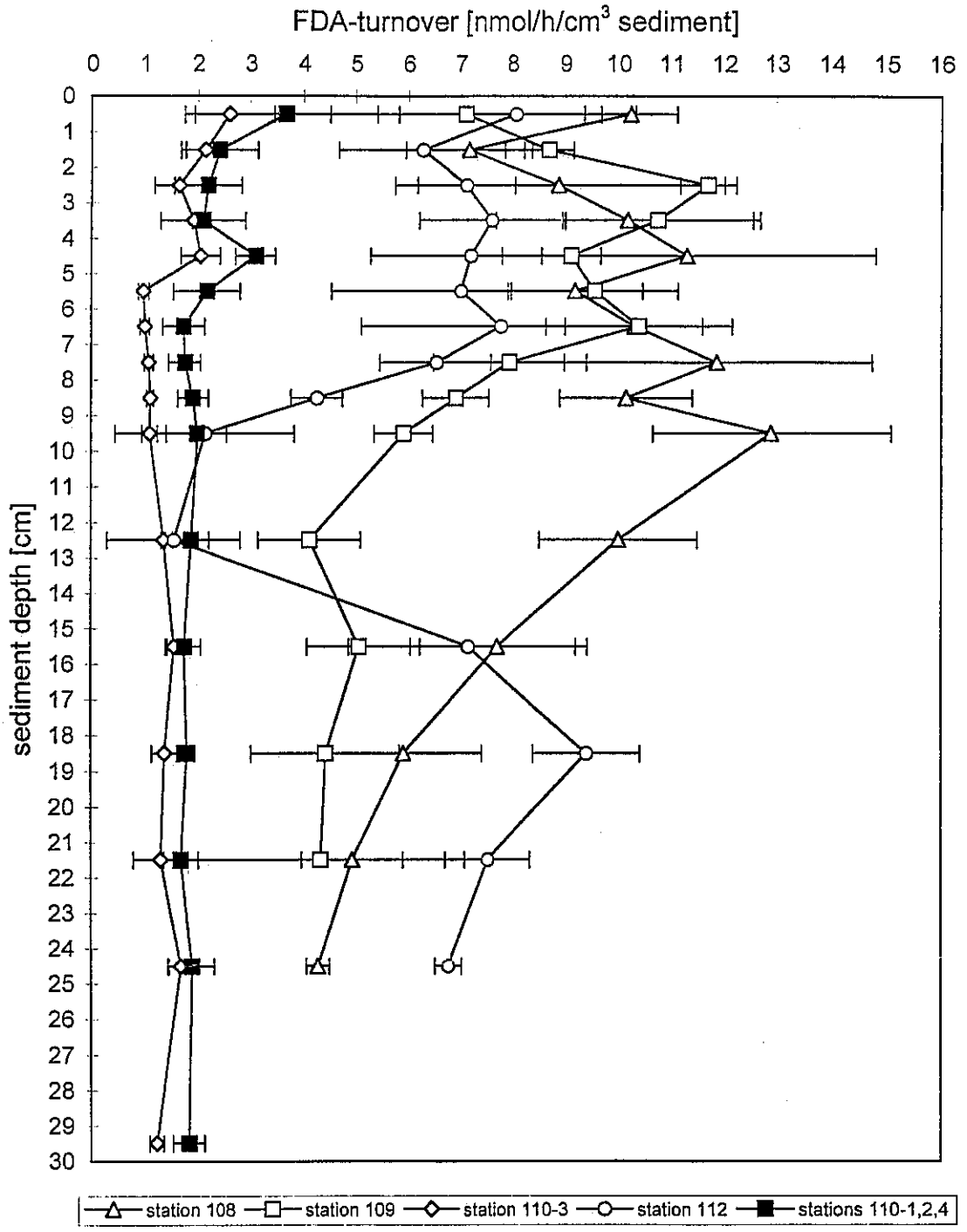

Fig. 68: Potential hydrolytic activity measured with fluorigenic substrate (Fluorescein-diacetate) in the top 25-30 cm of the sediment. The horizontal lines give the confidence limits at the 95 % probability level.

decreases rapidly and remains relatively constant beneath 10 cm. ETS activity was highest at the more productive stations 108 and 112 followed by stations 109 and 110.

Bacterial exoenzymatic activity (Figure 68) exhibited a pattern similar to the ETS activity although the depth gradients in the sediment column where rather smoothened indicating a relatively high bacterial activity below the oxic and suboxic sediment layer.

In comparison to the situation after the sedimentation of the spring phytoplankton bloom in the open NE-Atlantic benthic biological activity in the western Arabian Sea is significantly higher (factor 3-5).

5.3.3.3 Microbial Ecology

(A. Boetius)

In deep-sea sediments, bacterial enzymes are the primary agents of the early diagenesis of organic matter (OM). Since bacteria can only incorporate small molecules, polymeric organic compounds are degraded extracellularly. The hydrolysis of such polymers is the rate limiting step in the remineralization of OM.

Most extracellular enzymes are produced when their respective substrates become available (substrate induction), others are constantly produced but repressed in the presence of readily available nutrients. Previous investigations in different deep-sea regions indicated, that extracellular b-glucosidase and chitobiase can be assigned to the first group of positively controlled hydrolases and that peptidase belongs to the second group of negatively controlled enzymes. The production or inhibition of enzymes after a change of substrate availability in the environment can be detected after a few days. Therefore, the distribution of hydrolytic activities in the sediments is an indicator of the trophic status of the environment.

Samples for extracellular enzyme activities (EEA), microbial biomass and availability of specific organic compounds were collected at 11 stations between 1800 and 4100 m water depth (see station list). Microbial biomass and substrate availability will be determined in the home laboratory. Hydrolytic activities of a-, b-glucosidase, chitobiase, lipase and peptidase were measured on board using fluorescence-labelled MUF-substrates.

Along the west-east transect through the Arabian Sea, enzyme activities were only slightly decreasing with increasing water-depth (Figure 69). At the easternmost station WAST, several multicorers were obtained. EEA of a-, b-glucosidase, chitobiase and lipase were high compared to other deep-sea regions, indicating a higher supply with OM. This is supported by our observation of a layer of phytodetritus covering all cores that were recovered at the WAST station (see PFANNKUCHE, 5.3.3.2.2). The concentration of EEA at the sediment surface indicates that most of the OM is remineralized at the sediment-water interface (Figure 70). EEA of a-, b-glucosidase, chitobiase and lipase decreased quickly with increasing sediment depth and reached detection limit in the 3-4 cm, where oxygen was depleted (see WITTE,

5.3.3.2.1). Peptidase EEA reached 4-5 cm reflecting nitrate penetration depth (see WALLMANN, 5.3.4.2). At all stations, EEA of a-, b-glucosidase, chitobiase, lipase and peptidase were restricted to the oxic-suboxic sediment layer and not detectable deeper than 15 cm. The distribution of EEA will be compared to distribution of microbial biomass and substrate availability to detect the principle factors regulating microbial degradative activities. Seasonal and spatial variation in microbial activities and biomass, as well as the relationship between oxygen availability and degradation of specific substrates will be investigated during the following cruise to the Arabian Sea (M33/1).

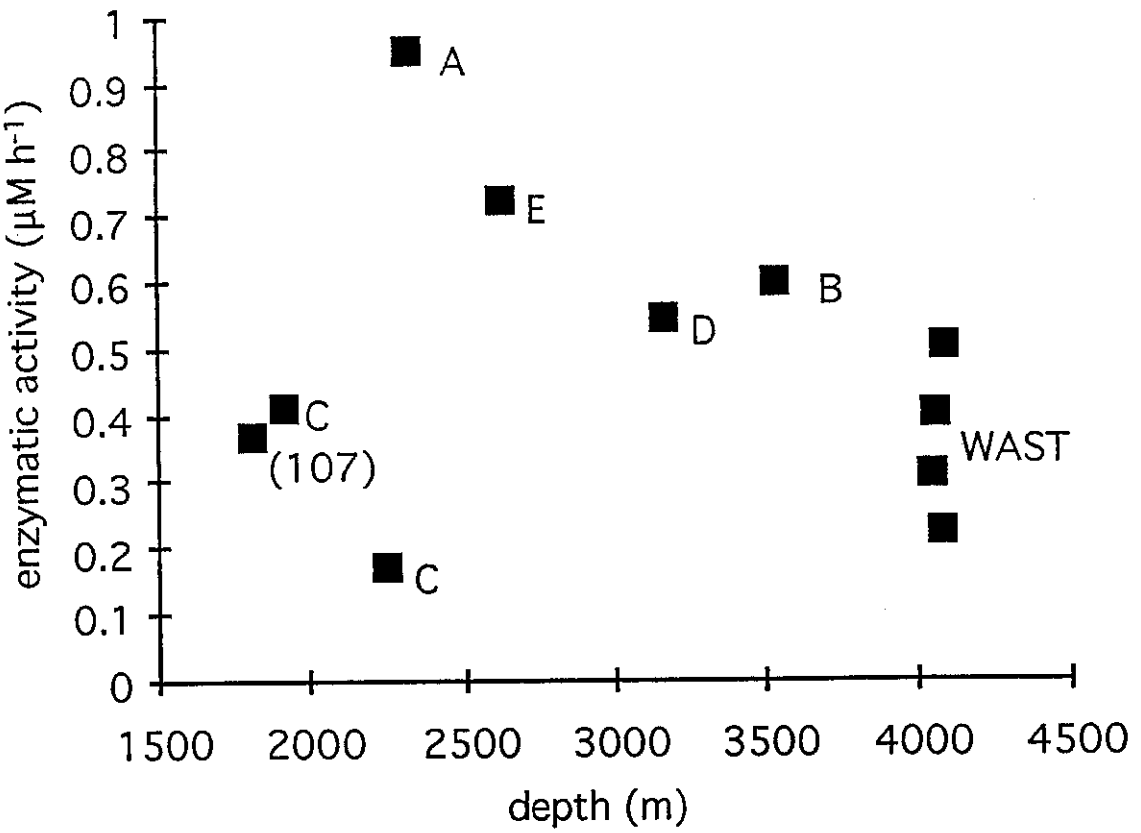

Fig. 69: Activity of b-glucosidase in surface sediments (O-1 cm). Letters indicate sample location (see list of stations).

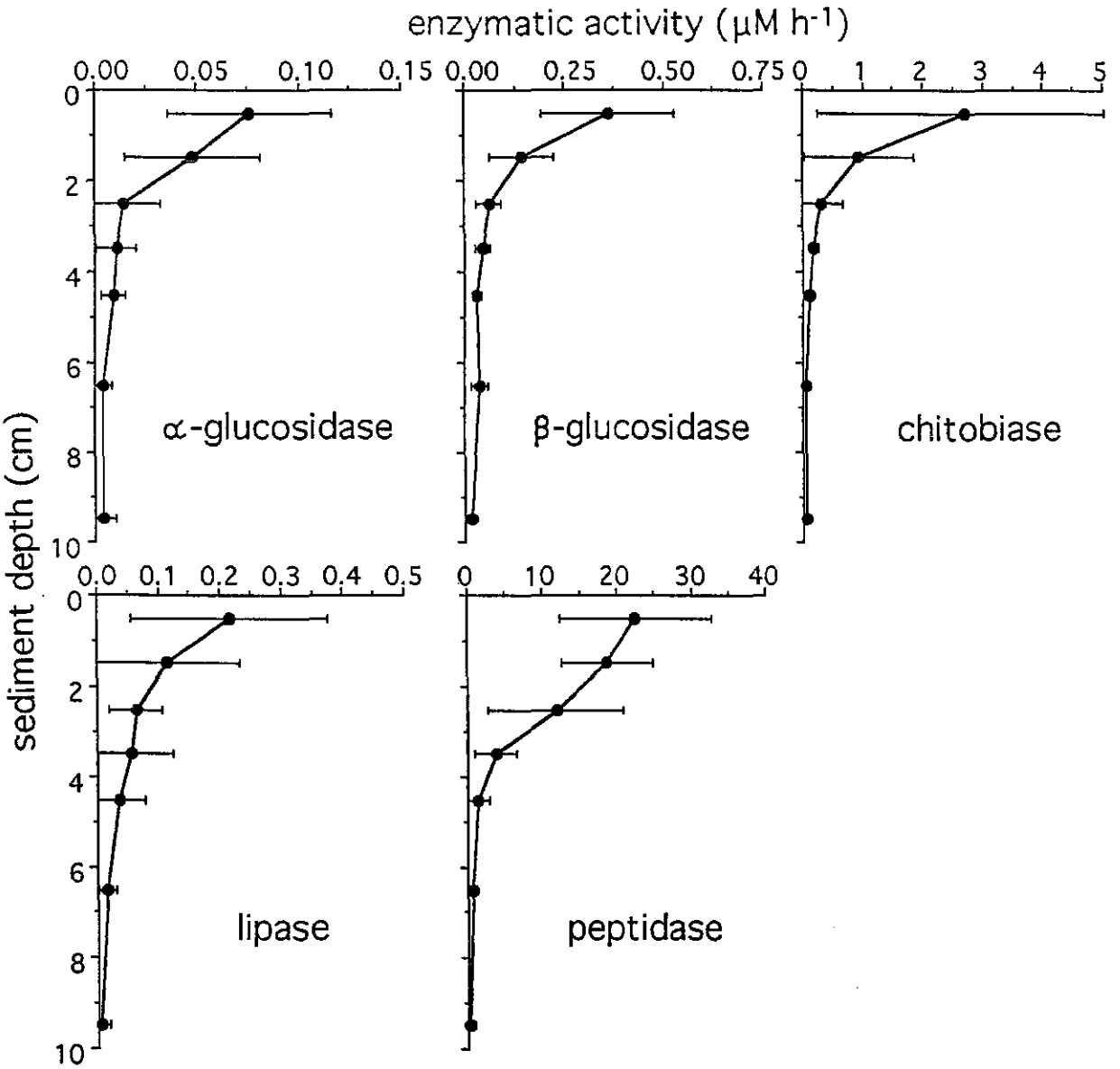

Fig. 70: Profiles of enzymatic activities at WAST. Dots indicate the average activities measured during 4 stations in the WAST area. Error bars represent 95 % confidence levels.

5.3.4 Marine Geoscience

Sediment Sampling

At 15 stations along the west-east transect through the Gulf of Aden, the Arabian Sea and the Oman Upwelling Area multicorer, boxcorer, gravity corer and piston corers were used to retrieve surface and late Quaternary deep sea sediments. The coring locations and respective water depths are given in the station list (7.3.2).This table also lists the devices used for the sediment sampling program at all stations as well as the core lengths recovered and the sample depths for water samples.

5.3.4.1 Multicorer

(K. Dehning, B. Jahn, H. Kitazato, G. Schmiedl, M. Scholz, R. Schneider, F. Wesselingh)

A multicorer was used as the main tool for sampling undisturbed surface sediments and the overlying bottom water. The model used on M31/3 was equipped with 10 larger plastic tubes of 8 cm and 4 smaller plastic tubes of 6 cm inner diameter, respectively. The multicorer was used at 14 stations. At all sites the retrieved cores were of good to very good quality reaching core recoveries from 13 to 35 cm (27 cm on average) (Table 15). In general the sediment cores and the overlying bottom water were sampled as follows:

- At each multicorer station the overlying bottom water was sampled for stable carbon and oxygen isotope measurements. To avoid ongoing biological fractionation the sample for carbon istotope measurements was immediately poisoned with 1ml of concentrated $HgCl_2$ solution.
- 2 large cores: intervals 0-0.5 cm, 0.5-1 cm and 1-10 cm in centimeter slices were stained with Rose Bengal methanol for studies on recent benthic foraminifera. From the 10th cm downward one core was sampled in centimeter slices (unstained) for downcore isotopic and faunal analyses.
- 3 large and 1 small core: the uppermost 3-5 cm were sampled for benthic foraminifera cultures and TEM fixation of selected individuals.
- 1 large core: sliced at 1 cm intervals for organic carbon geochemistry; these samples were frozen at -27° C.
- 1 large core (at several stations): interval 0-1cm of the sediment surface was sampled for geochemistry (C-org).
- 1 large core, sliced at 1 cm intervals for the analysis of dinoflagellates.
- 1 small core: interval 0-1 cm of the sediment surface was sampled for the investigation of diatoms.
- 2 large cores, sampled for macropaleontological studies.
- 2 small cores, frozen at -27° C as archive cores.

Tab. 15: Multicorer samples and assigned type of investigation

Station No.	GeoB No.	GPI TÜ No.	Water depth [m]	Core recovery [cm]	Bottom water: Isotopes	Benthic Foraminifera	Benthic For. Cultures	Organic C samples	Sed. surface: C-org	Dinoflagellates	Sed. surface: Diatoms	Macropaleontology	Archive: frozen cores
105	3001-1	MC368	175	25	x	x	x	x		x	x	x	2
105	3002-1	MC369	736	30	x	x	x	x		x	x	x	1
106	3003-5	MC370	2013	28	x	x	x	x		x	x	x	2
107	3004-4	MC371	1800	33	x	x	x	x		x	x	x	2
108	3005-3	MC372	2313	33	x	x	x	x		x	x	x	2
109	3006-2	MC373	3505	26	x	x	x	x	x	x	x	x	2
111-1	3007-3	MC374	1916	19	x	x	x	x	x	x	x	x	2
111-2	3008-5	MC375	2242	13	x	x	x	x		x	x	x	2
110-4	3009-2	MC376	4071	35	x	x	x	x	x	x	x	x	2
112	3010-2		3154	30	x		x	x		x	x		
112	3010-3	MC377	3136	30		x						x	1
113	3011-3	MC378	2624	22	x	x	x	x		x	x	x	2
114	3012-1	MC379	1539	32	x	x	x	x		x	x	x	2
115	3013-2	MC380	1729	27		x	x					x	
116	3014-2	MC381	1644	23	x	x	x	x	x	x	x	x	2
					GeoB	GPITü	GPITü	GeoB	GeoB	GeoB	GeoB	GPITü	GeoB

5.3.4.2 Sediment Geochemistry

(K. Wallmann)

Surface sediments were taken with a multicorer and brought into the cold room of RV METEOR immediately after recovery. In the cold room, cores were segmented and wet sediment samples were squeezed with argon gas at a pressure of 3 atm and a temperature of 2 - 6° C to gain undisturbed pore water samples. The following depth intervals were taken and analyzed (cm): 0-0.5, 0.5-1, 1-2, 2-3, 3-4, 4-5, 5-6, 6-7, 7-8, 8-9, 9-10, 10-13, 13-16, 16-19,

19-22, 22-25, 25-28, 28-31. Concentrations of dissolved nitrate, phosphate, ammonia, and silicate were determined in pore water and overlying water samples of the sediment cores using an autoanalyzer working with standard photometric procedures.

Pore water squeezing and analysis was performed at the following multicorer stations: MC1, MC6, MC7, MC9, MC12, MC13, MC14. With the exception of station MC1, all stations were located within the western Arabian Sea (WAST) working area. At station MC6, surface sediments were disturbed because the multicorer penetrated too deep into the soft sediment. The data from MC6 were therefore discarded. Sediments from station MC7 were extracted with 1 mol/l HCl for 24 h at room temperature immediately after sampling. In the home laboratory, extracted ferrous and ferric iron will be determined to study the reduction and oxidation of iron in surface sediments. Water samples from incubation experiments performed by the deep-sea biology group and from CTD deployments were also analyzed for nutrients.

Quantification of aerobic and anaerobic organic matter degradation in surface sediments of the Arabian Sea was the main scientific goal of the pore water investigations. Nitrate pore water profiles measured at WAST are plotted in Figure 71. They mirrow the release of nitrate from organic matter mineralisation during nitrification in the top oxic sediment layers and nitrate consumption caused by denitrification in deeper suboxic layers. The small nitrate penetration depth of approximately 5 cm indicates high rates of denitrification which are typical of high productivity areas. Sediments were very soft and had a redish brown colour in the top 2.5 cm. From 2.5 cm to 5 cm depth, sediments were tan and developed a greenish colouring with increasing depth. Below this transition zone, the colour was olive green till the bottom of the core. At stations MC12 and MC13, a lighter sediment colour was oberserved in the top 10 cm which indicates higher carbonate contents. The olive green colour is typical of suboxic sediments and is usually attributed to ferrous iron bearing clay minerals. A colour change at the nitrate penetration depth of 5 cm is consistent with the redox sequence usually found in deep sea sediments.

Nitrate pore water profiles may be affected by the sampling and storage procedure. Sediment temperature increased to 6-8° C during transport through the upper water column. This temperature effect and the pressure decrease may change microbial nitrification and denitrification rates and may thus disturbe the nitrate profile. Intact sediment cores covered with overlying bottom water were stored in the cold room at 2-6° C. One to 26 hours passed before segmentation and pore water squeezing was started. During this time, changing rates may have effected the profiles. The storage times for the individual cores were 1 h (MC14), 4 h (MC9), 6 h (MC12), 16 h (MC7), and 26 h (MC13). Cores MC 7 and MC 13 were stored much longer than the other ones and had significantely lower nitrate values below a depth of 1 cm. Therefore, it may be concluded that denitrification rates were artificially enhenced during coring and storage. It is thus necessary to process sediment cores within a few hours after sampling.

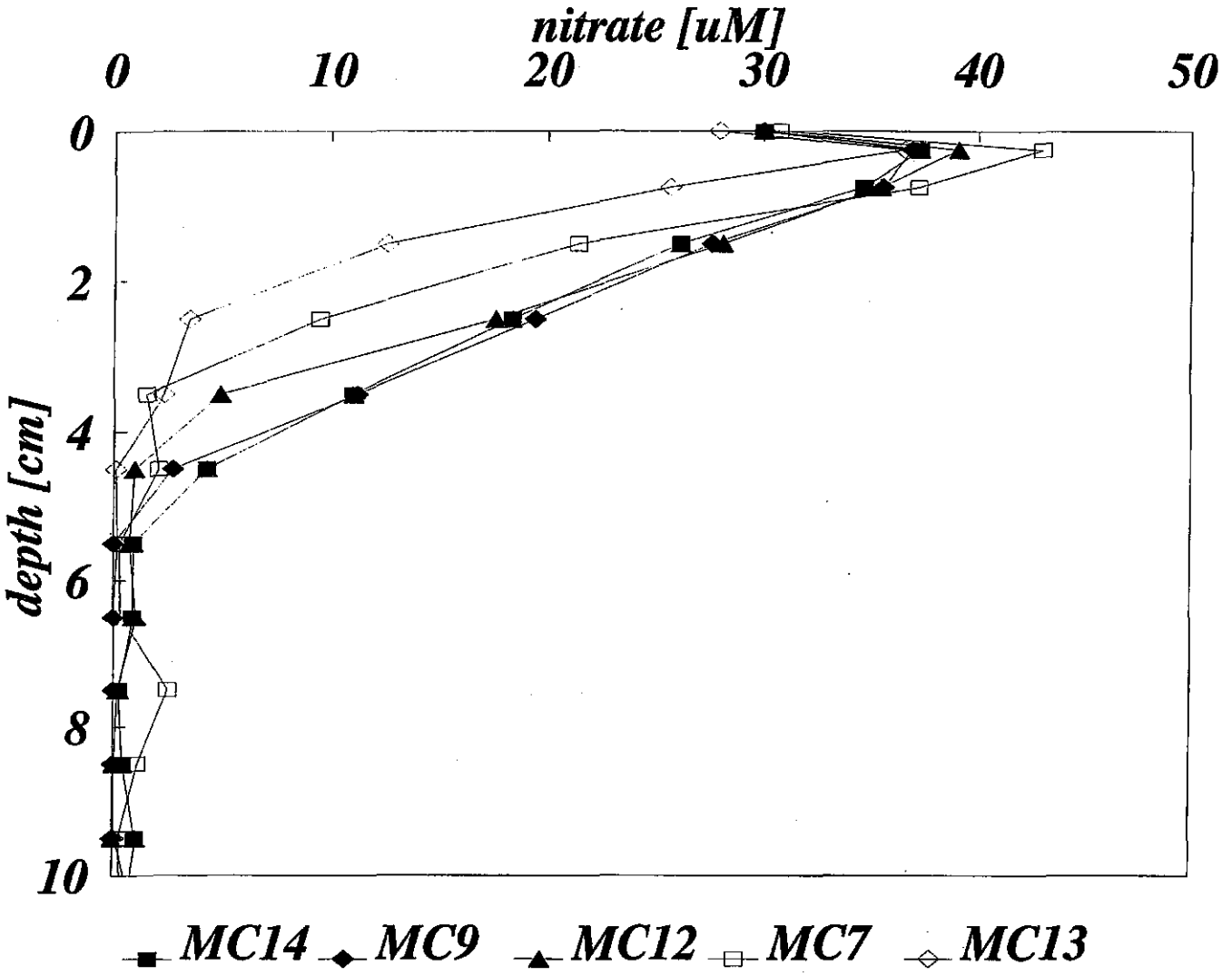

Fig. 71: Nitrate pore water data. Bottom water values measured in the overying water of multicorer cores are plotted at zero depth.

5.3.4.3 Radiolaria

(J. Erbacher)

Investigations on Radiolaria in Core Samples

Aim of Investigations

The investigation of radiolarian faunas from Leg 31-3 is concentrating on Sites 107 and 108. Site 108 is situated within an area of increased but annual fluctuating mixed layer primary productivities throughout the year (BROCK et al., 1994). The potential of upwelling-influences and rises in primary productivity of Site 107 which lies about 100 km WSW of Site 108, points to much stronger annual differences than at Site 108 (BROCK et al., 1994). Due to their positions close to the center and at the margin of the upwelling-area off Oman, a comparison of radiolarian faunas from these cores will serve the opportunity to describe high resolution changes of the intensity and spatial distribution of radiolarian accumulation rates and productivity during the last 500.000 years. Therefore we have chosen long piston cores of these sites to be investigated for radiolaria. The results shall serve to interpret monsoonal fluctuations during the Late Quaternary.

Material and Methods

Two multicorer-cores and two long piston cores have been sampled (approx. 400 samples). The multicorer cores were sampled in 0.5 to 1 cm intervals. The sampling interval of piston cores was 5 cm.

Samples will be washed and sieved at 63 µm. For each sample, semi-quantitative estimates of overall radiolarian abundance, preservation and specific abundances will be made.

First results

Shipboard-surveying of core catcher and sediment surface samples have shown that the highest radiolarian-abundances of all Sites occur at Sites 107 and 108. Site 108 shows the maximum values of radiolarian-abundances. The observed fauna shows great similarities to those being described by JOHNSON and NIGRINI (1980) from the western Indian Ocean, and VAN DE PAVERD (1995) from the northern Indian Ocean and the Banda Sea.

The ratio between Spumellaria and Nasselaria is about 2:1, which is typical for upwelling areas with a high abundance of upwelling endemic Spumellaria like e.g. *Acrosphaera murrayana* or *Collosphaera* cf. *huxleyi*. Upwelling endemic species and species that are typical for upwelling areas (NIGRINI, 1991; NIGRINI and CAULET, 1992) appear to be common parts of the fauna of sediment surface samples from Site 108 (see species list). We believe that a comparison of the lateral and vertical abundance of these upwelling forms between the two

cores will serve as a good tool to identify changes in the intensity of upwelling and therefore changes of the monsoon (see chapter 5.3.4.4)

List of the fifty most common taxa from a sediment surface sample of MC 372, Site 108, 0 - 0.5 cm:

Acanthodesmia renilla (Haeckel), very rare
Acanthodesmia vinculata (Müller), rare
Acanthodesmia reticulata (Ehrenberg), rare
Acrosphaera murrayana group*(Haeckel)*, rare, UPWELLING-Form!
Actinomma spp. group, common
Axoprunum stauraxonium Haeckel, very rare
Botryostrobus aquilonaris (Bailey), very rare
Carposphaera angulata group (Haeckel), very rare
Carposphaera ? *mellittosphaera* (Haeckel), very rare
Cladococcus abietinus (Haeckel), rare
Collosphaera aff. *C. huxleyi* Johnson and Nigrini, abundant, UPWELLING-Form!
Collosphaera macropora Popofsky, rare
? *Conicavus tipiopsis* Takahashi, rare
Dictyocoryne absyssorum (Ehrenberg)
Dictyocoryne truncatum (Ehrenberg), abundant
Dictyocoryne euclidis (Haeckel), abundant
Didymocyrtis messaensis (Müller), rare
Didymocyrtis tetrathalamus coronatus (Haeckel), very rare
Druppatractus ? sp. Dumitrica, rare
Eucyrtidium acuminatum (Ehrenberg), common
Eucyrtidium aderces ? Nigrini and Caulet, some, UPWELLING-Form!
Eucyrtidium tropezianum (Müller), very rare
Heliodiscus asteriscus Haeckel, common
Hexacontium heracliti (Haeckel), very rare
Hexacontium spp. group, common
Inversumbella macroceras (Haeckel), UPWELLING-Form!
Lacropyle butschlii Dreyer, very rare
? *Lacropyle haliomma* (Ehrenberg), some
Lamprocyclas maritalis maritalis Haeckel, common
Lamprocyclas maritalis Haeckel *polypora* Nigrini, common
Lamprocyclas maritalis Haeckel *ventricosa* Nigrini, common UPWELLING-Form!
Lamprocyrtis nigriniae (Caulet), rare but robust, UPWELLING-Form!
Pentapylonium implicatum Dumitrica, rare, UPWELLING-Form (displaced temperate)!
Perichlamydium arachium (Müller), abundant
Peripyramis circumtexta Haeckel, some
Pterocanium charybdeum Müller, some
Pterocanium grandiporus Nigrini, common, UPWELLING-Form!

Pterocanium praetextum (Ehrenberg), rare
Pterocorys zancleus (Müller), some
Pteroscenium pinnatum Haeckel, very rare
Euchitonia elegans (Ehrenberg), common
Sethoconus tricostatus (Haeckel), rare
Spongodiscus tetras (Haeckel), common
Spongodiscus biconcavus (Haeckel)
Spongurus cylindricus Haeckel, rare
Spongopyle osculosa Dreyer, rare
? *Spongosphaera* sp., very rare
Tholospirum aff. *venustum* (Bailey), some
Triacartus undulatum (Popofsky), rare
? *Tricranastrum* sp., rare

5.3.4.4 Benthic Foraminifera from Multicores and Boxcores

(H. Kitazato, G. Schmiedl)

One of the most important oceanographic features of the Arabian Sea is the oceanic upwelling which coincides with enhanced biological productivity (PRELL and CURRY, 1981). The seasonal maximum of the upwelling is reached in the summer months due to the prevailing southwest monsoon winds (BROCK et al., 1994). HERMELIN and SHIMMIELD (1990) found that the recent benthic foraminiferal faunas of the Arabian Sea are strongly related to the depositional environment which is influenced by the oceanic upwelling processes. The ancient response of benthic foraminifera to late Quaternary changes in upwelling intensity was investigated by HERMELIN and SHIMMIELD (1995). In accordance with results from different micropaleontological, sedimentological and geochemical proxies this study documented that during the Late Quaternary the upwelling underwent significant changes in intensity and spatial extension. Moreover, they showed that these paleoenvironmental changes are related to the dynamics of the monsoonal system.

The main goal of our faunal studies in the Gulf of Aden and the western Arabian Sea is to get more detailed informations on the ecology and paleoecology of deep water benthic foraminifera. Therefore, our studies include topics like trophic demands, benthic-pelagic coupling, distribution in the epibenthic zone, live horizons, distribution in the sediment, reaction on the O_2 content and the influence of the high saline Red Sea outflow water. This knowledge is necessary to finally use benthic foraminifera as a tool for paleoceanographic studies in the investigation area. For this purpose surface sediment samples were recovered at all geological stations for down-core studies as well as for TEM-fixations and live cultures of benthic foraminifera. Simultaneously, hydrographic (temperature, salinity, oxygen), sedimentological (carbonate, organic carbon) and pore water data (oxygen penetration, stable isotopes etc.) were collected to characterize the environment.

Benthic foraminiferal cultures

All culture bottles which were collected during this cruise for cultivating benthic foraminifera were transported from Djibouti to Tübingen by hand laggage. Deep-sea foraminifera were put in a cooling box to keep temperature conditions similar to the *in situ* conditions. In contrast, shallow-sea foraminifera were brought back under surrounding temperature conditions. After arriving at Tübingen deep-sea foraminifera were stored in a cooling room at about 4° C, shallow-sea foraminifera were stored both in 15° C and 20° C incubators. While at most of the deeper stations no benthic foraminifera survived in the laboratory, from the shallow water sites at station 105 (KG02, MC368, 180 m; KG03, 320 m; MC369, 736 m) a large number of living benthic foraminifera could be observed. Benthic foraminiferal genera of station 105 include *Allogromia, Bathysiphon, Trochammina, Quinqueloculina, Bolivina, Bulimina, Cassidulina, Dentalina, Epistominella, Fursenkoina, Hyalinea, Lenticulina, Nodosaria,* and *Uvigerina.* Additionally, from deep water station 107 (MC371, 1801 m) *Allogromia* and *Dentalina*, from station 111 (MC375, 2243 m) *Stainforthia*, and from station 114 (MC379, 1540 m) *Allogromia, Textularia* and *Bolivina* could be found alive.

Downcore studies of living deep-sea benthic foraminifera

As shown for the coastal upwelling areas off Southwest Africa (SCHMIEDL, 1995) deep water benthic foraminiferal faunas also in the Gulf of Aden and the western Arabian Sea mirror the recent flux rates of organic matter. Corresponding to elevated organic carbon fluxes at all sampled sites dissolved oxygen contents in bottom and pore waters were extremely depleted. Except of station 110 (WAST, 4073 m) where a O_2 concentration of 1.25 ml l^{-1} could be measured, values at all other sites never exeeded 1 ml l^{-1}, ranging between about 0.2 and 0.9 ml l^{-1}. Consequently, *Uvigerina peregrina, Bulimina aculeata, Globobulimina spp., Fursenkoina mexicana* and *Melonis barleeanum* were found to be dominant constituents of the benthic foraminiferal fauna. These species are well known to be adapted to these high productivity environmental conditions (summarized in SCHMIEDL, 1995). Additionally, below about 1800 m water depth the preferentially epifaunal living *E. exigua* is an important species of the benthic foraminiferal fauna. This cosmopolitan species is believed to indicate sudden inputs of freshly produced phytodetritus to the sea floor (GOODAY, 1988, GOODAY and LAMBSHEAD, 1989) that in the Arabian Sea occur during seasonal changes of the monsoon-driven upwelling.

Downcore fluctuations in the uppermost 5 sediment centimeters of station WAST (Western Arabian Sea Trap, station 110) from 4073 m water depth and station 111 from the adjacent seamount at 2243 m water depth are compared in detail. Since both stations are located close to each other primary productivity in the surface waters is very similar. However, the amount and quality of organic matter that is deposited on the sea floor is expected to exhibit striking differences (BERGER et al., 1989). At the shallow seamount station 111 high standing stocks around 100 living (stained) individuals per 10 cm^3 could be observed down to 4 cm sediment depth. Moreover, the distribution of endobenthic species exhibits a strong zonation where

Uvigerina peregrina prefers a shallow infaunal microhabitat from 0.5 to 2 cm, *Melonis barleeanum* an intermediate infaunal microhabitat from about 1 to 4 cm, and *Globobulimina* spp. a deep infaunal microhabitat from 3 to 5 cm depth below the sediment-water-interface. At the abyssal WAST station extraordinary high standing stocks of more than 100 living (stained) individuals per 10 cm^3 are restricted to the uppermost sediment centimeter. In contrast to station 111 from the seamount the fauna is dominated by epifaunal living species, e.g. *Epistominella exigua, Fontbotia wuellerstorfi, Rhizammina* spp., indicating food limitation in this abyssal basin environment.

5.3.4.5 Gravity Cores

(R. Schneider, K. Dehning, B. Jahn, P. Helmke, G. Kirst, M. Scholz)

With the gravity corer sediment cores of about 0.5 to 11.5 m in length were recovered at 11 stations. During M31/3 altogether about 96 m of sediment core were recovered with this device.

Before using the coring tools, the liners were marked with a straight line, lengthwise, in order to be able to sample the core segments afterwards in the same orientation, in particular for paleomagnetic purposes. When the core was retrieved on deck, the core liners were cut into 1 m segments, closed with caps at both ends and inscribed (Figure 72).

With exception of core GeoB 3003-2, all other cores were cutted along-core in two half pieces: one Archive and one Work half. The sediments were described, smear-slide samples were taken from specific layers and spectrophotometric measurements were done on the Archive half (see below). Both core halfs are stored in a cool room at +4° C in the Bremen core repository. Two parallel series of syringe samples (10 ccm) were taken from the Work half at a depth interval of 5 cm. These samples were taken for the measurements and determination of physical properties, stable isotopes, faunal assemblages and organic geochemistry.

A detailed list of samples (see also 7.3.4) available from the sediment cores taken on this cruise M31/3 can be requested from the core library of the Marine Geology Section, Fachbereich Geowissenschaften, University of Bremen.

Inscription:

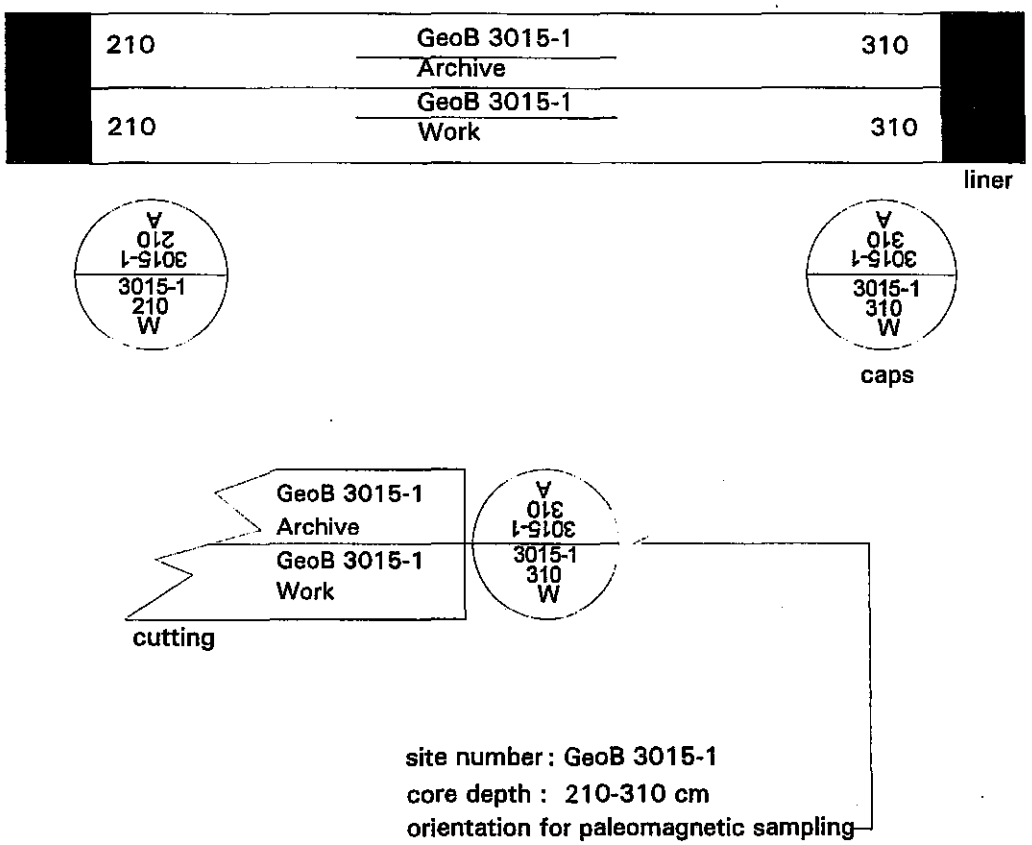

Fig. 72: Scheme of the inscription of gravity core segments.

Visual Core Description

The visual macroscopic description, carried out for the gravity cores opened directly onboard, comprises preliminary results for the general lithology and sediment structures, as well as its hue and croma attributes according to the MUNSELL soil color chart. The cores show no tremendous variation in lithology. All cores consist of intensivly bioturbated, foraminifera-bearing carbonate ooze with clay. All cores are visually more or less olive green, with a trend to generally lighter colors from the inner Gulf of Aden sediments to the more pelagic sediments in the Western Arabian Sea (Owen Ridge), which may indicate a decreasing influence of organic carbon and terrigenous input to the sites more distant from the coast. Additionally, there are alternating intervals of more grey, light color and of dark olive green color in every core, which can be determined more quantitatively by the color spectrophotometry (see below). Only in core GeoB 3007-1 two sandy foraminiferal layers where observed, which may indicate some winnowing of the fine fraction. No indications for sediment disturbances (hiatus, slumps, etc.) have been detected in the other cores (Figures 74 - 95, visual core descriptions for lithology, sediment structures, and color of the gravity cores GeoB 3003-4, 3004-1, 3005-1,.....3015-1).

Spectrophotometry

On M31/3 a Minolta CM - 2002 hand-held spectrophotometer was used to measure percent reflectance values of sediment color at 31 wavelength channels over the visible light range (400-700 nm). The digital reflectance data of the spectrophotometer readings were routinely obtained from the surfaces of the splitted cores to provide a continous record of the color variation from each core. Spectrophotometer readings were taken from the Archive half immediately after core opening. The surfaces of all core segments were scraped with a knife to expose a fresh, unsmeared surface for measurements at 2 cm intervals. A thin, transparent plastic film (food wrap) was used to cover the wet surface of the sediment to protect the photometer from being soiled. Before measuring each core the spectrophotometer was calibrated for white color reflectance by attaching a white calibration cap, which was also covered with the same plastic wrap to prevent bias in the readings when compared to the sediment values. The spectrophotometer readings were transfered to a personal computer using the "PROCOMM PLUS " software.

The reflectance of three selected wavelengths 450 nm (blue), 550 nm (green) and 700 nm (red) provide a detailed record of sediment color variability (Figures 75,77,79,81,.....,95). It is likely, that these color changes are due to changes in the sediment composition - especially the ratio of carbonate (light) to organic residue (dark) content - which are probably connected with variations in the upwelling history of the Western Arabian Sea. Some cores (Figure 73: GeoB 3003-4, 3004-1, 3005-1) show comparable reflectance curves which allow direct correlation between the cores. The most eastern core from the Owen Ridge (GeoB 3007-1) shows a reflectance pattern, which is strikingly similar to the glacial-interglacial climate variations, as for example is indicated in the global marine oxygen isotope record. The cores from the

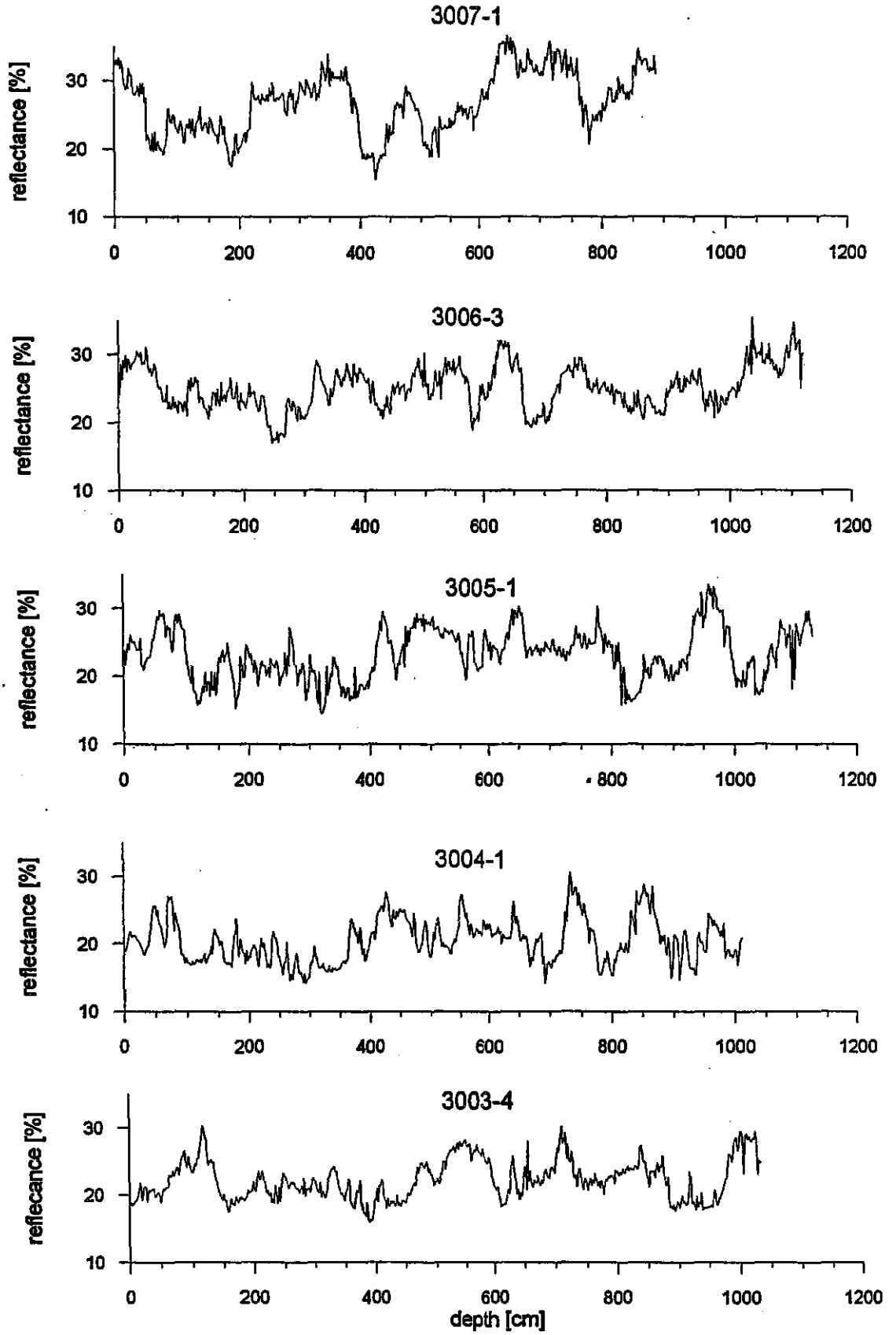

Fig. 73: Comparison of 550 nm waveband (10 nm increment) reflectance between selected cores on a west-east profile from the inner Gulf of Aden (GeoB 3004-1) to the Owen Ridge (GeoB 3007-1).

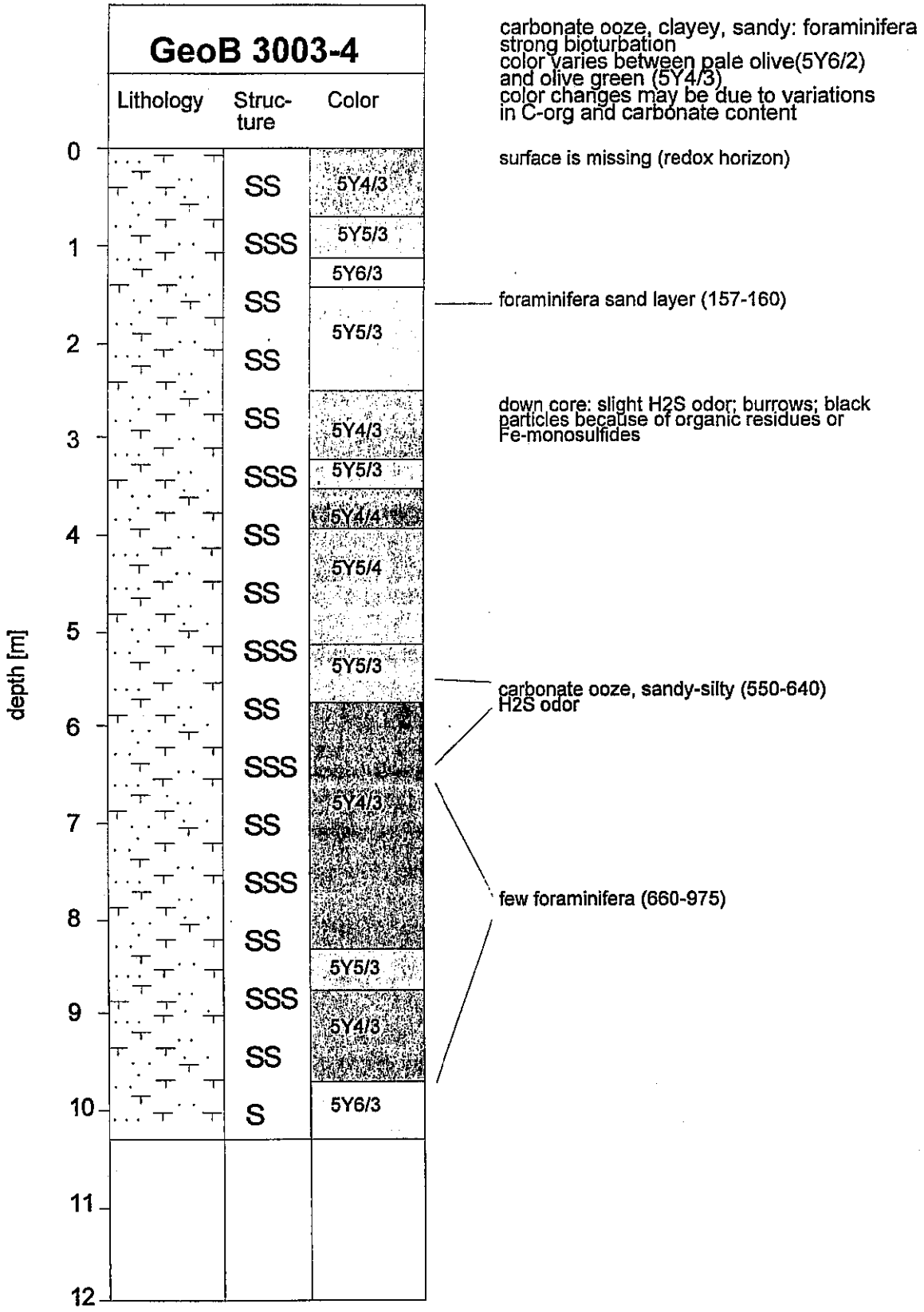

Fig. 74: Visual core description.

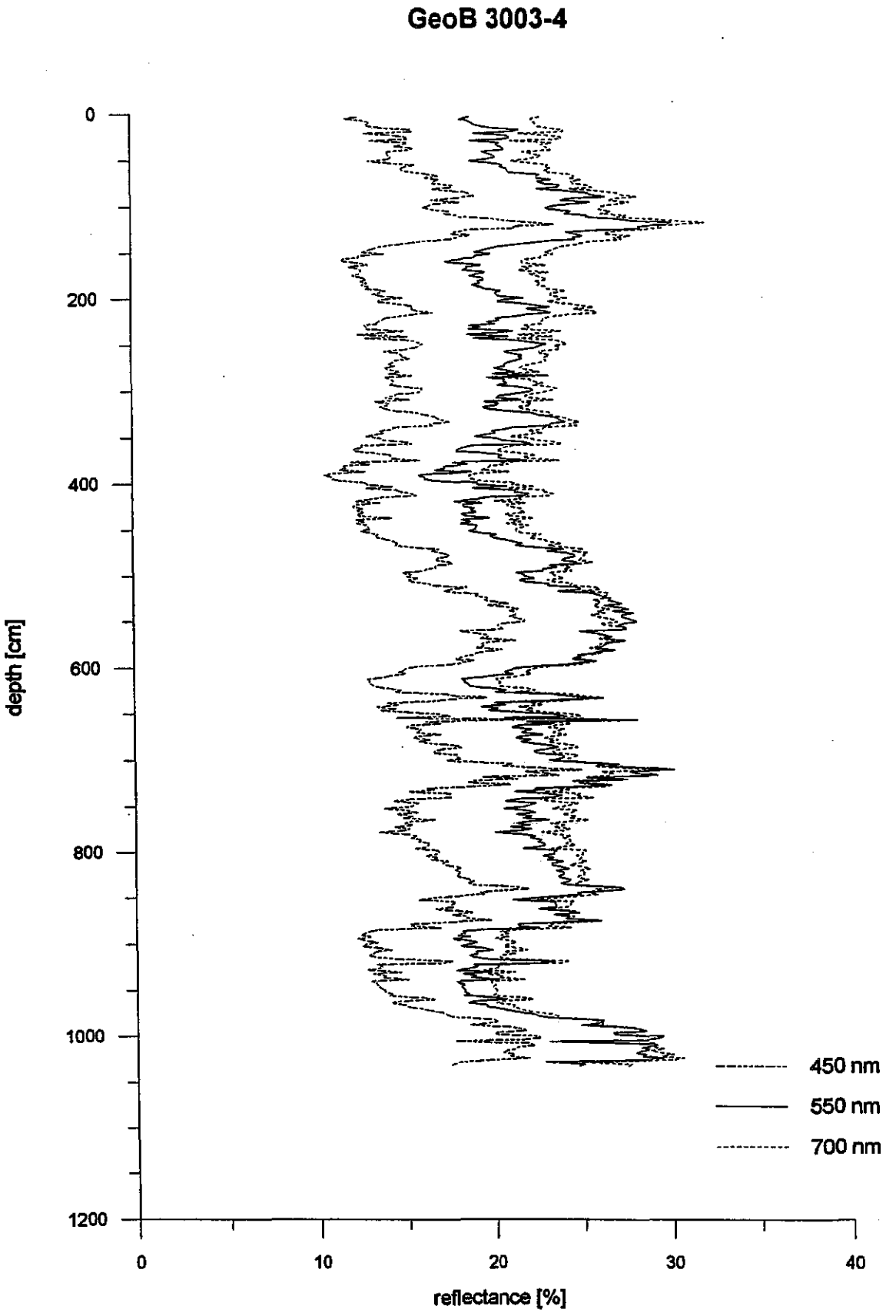

Fig. 75: Color reflectance measurements.

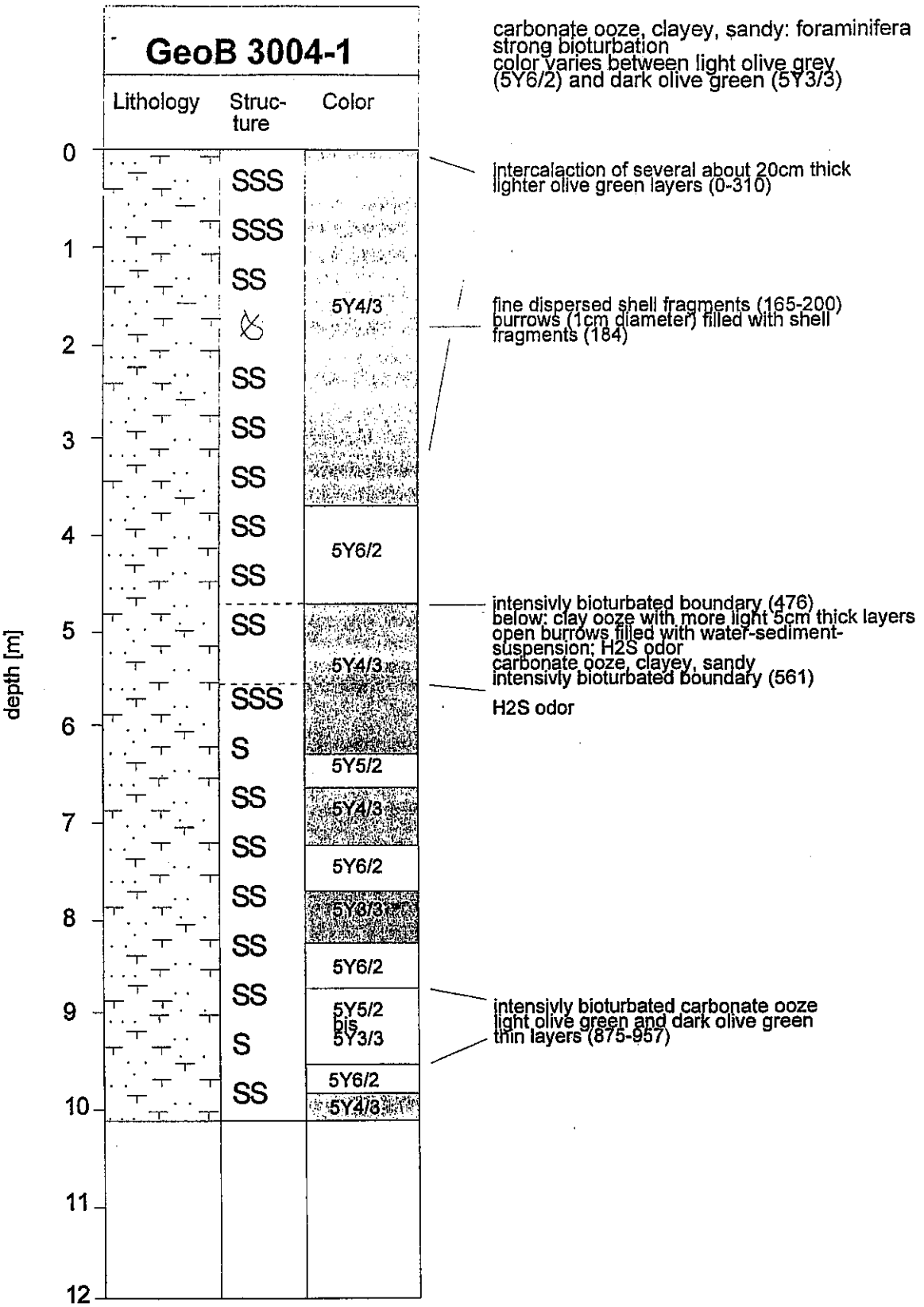

Fig. 76: Visual core description.

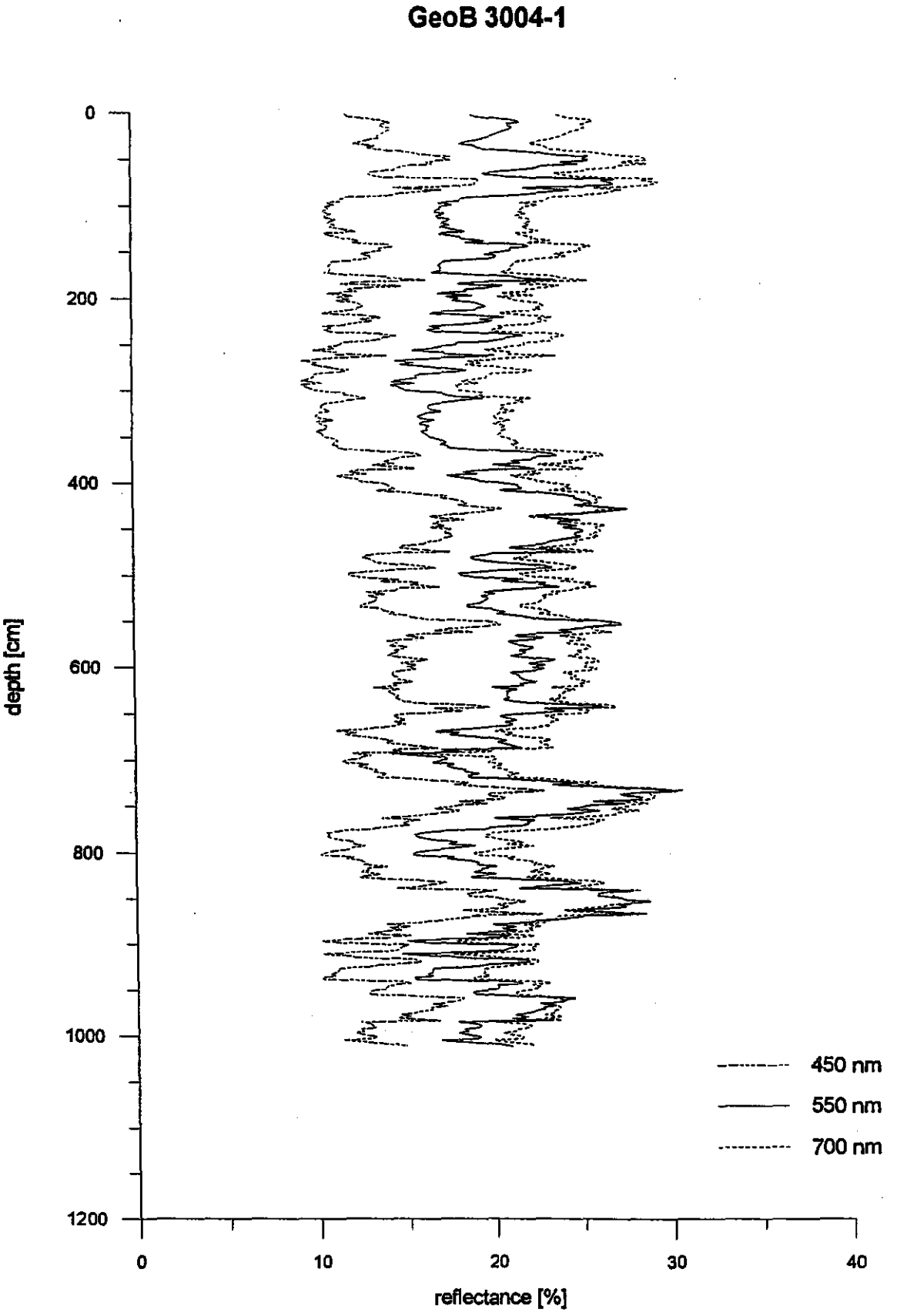

Fig. 77: Color reflectance measurements.

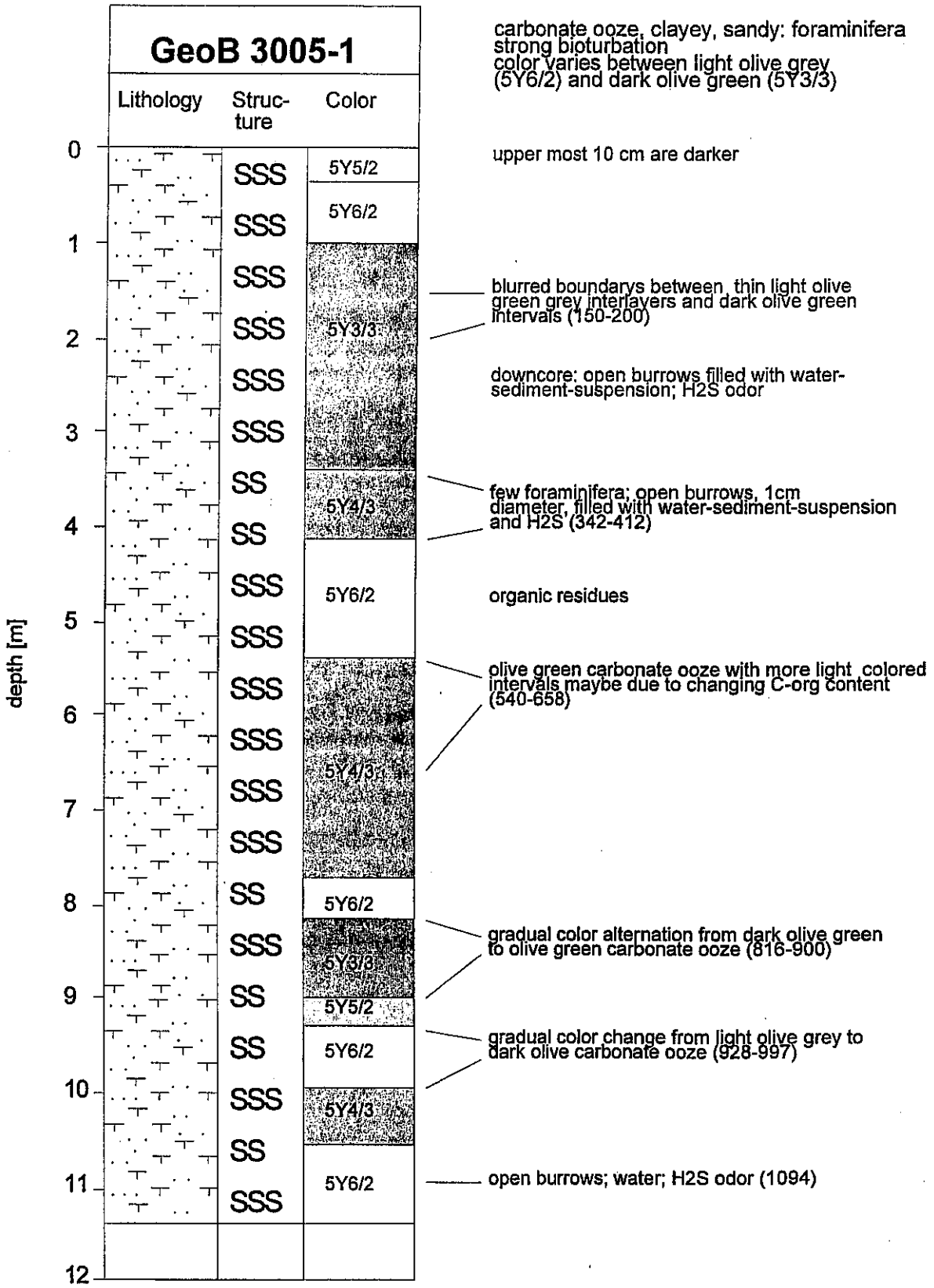

Fig. 78: Visual core description.

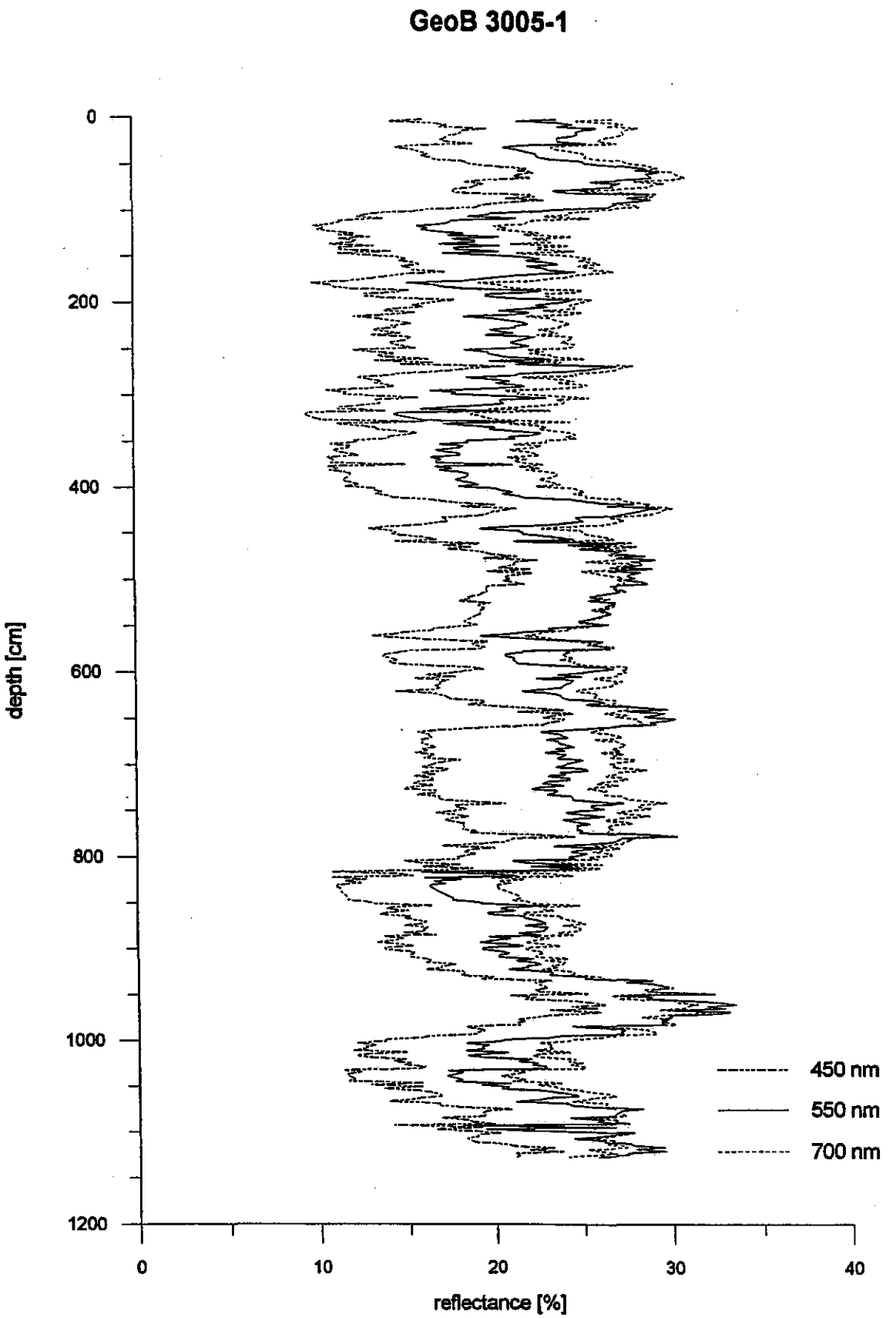

Fig. 79: Color reflectance measurements.

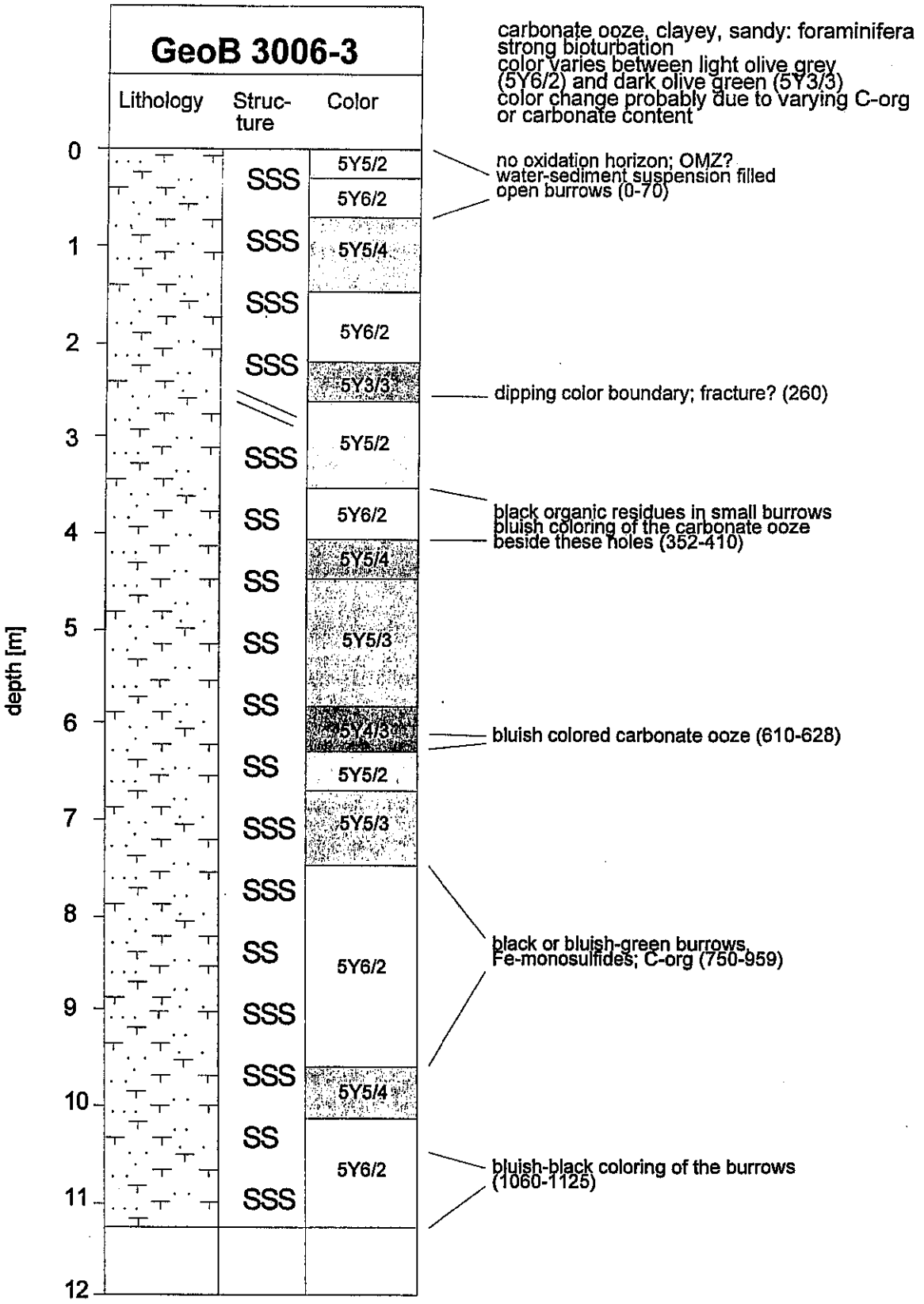

Fig. 80: Visual core description.

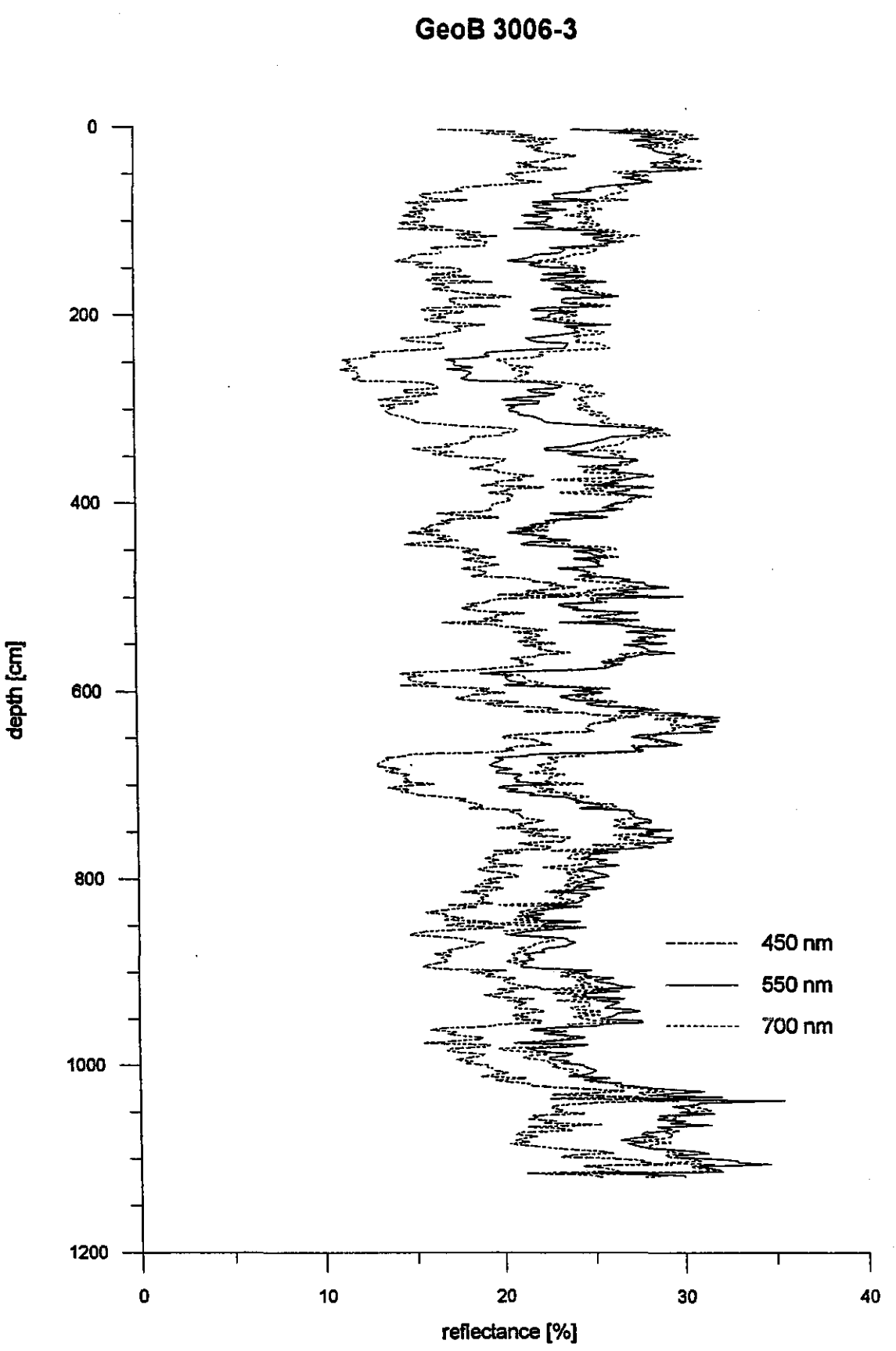

Fig. 81: Color reflectance measurements.

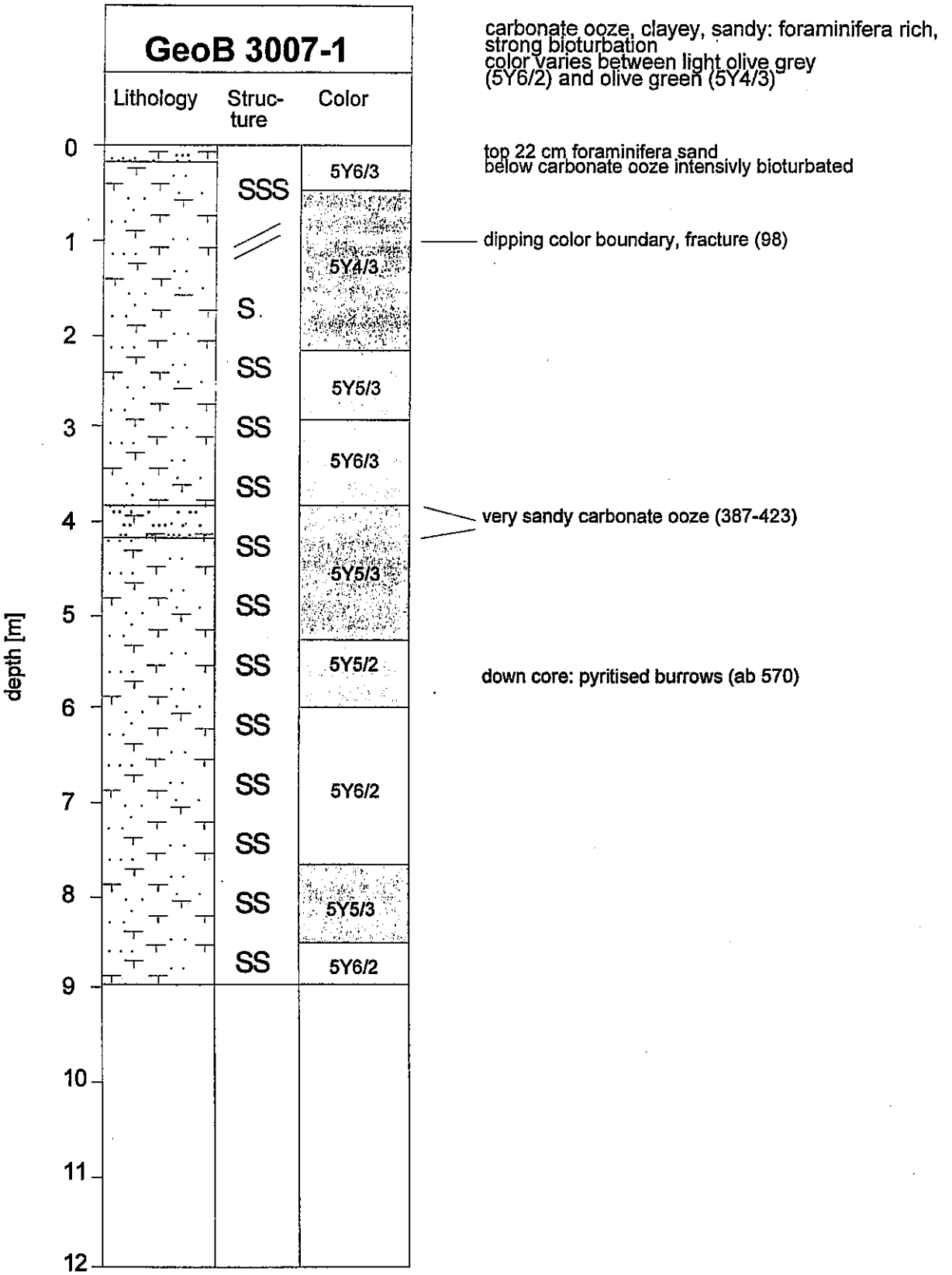

Fig. 82: Visual core description.

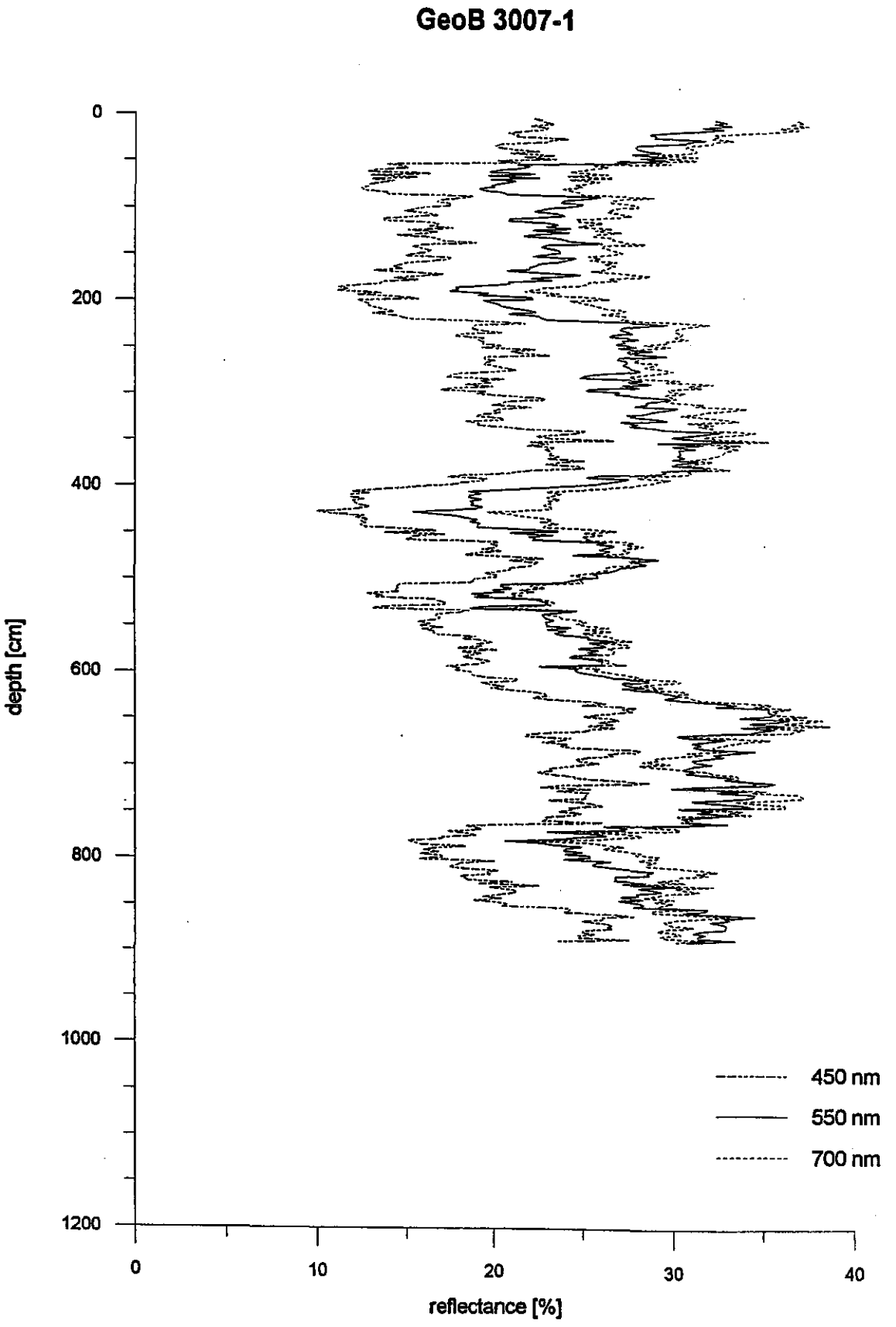

Fig. 83: Color reflectance measurements.

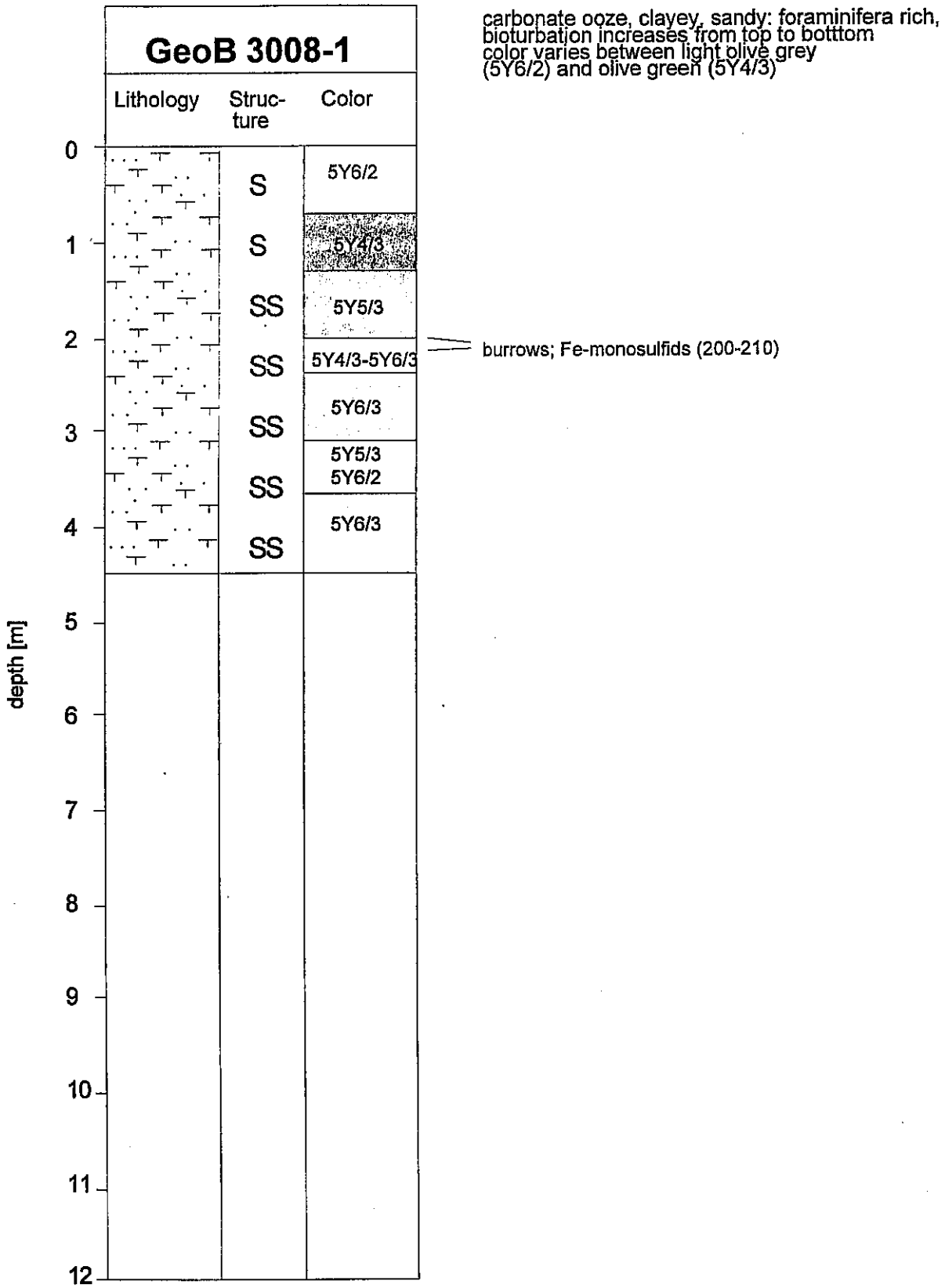

Fig. 84: Visual core description.

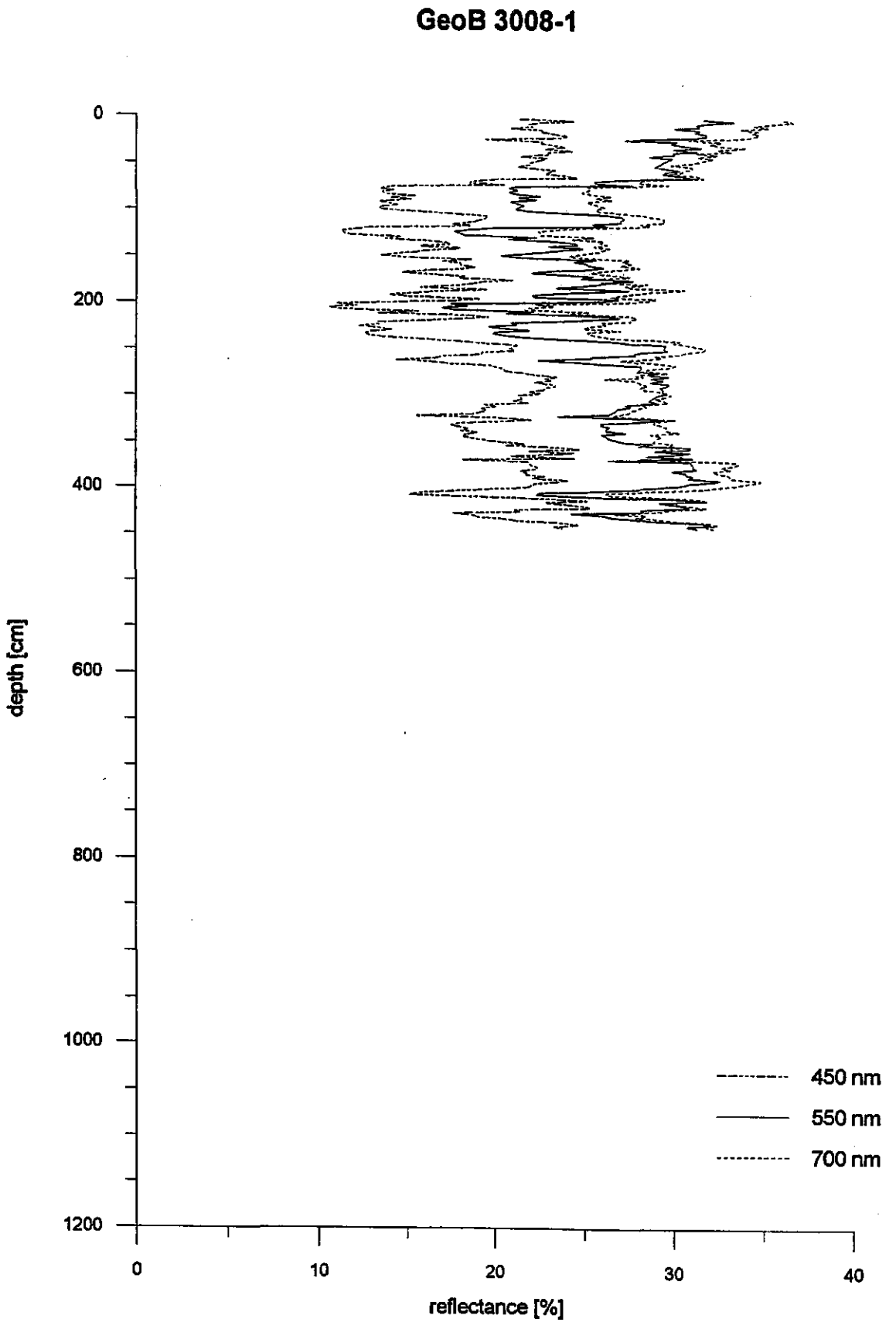

Fig. 85: Color reflectance measurements.

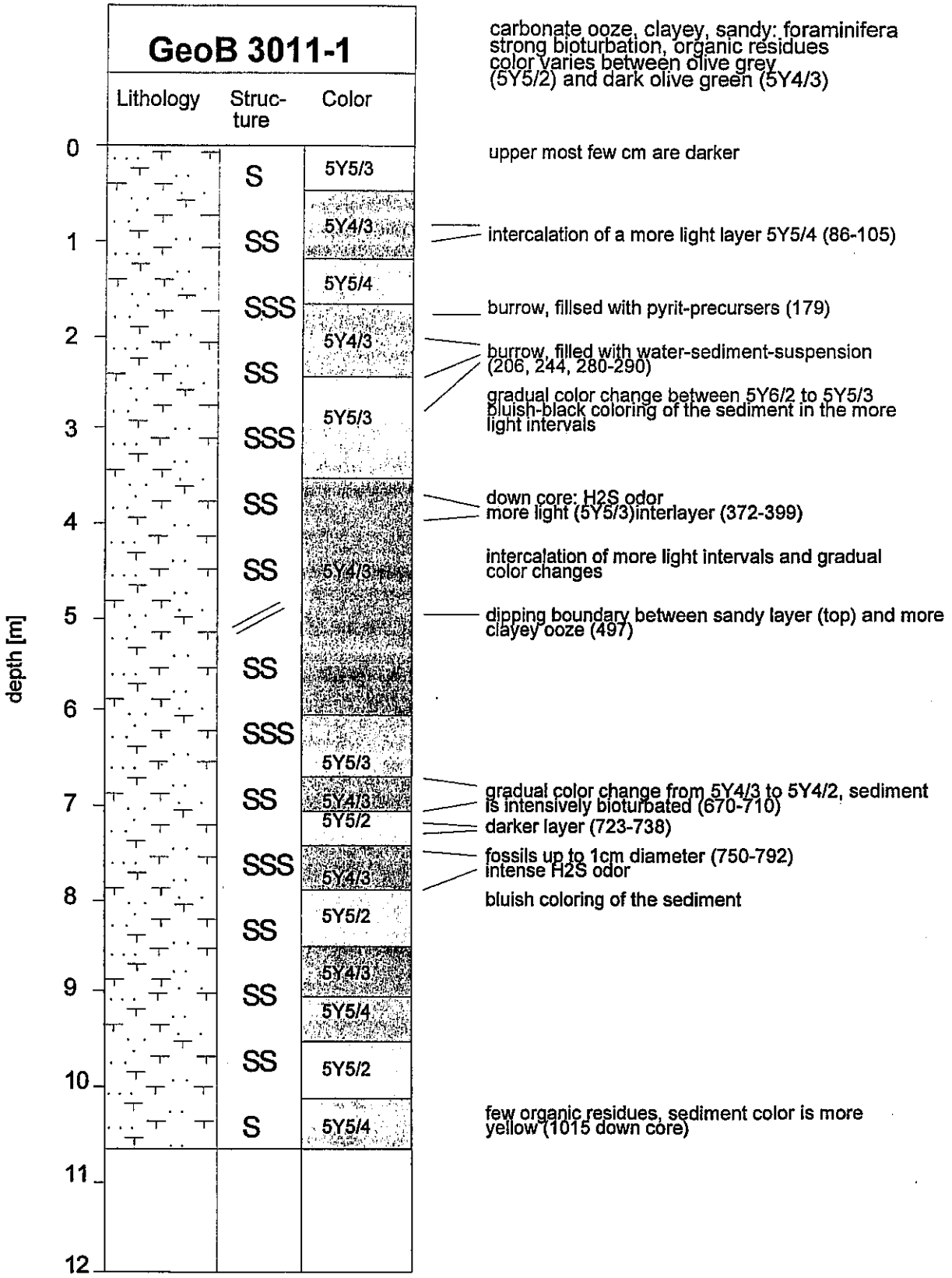

Fig. 86: Visual core description.

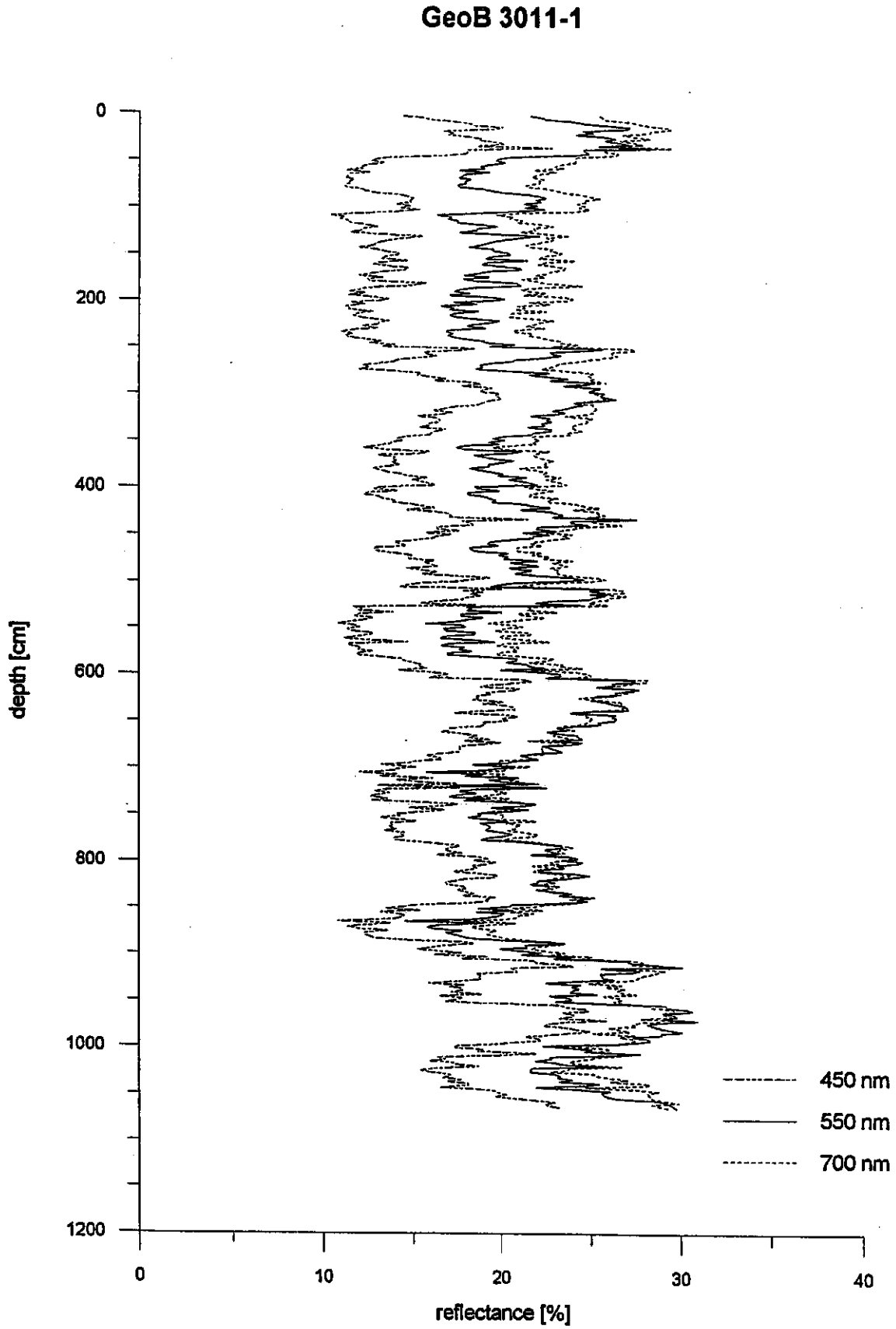

Fig. 87: Color reflectance measurements.

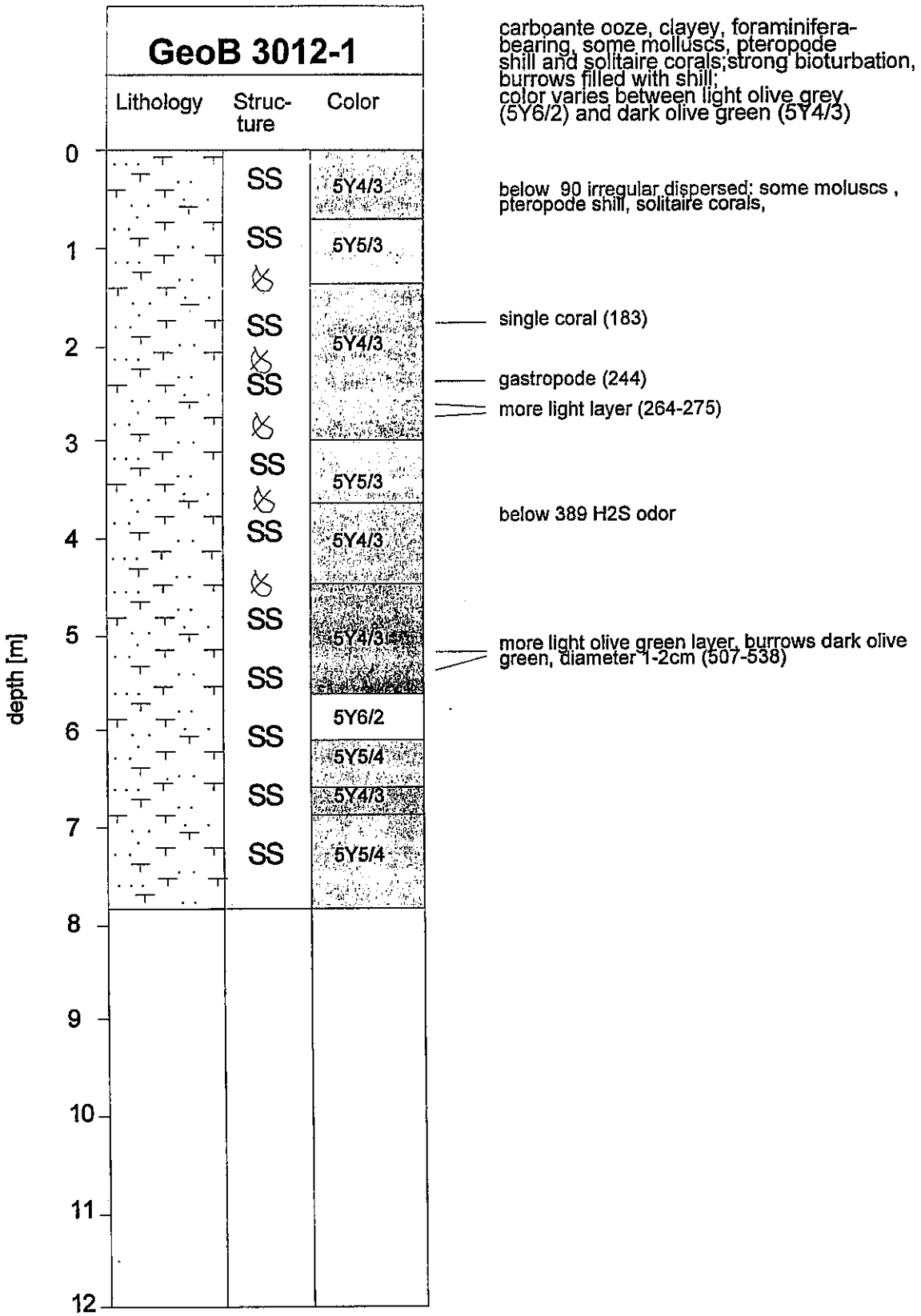

Fig. 88: Visual core description.

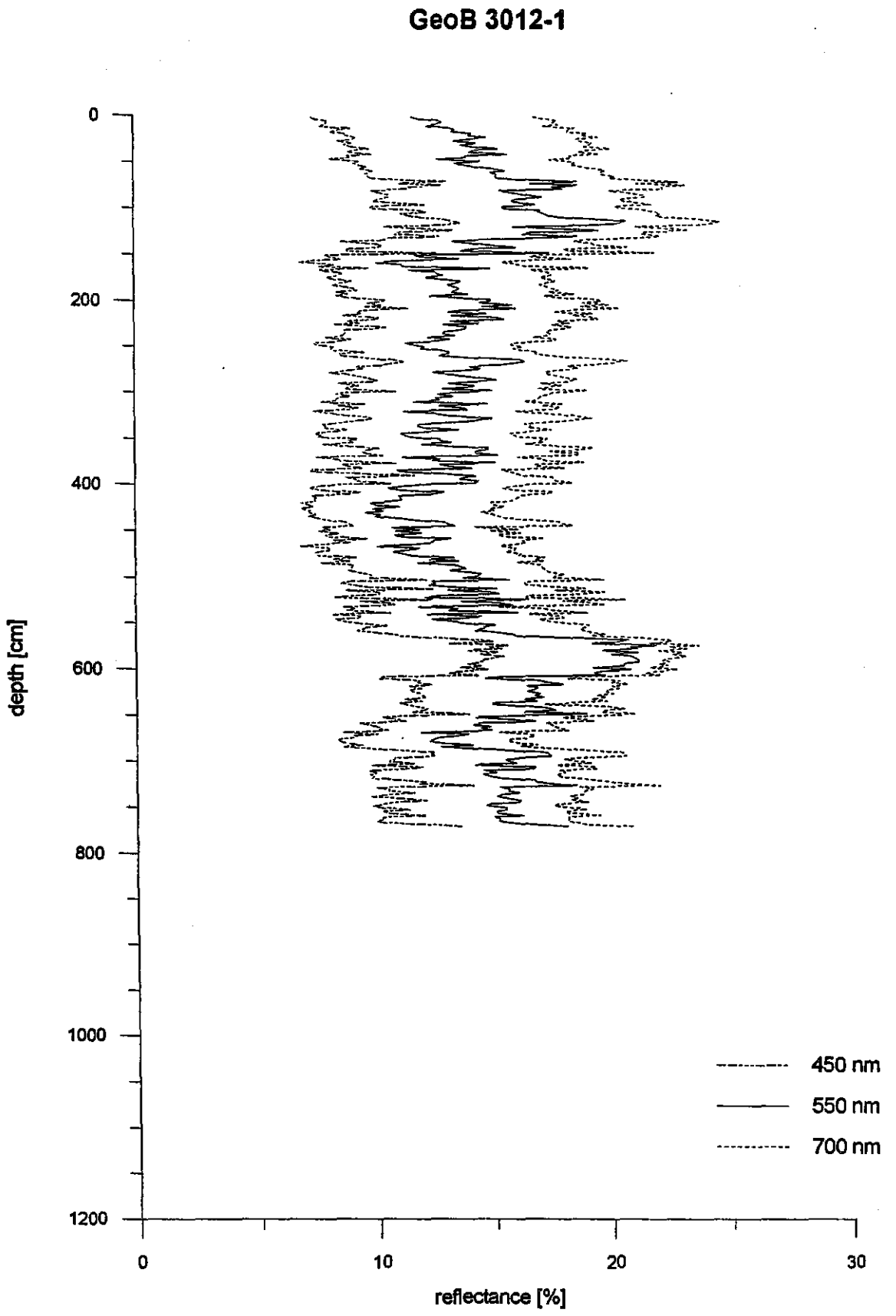

Fig. 89: Color reflectance measurements.

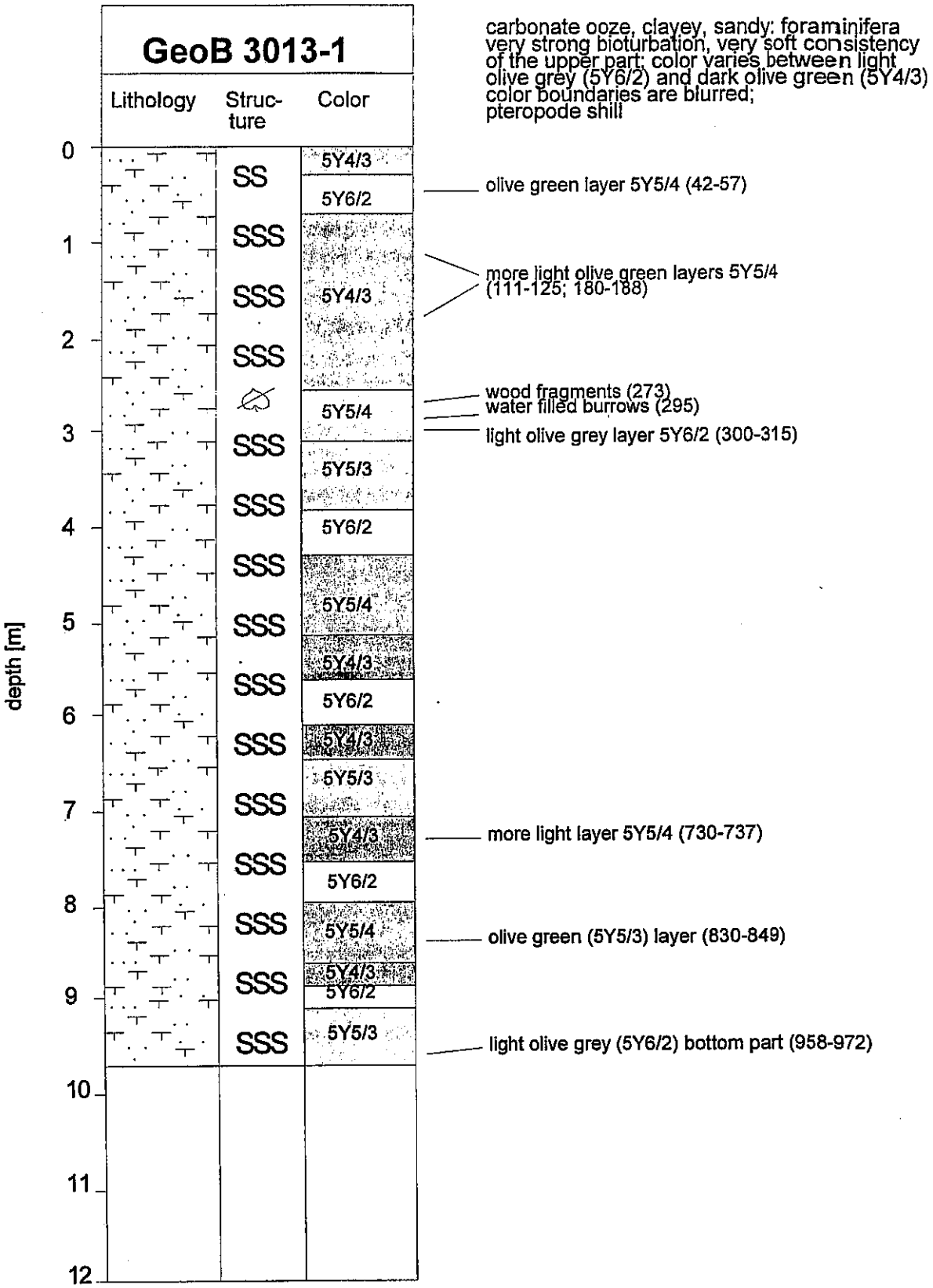

Fig. 90: Visual core description.

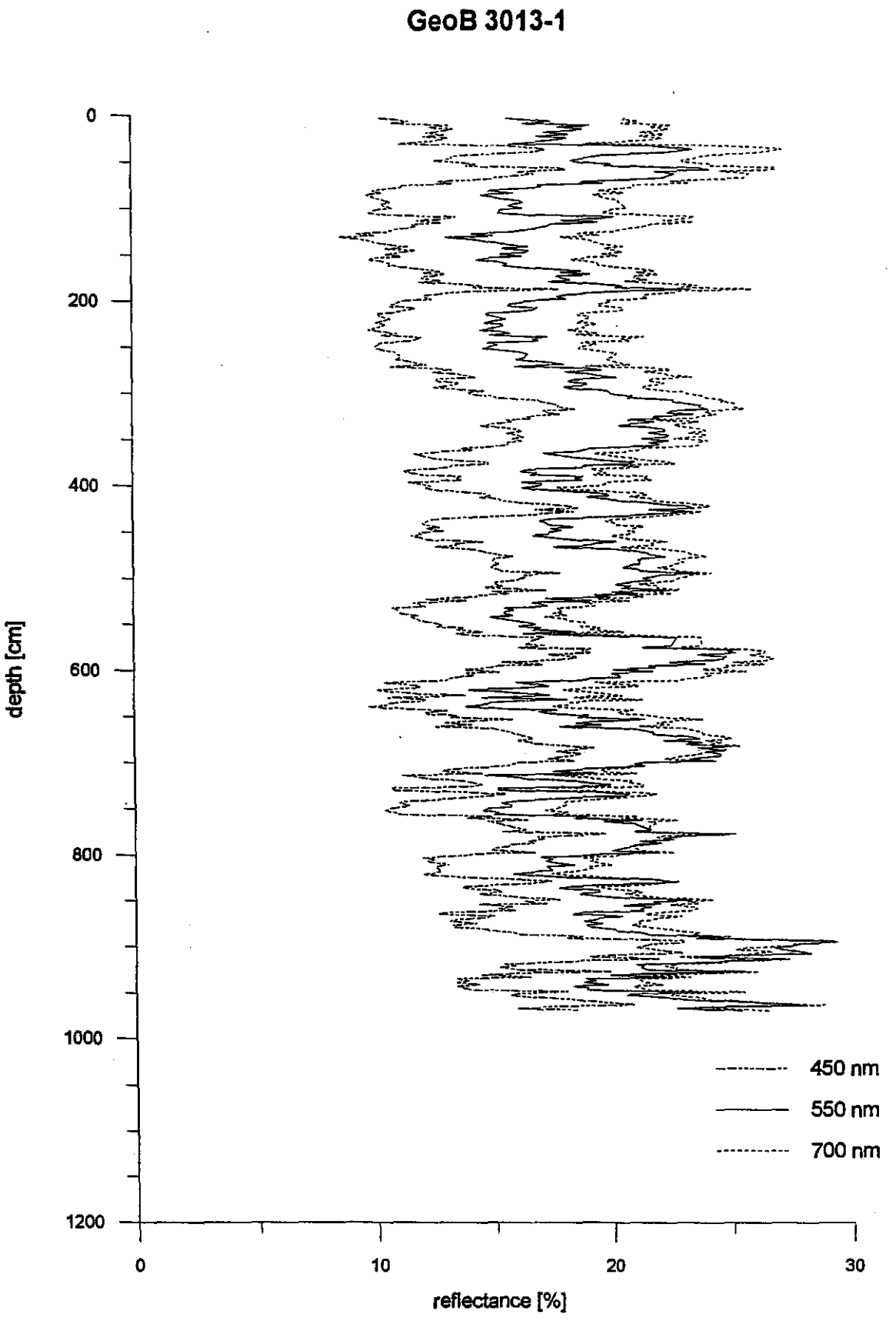

Fig. 91: Color reflectance measurements.

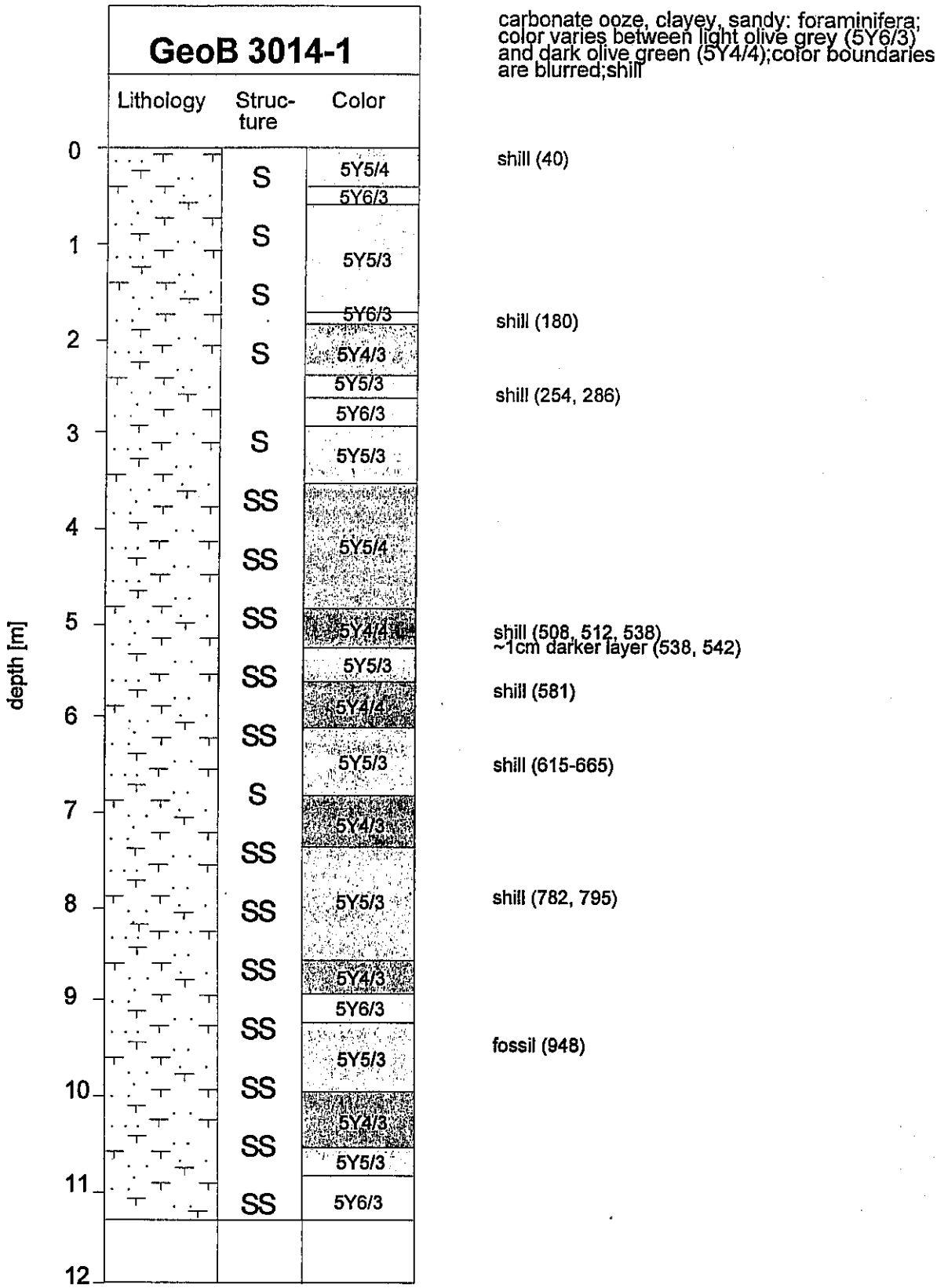

Fig. 92: Visual core description.

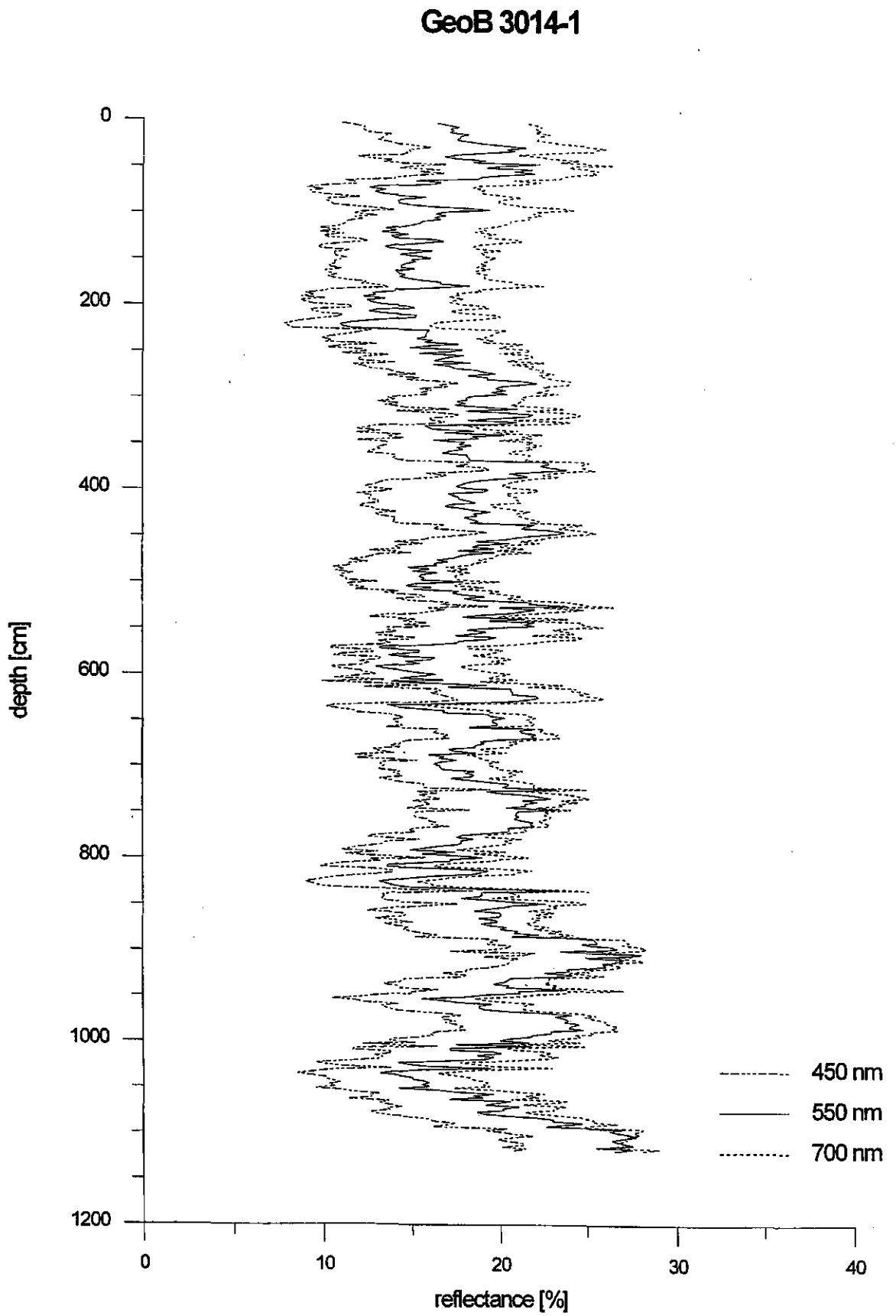

Fig. 93: Color reflectance measurements.

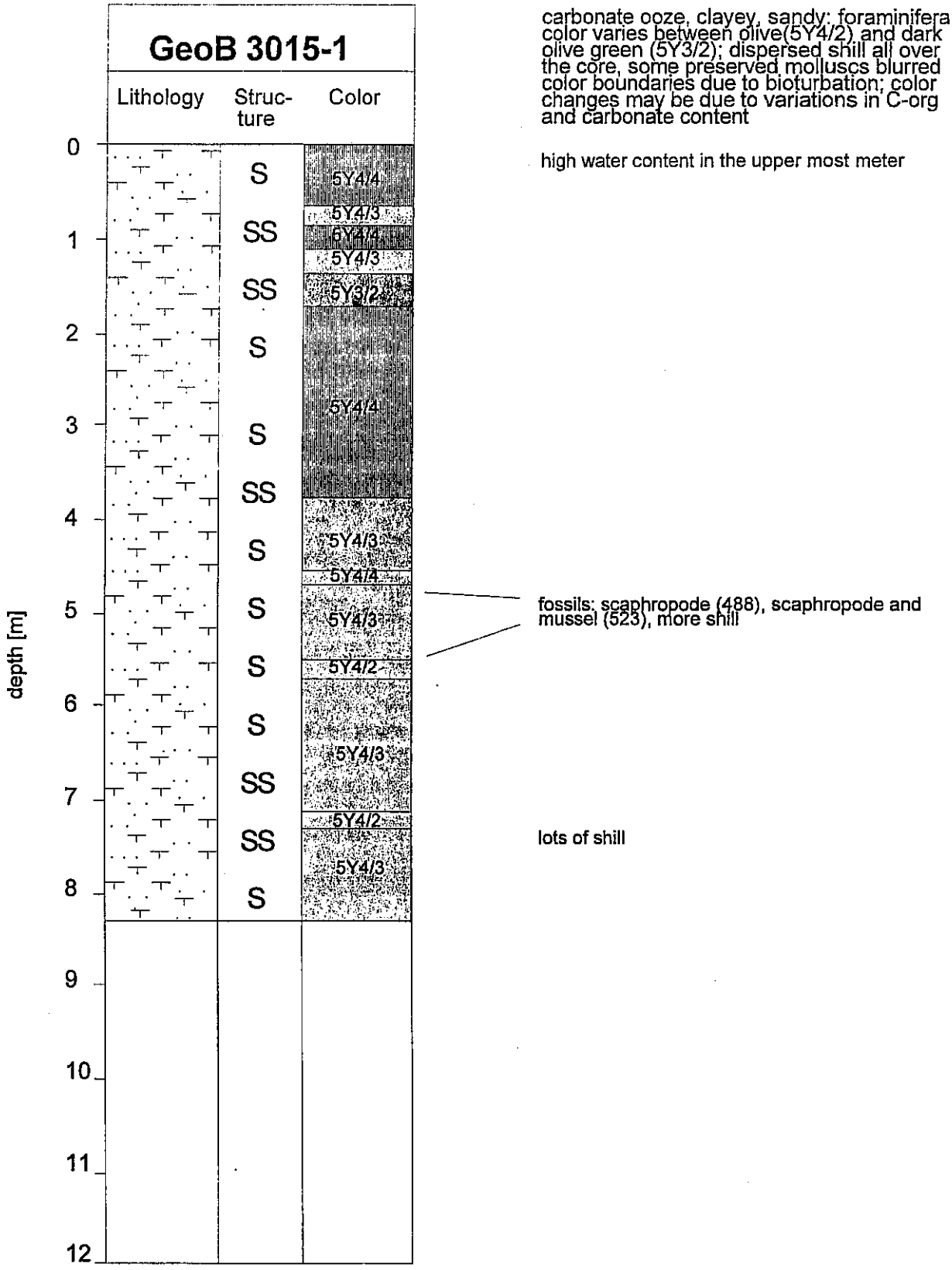

Fig. 94: Visual core description.

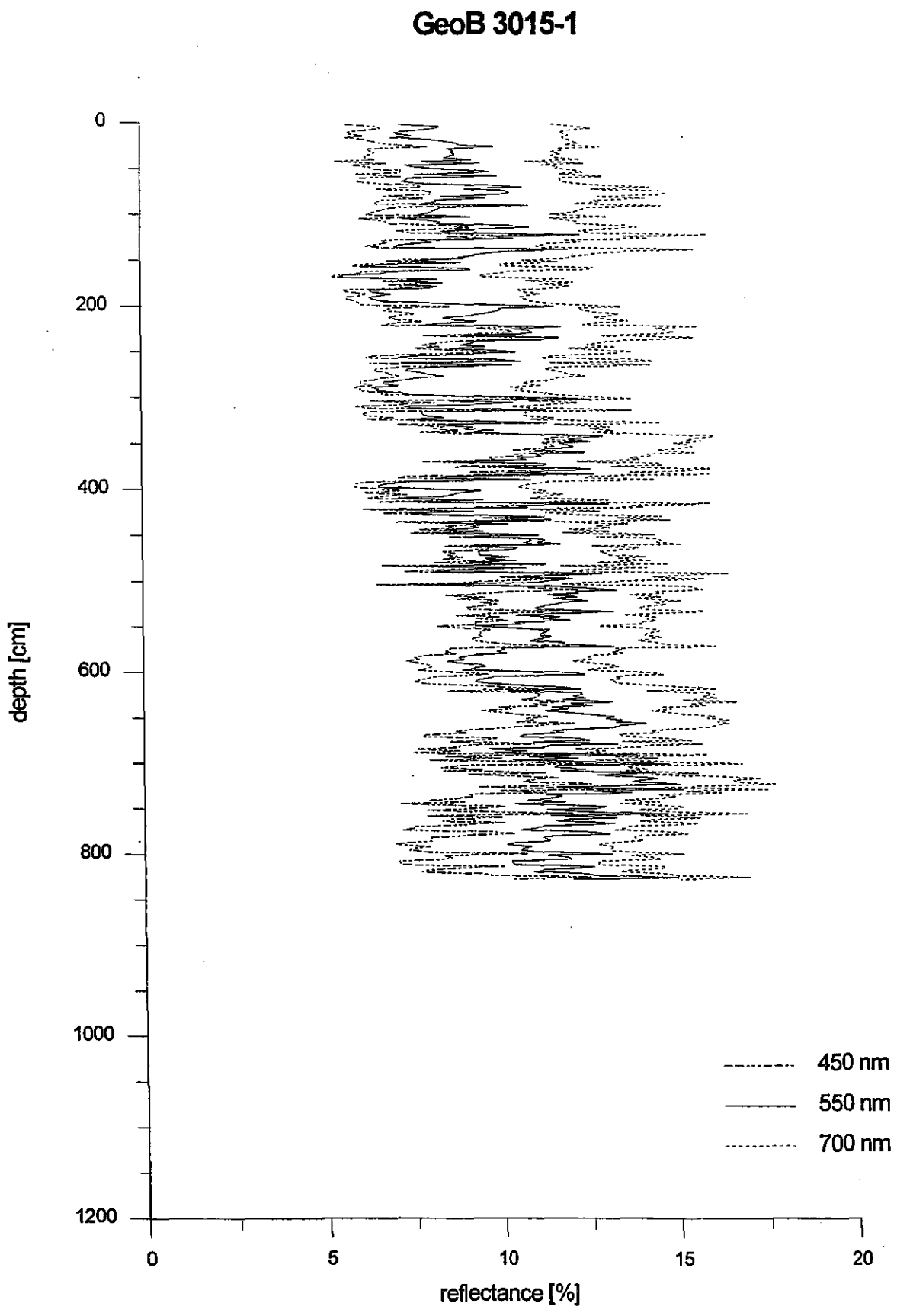

Fig. 95: Color reflectance measurements.

opening of the Gulf of Aden into the Arabian Sea have higher frequent variability in their reflectance pattern which might correspond cycling of monsoonal forcing of the upwelling off Somalia and Oman at precessional (23 kyr) and higher frequencies.

5.3.4.6 Piston Corers

(J. Erbacher, D. Fleitmann, H. Kitazato, J. Meyer, G. Schmiedl)

Two formats of the Göttingen piston corer were used to recover long sediment cores. For technical details see report on Leg M31/2, this volume.

Although the dead weight of the large piston corer had to be reduced by one ton, its performance was still satisfactory at 19 m or 80 % average core length (with exception of failed attempts on Station No. 111, where for unknown reasons only 6.2 m were recovered).

All cores collected on Leg M31/3 are stored, and will be described, at the University of Bremen (Prof. G. Wefer, Dr. R. Schneider).

Tab. 16: Core list of METEOR cruise 31/2
Arabian Sea

Station	Latitude	Longitude	Water depth	Core No.	Barrel (m)	GPI Tü No.	Core recovery
106	13 29,5N	50 17,8E	2023 m	KL 106-1	24	KL 33	18,9 m
107	14 36,3N	52 55,1E	1803 m	KL 107-1	24	KL 34	19,5 m
108	14 58,4N	54 22,8E	2330 m	KL 108-1	24	KL 35	19,4 m
109	15 51,2N	56 59,3E	3228 m	KL 109-1	24	KL 36	17,1 m
111-1	16 10,1N	59 45,9E	1918 m	KL 111-1	24	KL 37	6,2 m
111-2	16 05,5N	59 41,1E	2240 m	KL 111-2	12	KL 38	11,7 m
113	16 31,9N	55 19,9E	2624 m	KL 113-1	24	KL 39	20,4 m

Benthic foraminiferal faunal fluctuations during the Late Quaternary

Several late Quaternary sediment cores were sampled at 5 cm spacing to reconstruct global climatic changes and regional fluctuations in intensity and cyclicity of the mosoonal system. Based on a preliminary stratigraphy of the Bremen group (see report in this volume) selected samples of gravity core GeoB 3004-1 from station 107 were investigated on board for their benthic foraminiferal content. The core top sample and samples that are supposed to represent interglacial conditions are characterized by *Epistominella exigua*, which is a constituent of the epifauna. In contrast, samples that are supposed to mirror glacial conditions exhibit large portions of the preferentially infaunal species *Uvigerina peregrina* and *Bulimina aculeata*.

These preliminary results provide evidence for an increase of organic matter fluxes in the Arabian Sea upwelling area during glacial conditions. Future work will concentrate on the investigation of the benthic foraminiferal fauna and the corresponding stable isotope signal in a high temporal resolution to reconstruct high-frequency variations of the monsoonal system.

6 Ship's Meteorological Station

6.1 Weather and Meteorological Conditions during Leg M31/1

(J. Sußebach)

METEOR left the port of Hamburg on December 30, 1995 and sailed westward and southwest through the English Channel and the Bay of Biskay. The southwesterly winds in the North Sea reached strength between Bft 6-8 with gusts up to Bft 10 and reduced the ship speed in the beginning. The weather improved and was reasonably good between January 2 - 6 while METEOR passed the Bay of Biskaya and the Strait of Gibraltar into the western Mediterranean. A following period with unstable and stormy weather was caused by a low pressure system over Tunesia and lasted until January 8. METEOR cruised south of Sardinia and Sicliy in fair weather. On January 11 winds increased to Bft 8 and the northwesterly winds increased the speed of METEOR in the Strait of Sicily. Stormy winds from northwest to west continued on January 12 in connection with an approaching cold front from the northwest.

The cold front passed METEOR during the night of January 12. On its backside low veering winds could be observed during the morning hours of January 13. Cyclogenic processes in connection with a high pressure trough that reached from Russia to Tunesia had favoured the development of a low along the cold front just south of the position of METEOR and caused the decrease in wind speeds. An impressive development of the low pressure system could be observed in the following hours. The low pressure system deepened during the night of January 13 and reached a core pressure of 990 hpa in the eastern Ionian Sea. On the western flank of the low pressure system winds increased to hurricane strength during most of the day. Wind measurements at 14 UTC on January 14 yielded a 10 minute average of 73 knots with gusts of 85 knots. Winds did not decrease until the night of January 14 and remained at Bft 8-9 during January 15 during while the low pressure system moved slowly southward.

On the night of January 15 winds decreased distinctively when METEOR passed the Strait of Otranto. Station work in the southern Adriatic in the following two days was performed in fair weather. METEOR continued the cruise along the western coast of Greece under unstable weather conditions from January 18 to 20 with veering winds from northwest. Until January 30 METEOR was working in the Aegean and between Rhodes and the Turkish coast. During this period fair weather prevailed with the exceptions of January 25 and 28 when METEOR was passed by cold fronts with associated strong winds from southwest to northwest.

A high pressure system dominated the area west and south of Cypres during the period from January 31 to February 3 resulting in good weather with almost no winds and glassy seas. A

low over the Sinai peninsula which moved towards Israel caused an increase in clouds on February 4 but winds remainded moderate. METEOR reached Port Said on February 5.

6.2 Weather and Meteorological Conditions during Leg M31/2

(J. Sußebach)

On February 8, 1995 RV METEOR left Port Said for going through the Suez Canal. At this day the weather was cool with tempreatures about 9° C in the early morning and 14° C in the afternoon. Isolated rain showers and gusty southwesterly to westerly winds were observed at first. Later by day weather improved.

On February 9 and 10 weather was fair with light and variable winds in the Gulf of Suez and south of Sinai Peninsula.

During the following period until February 25 RV METEOR was in the northern half of the Red Sea. The weather situation was characterized by a flat low pressure trough extending nearly in northwest-southeast direction from Sinai to the region Ethiopia/Eritrea/Southern Red Sea/Yemen. At the same time relativ high pressure dominated over Saudi Arabia, Libya, Egypt and the northwestern part of Sudan. This pressure situation caused mainly northerly to northwesterly winds on our route. Other directions were seldom. The mean wind speed (10 minutes average) generally varied between force 4 and 6 Beaufort. Sometimes wind was light and variable.

The air was mainly dry with sunny or partly cloudly weather. Temperatures varied between 18° and 23° C during day and night. Only on February 13 moist air with dewpoints up to 18° C caused overcast sky for a time. On February 25 it was sultry, too.

From February 26 until March 1st RV METEOR was in the Southern Red Sea. The weather was sunny or cloudly. Temperatures varied between 22 and 26° C and increased to nearly 30° C later. The dewpoints gradually rised above 20° C. The wind blew from northwesterly to northerly directions with force 3 to 6 Beaufort at first. On March 1st the wind became southerly. It increased to force 6 to 7 Beaufort when RV METEOR passed the Strait Bab el Mandeb in the night to March 2nd.

6.3 Weather and Meterological Conditions during Leg M31/3

(E. Röd)

The Meteorological conditions during the cruise M 31/3 from the 3rd to 22nd of March 1995 (Djibouti-Djibouti).

The weather during this leg was still dominated by the winter monsoon. Its direction varied between E-SE and N-NE, depending on the particular distribution of the deciding pressure

centres.The typical pattern showed climatological normal conditions: a continental cold anticyclone over the Caspian Sea or Turkmenistan, thrusting a high pressure wedge over the Great Arabian Desert into the northern part of the Arabian Sea.

The intensity of the prevailing northeasterly outflow from this high was rather variable, but never achieved critical values. The highest wind force 6 Beaufort was observed in the Gulf of Aden, apparently due to coastal effects and to funnelling of the flow. (This could have been responsible also for the heavy cloudiness an the only rain of the whole cruise when leaving the bay of Djibouti). The most frequent wind forces were 3 and 4 Bft, so that nearly no movement of the ship was to be felt.

The temperature of the monsoon was quasi-constant 23 to 26° C, the relative moisture on the other hand varied between 90 % during the first rainy days and 45 % under a northerly flow advecting dry air from the desert of oman. The humidity thus showed a clear correlation with wind direction. The daily radiosoundings proved the monsoon to be limited to a rather shallow layer. Its top could be found mostly between 1500 and 2500 m. Above this level the wind was strictly westerly, increasing with height towards the maximum in 12-13 km with the tropopause in 15 km. Here the current often achieved jet-stream-intensity between 60 and 90 kts. Only once, on the 14th of March, the regime of the monsoon was interrupted by a ciclonic phase. A cloud patch showed up over central Arabia in the satellite image, became a big cloud formation and moved to the Strait of Hormuz. On the 14th of March cyclogenesis had formed already a complete frontal system.

The circulation of this low made the wind at the ship veer to S, after the passage of the weak upper cold front to NW and later to N-NE re-establishing thus the monsoon and high pressure conditions. Other fronts that appeared over the Arabian Peninsula moved E without touching the ship's route.

The visibility within the continental air was throughout good, mostly very good. No one fog event could be observed. The atmospheric pressure showed the well pronounced tropical daily variation of about 3 hPa. The interdiurnal variability was only of the same order.

The Intertropical Convergence Zone was still far away south of the equator. Only towards the end of the cruise convective cells appeared also in low northern latitudes when the ITCZ started moving slowly north.

The following distribution of wind direction and wind force illustrates the description given above (period 3. - 19. March 1995):

N	NE	E	SE	S	W	W	NW	
3	10	56	14	9	6	0	2 %	of all hourly measurements
0	1	2	3	4	5	6		Windforce in Beaufort
0	0	10	30	38	18	4 %		

7 Lists

7.1 Lists of Leg M31/1

7.1.1 List of CTD Stations

Station	Date	Time (UTC)	Cast	Profil-depth	Water-depth	Latitude	Longitude
001	05.01	05.37	(No. 1)	3499 m	3644 m	36° 10.9' N	009° 10.3' W
001	05.01	08.35	(No. 2)	1990 m	3633 m	36° 11.4' N	009° 10.1' W
001	05.01	10.44	(No. 3)	20 m	3641 m	36° 10.9' N	009° 09.7' W
002	06.01	18.57	(No. 1)	200 m	2616 m	36° 36.4' N	001° 00.7' W
002	06.01	19.25	(No. 2)	2591 m	2618 m	36° 36.2' N	001° 00.7' W
002	06.01	21.22	(No. 3)	289 m	2613 m	36° 36.0' N	001° 01.4' W
003	08.01	07.09	(No. 1)	2726 m	2743 m	37° 59.9' N	004° 34.9' E
003	08.01	09.20	(No. 2)	2603 m	2740 m	37° 59.9' N	004° 33.5' E
004	09.01	04.58	(No. 1)	200 m	2750 m	38° 10.0' N	007° 49.8' E
004	09.01	05.23	(No. 2)	2735 m	2750 m	38° 10.2' N	007° 50.0' E
005	10.01	17.38	(No. 1)	200 m	882 m	37° 32.3' N	011° 31.9' E
005	10.01	18.05	(No. 2)	852 m	887 m	37° 32.3' N	011° 31.8' E
005	10.01	19.00	(No. 3)	853 m	884 m	37° 32.5' N	011° 31.8' E
006	11.01	02.30	(No. 1)	1233 m	1285 m	36° 29.8' N	012° 32.9' E
007	11.01	12.19	(No. 1)	200 m	587 m	35° 28.0' N	014° 20.0' E
007	11.01	12.52	(No. 2)	571 m	586 m	35° 27.9' N	014° 19.8' E
008	12.01	08.20	(No. 1)	3560 m	3610 m	35° 47.5' N	015° 56.9' E
008	12.01	11.00	(No. 2)	196 m	3610 m	35° 47.2' N	015° 56.9' E
009	12.01	14.11	(No. 1)	201 m	3812 m	35° 47.9' N	016° 36.1' E
009	12.01	14.34	(No. 2)	3800 m	3812 m	35° 47.6' N	016° 35.8' E
010	12.01	20.52	(No. 1)	200 m	4070 m	35° 47.7' N	017° 30.0' E
010	12.01	21.20	(No. 2)	4025 m	4066 m	35° 46.8' N	017° 28.9' E
011	13.01	04.33	(No. 1)	200 m	4060 m	36° 09.8' N	018° 17.8' E
011	13.01	05.00	(No. 2)	4040 m	4060 m	36° 09.8' N	018° 17.7' E
013	15.01	11.10	(No. 1)	2262 m	2283 m	38° 48.0' N	018° 05.0' E
014	15.01	16.27	(No. 1)	1462 m	1469 m	38° 53.9' N	017° 30.0' E
014	15.01	17.33	(No. 2)	200 m	1463 m	38° 54.0' N	017° 29.9' E
015	16.01	05.13	(No. 1)	203 m	832 m	40° 24.1' N	018° 49.0' E
015	16.01	05.40	(No. 2)	826 m	832 m	40° 24.1' N	018° 48.9' E
016	16.01	19.00	(No. 1)	200 m	1160 m	41° 30.1' N	018° 17.8' E
016	16.01	19.28	(No. 2)	476 m	1135 m	41° 30.3' N	018° 17.8' E
016	16.01	20.17	(No. 3)	1131 m	1137 m	41° 30.5' N	018° 17.8' E
017	16.01	23.57	(No. 1)	199 m	1155 m	41° 24.1' N	017° 48.1' E
017	17.01	00.22	(No. 2)	1133 m	1155 m	41° 24.0' N	017° 47.9' E
018	17.01	03.28	(No. 1)	851 m	868 m	41° 16.0' N	017° 27.2' E

019	17.01	05.26	(No. 1)	155 m	161 m	41° 11.9' N	017° 18.0' E
020	18.01	10.26	(No. 1)	199 m	3202 m	38° 45.2' N	018° 47.6' E
020	18.01	10.50	(No. 2)	3189 m	3215 m	38° 45.5' N	018° 47.5' E
021	18.01	16.36	(No. 1)	160 m	3206 m	38° 10.0' N	019° 05.0' E
021	18.01	16.58	(No. 2)	3286 m	3316 m	38° 10.0' N	019° 04.6' E
022	18.01	22.21	(No. 1)	200 m	1413 m	38° 45.0' N	019° 24.0' E
022	18.01	22.48	(No. 2)	1391 m	1415 m	38° 44.8' N	019° 24.6' E
023	19.01	03.00	(No. 1)	203 m	2337 m	38° 45.0' N	020° 10.0' E
023	19.01	03.24	(No. 2)	2331 m	2335 m	38° 45.1' N	020° 10.0' E
024	19.01	12.56	(No. 1)	201 m	3348 m	37° 25.0' N	020° 45.0' E
024	19.01	13.29	(No. 2)	3330 m	3348 m	37° 25.0' N	020° 45.0' E
025	19.01	18.56	(No. 1)	198 m	3207 m	37° 02.0' N	020° 17.0' E
025	19.01	19.26	(No. 2)	3184 m	3207 m	37° 01.9' N	020° 16.7' E
026	20.01	03.22	(No. 1)	3252 m	3260 m	36° 25.0' N	019° 34.8' E
027	20.01	09.26	(No. 1)	199 m	3096 m	35° 40.0' N	019° 39.0' E
027	20.01	10.02	(No. 2)	3094 m	3100 m	35° 40.1' N	019° 38.9' E
028	20.01	17.16	(No. 1)	199 m	3191 m	34° 40.0' N	019° 42.0' E
028	20.01	17.43	(No. 2)	3074 m	3191 m	34° 40.0' N	019° 42.1' E
029	21.01	00.54	(No. 1)	199 m	3034 m	33° 48.0' N	020° 17.0' E
029	21.01	01.25	(No. 2)	3011 m	3034 m	33° 48.0' N	020° 17.0' E
030	21.01	11.16	(No. 1)	200 m	2433 m	34° 04.1' N	022° 07.2' E
030	21.01	11.46	(No. 2)	2406 m	2433 m	34° 04.0' N	022° 07.3' E
031	21.01	16.47	(No. 1)	204 m	2891 m	34° 31.1' N	022° 32.8' E
031	21.01	17.12	(No. 2)	2787 m	2891 m	34° 31.0' N	022° 32.9' E
032	21.01	22.25	(No. 1)	200 m	3202 m	34° 58.0' N	022° 58.9' E
032	22.01	23.04	(No. 2)	3188 m	3202 m	34° 58.0' N	022° 58.9' E
033	22.01	03.45	(No. 1)	198 m	3196 m	35° 20.0' N	023° 18.9' E
033	22.01	04.12	(No. 2)	3198 m	3196 m	35° 20.0' N	023° 19.0' E
034	22.01	08.18	(No. 1)	1412 m	1529 m	35° 30.1' N	023° 23.2' E
035	22.01	11.59	(No. 1)	911 m	918 m	35° 52.5' N	023° 01.0' E
036	22.01	16.20	(No. 1)	1365 m	1371 m	36° 26.0' N	022° 46.5' E
037	22.01	21.06	(No. 1)	200 m	2869 m	36° 03.1' N	022° 29.9' E
037	22.01	21.30	(No. 2)	2849 m	2869 m	36° 03.3' N	022° 29.7' E
038	23.01	01.55	(No. 1)	202 m	4627 m	35° 38.9' N	022° 29.9' E
038	23.01	02.25	(No. 1)	4595 m	4627 m	35° 38.8' N	022° 30.2' E
039	23.01	09.40	(No. 1)	748 m	853 m	35° 45.0' N	023° 27.2' E
040	23.01	13.26	(No. 1)	1123 m	1142 m	35° 53.0' N	024° 07.5' E
041	23.01	18.44	(No. 1)	248 m	1864 m	35° 52.8' N	025° 11.2' E
041	23.01	19.20	(No. 2)	1850 m	1864 m	35° 52.6' N	025° 11.4' E
042	24.01	01.05	(No. 1)	240 m	2294 m	35° 42.6' N	026° 12.1' E
042	24.01	01.35	(No. 2)	2273 m	2294 m	35° 42.5' N	026° 12.1' E
043	24.01	05.48	(No. 1)	201 m	2400 m	35° 36.5' N	026° 47.0' E
043	24.01	06.15	(No. 2)	2406 m	2415 m	35° 36.8' N	026° 47.1' E
043	24.01	08.00	(No. 3)	2311 m	2415 m	35° 36.8' N	026° 47.7' E

044	24.01	14.11	(No. 1)	942 m	970 m	35° 16.5' N	026° 39.1' E
045	24.01	18.31	(No. 1)	200 m	1770 m	34° 46.9' N	026° 19.2' E
045	24.01	18.55	(No. 2)	1911 m	1938 m	34° 46.4' N	026° 19.2' E
046	24.01	22.47	(No. 1)	200 m	3295 m	34° 30.0' N	026° 00.0' E
046	24.01	23.12	(No. 2)	3264 m	3295 m	34° 29.9' N	025° 59.9' E
047	25.01	04.37	(No. 1)	200 m	2854 m	34° 00.0' N	025° 51.5' E
047	25.01	05.08	(No. 2)	2885 m	2904 m	34° 00.1' N	025° 51.3' E
048	25.01	10.24	(No. 1)	2468 m	2499 m	33° 28.0' N	025° 43.0' E
048	25.01	12.23	(No. 2)	299 m	2496 m	33° 28.0' N	025° 43.0' E
049	25.01	15.35	(No. 1)	199 m	2429 m	32° 57.7' N	025° 33.9' E
049	25.01	16.00	(No. 2)	2374 m	2441 m	32° 57.6' N	025° 34.0' E
050	25.01	20.16	(No. 1)	199 m	2957 m	32° 28.5' N	025° 25.4' E
050	25.01	20.43	(No. 2)	3097 m	3128 m	32° 28.2' N	025° 25.6' E
051	26.01	07.55	(No. 1)	305 m	2485 m	33° 35.9' N	026° 58.7' E
051	26.01	08.25	(No. 2)	2479 m	2503 m	33° 35.6' N	026° 58.8' E
052	26.01	18.31	(No. 1)	304 m	2402 m	35° 02.7' N	026° 55.2' E
052	26.01	19.01	(No. 2)	2382 m	2402 m	35° 02.6' N	026° 55.4' E
053	27.01	00.14	(No. 1)	201 m	2700 m	34° 31.5' N	027° 28.4' E
053	27.01	00.38	(No. 2)	2676 m	2719 m	34° 31.5' N	027° 28.6' E
054	27.01	06.11	(No. 1)	310 m	2787 m	34° 00.3' N	027° 49.9' E
054	27.01	06.47	(No. 2)	2818 m	2856 m	33° 59.9' N	028° 00.0' E
055	27.01	13.17	(No. 1)	305 m	3094 m	33° 11.9' N	028° 24.0' E
055	27.01	13.46	(No. 2)	3076 m	3095 m	33° 12.0' N	028° 24.2' E
056	27.01	22.36	(No. 1)	292 m	2606 m	34° 24.0' N	029° 06.0' E
056	27.01	23.11	(No. 2)	2599 m	2634 m	34° 23.9' N	029° 06.0' E
057	28.01	05.27	(No. 1)	300 m	2384 m	34° 59.9' N	029° 48.1' E
057	28.01	05.57	(No. 2)	2371 m	2391 m	34° 59.7' N	029° 48.2' E
058	28.01	12.07	(No. 1)	302 m	2974 m	35° 35.9' N	029° 20.0' E
058	28.01	12.30	(No. 2)	2957 m	3004 m	35° 36.0' N	029° 20.0' E
059	28.01	18.46	(No. 1)	269 m	4452 m	36° 00.8' N	028° 42.1' E
059	28.01	19.15	(No. 2)	4305 m	4327 m	36° 01.1' N	028° 41.8' E
060	29.01	00.26	(No. 1)	206 m	3554 m	35° 45.5' N	028° 20.9' E
060	29.01	00.53	(No. 2)	3542 m	3575 m	35° 45.5' N	028° 20.4' E
061	29.01	05.16	(No. 1)	300 m	1925 m	35° 29.8' N	027° 59.9' E
061	29.01	05.43	(No. 2)	1826 m	1844 m	35° 29.7' N	027° 59.7' E
062	29.01	15.52	(No. 1)	317 m	1311 m	35° 21.3' N	027° 17.4' E
062	29.01	16.20	(No. 2)	1242 m	1286 m	35° 21.1' N	027° 17.0' E
063	30.01	01.23	(No. 1)	291 m	2905 m	35° 00.0' N	028° 25.0' E
063	30.01	01.53	(No. 2)	2893 m	2905 m	35° 00.0' N	028° 24.1' E
064	30.01	05.52	(No. 1)	2758 m	2788 m	34° 59.8' N	028° 35.2' E
065	30.01	16.36	(No. 1)	300 m	1755 m	35° 40.0' N	030° 20.0' E
065	30.01	17.02	(No. 2)	1715 m	1755 m	35° 40.0' N	030° 20.0' E
066	30.01	21.54	(No. 1)	200 m	2592 m	36° 06.0' N	031° 00.0' E
066	30.01	22.18	(No. 2)	2571 m	2593 m	36° 06.1' N	030° 59.9' E

067	31.01	03.26	(No. 1)	200 m	2521 m	35° 36.1' N	031° 30.0' E
067	31.01	03.54	(No. 2)	2498 m	2519 m	35° 36.0' N	031° 30.1' E
068	31.01	09.17	(No. 1)	300 m	2176 m	34° 59.9' N	031° 59.9' E
068	31.01	09.48	(No. 2)	2134 m	2161 m	35° 00.0' N	032° 00.0' E
069	31.01	15.20	(No. 1)	300 m	2421 m	34° 23.9' N	031° 24.0' E
069	31.01	15.51	(No. 2)	2413 m	2421 m	34° 24.0' N	031° 24.0' E
070	31.01	23.27	(No. 1)	301 m	2301 m	33° 12.0' N	031° 00.0' E
070	31.01	23.54	(No. 2)	2274 m	2302 m	33° 11.8' N	031° 00.0' E
071	01.02	08.17	(No. 1)	308 m	2420 m	34° 23.9' N	030° 24.2' E
071	01.02	08.43	(No. 2)	2434 m	2483 m	34° 23.1' N	030° 24.6' E
072	01.02	19.14	(No. 1)	299 m	2278 m	35° 00.1' N	030° 54.0' E
072	01.02	19.45	(No. 2)	2255 m	2276 m	35° 00.0' N	030° 53.7' E
073	02.02	04.53	(No. 1)	204 m	2395 m	34° 25.1' N	032° 11.7' E
073	02.02	05.23	(No. 2)	2358 m	2407 m	34° 25.0' N	032° 11.5' E
073	02.02	07.16	(No. 3)	2260 m	2418 m	34° 25.2' N	032° 11.4' E
074	02.02	16.17	(No. 1)	299 m	2231 m	33° 50.0' N	033° 30.1' E
074	02.02	16.46	(No. 2)	2228 m	2240 m	33° 50.0' N	033° 30.1' E
075	02.02	23.52	(No. 1)	300 m	2629 m	33° 42.0' N	032° 12.2' E
075	03.02	00.18	(No. 2)	2614 m	2630 m	33° 42.1' N	032° 12.2' E
076	03.02	06.16	(No. 1)	305 m	1423 m	33° 00.1' N	032° 42.0' E
076	03.02	06.48	(No. 2)	1421 m	1425 m	33° 00.4' N	032° 42.2' E
077	03.02	11.38	(No. 1)	301 m	1150 m	32° 18.1' N	032° 54.0' E
077	03.02	12.08	(No. 2)	1131 m	1150 m	32° 18.1' N	032° 54.0' E

7.1.2 List of Stations with Tracer Measurements

Station	Date	Time (UTC)	Cast	Latitude	Longitude	CFC samples	Helium samples	Tritium samples	Stable Isotopes
001	05.01	05.37	(No. 1)	36° 10.9' N	009° 10.3' W	34			
001	05.01	08.35	(No. 2)	36° 11.4' N	009° 10.1' W	10			
002	06.01	19.25	(No. 2)	36° 36.2' N	001° 00.7' W	23	17	17	16
003	08.01	07.09	(No. 1)	37° 59.9' N	004° 34.9' E	20	14	14	14
004	09.01	05.23	(No. 2)	38° 10.2' N	007° 50.0' E	24	17	17	14
005	10.01	19.00	(No. 3)	37° 32.5' N	011° 31.8' E	13	9	6	
006	11.01	02.30	(No. 1)	36° 29.8' N	012° 32.9' E	13	13	13	13
007	11.01	12.52	(No. 2)	35° 27.9' N	014° 19.8' E	11	5	8	
008	12.01	08.20	(No. 1)	35° 47.5' N	015° 56.9' E	23	15	22	14
009	12.01	14.34	(No. 2)	35° 47.6' N	016° 35.8' E	19	7	7	
010	12.01	21.20	(No. 2)	35° 46.8' N	017° 28.9' E	16	17	18	18
011	13.01	05.00	(No. 2)	36° 09.8' N	018° 17.7' E	21			
013	15.01	11.10	(No. 1)	38° 48.0' N	018° 05.0' E	20	13	17	13
014	15.01	16.27	(No. 1)	38° 53.9' N	017° 30.0' E	14	4	4	
015	16.01	05.40	(No. 2)	40° 24.1' N	018° 48.9' E	19	4	4	
016	16.01	20.17	(No. 3)	41° 30.5' N	018° 17.8' E	16	4	4	4
017	17.01	00.22	(No. 2)	41° 24.0' N	017° 47.9' E	14	11	11	11
018	17.01	03.28	(No. 1)	41° 16.0' N	017° 27.2' E	11			
019	17.01	05.26	(No. 1)	41° 11.9' N	017° 18.0' E			6	6
020	18.01	10.50	(No. 2)	38° 45.5' N	018° 47.5' E	20	5	5	5
021	18.01	16.58	(No. 2)	38° 10.0' N	019° 04.6' E	22	17	17	17
022	18.01	22.48	(No. 2)	38° 44.8' N	019° 24.6' E	12	4	4	4
023	19.01	03.24	(No. 2)	38° 45.1' N	020° 10.0' E	15	16	18	11
024	19.01	13.29	(No. 2)	37° 25.0' N	020° 45.0' E	17	16	16	11
025	19.01	19.26	(No. 2)	37° 01.9' N	020° 16.7' E	14		6	
026	20.01	03.22	(No. 1)	36° 25.0' N	019° 34.8' E	21	20	20	20
027	20.01	10.02	(No. 2)	35° 40.1' N	019° 38.9' E	13			
028	20.01	17.43	(No. 2)	34° 40.0' N	019° 42.1' E	19	15	17	12
029	21.01	01.25	(No. 2)	33° 48.0' N	020° 17.0' E	20	13	14	12
030	21.01	11.46	(No. 2)	34° 04.0' N	022° 07.3' E	19	15	18	12
031	21.01	17.12	(No. 2)	34° 31.0' N	022° 32.9' E	13	6	6	
032	22.01	23.04	(No. 2)	34° 58.0' N	022° 58.9' E	12	12	13	11
033	22.01	04.12	(No. 2)	35° 20.0' N	023° 19.0' E		10	13	

034	22.01	08.18	(No. 1) 35° 30.1' N	023° 23.2' E	11	9	9	
036	22.01	16.20	(No. 1) 36° 26.0' N	022° 46.5' E	12			
037	22.01	21.30	(No. 2) 36° 03.3' N	022° 29.7' E	14	14	14	12
038	23.01	02.25	(No. 1) 35° 38.8' N	022° 30.2' E	19	6	8	6
039	23.01	09.40	(No. 1) 35° 45.0' N	023° 27.2' E	8	6	6	
040	23.01	13.26	(No. 1) 35° 53.0' N	024° 07.5' E	11			
041	23.01	19.20	(No. 2) 35° 52.6' N	025° 11.4' E	14	12	13	11
042	24.01	01.35	(No. 2) 35° 42.5' N	026° 12.1' E	4	4	4	
043	24.01	06.15	(No. 2) 35° 36.8' N	026° 47.1' E	12	14	14	6
044	24.01	14.11	(No. 1) 35° 16.5' N	026° 39.1' E	10	6	6	6
045	24.01	18.55	(No. 2) 34° 46.4' N	026° 19.2' E	11	5	5	
046	24.01	23.12	(No. 2) 34° 29.9' N	025° 59.9' E	14	12	13	12
047	25.01	05.08	(No. 2) 34° 00.1' N	025° 51.3' E	14			
048	25.01	10.24	(No. 1) 33° 28.0' N	025° 43.0' E	14	13	14	11
049	25.01	16.00	(No. 2) 32° 57.6' N	025° 34.0' E	6			
050	25.01	20.43	(No. 2) 32° 28.2' N	025° 25.6' E	22	19	19	14
051	26.01	08.25	(No. 2) 33° 35.6' N	026° 58.8' E	12	4		
052	26.01	19.01	(No. 2) 35° 02.6' N	026° 55.4' E	15	7	12	
053	27.01	00.38	(No. 2) 34° 31.5' N	027° 28.6' E	16	17	17	13
054	27.01	06.47	(No. 2) 33° 59.9' N	028° 00.0' E	16	5	6	
055	27.01	13.46	(No. 2) 33° 12.0' N	028° 24.2' E	23	15	21	14
056	27.01	23.11	(No. 2) 34° 23.9' N	029° 06.0' E	14	6	6	
057	28.01	05.57	(No. 2) 34° 59.7' N	029° 48.2' E	12	12	12	10
058	28.01	12.30	(No. 2) 35° 36.0' N	029° 20.0' E	11	5	5	
059	28.01	19.15	(No. 2) 36° 01.1' N	028° 41.8' E	23	18	19	13
060	29.01	00.53	(No. 2) 35° 45.5' N	028° 20.4' E	14	6	7	
061	29.01	05.43	(No. 2) 35° 29.7' N	027° 59.7' E	16	8	8	
062	29.01	16.20	(No. 2) 35° 21.1' N	027° 17.0' E	19	12	12	9
063	30.01	01.53	(No. 2) 35° 00.0' N	028° 24.1' E	10	13	15	11
064	30.01	05.52	(No. 1) 34° 59.8' N	028° 35.2' E	7	7	7	
065	30.01	17.02	(No. 2) 35° 40.0' N	030° 20.0' E	12	6	6	
066	30.01	22.18	(No. 2) 36° 06.1' N	030° 59.9' E	14	14	14	14
067	31.01	03.54	(No. 2) 35° 36.0' N	031° 30.1' E	14			
068	31.01	09.48	(No. 2) 35° 00.0' N	032° 00.0' E	15	14	14	11
069	31.01	15.51	(No. 2) 34° 24.0' N	031° 24.0' E	15			
070	31.01	23.54	(No. 2) 33° 11.8' N	031° 00.0' E	13	14	14	12
071	01.02	08.43	(No. 2) 34° 23.1' N	030° 24.6' E	21			
072	01.02	19.45	(No. 2) 35° 00.0' N	030° 53.7' E	21	14	14	14
073	02.02	05.21	(No. 2) 34° 25.1' N	032° 11.7' E	16			
074	02.02	16.46	(No. 2) 33° 50.0' N	033° 30.1' E	19	15	15	14
075	03.02	00.18	(No. 2) 33° 42.1' N	032° 12.2' E	18	13	13	12
076	03.02	06.48	(No. 2) 33° 00.4' N	032° 42.2' E	18			
077	03.02	12.08	(No. 2) 32° 18.1' N	032° 54.0' E	7	9	11	10

7.1.3 List of XBT Drops

Latitude	Longitude	Max. Depth	Date	Hour:Minute	XBT No.
37.3000	11.7167	122.80	10.01	21:21	2
37.2167	11.8000	166.80	10.01	21:56	3
37.1000	11.9167	136.20	10.01	22:28	4
37.0000	12.0167	117.00	10.01	23:11	5
36.9000	12.1167	760.00	10.01	23:53	6
36.8000	12.2167	760.00	11.01	0:30	7
36.7000	12.3333	760.00	11.01	1:08	8
36.6000	12.4167	760.00	11.01	1:43	9
36.4167	12.6833	760.00	11.01	4:13	10
36.3500	12.8167	760.00	11.01	4:50	11
36.2667	12.9500	760.00	11.01	5:27	12
36.2000	13.0833	682.70	11.01	6:07	13
36.0167	13.3833	631.00	11.01	7:34	15
35.9500	13.5167	683.30	11.01	8:16	16
35.8667	13.6500	664.70	11.01	8:53	17
35.7833	13.7833	538.00	11.01	9:33	18
35.6167	14.0500	527.00	11.01	10:52	20
35.5500	14.1833	369.90	11.01	11:32	21
35.5000	14.4833	387.20	11.01	14:25	23
35.5333	14.6500	277.40	11.01	15:00	24
35.5667	14.8000	141.80	11.01	15:40	25
35.6000	14.9667	121.50	11.01	16:20	26
35.6333	15.1333	122.80	11.01	17:02	27
35.6667	15.3000	219.40	11.01	17:41	28
35.7000	15.4500	360.00	11.01	18:19	29
35.7333	15.6167	508.80	11.01	19:03	30
35.7667	15.8000	760.00	11.01	19:45	31
35.8000	16.1000	760.00	12.01	12:09	32
35.8000	16.2667	760.00	12.01	12:47	33
35.8000	16.4167	760.00	12.01	13:22	34
35.8000	16.7667	760.00	12.01	17:46	35
35.8000	16.9500	760.00	12.01	18:33	36
35.8000	17.1167	760.00	12.01	19:15	37
35.8333	17.6167	760.00	13.01	1:15	39
35.9000	17.7667	760.00	13.01	1:57	40
36.1000	18.1500	760.00	13.01	3:49	43
36.3000	18.3000	760.00	13.01	8:34	44
36.4333	18.3000	760.00	13.01	9:28	45
36.5833	18.3000	760.00	13.01	16:36	46
36.7167	18.3000	760.00	13.01	17:55	47
36.8500	18.3000	760.00	13.01	20:37	48

37.0000	18.3000	760.00	14.01	0:40	49
37.1333	18.3000	760.00	14.01	4:08	50
37.7000	18.1833	194.70	14.01	19:13	51
37.9667	18.1333	760.00	14.01	22:34	53
38.2500	18.1000	760.00	15.01	2:06	55
38.4000	18.0833	760.00	15.01	4:22	56
38.5167	18.0667	760.00	15.01	6:26	57
38.6667	18.0667	760.00	15.01	8:39	58
38.8333	17.8833	533.20	15.01	14:13	59
38.8667	17.7000	760.00	15.01	15:21	60
39.1000	17.7333	760.00	15.01	20:13	62
39.2167	17.8500	760.00	15.01	21:16	63
39.3167	17.9833	760.00	15.01	22:05	64
39.4167	18.0833	760.00	15.01	22:50	65
39.5167	18.2000	760.00	15.01	23:34	66
39.6333	18.3167	271.10	16.01	0:26	67
39.7333	18.4500	131.70	16.01	1:10	68
39.8833	18.5333	113.20	16.01	2:09	69
40.0167	18.6167	90.10	16.01	2:55	70
40.2833	18.7500	699.50	16.01	4:29	72
40.5500	18.7500	749.70	16.01	7:22	73
40.6833	18.6833	760.00	16.01	8:09	74
40.8167	18.6167	760.00	16.01	8:55	75
40.9500	18.5500	760.00	16.01	9:45	76
41.1000	18.5000	760.00	16.01	10:36	77
41.2167	18.4333	760.00	16.01	11:20	78
41.3667	18.3667	760.00	16.01	12:07	79
41.5000	18.3000	760.00	16.01	18:56	80
41.4667	18.1333	760.00	16.01	22:17	81
41.4333	17.9833	760.00	16.01	23:06	82
41.4000	17.7833	760.00	17.01	1:31	83
41.3333	17.6333	760.00	17.01	2:32	84
41.2667	17.4500	760.00	17.01	3:30	85
41.2000	17.3000	156.60	17.01	5:58	87
40.0833	18.8000	653.90	18.01	1:31	88
40.0000	18.9167	760.00	18.01	2:09	89
39.9167	19.0167	760.00	18.01	2:39	90
39.8500	19.1333	760.00	18.01	3:14	91
39.8333	19.0667	760.00	18.01	3:33	92
39.8333	19.0167	760.00	18.01	3:45	93
39.8333	18.9500	760.00	18.01	3:59	94
39.8333	18.8833	752.50	18.01	4:13	95
39.8333	18.8333	657.50	18.01	4:24	96
39.8333	18.7833	457.20	18.01	4:38	97

39.8333	18.7167	221.90	18.01	4:52	98
39.8333	18.6667	121.50	18.01	5:04	99
39.7000	18.6667	559.50	18.01	5:46	100
39.5667	18.6833	731.20	18.01	6:26	101
39.4000	18.7167	760.00	18.01	7:15	102
39.3000	18.7167	760.00	18.01	7:41	103
39.1500	18.7500	760.00	18.01	8:25	104
39.0167	18.7667	760.00	18.01	9:02	105
38.8833	18.7833	760.00	18.01	9:40	106
38.6333	18.8500	760.00	18.01	13:55	107
38.5333	18.9000	760.00	18.01	14:30	108
38.4167	18.9667	760.00	18.01	15:23	109
38.2833	19.0167	760.00	18.01	15:59	110
38.1667	19.0833	760.00	18.01	19:03	111
38.2833	19.1500	760.00	18.01	19:45	112
38.4000	19.2000	760.00	18.01	20:23	113
38.5167	19.2833	760.00	18.01	21:00	114
38.6333	19.3333	760.00	18.01	21:40	115
38.7500	19.7833	760.00	19.01	1:31	117
38.7500	19.9667	760.00	19.01	2:16	118
38.6333	20.1333	760.00	19.01	5:53	119
38.5000	20.1167	760.00	19.01	6:28	120
38.3667	20.1000	760.00	19.01	7:13	122
38.2500	20.0667	760.00	19.01	7:43	123
38.1333	20.0667	760.00	19.01	8:18	124
38.0000	20.0667	760.00	19.01	8:58	125
37.9167	20.1667	760.00	19.01	9:33	126
37.8167	20.2833	760.00	19.01	10:15	127
37.7167	20.4000	760.00	19.01	10:52	128
37.6167	20.5000	760.00	19.01	11:32	129
37.5167	20.6167	760.00	19.01	12:12	130
37.3333	20.6500	760.00	19.01	16:31	132
37.2333	20.5333	760.00	19.01	17:16	133
37.1333	20.4000	760.00	19.01	18:05	134
37.0333	20.2833	760.00	19.01	21:45	135
36.9333	20.1833	760.00	19.01	22:43	136
36.8333	20.0667	760.00	19.01	23:39	137
36.7333	19.9333	760.00	20.01	0:40	138
36.6167	19.8167	760.00	20.01	1:36	139
36.5167	19.7000	760.00	20.01	2:34	140
36.3167	19.5833	760.00	20.01	6:16	141
36.1667	19.6000	760.00	20.01	6:59	142
36.0500	19.6167	760.00	20.01	7:36	143
35.9333	19.6167	760.00	20.01	8:18	145

35.8000	19.6333	760.00	20.01	8:48	146
35.5500	19.6500	760.00	20.01	13:03	148
35.4000	19.6667	760.00	20.01	13:48	149
35.2500	19.6500	760.00	20.01	14:32	150
35.1000	19.6667	760.00	20.01	15:09	151
34.9667	19.6833	760.00	20.01	15:54	152
34.8167	19.7000	760.00	20.01	16:36	153
34.5667	19.7833	760.00	20.01	20:41	154
34.4333	19.8500	760.00	20.01	21:23	155
34.3000	19.9333	760.00	20.01	22:05	156
34.1833	20.0333	760.00	20.01	22:48	157
34.0667	20.1167	760.00	20.01	23:27	158
33.9333	20.2000	760.00	21.01	0:12	159
33.8000	20.2833	760.00	21.01	3:33	160
33.8167	20.3833	760.00	21.01	4:03	161
33.8333	20.4833	760.00	21.01	4:29	162
33.8500	20.6000	760.00	21.01	4:57	163
33.8667	20.7000	760.00	21.01	5:23	164
33.8833	20.8167	760.00	21.01	5:53	165
33.9000	20.9333	760.00	21.01	6:16	166
33.9167	21.0333	760.00	21.01	6:45	167
33.9167	21.1333	760.00	21.01	7:10	168
33.9333	21.2333	760.00	21.01	7:36	169
33.9500	21.3333	760.00	21.01	7:99	170
33.9667	21.4500	760.00	21.01	8:30	171
33.9833	21.5500	760.00	21.01	8:55	172
34.0000	21.6833	760.00	21.01	9:26	173
34.0167	21.7833	760.00	21.01	9:52	174
34.0500	21.9833	760.00	21.01	10:45	176
34.0667	22.1167	760.00	21.01	13:43	177
34.1333	22.1833	760.00	21.01	14:16	178
34.2167	22.2667	760.00	21.01	14:51	180
34.2833	22.3333	760.00	21.01	15:16	181
34.3667	22.4000	288.70	21.01	15:47	182
34.4333	22.4833	760.00	21.01	16:17	183
34.5167	22.5167	760.00	21.01	19:22	184
34.5833	22.6000	760.00	21.01	19:55	185
34.6500	22.6833	760.00	21.01	20:23	186
34.7333	22.7667	760.00	21.01	20:55	188
34.8000	22.8333	760.00	21.01	21:23	189
34.8833	22.9000	760.00	21.01	21:49	190
34.9667	22.9833	760.00	21.01	1:34	191
35.0333	23.0500	760.00	22.01	2:02	192
35.1000	23.1167	760.00	22.01	2:27	193

35.1833	23.1667	760.00	22.01	2:53	194
35.2667	23.2500	760.00	22.01	3:21	195
35.3333	23.3167	760.00	22.01	6:30	196
35.3833	23.3667	760.00	22.01	6:61	197
35.4500	23.4333	760.00	22.01	7:27	198
35.5000	23.3833	760.00	22.01	8:30	199
35.5500	23.3500	475.00	22.01	9:61	200
35.5667	23.3000	390.40	22.01	10:13	201
35.6000	23.2833	395.40	22.01	10:24	202
35.6500	23.2333	760.00	22.01	10:38	203
35.6667	23.2000	760.00	22.01	10:52	204
35.7167	23.1667	718.70	22.01	11:02	205
35.7333	23.1500	444.90	22.01	11:13	206
35.7833	23.1167	622.50	22.01	11:25	207
35.8167	23.0667	660.50	22.01	11:39	208
35.8667	23.0167	760.00	22.01	13:05	209
35.9500	22.9500	467.10	22.01	13:34	210
35.9833	22.9167	529.00	22.01	13:45	211
36.0167	22.8667	506.30	22.01	13:99	212
36.0833	22.8000	394.20	22.01	14:25	213
36.1667	22.7333	505.70	22.01	14:53	214
36.2667	22.7500	760.00	22.01	15:19	215
36.3500	22.7667	760.00	22.01	15:40	216
36.4333	22.7833	760.00	22.01	17:32	217
36.5333	22.8000	760.00	22.01	18:07	218
36.1833	22.7333	498.40	22.01	19:55	219
36.1333	22.6667	760.00	22.01	20:18	220
36.1000	22.5833	760.00	22.01	20:41	221
35.9500	22.5000	760.00	23.01	0:23	222
35.8500	22.5000	760.00	23.01	0:49	223
35.7333	22.5000	760.00	23.01	1:24	224
35.6667	22.6000	760.00	23.01	5:53	225
35.6667	22.7167	503.30	23.01	6:19	226
35.6833	22.8167	760.00	23.01	6:45	227
35.7000	22.9000	760.00	23.01	7:05	228
35.7000	23.0167	760.00	23.01	7:34	229
35.7000	23.1167	760.00	23.01	7:59	230
35.7333	23.2333	564.30	23.01	8:27	231
35.7333	23.3000	397.90	23.01	8:46	233
35.7333	23.3667	274.90	23.01	9:00	234
35.7667	23.5333	388.60	23.01	11:02	235
35.7833	23.6000	760.00	23.01	11:18	236
35.8333	23.8833	723.40	23.01	12:28	240
35.8667	24.0000	760.00	23.01	12:54	241

35.8833	24.2333	760.00	23.01	14:55	242
35.8833	24.3333	760.00	23.01	15:21	243
35.8833	24.4500	760.00	23.01	15:47	244
35.8833	24.5500	760.00	23.01	16:10	245
35.8833	24.6500	760.00	23.01	16:34	246
35.8833	24.7667	760.00	23.01	17:02	248
35.8833	24.8500	760.00	23.01	17:23	249
35.8833	24.9667	760.00	23.01	17:51	250
35.8833	25.0667	760.00	23.01	18:14	251
35.8667	25.2833	760.00	23.01	21:26	252
35.8167	25.5167	760.00	23.01	22:20	254
35.8000	25.6333	760.00	23.01	22:38	255
35.7833	25.7500	760.00	23.01	23:04	256
35.7667	25.8500	760.00	23.01	23:30	257
35.7500	25.9667	760.00	23.01	23:55	258
35.7333	26.0833	760.00	24.01	0:21	259
35.6833	26.3000	760.00	24.01	3:52	260
35.6667	26.4333	760.00	24.01	4:20	261
35.6500	26.5667	760.00	24.01	4:52	263
35.6333	26.6500	760.00	24.01	5:11	264
35.5333	26.7500	760.00	24.01	11:09	265
35.4667	26.6833	760.00	24.01	11:32	266
35.4000	26.7000	646.00	24.01	11:58	267
35.3000	26.7000	560.00	24.01	12:40	268
35.2667	26.6500	760.00	24.01	15:00	269
35.2500	26.6167	554.00	24.01	15:14	270
35.2333	26.5833	260.40	24.01	15:28	271
35.2000	26.5333	414.00	24.01	15:42	272
35.1667	26.4833	760.00	24.01	15:56	273
35.1333	26.4500	201.00	24.01	16:10	274
35.0333	26.4167	457.80	24.01	16:50	275
34.9000	26.3667	392.20	24.01	17:34	276
34.7000	26.2333	760.00	24.01	21:07	277
34.6000	26.1000	760.00	24.01	21:56	278
34.4167	25.9833	760.00	25.01	2:09	279
34.3000	25.9500	760.00	25.01	2:46	280
34.2167	25.9167	760.00	25.01	3:16	281
34.1000	25.8833	760.00	25.01	3:54	282
33.9000	25.8167	760.00	25.01	7:50	283
33.8000	25.8000	760.00	25.01	8:25	284
33.6500	25.7667	760.00	25.01	9:07	286
33.5833	25.7500	760.00	25.01	9:30	287
33.3833	25.6833	760.00	25.01	13:31	288
33.2667	25.6500	760.00	25.01	14:04	289

33.1500	25.6167	760.00	25.01	14:32	290
33.0667	25.6000	760.00	25.01	14:60	291
32.8833	25.5500	760.00	25.01	18:07	292
32.7833	25.5167	760.00	25.01	18:35	293
32.6833	25.4833	760.00	25.01	19:03	294
32.5833	25.4500	760.00	25.01	19:31	295
32.5667	25.5500	760.00	25.01	23:55	297
32.6333	25.6667	760.00	26.01	0:28	298
32.7333	25.7833	760.00	26.01	1:08	299
32.8167	25.9000	760.00	26.01	1:48	300
32.9000	26.0167	760.00	26.01	2:23	301
33.0833	26.2667	760.00	26.01	3:40	303
33.1667	26.3833	760.00	26.01	4:17	304
33.2500	26.5000	760.00	26.01	4:57	305
33.3333	26.6333	760.00	26.01	5:37	307
33.4167	26.7500	760.00	26.01	6:16	308
33.5000	26.8667	760.00	26.01	6:61	310
33.6833	26.9667	760.00	26.01	11:02	311
33.7667	26.9667	760.00	26.01	11:30	312
33.8500	26.9667	760.00	26.01	11:60	313
33.9500	26.9667	760.00	26.01	12:33	314
34.0500	26.9667	760.00	26.01	13:08	315
34.1333	26.9667	760.00	26.01	13:36	316
34.2333	26.9667	760.00	26.01	14:06	317
34.4000	26.9500	760.00	26.01	15:12	320
34.5000	26.9500	760.00	26.01	15:40	321
34.5833	26.9500	760.00	26.01	16:05	322
34.6833	26.9500	760.00	26.01	16:34	323
34.7667	26.9333	760.00	26.01	16:59	324
34.8667	26.9333	760.00	26.01	17:25	325
34.9500	26.9333	760.00	26.01	17:53	326
34.9833	26.9833	760.00	26.01	21:16	327
34.9167	27.0500	760.00	26.01	21:42	328
34.8500	27.1167	760.00	26.01	22:08	329
34.7833	27.2000	760.00	26.01	22:34	330
34.7167	27.2667	760.00	26.01	22:59	331
34.6500	27.3333	760.00	26.01	23:20	332
34.5833	27.4000	760.00	26.01	23:44	333
34.4667	27.5167	760.00	27.01	3:05	334
34.4000	27.6000	760.00	27.01	3:30	335
34.3333	27.6667	760.00	27.01	3:54	336
34.2667	27.7333	760.00	27.01	4:17	337
34.2000	27.8000	760.00	27.01	4:45	338
34.1333	27.8667	760.00	27.01	5:09	339

34.0667	27.9333	760.00	27.01	5:37	340
33.9333	28.0500	760.00	27.01	9:28	341
33.8500	28.0833	760.00	27.01	9:54	342
33.7667	28.1167	760.00	27.01	10:20	343
33.6667	28.1667	760.00	27.01	10:45	344
33.6167	28.2000	760.00	27.01	11:06	345
33.5333	28.2333	760.00	27.01	11:30	346
33.4500	28.2833	760.00	27.01	11:58	347
33.3500	28.3167	760.00	27.01	12:21	348
33.3000	28.3500	760.00	27.01	12:40	349
33.2667	28.4333	760.00	27.01	16:15	350
33.3500	28.4833	760.00	27.01	16:41	351
33.4167	28.5333	760.00	27.01	17:04	352
33.5000	28.5833	760.00	27.01	17:34	353
33.5833	28.6167	760.00	27.01	17:59	354
33.7500	28.7167	760.00	27.01	18:54	356
33.8333	28.7667	760.00	27.01	19:27	357
33.9000	28.8000	760.00	27.01	19:45	358
34.0000	28.8667	760.00	27.01	20:13	359
34.0667	28.9000	760.00	27.01	20:37	360
34.1500	28.9500	760.00	27.01	21:02	361
34.2167	29.0000	760.00	27.01	21:28	362
34.3000	29.0333	760.00	27.01	21:54	363
34.4667	29.1833	760.00	28.01	1:41	364
34.5333	29.2500	760.00	28.01	2:04	365
34.5833	29.3167	760.00	28.01	2:30	366
34.6667	29.4167	760.00	28.01	3:05	367
34.7333	29.4833	760.00	28.01	3:28	368
34.7833	29.5500	760.00	28.01	3:54	369
34.8667	29.6333	760.00	28.01	4:22	370
34.9167	29.7167	760.00	28.01	4:50	371
35.0667	29.7500	760.00	28.01	8:20	372
35.1500	29.6833	760.00	28.01	8:48	373
35.2167	29.6167	760.00	28.01	9:21	374
35.2833	29.5833	760.00	28.01	9:47	375
35.3500	29.5167	760.00	28.01	10:15	376
35.4333	29.4500	760.00	28.01	10:48	377
35.5000	29.4000	760.00	28.01	11:18	378
35.6500	29.2333	760.00	28.01	15:21	379
35.7167	29.1500	760.00	28.01	15:52	380
35.7667	29.0667	760.00	28.01	16:27	381
35.8333	28.9833	760.00	28.01	16:57	382
35.8833	28.9000	760.00	28.01	17:32	383
35.9500	28.8000	760.00	28.01	18:02	384

35.9667	28.6167	760.00	28.01	22:38	385
35.9000	28.5167	760.00	28.01	23:11	386
35.8333	28.4500	760.00	28.01	23:41	387
35.7000	28.2667	760.00	29.01	3:42	388
35.6333	28.1833	760.00	29.01	4:10	389
35.5667	28.1000	760.00	29.01	4:38	390
35.5500	27.9167	760.00	29.01	7:48	391
35.6167	27.8333	760.00	29.01	8:18	392
35.7000	27.7667	760.00	29.01	8:46	393
35.7667	27.7000	164.80	29.01	9:14	394
35.7167	27.6167	760.00	29.01	13:22	395
35.6333	27.5667	760.00	29.01	13:43	396
35.5667	27.5000	315.00	29.01	14:09	397
35.5667	27.4833	760.00	29.01	14:11	398
35.5000	27.4333	760.00	29.01	14:32	399
35.4333	27.3833	760.00	29.01	14:53	400
35.3000	27.2333	760.00	29.01	17:39	401
35.2333	27.1667	760.00	29.01	18:05	402
35.1000	27.0000	760.00	29.01	18:54	405
35.0500	26.9333	760.00	29.01	19:22	406
35.0333	27.0167	760.00	29.01	19:50	407
35.0333	27.1500	760.00	29.01	20:18	408
35.0167	27.2500	760.00	29.01	20:44	409
35.0333	27.3667	742.50	29.01	21:07	410
35.0333	27.4833	760.00	29.01	21:33	411
35.0167	27.6167	760.00	29.01	22:03	412
35.0167	27.7167	760.00	29.01	22:29	413
35.0167	27.8333	760.00	29.01	22:57	414
35.0167	27.9500	760.00	29.01	23:25	415
35.0167	28.0500	760.00	29.01	23:48	416
35.0000	28.1667	760.00	30.01	0:14	417
35.0000	28.2833	760.00	30.01	0:45	418
35.0000	28.5000	760.00	30.01	4:22	419
35.0000	28.5667	760.00	30.01	4:36	420
35.0000	28.5833	760.00	30.01	5:48	422
35.0000	28.6667	760.00	30.01	4:59	421
35.0000	28.7000	760.00	30.01	8:30	423
35.0000	28.8333	760.00	30.01	8:55	424
35.0000	28.9167	760.00	30.01	9:16	425
35.0000	29.0167	760.00	30.01	9:42	426
35.0000	29.1333	760.00	30.01	10:05	427
35.0000	29.2500	760.00	30.01	10:31	428
35.0000	29.3667	760.00	30.01	10:57	429
35.0000	29.4833	760.00	30.01	11:30	430

35.0000	29.5667	760.00	30.01	11:46	431
35.0000	29.6833	760.00	30.01	12:14	432
35.0000	29.7833	760.00	30.01	12:38	433
35.0667	29.8500	760.00	30.01	13:03	434
35.1500	29.9167	760.00	30.01	13:29	435
35.2167	29.9667	760.00	30.01	13:55	436
35.2833	30.0333	760.00	30.01	14:18	437
35.3667	30.1000	760.00	30.01	14:46	438
35.4500	30.1500	760.00	30.01	15:12	439
35.5000	30.2000	760.00	30.01	15:33	440
35.5833	30.2667	760.00	30.01	16:01	441
35.7167	30.4167	760.00	30.01	18:49	442
35.7667	30.4833	760.00	30.01	19:10	443
35.8167	30.5667	760.00	30.01	19:41	444
35.8667	30.6500	760.00	30.01	20:02	445
35.9333	30.7333	760.00	30.01	20:27	446
35.9833	30.8167	760.00	30.01	20:53	447
36.0333	30.9000	760.00	30.01	21:19	448
36.0333	31.0667	760.00	31.01	0:38	449
35.9667	31.1333	760.00	31.01	1:03	450
35.9000	31.2167	760.00	31.01	1:29	451
35.8167	31.2667	760.00	31.01	1:57	452
35.7500	31.3500	760.00	31.01	2:25	453
35.6833	31.4167	760.00	31.01	2:51	454
35.5333	31.5667	760.00	31.01	6:12	455
35.4500	31.6167	760.00	31.01	6:38	456
35.3833	31.6833	760.00	31.01	7:03	457
35.3000	31.7500	760.00	31.01	7:27	458
35.2167	31.8167	760.00	31.01	7:57	459
35.1667	31.8667	760.00	31.01	8:18	460
35.0833	31.9333	760.00	31.01	8:44	461
34.9167	31.9167	760.00	31.01	12:02	462
34.8333	31.8333	760.00	31.01	12:33	463
34.7500	31.7500	760.00	31.01	13:05	464
34.6667	31.6500	760.00	31.01	13:38	465
34.5833	31.5833	760.00	31.01	14:06	466
34.4833	31.4833	760.00	31.01	14:41	467
34.3000	31.3667	760.00	31.01	18:00	468
34.1833	31.3333	760.00	31.01	18:33	469
34.0833	31.3000	760.00	31.01	19:03	470
33.9667	31.2500	760.00	31.01	19:36	471
33.8667	31.2167	760.00	31.01	20:06	472
33.7500	31.1667	760.00	31.01	20:44	473
33.6333	31.1333	760.00	31.01	21:12	474

33.5333	31.1000	760.00	31.01	21:42	475
33.4167	31.0667	756.80	31.01	22:15	476
33.3000	31.0333	760.00	31.01	22:48	477
33.2833	30.9500	760.00	01.02	2:06	478
33.3833	30.9000	760.00	01.02	2:41	479
33.5000	30.8500	760.00	01.02	3:14	480
33.5833	30.8000	760.00	01.02	3:45	481
33.6833	30.7500	760.00	01.02	4:15	482
33.8000	30.7000	760.00	01.02	4:48	483
33.9000	30.6500	760.00	01.02	5:20	484
34.0000	30.6000	760.00	01.02	5:51	485
34.1000	30.5500	760.00	01.02	6:23	486
34.2000	30.5000	760.00	01.02	6:56	487
34.2833	30.4500	760.00	01.02	7:34	488
34.4667	30.3167	760.00	01.02	11:23	489
34.5500	30.2333	760.00	01.02	11:55	490
34.6667	30.1333	760.00	01.02	12:35	491
34.7333	30.0667	760.00	01.02	13:03	492
34.8333	29.9500	760.00	01.02	13:38	493
34.9167	29.8833	760.00	01.02	14:09	494
35.0000	29.8000	760.00	01.02	14:39	495
35.0000	29.9333	760.00	01.02	15:12	496
35.0000	30.0667	760.00	01.02	15:45	497
35.0000	30.2167	760.00	01.02	16:17	498
35.0000	30.3500	760.00	01.02	16:50	499
35.0000	30.4833	760.00	01.02	17:23	500
35.0000	30.6167	760.00	01.02	17:53	501
35.0000	30.7500	760.00	01.02	18:26	502
35.0000	31.0500	760.00	01.02	22:17	503
35.0000	31.1833	760.00	01.02	22:50	504
35.0000	31.3167	760.00	01.02	23:16	505
35.0000	31.4500	760.00	01.02	23:46	506
35.0000	31.5667	760.00	02.02	0:14	507
35.0000	31.7167	760.00	02.02	0:47	508
35.0000	31.8500	760.00	02.02	1:17	509
35.0000	32.0000	760.00	02.02	1:55	510
34.9000	32.0333	760.00	02.02	2:25	511
34.7833	32.0667	760.00	02.02	2:59	512
34.6667	32.1167	760.00	02.02	3:33	513
34.5333	32.1500	760.00	02.02	4:10	514
34.3500	32.3500	760.00	02.02	11:02	515
34.2833	32.4833	760.00	02.02	11:41	516
34.2167	32.6333	760.00	02.02	12:21	517
34.1500	32.7833	760.00	02.02	12:59	518

34.1000	32.9167	760.00	02.02	13:36	519
34.0333	33.0667	760.00	02.02	14:13	520
33.9667	33.2000	760.00	02.02	14:53	521
33.9000	33.3500	760.00	02.02	15:30	522
33.8167	33.3333	760.00	02.02	19:10	523
33.8000	33.1833	760.00	02.02	19:43	524
33.7833	33.0167	760.00	02.02	20:25	525
33.7667	32.8667	760.00	02.02	21:05	526
33.7500	32.7000	760.00	02.02	21:42	527
33.7333	32.5333	760.00	02.02	22:24	528
33.7167	32.3667	760.00	02.02	23:02	529
33.6000	32.2667	760.00	03.02	2:48	530
33.4667	32.3667	760.00	03.02	3:30	531
33.3500	32.4500	760.00	03.02	4:08	532
33.2333	32.5333	760.00	03.02	4:45	533
33.1167	32.6167	760.00	03.02	5:25	534
33.0167	32.7167	760.00	03.02	7:55	535
32.8833	32.7333	760.00	03.02	8:39	536
32.7167	32.7833	760.00	03.02	9:28	537
32.5833	32.8167	760.00	03.02	10:03	538
32.4333	32.8500	760.00	03.02	10:48	539

7.2 Lists of Leg M31/2

7.2.1 Station List of Leg M31/2

Abbreviations:

CTD	Rosette water sample equipped with conductivity-temperature-depth-oxygen sensor and 12 Niskin bottles (10 l)
CTD/ADM	Single CTD for high temperature measurements
WB	Niskin water bottles (5 l)
PC	Piston core
KL	Kasten corer
MC	Multicorer
GC	Gravity corer
GKG	Giant boxcorer
DR	Dredge
DR B	Benthos-dredge
MSN	Opening-closing net
OFOS	Ocean Floor Observation System
GTV	TV-Grab
HS/PN	Hydrosweep-/Parasound profiles

STATION	SPEC. NO	DATE (1995)	TIME (UTC +2h)	LATITUDE N	LONGITUE E	WATER DEPTH (m)	CORE RECOVERY
M31/2 - 78 HS/PN Start		9.02.	22:33	27 40,0	034 30,0		
End		10.02	02:30	27 41,2	034 36,1		
M31/2 - 78 CTD/RO 1		10.02	02:43	27 41,2	034 35,9	1044	
M31/2 - 78 MSN 2		10.02	04:25	27 41,2	034 35,9	1013	
M31/2 - 78 MSN 3		10.02	05:28	27 41,2	034 35,6	1016	
M31/2 - 78 MC 4		10.02	06:40	27 41,2	034 35,8	1018	
M31/2 - 78 PC 5		10.02	08:35	27 41,2	034 35,9	1018	
M31/2 - 78 PC 6		10.02	12:04	27 41,2	034 35,9	1018	
M31/2 - 79 HS/PN Start		10.02	17:52	26 47,2	034 30,0		
End		10.02	19:08	26 43,8	034 30,6		
M31/2 - 80 HS/PN Start		10.02	00:18	16 13,4	035 22,0		
End		11.02	01:54	26 17,1	035 20,9		
M31/2 - 80 CTD 1		11.02	02:25	26 17,5	035 21,0	1154	
M31/2 - 80 MNS 2		11.02	03:25	26,17,9	035 21,2		
M31/2 - 80 MSN 3		11.02	04:35	26,18,2	035 21,9	1137	
M31/2 - 80 PC 4		11.02	07:31	26 16,7	035 20,8	1111	
M31/2 - 80 PC 5		11.02	11:39	26 16,8	035 21,1	1126	
M31/2 - 80 MC 6		11.02	14:18	26 17,5	035 21,6	1175	
M31/2 - 81 CTD/RO 1	GIK 17000-1	11.02	16:07	26 15,5	035 19,8	1273	
M31/2 - 81 GKG 2	GIK 17000-2	11.02	19:35	26 15,5	035 19,8	1327	
M31/2 - 81 KL 3		11.02	21:15	26 15,5	035 19,6	1290	

M31/2 - 81 GKG 4		11.02	22:50	26 15,5	035 19,5	1351	
M31/2 - 81 CTD/RO 5	GIK 17001-1	12.02.	00:52	26 13,7	035 22,5	1477	
M31/2 - 81 KL 6		12.02.	03:25	26 14,0	035 22,5	1552m	
M31/2 - 81 CTD/RO7	GIK 17002-1	12.02.	06:36	26 12,6	035 21,1	1475	
M31/2 - 81 KL 8		12.02.	08:30	26 12,6	035 21,1	1503	
M31/2 - 81 CTD/RO 9	GIK 17003-1	12.02.	11:56	26 15,2	035 18,7	1346	
M31/2 - 81 KL 10	GIK 17003-2	12.02	13:39	26 15.1	035 18,8	1345	
M31/2 - 81 DR 1 Start	GIK 17003A-1	12.02.	15:58	26 12,4	035 21,7	1497	
End		12.02.	18:07	26 13,4	035 21,4	1224	
M31/2 - 81 DR 2 Start	GIK 17003A-2	12.02.	19:40	26 14,0	035 21,6	1316	
End		12.02.	20:25	26 14,1	035 20,7		
M31/2 - 81 DR 2b Start	GIK 17003A-3	12.02.	21:53	26 13,9	035 21,4	1302	
End		12.02.	22:29	26 14,2	035 20,6	860	
M31/2 - 81 DR 3 Start	GIK 17003A-4	13.02.	01:32	26 13,2	035 22,4	1295	
End		13.02.	02:32	26 13,0	035 22,4	1329	
M31/2 - 81 DR 4 Start	GIK 17003A-5	13.02.	04:05	26 14,9	035 19,2	1321	
End		13.02.	04:28	26 15,5	035 18,6		
M31/2 - DR 5 Start	GIK 17003-6	13.02.	07:06	26 13,2	035 21,2	1410	
End		13.02.	07:54	26 14,2	035 20,7	841	
HS/PS Start		13.02.	09:31	26 13,3	035 25,0		
End		13.02.	18:25	26 17,4	035 21,4		
M31/2 - 82 PC 1		13.02.	18:13	26 17,4	035 21,5	1145	
M31/2 - 82 CTD/RO 2		13.02.	19:33	26 17,5	035 21,5	1145	
M31/2 - 82 MSN 3		13.02.	20:40	26 17,4	035 21,4	1175	
M31/2 - 82 MSN 4		13.02.	21:20	26 17,5	035 21,3	1186	

M31/2 - 82 PC 5		13.02.	22:46	26 17,5	035 21,4	1175	
M31/2 - 83 KL 1	GIK 17004-1	14.02.	03:00	26 13,6	035 22,5	1454	
M31/2 - 83 KL 2	GIK 17005-1	14.02.	05:07	26 15,0	035 18,8	1351	
M31/2 - 84 CTD 1		14.02.	09:39	25 44,8	034 52,0	735	
M31/2 - 84 MC 2		14.02.	10:55	25 44,9	034 52,0	736	
M31/2 - 84 HS/PN Start		14.02.	11:20	25 45,0	034 52,0		
End		14.02.	13:16	25 45,0	035 05,1		
M31/2 - 84 MC 3		14.02.	13:33	25 45,0	035 05,1	666	
M31/2 - 84 PC 4		14.02.	15:15	25 44,6	035 04,4	698	
M31/2 - 84 CTD/RO 5		14.02.	17:17	25 44,9	035 03,3	702	
M31/2 - 84 PC 6		14.02.	19:11	25 44,9	035 03,3	702	
M31/2 - 85 HS/PN Start		14.02.	20:00	25 45,1	035 03,8		
End		15.02.	00:16	25 31,3	035 36,5		
M31/2 - 86 MC		15.02.	00:36	25 31,3	035 36,5	941	
M31/2 - 87 HS/PN1 Start		15.02.	06:20	24 44,0	036 17,0		
Ende		15.02.	07:58	24 43,3	036 16,7		
M31/2 - 87 CTD/RO 2	GIK 17006-1	15.02.	08:30	24 43,3	036 16,6	1536	
M31/2 - 87 HS/PN 3 Start		15.02.	10:20	24 41,0	036 14,0		
End		15.02.	15:15	24 41,0	036 20,0		
M31/2 - 87 CTD/RO 4	GIK 17006-2	15.02.	16:38	24 43,2	036 16,5	1535	
M31/2 - 87 CTD/RO 5	GIK 17006-3	15.02.	18:48	24 43,3	036 16,5	1536	
M31/2 - 87 GKG 6	GIK 17006-4	15.02.	20:04	24 43,3	036 16,5	1534	
M31/2 - 87 KL 7	GIK17006-5	15.02.	22:08	24 43,2	036 16,5	1536	

M31/2 - 87 DR 1 Start	GIK 17006-6	15.02.	23:39	24 43,3	036 16,4	1537	
End		16.02.	00:28	24 43,7	036 15,9	1359	
M31/2 - 87 DR 2 Start	GIK 17006-7	16.02.	01:53	24 43,2	036 16,4	1536	
End		16.02.	02:39	24 43,5	036 15,9	1406	
M31/2 - 87 DR 3 Start	GIK 17006-8	16.02.	04:00	24 43,2	036 16,4	1533	
End		16.02.	04:38	24 43,1	036 16,0	1458	
M31/2 - 87 DR 4 Start	GIK 17006-8	16.02.	05:43	24 43,4	036 16,5	1536	
End		16.02.	06:37	24 44,0	036 16,3	1367	
M31/2 - 87 HS/PS Start		16.02.	08:46	24 43,0	036 16,6		
End		16.02.	12:10	24 45,5	036 18,0		
M31/2 - 87 GTV 1 Start	GIK 17006-10	16.02.	14:25	24 43,5	036 16,0	1411	
End		16.02.	15:19	24 43,4	036 16,1	1435	
M31/2 - 87 GTV 2	GIK 17006-11	16.02.	17:32	24 43,4	036 16,0	1410	
M31/2 - 87 GTV 3 Start	GIK 17006-11	16.02.	19:09	24 43,6	036 15,9	1380	
End		16.02.	20:34	24 43,3	036 16,1	1463	
M31/2 - 88 GTV Start	GIK 17007-1	16.02.	10:03	26 14,2	035 20,5	1117	
End		17.02	11:48	26 13,3	035 21,4	1280	
M31/2 - 88 DR 1 Start	GIK 17007-2	17.02	16:00	26 13,4	035 21,4	1410	
End	GIK 17007-2	17.02	17:48	26 13,6	035 21,2	1150	
M31/2 - 88 DR 2 Start	GIK 17007-3	17.02	19:32	26 13,5	035 21,2	1225	
End		17.02	19:53	26 14,0	035 21,0		
M31/2 - 88 DR 3 Start	GIK 17007-4	17.02	22:02	26 13,7	035 21,9	1504	
End		17.02	23:15	26 13,6	035 21,8	1324	
M31/2 - 88 DR 4 Start	GIK 17007-5	18.02.	00:29	26 13,9	035 20,5	1179	
End		18.02.	00:46	26 14,0	035 20,6	1019	
M31/2 - 88 DR 5 Start	GIK 17007-6	18.02.	02:24	26 13,5	035 20,3	1381	
End		18.02.	03:39	26 14,0	035 20,7	1197	
M31/2 - 88 DR 6 Start	GIK 17007-7	18.02.	05:18	26 15,1	035 18,7	1344	

End		18.02.	08:32	26 15,2	035 18,7	1295	
M31/2 - 88 PC 1	GIK 17008-1	18.02.	11:32	26 14,0	035 22,3	1441	
M31/2 - 88 DR 7 Start	GIK 17009-1	18.02.	14:30	26 13,2	035 20,1	1489	
End		18.02.	15:23	26 13,7	035 20,4	1296	
M31/2 - 88 DR 8 Start	GIK 17009-2	18.02.	17:01	26 13,4	035 20,3	1449	
End		18.02.	17:48	26 13,9	035 20,8	998	
M31/2 - 88 PC 2	GIK 17009-3	18.02.	19:41	26 13,9	035 22,7	1474	
M31/2 - 89 MC 1		20.02.	04:49	24 50,5	035 36,4	419	
M31/2 - 89 MC 2		20.02.	05:48	24 50,4	035 36,6	405	
M31/2 - 90 MC 1		20.02.	11:32	24 45,6	036 13,8	1185	
M31/2 - 90 PC 2		20.02.	15:26	24 45,6	036 13,8	1195	
M31/2 - 90 MSN 3		20.02.	16:34	24 45,6	036 13,7	1195	
M31/2 - 90 MSN 4		20.02.	17:19	24 45,6	036 13,5	1190	
M31/2 - 90 PC 5		20.02.	19:10	24 45,6	036 17,7	1196	
M31/2 - 91 CTD/RO 1	GIK 17010-1	20.02.	21:44	24 43,0	036 16,4	1539	
M31/2 - 91 KL 2	GIK 17010-2	20.02.	23:14	24 43,2	036 16,1	1474	
M31/2 - 91 DR 1 Start	GIK 17010-3	21.02.	01:11	24 42,9	036 16,4	1530	
End		21.02.	01:34	24 42,6	036 16,5	1372	
M31/2 - 91 DR 2 Start	GIK 17010-4	21.02.	02:31	24 43,0	036 16,6	1517	
End		21.02.	02:45	24 42,8	036 16,7	1400	
M31/2 - 91 DR 3 Start	GIK 17010-5	21.02.	04:13	24 43,0	036 16,6	1519	
End		21.02.	04:32	24 43,2	036 17,1	1420	
M31/2 - 91 DR 4 Start	GIK 17010-6	21.02.	05:56	24 43,1	036 16,3	1521	
End		21.02.	06:18	24 43,5	036 15,9	1383	
M31/2 - 91 DR 5 Start	GIK 17010-7	21.02.	07:28	24 42,9	036 15,9	1470	

End		21.02.	07:45	24 43,1	036 16,0	1462	
M31/2 - 91 CTD 3	GIK 17010-8	21.02.	10:44	24 42,7	036 16,2	1304	
M31/2 - 91 DR 6 Start	GIK 17010-9	21.02.	13:12	24 42,9	036 15,5	1443	
Ende		21.02.	14:35	24 44,0	036 16,6	1413	
M31/2 - 92 HS/PN Start		21.02.	22:00	23 31.5	036 34,0		
End		21.02.	00:35	23 18,7	036 42,7		
M31/2 - 92 MC 1		22.02.	01:02	23 18.7	036 42,7	1024	
M31/2 - 92 PC 2		22.02.	02:45	23 18,6	036 42,8	1025	
M31/2 - 92 CTD/RO 3		22.02.	04:26	23 18,6	036 42,9	1023	
M31/2 - 92 PC 4		22.02.	06:28	23 18,6	036 42,8	1024	
M31/2 - 92 MSN 5		22.02.	08:30	23 13.0	036 43,9	1033	
M31/2 - 92 MSN 6		22.02.	09:10	23 13,3	036 43,2	1038	
M31/2 - 93 GKG 1		22.02.	23:11	20 57,9	037 26,6	589	
M31/2 - 93 GKG 2		22.02.	23:57	to Abington Riff rw 170° 4,26sm		663	
M31/2 - 93 GKG 3		23.02.	00:53	to Abington Riff rw 164° 4,26sm		685	
M31/2 - 93 GKG 4		23.02.	02:01	to Abington Riff rw 159° 4,45sm		657	
M31/2 - 93 GKG 5		23.02.	02:50	to Abington Riff rw 153° 4,70sm		595	
M31/2 - 93 GKG 6		23.02.	03:36	to Abington Riff rw 148° 4,90sm		568	
M31/2 - 93 DR B 1		23.02.	04:57	to Abington Riff rw 167° 4,10sm		670	

M31/2 - 93 GKG 7		23.02.	06:08	to Abington Riff rw 143° 4,80sm		374	
M31/2 - 93 GKG 8		23.02.	06:45	to Abington Riff rw 141° 5,20sm		80	
M31/2 - 93 GKG 9		23.02.	07:16	to Abington Riff rw 136° 5,50sm		313	
M31/2 - 93 GKG 10		23.02.	07:46	to Abington Riff rw 133° 5,94sm		56	
M31/2 - 93 GKG 11		23.02.	08:28	to Abington Riff rw 131° 6,7sm		52	
M31/2 - 93 DR B 2 Start		23.02.	09:32	to Abington Riff rw 147° 5,06sm		540	
End		23.02.	09:52	to Abington Riff rw 143° 5,09sm		378	
M31/2 - 94 KL 1		23.02.	11:58	to Abington Riff rw 094° 1,17sm		517	
M31/2 - 94 KL 02	M31/2-94-AL	23.02.		20 53.7	037 25,7	498	
M31/2 - 95 GKG 1		23.02.	15:01	to Abington Riff rw 063° 6,96sm		42	
M31/2 - 95- GKG 2		23.02	15:18	to Abington Reef 059° 6,2 sm		40	
M31/2 - 95 GKG 3		23.02.	15:39	to Abington Riff rw 059° 6,10sm		32	
M31/2 - 95 GKG 4		23.02.	16:13	to Abington Riff rw 054° 6,50sm		78	
M31/2 - 95 GKG 5		23.02.	16:41	to Abington Riff rw 053° 6,60sm		237	

M31/2 - 95 GKG 6		23.02.	17:07	to Abington Riff rw 052° 6,50sm		418	
M31/2 - 95 GKG 7		23.02.	18:42	to Abington Riff rw 47,5° 6,40sm		575	
M31/2 - 95 GKG 8		23.02.	19:25	to Abington Riff rw 44° 6,40sm		580	
M31/2 - 95 GKG 9		23.02.	20:15	to Abington Riff rw 40° 6,50sm		569	
M31/2 - 95 GKG 10		23.02.	20:55	to Abington Riff rw 32° 6,50sm		508	
M31/2 - 95 GKG 11		23.02.	21:39	to Abington Riff rw 28° 6,50sm		497	
M31/2 - 95 GKG 12		23.02.	22:12	to Abington Riff rw 21° 6,70sm		308	
M31/2 - 95 GKG 13		23.02.	22:42	to Abington Riff rw 22° 6,65sm		311	
M31/2 - 95 GKG 14		23.02.	23:21	to Abington Riff rw 16° 6,90sm		533	
M31/2 - 96 KL	M31/2-96-AW	24.02.	02:27	20 53,8	037 28,3	513	
M31/2 - 97 DR B Start		24.02.	04:25	to Abington Riff rw 145° 5,60sm		90	
End		24.02.	04:38	to Abington Riff rw 142° 5,60sm			
M31/2 - 98 CTD/RO 1	GIK 17011-1	24.02.	09:31	21 20,5	038 04,8	2170	
M31/2 - 98 CTD/ADM 2	GIK 17011-2	24.02.	13:26	21 21,6	038 04,5	2158	
M31/2 - 98 WB 3	GIK 17011-3	24.02.	16:52	21 20,8	038 04,7	2167	
M31/2 - 98 GTV 4 Start	GIK 17012	24.02	20:08	21 19,4	038 06,4	1897	
End		24.02.	22:25	21 19,4	038 06,4	1898	

M31/2 - 98 CTD/ADM 5	GIK 17013-1	25.02.	02:03	21 25,9	038 04,4	2113	
M31/2 - 98 WB 6	GIK 17013-2	25.02.	04:44	21 25.9	038 04,4	2118	
M31/2 - 98 CTD/ADM 7	GIK 17014-1	25.02.	08:30	21 17.0	038 02,8	2106	
M31/2 - 98 WB 8	GIK 17014-2	25.02.	11:20	21 17.0	038 02,8	2116	
M31/2 - 98 KL 9	GIK 17015-1	25.02.	14:30	21 20.9	038 04,8	2163	
M31/2 - 98 KL 10	GIK 17015-2	25.02.	17:39	21 21,9	038 04,1	2138	
M31/2 - 99 KL 1	M31/2-99-S1	26.02.	04:56	19 45,1	037 24.7	771	
M31/2 - 99 Kl 2	M31/2-99 Sb	26.02.	07:12	1943,7	037 24,7	810	
M31/2 - 99 Kl 3	M31/2 - 99-S2	26.02.	10:55	19 45,8	037 24,7	810	
M31/2 - 99 KL 4	M31/2-99-S3	26.02.	12:28	19 44,3	037 29,1	757	
M31/2 - 99 KL 5	M31/2-99-S4	26.02.	15:21	19 44,6	037 29,1	762	
M31/2 - 99 GC 6	M31/2-99-S5	26.02.	17:34	19 43,9	037 27,6	694	
M31/2 - 99 GC 7	M31/2-99-S6	26.02.	18:58	19 44,6	037 27,9	744	
M31/2 - 100 GKG 1		27.02.	02:48	19 06,3	038 36,6	393	
M31/2 - 100 GKG 2		27.02.	03:47	19 05,1	038 33,8	404	
M31/2 - 100 GKG 3		27.02.	04:46	19 04,0	038 31,2	557	
M31/2 - 100 GKG 4		27.02.	05:42	19 03,1	038 28,7	380	
M31/2 - 100 GKG 5		27.02.	06:42	19 01,3	038 25,1	343	
M31/2 - 100 GKG 6		27.02.	07:43	19 00,2	038 22,1	669	
M31/2 - 100 GKG 7		27.02.	09:25	18 57,9	038 16,8	646	
M31/2 - 100 GKG 8		27.02.	10:10	18 57,5	038 15,8	90	

M31/2 - 100 GKG 9		27.02.	10:38	18 57,5	038 15,7	101	
M31/2 - 100 GKG 10		27.02.	11:23	18 56,5	038 13,9	46	
M31/2 - 100 GKG 11		27.02.	11:50	18 56,3	038 12,8	79	
M31/2 - 101 MC 1		28.02.	02:03	17 21,7	040 01,3	475	
M31/2 - 101 PC 2		28.02.	03:18	17 22,0	040 00,6	474	
M31/2 - 102 PC		28.02.	19:39	15 33,0	041 41,1	583	
M31/2 - 103 PC 1		01.03.	01:47	15 33,4	041 40,4	598	
M31/2 - 103 CTD/RO 2		01.03.	03:20	15 33,6	041 40,0	607	
M31/2 - 103 MC 3		01.03.	04:19	15 33,6	041 40,2	604	
M31/2 - 103 MSN 4		01.03.	04:48	15 33,7	041 40,2	603	
M31/2 - 104 DR 1 Start		01.03.	06:40	15 23,4	041 42,6	72	
End		01.03.	06:46	15 23,3	041 42,6		
M31/2 - 104 DR 2 Start		01.03.	07:02	15 23,1	041 42,7	74	
End		01.03.	07:06	15 23,0	041 42,7		
M31/2 - 104 DR 3 Start		01.03.	07:23	15 22,6	041 42,9	76	
End		01.03.	07:35	15 22,4	041 42,9		
M31/2 - 104 DR 4		01.03.	07:50	15 22,3	041 43,0	73	
M31/2 - 104 DR 5		01.03.	08:35	15 23,0	041 42,7	73	
M31/2 - 104 DR 6 Start		01.03.	09:39	15 23,1	041 45,4	447	
End		01.03.	10:21	15 22,9	041 44,4	227	

7.2.2 Results of Hydrocarbon Measurements during M31/2

Deep	Station	Depth dbar	Temp. °C	CH_4 nl/l	C_2H_6 nl/l
	Surface	0.0	22.00	25	0
	Surface	0.0	22.00	39	0
	Surface	0.0	22.00	28	0
Shaban	17000-1	50.3	22.45	266	25
Shaban	17000-1	150.2	22.04	74	3
Shaban	17000-1	599.7	21.50	58	2
Shaban	17000-1	1333.0	21.50	178	6
Shaban	17000-1	1336.8	21.50	726	24
Shaban	17000-1	1338.2	22.70	573	19
Shaban	17000-1	1356.0	22.70	29037	2239
Shaban	17000-1	1367.5	22.70	27730	2100
Shaban	17001-1	14.8	22.54	182	15
Shaban	17001-1	50.3	22.44	138	7
Shaban	17001-1	400.0	21.49	199	7
Shaban	17001-1	1326.9	21.48	389	11
Shaban	17001-1	1336.8	21.48	460	16
Shaban	17001-1	1338.2	22.88	19798	1365
Shaban	17001-1	1473.9	24.09	52164	3616
Shaban	17001-1	1498.3	24.63	24586	2827
Shaban	17001-1	1531.0	24.60		
Shaban	17001-1	1531.0	24.60	29566	2523
Shaban	17002-1	50.0	22.47	130	10
Shaban	17002-1	449.3	21.48	344	15
Shaban	17002-1	749.7	21.49	444	19
Shaban	17002-1	1050.2	21.46	575	24
Shaban	17002-1	1334.8	21.48	1414	45
Shaban	17002-1	1339.9	24.01	61064	4382
Shaban	17002-1	1481.6	24.09	66815	4782
Shaban	17002-1	1567.6	25.25	31995	2600
Shaban	17003-1	4.2	22.61	46	1
Shaban	17003-1	36.9	22.51		
Shaban	17003-1	199.7	21.74	57	3
Shaban	17003-1	1098.1	21.45	110	5
Shaban	17003-1	1335.8	21.47	329	11
Shaban	17003-1	1337.0	22.07	6494	444
Shaban	17003-1	1342.2	22.73	25130	1757
Shaban	17003-1	1356.7	22.00	60829	3993
Kebrit	17006-1	50.3	22.87	4812	94
Kebrit	17006-1	511.9	21.52	75559	758
Kebrit	17006-1	989.0	21.45	99435	878
Kebrit	17006-1	1200.3	21.42	136463	1103
Kebrit	17006-1	1399.8	21.45	254598	2145
Kebrit	17006-1	1478.7	21.46	21423007	447316
Kebrit	17006-1	1482.1	22.58	11265699	226404
Kebrit	17006-1	1485.0	23.33	12889457	242483
Kebrit	17006-1	1516.0	23.36	22586553	437333
Kebrit	17006-1	1570.2	23.37	20697	333

Deep	Station	Depth dbar	Temp. °C	CH_4 nl/l	C_2H_6 nl/l	
Kebrit	17006-2	0.0		88	1	
Kebrit	17006-2	24.5	23.14	203	4	
Kebrit	17006-2	49.9	22.79	112	21	
Kebrit	17006-2	299.0	21.53	1143	58	
Kebrit	17006-2	499.4	21.52	1464	27	
Kebrit	17006-2	1200.2	21.45	6097	220	
Kebrit	17006-2	1399.8	21.45	5731	104	
Kebrit	17006-2	1469.0	21.46	3253	64	
Kebrit	17006-3	24.5	23.08	8719	198	
Kebrit	17006-3	1478.1	21.46	85737	757	
Kebrit	17006-3	1478.1	21.46	864	8	
Kebrit	17006-3	1482.1	22.64	17836670	363913	
Kebrit	17006-3	1484.7	23.32			
Kebrit	17006-3	1519.7	23.36			
Kebrit	17006-3	1580.2	23.38			
Kebrit	17010-1	0.0		26	1	
Kebrit	17010-1	6.2	23.00	34	1	
Kebrit	17010-1	50.2	23.05	3151	62	
Kebrit	17010-1	50.2	23.05	182	0	
Kebrit	17010-1	175.4	21.58	188	0	
Kebrit	17010-1	300.5	21.52	1177	18	
Kebrit	17010-1	300.5	21.52	342	6	
Kebrit	17010-1	600.3	21.50	237	6	
Kebrit	17010-1	900.6	21.46	24	0	
Kebrit	17010-1	1199.9	21.43	35	2	
Kebrit	17010-1	1400.2	21.45	360	2	
Kebrit	17010-8	4.8	22.90	20	0	
Kebrit	17010-8	49.0	22.94	134	2	
Kebrit	17010-8	100.2	22.33	124	2	
Kebrit	17010-8	175.5	21.60	39	1	
Kebrit	17010-8	297.9	21.51	54	1	
Kebrit	17010-8	604.4	21.50	26	0	
Kebrit	17010-8	900.2	21.46	20	0	
Kebrit	17010-8	1200.1	21.42	30	1	
Atlantis II	17011-1	5.5	25.26	32	0	
Atlantis II	17011-1	51.7	24.19	75	1	
Atlantis II	17011-1	149.3	21.80	52	1	
Atlantis II	17011-1	300.0	21.62	53	1	
Atlantis II	17011-1	600.4	21.65	23	0	
Atlantis II	17011-1	1199.7	21.53	28	0	
Atlantis II	17011-1	1921.5	21.89	19	0	
Atlantis II	17011-1	1998.0	25.04	47	0	
Atlantis II	17011-1	2016.8	31.88	4023	3	
Atlantis II	17011-3	2015.0		107838	44	Depth: m cable
Atlantis II	17011-3	2030.0		123478	90	Depth: m cable
Atlantis II	17011-3	2040.0		84925	1645	Depth: m cable
Atlantis II	17011-3	2050.0		92044	1826	Depth: m cable
Atlantis II	17011-3	2060.0		120406	2327	Depth: m cable
Atlantis II	17011-3	2070.0		104490	1935	Depth: m cable
Atlantis II	17011-3	2080.0		112083	2062	Depth: m cable
Atlantis II	17011-3	2140.0		94215	1740	Depth:

Deep	Station	Depth dbar	Temp. °C	CH_4 nl/l	C_2H_6 nl/l	
Atlantis II	17013-2	1985.0		107	0	Depth: m cable
Atlantis II	17013-2	2005.0		210	0	Depth: m cable
Atlantis II	17013-2	2035.0		26109	12	Depth: m cable
Atlantis II	17013-2	2045.0		102599	22	Depth:
Atlantis II	17013-2	2065.0		135811	113	Depth:
Atlantis II	17013-2	2075.0		108505	2069	Depth: m cable
Atlantis II	17013-2	2100.0		106483	1972	Depth: m cable
Discovery	17014-2	2025.0		10311	6	Depth: m cable
Discovery	17014-2	2035.0		19636	91	Depth: m cable
Discovery	17014-2	2045.0		26274	144	Depth: m cable
Discovery	17014-2	2055.0		25479	140	Depth: m cable
Discovery	17014-2	2065.0		28965	158	Depth: m cable
Discovery	17014-2	2075.0		28348	156	Depth: m cable
Discovery	17014-2	2085.0		27641	160	Depth: m cable
Discovery	17014-2	2165.0		27026	162	Depth: m cable

7.2.3 M 31/2 Multi-Opening/Closing Hauls

Date	Station	Latitude	Longitude	Haul	no.	Net no.	Water depth (m)
10.02.95	78	27°41,109N	34°35,497E	MSN	887	1	100-80
10.02.95	78	27°41,109N	34°35,497E	MSN	887	2	80-60
10.02.95	78	27°41,109N	34°35,497E	MSN	887	3	60-40
10.02.95	78	27°41,109N	34°35,497E	MSN	887	4	40-20
10.02.95	78	27°41,109N	34°35,497E	MSN	887	5	20-0
10.02.95	78	27°41,166N	34°35,616E	MSN	888	1	700-500
10.02.95	78	27°41,166N	34°35,616E	MSN	888	2	500-300
10.02.95	78	27°41,166N	34°35,616E	MSN	888	3	300-200
10.02.95	78	27°41,166N	34°35,616E	MSN	888	4	200-100
10.02.95	78	27°41,166N	34°35,616E	MSN	888	5	100-0
11.02.95	80	26°17,478N	35°21,255E	MSN	889	1	100-80
11.02.95	80	26°17,478N	35°21,255E	MSN	889	2	80-60
11.02.95	80	26°17,478N	35°21,255E	MSN	889	3	60-40
11.02.95	80	26°17,478N	35°21,255E	MSN	889	4	40-20
11.02.95	80	26°17,478N	35°21,255E	MSN	889	5	20-0
11.02.95	80	26°18,121N	35°21,693E	MSN	890	1	700-500
11.02.95	80	26°18,121N	35°21,693E	MSN	890	2	500-300
11.02.95	80	26°18,121N	35°21,693E	MSN	890	3	300-200
11.02.95	80	26°18,121N	35°21,693E	MSN	890	4	200-100
11.02.95	80	26°18,121N	35°21,693E	MSN	890	5	100-0
13.02.95	82	26°17,472N	35°21,427E	MSN	891	1	100-80
13.02.95	82	26°17,472N	35°21,427E	MSN	891	2	80-60
13.02.95	82	26°17,472N	35°21,427E	MSN	891	3	60-40
13.02.95	82	26°17,472N	35°21,427E	MSN	891	4	40-20

13.02.95	82	26°17,472N	35°21,427E	MSN	891	5	20-0
13.02.95	82	26°17,582N	35°21,342E	MSN	892	1	700-500
13.02.95	82	26°17,582N	35°21,342E	MSN	892	2	500-300
13.02.95	82	26°17,582N	35°21,342E	MSN	892	3	300-200
13.02.95	82	26°17,582N	35°21,342E	MSN	892	4	200-100
13.02.95	82	26°17,582N	35°21,342E	MSN	892	5	100-0
20.02.95	90	24°45,605N	36°13,693E	MSN	893	1	100-80
20.02.95	90	24°45,605N	36°13,693E	MSN	893	2	80-60
20.02.95	90	24°45,605N	36°13,693E	MSN	893	3	60-40
20.02.95	90	24°45,605N	36°13,693E	MSN	893	4	40-20
20.02.95	90	24°45,605N	36°13,693E	MSN	893	5	20-0
20.02.95	90	24°45,423N	36°13,521E	MSN	894	1	700-500
20.02.95	90	24°45,423N	36°13,521E	MSN	894	2	500-300
20.02.95	90	24°45,423N	36°13,521E	MSN	894	3	300-200
20.02.95	90	24°45,423N	36°13,521E	MSN	894	4	200-100
20.02.95	90	24°45,423N	36°13,521E	MSN	894	5	100-0
22.02.95	92	23°13,154N	36°43,911E	MSN	895	1	100-80
22.02.95	92	23°13,154N	36°43,911E	MSN	895	2	80-60
22.02.95	92	23°13,154N	36°43,911E	MSN	895	3	60-40
22.02.95	92	23°13,154N	36°43,911E	MSN	895	4	40-20
22.02.95	92	23°13,154N	36°43,911E	MSN	895	5	20-0
22.02.95	92	23°13,328N	36°43,240E	MSN	896	1	700-500
22.02.95	92	23°13,328N	36°43,240E	MSN	896	2	500-300
22.02.95	92	23°13,328N	36°43,240E	MSN	896	3	300-200
22.02.95	92	23°13,328N	36°43,240E	MSN	896	4	200-100
22.02.95	92	23°13,328N	36°43,240E	MSN	896	5	100-0
1.3.95	102	15°33,734N	41°40,168E	MSN	897	1	100-80
1.3.95	102	15°33,734N	41°40,168E	MSN	897	2	80-60
1.3.95	102	15°33,734N	41°40,168E	MSN	897	3	60-40
1.3.95	102	15°33,734N	41°40,168E	MSN	897	4	40-20
1.3.95	102	15°33,734N	41°40,168E	MSN	897	5	20-0

7.2.4 List of collected Red Sea Samples

station number	tool	depth (m)	number of subsamples
78	MC 4	1040	1
80	MC 6	1147	1
81	DR 1	1330	1
	DR 2	~1200	1
	DR 3	~1200	1
	DR 4	~1200	1
	DR 5	~1200	1
	GKG 4	1330	1
84	MC 2	719	2
	MC 3	648	1
	PC 6	702	1
86	MC	933	2
87	GTV 1	1435	1
	GTV 2	1463	1
	DR 1	~1400	1
	DR 2	~1400	1
	DR 3	~1400	1
90	MC 1	1173	2
91	DR 1	~1400	1
92	MC	998	2
93	GKG 1	593	1
	GKG 2	652	3
	GKG 3	678	1
	GKG 4	645	3
	GKG 5	589	3
	GKG 6	567	3
	GKG 7	370	2
	GKG 8	79	2
	GKG 9	310	3
	GKG 10	58	2
95	GKG 6	441	1
	GKG 7	568	1
	GKG 8	568	1
	GKG 9	575	2
	GKG 10	563	2
	GKG 11	504	2
	GKG 12	494	2
	GKG 13	306	3

	GKG 14	533	3
98	GTV 4	1903	1
99	KL 1	771	1
	KL 3	810	1
	KL 4	757	1
Sanganeb Atoll	diving sample	4	1

(GKG = Giant boxcore, GTV = TV-Grab, MC = Multicorer, DR = Dredge, PC= Piston corer, KL = Kasten corer)

7.2.5 Volcanic Rocks recovered during METEOR 31/2

Station	Gik-Nr.	Sample No.	Description	Remarks
M31/2-81	17003A-1	DR1-1	vesicular (10%) basalts, sheet flow, dark colour. Glassy rims (10mm) Ol and plag-phyric (ca. 5 mm)	glassy rims are palagonitized (1-2mm), both types exhibit porous zones with coloured precipitations of smetitic material, biogenic carbonate hard layer (10mm) abundant serpulidae
	17003A-3	DR 1-2	one piece shows large phenocrysts of olivine, plagioclase and pyroxene of >10mm	and the rock has a distinct palagonite rind, carbonate layers etc.
	17003A-4	DR 1-3	elongated sheet flow (10 cm long) glassy rim, vesicular 10%	glassy rims are palagonitized (1-2mm), porous zones with coloured precipitations of smetitic material biogenic carbonate hard layer (10mm) abundant serpulidae
	17003A-5	DR 1-4	little pillow 7 cm moderately vesicular 10 % plag-phyric (4mm)	palagonitic rim, little carbonate with serpulidae no manganese coating
	17003A-6	DR 1	various small pieces of volcanic rocks, named "rests"	palagonitic rim, little carbonate with serpulidae

M31/2-81 17003-2	KL-10-1 core catcher	vesicular (<10%) porphyric basalt, plagioclase phenos (10mm), glassy rim (4mm)	encrusted with foraminiferal ooze
M31/2-81 17003-2	KL-10-2 core catcher	5 small (<3cm) vesicular (<10%) porphyric pieces of glassy basalt, plagioclase phenos (10mm)	encrusted with foraminiferal ooze
M31/2-88 17007-1	GTV	small pieces (<60mm) of basalt, highly veiscular plagphyric (8mm) glassy rim	palagonite rind (1mm) coated by carbonate and in part by manganese (2-4mm)
M31/2-88 17007-3	DR 2-1	highly vesicular, porphyric pillow basalt Phenocrysts of olivine (8 mm) and plagioclase (8 mm), glassy rim up to 15 mm.	hard layer of carbonate (grey-yellow) of 30 mm thickness on surface above a thin palagonitic rim (1 mm), in parts manganese coating abundant sessile organisms (serpulidae) carbonate fillings of vesicles occur, partly clear crystals in vesicles
M31/2-88 17007-3	DR 2-2	highly vesicular, porphyric pillow basalt Phenocrysts of olivine (8 mm) and plagioclase (8 mm), glassy rim up to 15 mm.	hard layer of carbonate (grey-yellow) of <10 mm thickness on surface above a thin palagonitic rim (1 mm), in parts manganese coating abundant sessile organisms (serpulidae) carbonate fillings of vesicles occur, partly clear crystals in vesicles
M31/2-88 17007-4	DR 3-1	vesicular (10%) aphyric pillow basalt diameter 10 cm	interior fracture surfaces of pillows are partly coated with thin <2mm manganese crust glassy rim nearly completely altered into reddish palagonite outer surface of pillow coated with soft foraminiferal-ooze and hard layer (10mm) of greyish-yellowish carbonatic material

M31/2-88 17007-4	DR 3-2	vesicular (10%) aphyric pillow basalt	interior fracture surfaces of pillows are partly coated with thin <2mm manganese crust glassy rim nearly completely altered into reddish palagonite outer surface of pillow coated with soft foraminiferal-ooze and hard layer (10mm) of greyish-yellowish carbonatic material
M31/2-88 17007-4	DR 3-3	vesicular (10%) aphyric pillow basalt	glassy rim nearly completely altered into reddish palagonite outer surface of pillow coated with hard layer (10mm) of greyish-yellowish carbonatic material and greyish upper coat
M31/2-88 17007-4	DR 3	single small piece similar to DR 3-3	
M31/2-88 17009-3	PCorer	Glass-breccia in core catcher	fresh glass breccia in fine grained glassy matrix
M31/2-92	92 MC 1	one small (10mm) piece of vesicular material (basalt ?) looks more like metal slag	
M31/2-102	102 PC 1	five small pieces of highly vesicular, brittle basalt glass, no phenos	

7.3 Lists of Leg M31/3

7.3.1 Station List of Leg M31/3

Abbreviations:

CTD/Ro	Rosette water sample equipped with conductivity-temperature-depth-oxygen sensor and 12 Niskin bottles (10 l)
GC	Gravity corer
KL	Piston corer / Kasten corer
MC1	Multicorer (Pfannkuche)
MC2	Multicorer (Graf)
GKG	Giant boxcorer
DR B	Benthos-dredge
MSN	Opening-closing net
HS/PN	Hydrosweep-/Parasound profiles

Station	Date 1995	Time (UTC + 3h)	Latitude N	Longitude E	Water depth (m)	Core recovery
M31/3 - 105 GKG1	04.03.	8:42	12 27,6	044 25,3	71	
M31/3 - 105 GKG2	04.03.	10:16	12 24,1	044 29,6	179	
M31/3 - 105 MC1/1	04.03.	10:47	12 24,2	044 29,6	174	
M31/3 - 105 GKG3	04.03.	11:51	12 22,8	044 31,5	321	
M31/3 - 105 GKG4	04.03.	13:06	12 21,5	044 33,0	506	
M31/3 - 105 GKG5	04.03.	14:40	12 17,1	044 38,8	761	
M31/3 - 105 MC1/2	04.03.	15:30	12 17,3	044 38,2	752	

M31/3 - 105 CTD/Ro	04.03.	16:31	12 17,1	044 37,3	729	
M31/3 - 105 MSN	04.03.	17:49	12 17,0	044 37,5	733	
M31/3 - 105 MSN	04.03.	18:34	12 17,2	044 37,5	730	
M31/3 - 106 CTD/Ro	06.03	05:38	13 29,1	050 18,0	1948	
M31/3 - 106 GC 12m	06.03	07:22	13 29,48	050 17,84	2023	1,5 m
M31/3 - 106 MSN	06.03	08:27	13 29,5	050 17,9	2025	
M31/3 - 106 MSN	06.03	09:13	13 29,5	050 17,8	2022	
M31/3 - 106 KL 24m	06.03	10:46	13 29,44	050 17,81	2022	18,9 m
M31/3 - 106 GC 12m	06.03	13:58	13 29,7	050 17,6	2016	10,5 m
M31/3 - 106 MC1	06.03	15:52	13 29,6	050 17,7	2013	
M31/3 - 106 GKG	06.03	17:26	13 29,6	050 17,7	2016	
M31/3 - 106 MSN	06.03	19:26	13 30,2	050 18,5	2053	
M31/3 - 106 CTD/Ro	06.03	21:11	13 29,8	050 18,7	2055	
M31/3 - 107 HS/PS Start	07.03.	12:00				
End	07.03.	16:11				
M31/3 - 107 GC 12m	07.03.	16:44	14 36,3	052 55,2	1803	10,5 m
M31/3 - 107 MSN	07.03.	18:01	14 36,3	052 55,1	1801	

M31/3 - 107 KL 24m	07.03.	19:26	14 36,3	052 55,15	1802	19,5 m
M31/3 - 107 CTD/Ro	07.03.	21:39	14 36,3	052 55,2	1802	
M31/3 - 107 MC1	07.03.	23:11	14 36,3	052 55,2	1801	
M31/3 - 107 MSN	08.03.	00:33	14 36,7	052 56,1	1840	
M31/3 - 107 CTD/Ro	08.03.	01:18	14 36,6	052 56,0	1842	
M31/3 - 108 HS/PS Start	08.03.	09:18				
End	08.03.	10:20				
M31/3 - 108 GC 12m	08.03.	11:08	14 58,3	054 22,2	2316	11 m
M31/3 - 108 KL 24m	08.03.	14:20	14 58,3	054 22,0	2309	20 m
M31/3 - 108 MC2	08.03.	17:05	14 58,1	054 22,2	2316	
M31/3 - 108 MC1	08.03.	18:35	14 58,2	054 22,25	2315	
M31/3 - 108 MC1	08.03.	20:08	14 58,1	054 22,2	2322	
M31/3 - 108 MC1	08.03.	21:31	14 58,2	054 22,2	2314	
M31/3 - 108 GKG	08.03.	22:55	14 58,3	054 22,2	2316	

M31/3 - 108 MSN	09.03.	00:20	14 59,3	054 23,7	2583	
M31/3 - 108 MSN	09.03.	01:13	14 59,7	054 24,7	2800	
M31/3 - 108 CTD/Ro	09.03.	02:50	15 00,0	054 26,8	2893	
M31/3 - 108 MSN	09.03.	05:24	15 00,7	054 28,3	2901	
M31/3 - 108 CTD/Ro	09.03.	07:07	15 01,3	054 29,4	2893	
M31/3 - 108 DR B Start	09.03.	10:25	14 58,2	054 22,25	2313	
End	09.03.	10:59	14 58,2	054 22,3	2313	
M31/3 - 109 MSN	10.03.	2:00	15 50,0	057 00,1	3473	
M31/3 - 109 MSN	10.03.	02:45	15 49,8	056 59,9	3470	
M31/3 - 109 CTD/Ro	10.03.	04:16	15 50,0	056 59,65	3467	
M31/3 - 109 MC1	10.03.	06:41	15 49,7	056 59,7	3521	
M31/3 - 109 CTD/Ro	10.03.	08:00	15 49,5	056 59,6	3524	
M31/3 - 109 MC2	10.03.	09:25	15 49,6	056 59,6	3520	
M31/3 - 109 GC 12m	10.03.	12:00	15 51,1	056 59,3	3225	10,5 m

M31/3 - 109 KL 24m	10.03.	15:15	15 51,1	056 59,3	3157	17,1 m
M31/3 - 109 HS/PS Start	11.03.	10:50	16 09,7	059 42,9	4031	
End	11.03.	11:20	16 10,1	059 45,9		
M31/3 - 110.1 DR B Start	11.03	16:00	16 13,2	060 16,0	4048	
End	11.03.	16:45	16 13,2	060 16,0		
M31/3 - 110.1 GKG	11.03.	19:20	16 13,2	060 16,0	4048	
M31/3 - 110.1 MC1	11.03.	22:31	16 13,2	060 16,1	4043	
M31/3 - 110.1 MC2	12.03.	01:42	16 13,1	060 16,0	4032	
M31/3 - 111.1 GC 12m	12.03.	07:18	16 10,1	059 45,65	1920	...
M31/3 - 111.1 KL 12m	12.03.	09:23	16 10,1	059 45,9	1916	9 m
M31/3 - 111.1 MSN	12.03.	10:24	16 10,1	059 45,9	1915	
M31/3 - 111.1 MSN	12.03.	11:06	16 10,1	059 46,0	1914	
M31/3 - 111.1 CTD/Ro	12.03.	12:00	16 10,1	059 46,0	1914	
M31/3 - 111.1 MC1	12.03.	13:10	16 10,2	059 46,2	1914	

M31/3 - 111.1 HS/PS Start	12.03.	15:00	16 05,7	059 41,2		
End	12.03.	19:57	16 12,9	060 15,9		
M31/3 - 110.2 DR B Start	12.03.	21:30	16 13,1	060 16,0	4054	
End	12.03.	22:15	16 13,1	060 16,0		
M31/3 - 110.2 GKG	13.03.	00:50	16 12,8	060 15,8	4031	
M31/3 - 110.2 MC2	13.03.	04:05	16 12,8	060 16,2	4031	
M31/3 - 110.2 CTD/Ro	13.03.	06:06	16 13,0	060 16,3	4049	
M31/3 - 110.2 MC1	13.03.	08:01	16 13,0	060 16,0	4046	
M31/3 - 111.2 GC 12m	13.03.	13:33	16 05,4	059 41,0	2224	7 m
M31/3 - 111.2 KL 12m	13.03.	16:06	16 05,45	059 41,1	2239	11,7 m
M31/3 - 111.2 MSN	13.03.	18:47	16 05,45	059 41,2	2237	
M31/3 - 111.2 CTD/Ro	13.03.	20:16	16 05,5	059 41,1	2238	
M31/3 - 111.2 KL 24m	13.03.	21:58	16 05,4	059 41,09	2243	...
M31/3 - 111.2 CTD/Ro	13.03.	23:54	16 05,5	059 41,2	2236	
M31/3 - 111.2 MC1	14.03.	01:42	16 05,4	059 41,0	2223	

M31/3 - 110.3 DR B Start	14.03.	07:32	16 03,0	060 16,0	4041	
End	14.03.	07:34	16 03,0	060 16,0		
M31/3 - 110.3 GKG	14.03.	10:00	16 03,0	060 16,0	4040	
M31/3 - 110.3 MC1	14.03.	12:25	16 03,0	060 16,0	4040	
M31/3 - 110.3 MC2	14.03.	15:20	16 02,8	060 16,0	4040	
M31/3 - 110.3 CTD/Ro	14.03.	18:25	16 02,9	060 16,0	4080	
M31/3 - 110.4 MSN	14.03.	21:22	16 13,0	060 16,6,11	4040	
M31/3 - 110.4 MSN	14.03.	22:01	16 13,0	060 16,1	4040	
M31/3 - 110.4 MSN	14.03.	23:56	16 13,1	060 16,9	4040	
M31/3 - 110.4 CTD/Ro	15.03.	01:51	16 13,2	060 16,8	4030	
M31/3 - 110.4 MC1	15.03.	04:00	16 12,6	060 16,0	4031	
M31/3 - 110.4 GKG	15.03.	07:09	16 13,05	060 16,0	4071	
M31/3 - 110.4 MC2	15.03.	10:12	16 13,0	060 16,0	4031	
M31/3 - 110.4 MC1	15.03.	12:47	16 12,9	060 15,6	4030	

M31/3 - 110.4 DR B Start	15.03.	15:55	16 12,9	060 15,5	4031	
End	15.03.	17:16	16 13,1	060 17,7	4050	
M31/3 - 112 DR B Start	16.03.	09:15	17 45,1	058 09,2	3165	
End	16.03.	10:30	17 44,9	058 09,0	3145	
M31/3 - 112 CTD/Ro	16.03.	14:55	17 45,1	058 09,0	3146	
M31/3 - 112 GKG	16.03.	16:30	17 44,9	058 09,0	3164	
M31/3 - 112 MC2	16.03.	18:56	17 45,0	058 09,0	3166	
M31/3 - 112 MC1	16.03.	21:09	17 45,0	058 09,0	3165	
M31/3 - 112 GKG	16.03.	23:10	17 44,9	058 09,0	3161	
M31/3 - 112 HS/PN Start	17.03.	00:17				
End	17.03.	18:42				
M31/3 - 113 GC 12m	17.03.	18:50	16 32,1	055 19,85	2636	11,6 m
M31/3 - 113 KL 24m	18.03.	01:27	16 31,9	055 19,9	2624	20,7 m
M31/3 - 113 MC1	18.03.	05:01	16 31,9	055 19,9	2624	
M31/3 - 113 MSN	18.03.	06:13	16 32,2	055 20,0	2636	

M31/3 - 113 MSN	18.03.	06:51	16 32,8	055 20,1	2692	
M31/3 - 113 CTD/Ro	18.03.	08:24	16 31,9	055 19,9	2627	
M31/3 - 114 GC 12m	19.03.	08:24	14 32,4	051 44,8	1539	8,5 m
M31/3 - 114 MC1	19.03.	09:45	14 32,4	051 44,9	1538	
M31/3 - 114 MSN	19.03.	10:32	14 32,4	051 45,6	1538	
M31/3 - 114 MSN	19.03.	11:08	14 32,6	051 46,5	1540	
M31/3 - 114 MSN	19.03.	12:30	14 32,3	051 48,1	1539	
M31/3 - 114 CTD	19.03.	14:45	14 32,8	051 46,1	1531	
M31/3 - 115 GC 12m	20.03.	10:13	13 18,5	048 47,0	1717	9,6 m
M31/3 - 115 MC1	20.03.	11:37	13 18,6	048 47,0	1731	
M31/3 - 115 MSN	20.03.	12:37	13 18,3	048 47,1	1708	
M31/3 - 115 MSN	20.03.	13:15	13 18,7	048 47,0	1708	
M31/3 - 115 CTD/Ro	20.03.	14:31	13 18,3	048 46,9	1707	

M31/3 - 115 Foto-schlitten Start	20.03.	16:21	13 18,5	048 46,9	1732	
End	20.03.	16:34	Kamera löst	nicht aus		
M31/3 - 116 GC 12m	21.03.	01:59	12 51,76	047 26,1	1646	11 m
M31/3 - 116 MC1	21.03.	03:13	12 51,7	047 26,1	1626	
M31/3 - 116 MSN	21.03.	04:16	12 52,0	047 26,6	1687	
M31/3 - 116 MSN	21.03.	04:56	12 51,9	047 26,5	1677	
M31/3 - 116 CTD/Ro	21.03.	06:01	12 52,0	047 26,5	1682	
M31/3 - 117 GC 12m	21.03.	20:51	12 17,2	044 37,4	736	8 m
M31/3 - 117 DR B Start	21.03.	21:41	12 17,5	044 37,6	734	
End	21.03.	22:15	12 17,7	044 37,6	730	

7.3.2 M31/3 Multi-Opening/Closing Hauls

Date	Station	Latitude	Longitude	Haul	no.	Net no.	Water depth (m)
4.3.95	105	12°17,336N	44°37,471E	MSN	898	1	100-80
4.3.95	105	12°17,336N	44°37,471E	MSN	898	2	80-60
4.3.95	105	12°17,336N	44°37,471E	MSN	898	3	60-40
4.3.95	105	12°17,336N	44°37,471E	MSN	898	4	40-20
4.3.95	105	12°17,336N	44°37,471E	MSN	898	5	20-0
4.3.95	105	12°17,336N	44°37,471E	MSN	899	1	700-500
4.3.95	105	12°17,336N	44°37,471E	MSN	899	2	500-400
4.3.95	105	12°17,336N	44°37,471E	MSN	899	3	400-300
4.3.95	105	12°17,336N	44°37,471E	MSN	899	4	300-200
4.3.95	105	12°17,336N	44°37,471E	MSN	899	5	200-0
6.3.95	106	13°29,467N	50°17,847E	MSN	900	1	100-80
6.3.95	106	13°29,467N	50°17,847E	MSN	900	2	80-60
6.3.95	106	13°29,467N	50°17,847E	MSN	900	3	60-40
6.3.95	106	13°29,467N	50°17,847E	MSN	900	4	40-20
6.3.95	106	13°29,467N	50°17,847E	MSN	900	5	20-0
6.3.95	106	13°29,451N	50°17,788E	MSN	901	1	700-500
6.3.95	106	13°29,451N	50°17,788E	MSN	901	2	500-300
6.3.95	106	13°29,451N	50°17,788E	MSN	901	3	300-200
6.3.95	106	13°29,451N	50°17,788E	MSN	901	4	200-100
6.3.95	106	13°29,451N	50°17,788E	MSN	901	5	100-0
6.3.95	106	13°30,164N	50°18,548E	MSN	902	1	2000-1500
6.3.95	106	13°30,164N	50°18,548E	MSN	902	2	1500-1000
6.3.95	106	13°30,164N	50°18,548E	MSN	902	3	1000-700
6.3.95	106	13°30,164N	50°18,548E	MSN	902	4	700-200
6.3.95	106	13°30,164N	50°18,548E	MSN	902	5	200-0
7.3.95	107	14°36,299N	52°55,145E	MSN	903	1	100-80
7.3.95	107	14°36,299N	52°55,145E	MSN	903	2	80-60
7.3.95	107	14°36,299N	52°55,145E	MSN	903	3	60-40
7.3.95	107	14°36,299N	52°55,145E	MSN	903	4	40-20
7.3.95	107	14°36,299N	52°55,145E	MSN	903	5	20-0
8.3.95	107	14°36,781N	52°56,201E	MSN	904	1	700-500
8.3.95	107	14°36,781N	52°56,201E	MSN	904	2	500-300
8.3.95	107	14°36,781N	52°56,201E	MSN	904	3	300-200
8.3.95	107	14°36,781N	52°56,201E	MSN	904	4	200-100
8.3.95	107	14°36,781N	52°56,201E	MSN	904	5	100-0
9.3.95	108	14°59,315N	54°23,660E	MSN	905	1	100-80
9.3.95	108	14°59,315N	54°23,660E	MSN	905	2	80-60
9.3.95	108	14°59,315N	54°23,660E	MSN	905	3	60-40
9.3.95	108	14°59,315N	54°23,660E	MSN	905	4	40-20
9.3.95	108	14°59,315N	54°23,660E	MSN	905	5	20-0

9.3.95	108	14°59,709N	54°24,776E	MSN	906	1	700-500
9.3.95	108	14°59,709N	54°24,776E	MSN	906	2	500-300
9.3.95	108	14°59,709N	54°24,776E	MSN	906	3	300-200
9.3.95	108	14°59,709N	54°24,776E	MSN	906	4	200-100
9.3.95	108	14°59,709N	54°24,776E	MSN	906	5	100-0
9.3.95	108	15°00,848N	54°28,439E	MSN	907	1	2500-2000
9.3.95	108	15°00,848N	54°28,439E	MSN	907	2	2000-1500
9.3.95	108	15°00,848N	54°28,439E	MSN	907	3	1500-1000
9.3.95	108	15°00,848N	54°28,439E	MSN	907	4	1000-700
9.3.95	108	15°00,848N	54°28,439E	MSN	907	5	700-0
10.3.95	109	15°50,012N	57°00,147E	MSN	908	1	100-80
10.3.95	109	15°50,012N	57°00,147E	MSN	908	2	80-60
10.3.95	109	15°50,012N	57°00,147E	MSN	908	3	60-40
10.3.95	109	15°50,012N	57°00,147E	MSN	908	4	40-20
10.3.95	109	15°50,012N	57°00,147E	MSN	908	5	20-0
10.3.95	109	15°49,769N	56°59,762E	MSN	909	1	700-500
10.3.95	109	15°49,769N	56°59,762E	MSN	909	2	500-300
10.3.95	109	15°49,769N	56°59,762E	MSN	909	3	300-200
10.3.95	109	15°49,769N	56°59,762E	MSN	909	4	200-100
10.3.95	109	15°49,769N	56°59,762E	MSN	909	5	100-0
12.03.95	111-1	16°10,137N	59°45,864E	MSN	910	1	100-80
12.03.95	111-1	16°10,137N	59°45,864E	MSN	910	2	80-60
12.03.95	111-1	16°10,137N	59°45,864E	MSN	910	3	60-40
12.03.95	111-1	16°10,137N	59°45,864E	MSN	910	4	40-20
12.03.95	111-1	16°10,137N	59°45,864E	MSN	910	5	20-0
12.03.95	111-1	16°10,137N	59°45,864E	MSN	911	1	700-500
12.03.95	111-1	16°10,137N	59°45,864E	MSN	911	2	500-300
12.03.95	111-1	16°10,137N	59°45,864E	MSN	911	3	300-200
12.03.95	111-1	16°10,137N	59°45,864E	MSN	911	4	200-100
12.03.95	111-1	16°10,137N	59°45,864E	MSN	911	5	100-0
13.03.95	111-2	16°05,453N	59°41,158E	MSN	912	1	2000-1500
13.03.95	111-2	16°05,453N	59°41,158E	MSN	912	2	1500-1000
13.03.95	111-2	16°05,453N	59°41,158E	MSN	912	3	1000-700
13.03.95	111-2	16°05,453N	59°41,158E	MSN	912	4	700-200
13.03.95	111-2	16°05,453N	59°41,158E	MSN	912	5	200-0
14.03.95	110-4	16°12,975N	60°16,153E	MSN	913	1	100-80
14.03.95	110-4	16°12,975N	60°16,153E	MSN	913	2	80-60
14.03.95	110-4	16°12,975N	60°16,153E	MSN	913	3	60-40
14.03.95	110-4	16°12,975N	60°16,153E	MSN	913	4	40-20
14.03.95	110-4	16°12,975N	60°16,153E	MSN	913	4	40-20
14.03.95	110-4	16°12,975N	60°16,153E	MSN	913	5	20-0
14.03.95	110-4	16°12,981N	60°16,127E	MSN	914	1	700-500
14.03.95	110-4	16°12,981N	60°16,127E	MSN	914	2	500-300
14.03.95	110-4	16°12,981N	60°16,127E	MSN	914	3	300-200

14.03.95	110-4	16°12,981N	60°16,127E	MSN 914	4	200-100
14.03.95	110-4	16°12,981N	60°16,127E	MSN 914	5	100-0
15.03.95	110-4	16°13,022N	60°16,222E	MSN 915	1	2500-200O
15.03.95	110-4	16°13,022N	60°16,222E	MSN 915	2	2000-150O
15.03.95	110-4	16°13,022N	60°16,222E	MSN 915	3	1500-100O
15.03.95	110-4	16°13,022N	60°16,222E	MSN 915	4	1000-70O
15.03.95	110-4	16°13,022N	60°16,222E	MSN 915	5	700-0
18.03.95	113	16°32,181N	55°19,987E	MSN 916	1	100-80
18.03.95	113	16°32,181N	55°19,987E	MSN 916	2	80-60
18.03.95	113	16°32,181N	55°19,987E	MSN 916	3	60-40
18.03.95	113	16°32,181N	55°19,987E	MSN 916	4	40-20
18.03.95	113	16°32,181N	55°19,987E	MSN 916	5	20-0
18.03.95	113	16°32,852N	55°20,107E	MSN 917	1	700-500
18.03.95	113	16°32,852N	55°20,107E	MSN 917	2	500-300
18.03.95	113	16°32,852N	55°20,107E	MSN 917	3	300-200
18.03.95	113	16°32,852N	55°20,107E	MSN 917	4	200-100
18.03.95	113	16°32,852N	55°20,107E	MSN 917	5	100-0
19.03.95	114	14°32,367N	51°45,557E	MSN 918	1	100-80
19.03.95	114	14°32,367N	51°45,557E	MSN 918	2	80-60
19.03.95	114	14°32,367N	51°45,557E	MSN 918	3	60-40
19.03.95	114	14°32,367N	51°45,557E	MSN 918	4	40-20
19.03.95	114	14°32,367N	51°45,557E	MSN 918	5	20-0
19.03.95	114	14°32,587N	51°45,444E	MSN 919	1	700-500
19.03.95	114	14°32,587N	51°45,444E	MSN 919	2	500-300
19.03.95	114	14°32,587N	51°45,444E	MSN 919	3	300-200
19.03.95	114	14°32,587N	51°45,444E	MSN 919	4	200-100
19.03.95	114	14°32,587N	51°45,444E	MSN 919	5	100-0
19.03.95	114	14°32,343N	51°48,189E	MSN 920	1	1500-1250
19.03.95	114	14°32,343N	51°48,189E	MSN 920	2	1250-1000
19.03.95	114	14°32,343N	51°48,189E	MSN 920	3	1000-700
19.03.95	114	14°32,343N	51°48,189E	MSN 920	4	700-500
19.03.95	114	14°32,343N	51°48,189E	MSN 920	5	500-0
20.03.95	115	13°18,374N	48°47,089E	MSN 921	1	100-80
20.03.95	115	13°18,374N	48°47,089E	MSN 921	2	80-60
20.03.95	115	13°18,374N	48°47,089E	MSN 921	3	60-40
20.03.95	115	13°18,374N	48°47,089E	MSN 921	4	40-20
20.03.95	115	13°18,374N	48°47,089E	MSN 921	5	20-0
20.03.95	115	13°18,762N	48°47,011E	MSN 922	1	700-500
20.03.95	115	13°18,762N	48°47,011E	MSN 922	2	500-300
20.03.95	115	13°18,762N	48°47,011E	MSN 922	3	300-200
20.03.95	115	13°18,762N	48°47,011E	MSN 922	4	200-100
20.03.95	115	13°18,762N	48°47,011E	MSN 922	5	100-0
21.03.95	116	12°52,022N	47°26,559E	MSN 923	1	100-80
21.03.95	116	12°52,022N	47°26,559E	MSN 923	2	80-60

21.03.95	116	12°52,022N	47°26,559E	MSN	923	3	60-40
21.03.95	116	12°52,022N	47°26,559E	MSN	923	4	40-20
21.03.95	116	12°52,022N	47°26,559E	MSN	923	5	20-0
21.03.95	116	12°51,924N	47°26,527E	MSN	924	1	700-500
21.03.95	116	12°51,924N	47°26,527E	MSN	924	2	500-300
21.03.95	116	12°51,924N	47°26,527E	MSN	924	3	300-200
21.03.95	116	12°51,924N	47°26,527E	MSN	924	4	200-100
21.03.95	116	12°51,924N	47°26,527E	MSN	924	5	100-0

7.3.3 Plankton Pump Samples

	Start Filtration						Stop Filtration						
	Position						Position						
Date	Time	Latitude	Longitude	Sal.(°/oo)	Temp. (°C)	Waterclock	Time	Latitude	Longitude	Sal.(°/oo)	Temp. (°C)	Waterclock	pumped Liters
04.03.95	10:45	12°24,3	44°29,6	35,7	26,0	270916	17:24	17°12,5	37°57,4	35,7	26,3	274058	3142
05.03.95	08:19	12°74,3	46°59,9	35,2	26,1	274058	17:29	13°06,4	48°31,1	35,5	26,4	276058	2000
06.03.95	10:25	13°29,4	50°17,8	35,6	26,1	277794	17:25	13°29,6	50°17,7	35,6	26,0	281131	3337
07.03.95	07:30	14°03,7	51°57,9	34,89	27,2	281131	20:04	14°36,3	52°55,2	35,5	25,6	286270	5139
08.03.95	08:00	14°55,8	54°04,0	35,56	25,5	286595	19:05	14°58,7	54°22,1	35,5	25,8	290955	4360
09.03.95	09:00	14°58,5	54°22,5	35,48	25,7	290955	18:45	15°26,7	55°45,0	34,89	26,6	294552	3597
10.03.95	07:45	15°49,6	56°59,6	35,62	25,3	294552	18:45	15°52,5	57°11,7	35,3	25,6	298686	4134
11.03.95	08:20	16°06,5	59°14,8	35,6	25,1	298686	18:30	16°13,2	60°16,0	35,62	25,2	302617	3931
12.03.95	07:55	16°10,1	59°45,7	35,6	25,1	302618	18:10	16°08,0	60°15,8	35,62	25,2	305761	3143
13.03.95	08:35	16°13,1	60°16,0	35,63	25,2	305761	18:40	16°05,5	59°41,1	35,60	25,4	308414	2653
14.03.95	07:35	16°03,1	60°16,0	35,66	25,2	308414	18:30	16°02,9	60°16,0	35,65	25,4	312738	4324
15.03.95	07:45	16°13,0	60°16,0	35.59	25.4	312740	17:25	16°13,2	60°15,5	35,57	25,4	317312	4572
16.03.95	07:45	17°44,9	58°08,0	35,74	24,9	317312	17:55	17°45,0	58°08,9	35,71	25,3	320121	2809
17.03.95	08:40	17°22,4	57°00.8	35.52	25,2	320125	18:05	16°34,1	55°24,8	34.95	27,0	323952	3827
18.03.95	08:10	16°31,8	55°20,0	34,94	26,8	323953	18:23	15°44,4	53°53,8	35,80	25,9	326054	2101
19.03.95	07:40	14°32,1	51°44,0	35,02	27,0	326068	01:20	13°53,2	50°19,0	35,54	26,6	331521	5453
20.03.95	08:05	13°23,9	49°01,2	35,67	36,7	331521	17:30	13°17,8	48°44,0	35,67	28,8	335010	3489

7.3.4 Station list of Sediment Samples

Station GeoB #	Date 1995	Coring device	Sample/Seafloor Time	Latitude (° N)	Longitude (° E)	Water-depth (m)	core-length (cm)	Remarks
Gulf of Aden								
Sta.105								
3001-1	04.03	MC	10:47	12°24.2	44°29.6	174	25	Sandy mud, olive-green, mollusk shells
3001-2		GKG	11:51	12°22.8	44°31.5	321		Corg surface sample
3001-3		GKG	13:06	12°21.5	44°33.0	506		Corg surface sample
also Sta.105								
3002-1	04. 03	MC	15:30	12°17.3	44°38.2	752	30	2 big, 2 small tubes, olive green mud
3002-2		ROS	16:31	12°17.1	44°37.3	716	12 (bt.)	O^{18} + C^{13} samples: 3 x 50 ml
Sta.106								
3003-1	06.03	ROS	05:38	13°29.1	50°18.0	1938	12 (bt.)	O^{18} + C^{13} samples: 3 x 50 ml
3003-2		SL 12	07:22	13°29.5	50°17.8	2023	62	Penetration until weight
3003-3		KL 24	10:46	13°29.4	50°17.8	2022	1890	CC: clayey carbonate ooze, olive-green
3003-4		SL 12	13:58	13°29.7	50°17.6	2016	1048	CC: clayey carbonate ooze, olive-green
3003-5		MC1	15:52	13°29.6	50°17.7	2013	25	2 big, 2 small tubes: clay/carbonate ooze, 0- 2 cm brown, else olive-green
Sta.107								
3004-1	07.03	SL 12	16:44	14°36.3	52°55.2	1803	1028	Penetration until weight, CC: H_2S, clayey carbonate ooze, oliv-green
3004-2		KL 24	19:26	14°36.3	52°55.2	1802	1950	CC: carbonate ooze, olive green
3004-3		ROS	21:39	14°36.3	52°55.2	1793	12(bt.)	O^{18} + C^{13} samples: 3 x 50 ml
3004-4		MC	23:11	14°36.3	52°55.2	1801	30	2 big, 2 small tubes: clay/carbonate ooze
Western Arabian Sea								
Sta.108								
3005-1	08.03	SL 12	11:08	14°58.3	54°22.2	2316	1148	Penetration until weight, 0 - 5 cm missing, CC: carbonate ooze, olive-green

3005-2		KL 24	14:20	14°58.3	54°22.0	2309	1950	CC: carbonate ooze, olive green
3005-3		MC	21:31	14°58.2	54°22.2	2313	30	2 big, 2 small tubes, carbonate ooze, olive-green
3005-4	09.03	ROS	02:50	15°00.0	54°26.8	2694	12(bt)	$O^{18} + C^{13}$ samples: 3 x 50 ml
Sta.109								
3006-1	10.03	ROS	04.16	15°50.0	56°59.7	2966	12(bt)	$O^{18} + C^{13}$ samples: 3 x 50 ml
3006-2		MC	06.41	15°49.7	56°59.7	3521	26	2 big, 2 small tubes, clay/carbonate-ooze, olive-green
3006-3		SL 12	12:00	15°51.1	56°59.3	3225	1134	CC: sandy carbonate-ooze, green-gray between 70 and 132 cm disturbed
3006-4		KL 24	15:15	15°51.1	56°59.3	3157	1710	CC: clayey carbonate ooze, olive green

Owen Ridge

Sta.111-1								
3007-1	12.03	SL 12	07:18	16°10.2	59°45.3	1920	892	CC: sandy carbonate-ooze, green
3007-2		KL 12	09:23	16°10.1	59°45.9	1916	680	CC: carbonate-ooze, green-grey
3007-3		MC	13:10	16°10.2	59°46.2	1914	19	2 big, 2 small tubes, 2 surface
Sta.111-2								
3008-1	13.03	SL 12	13:33	16°05.4	59°41.0	2224	447	CC: carbonate-ooze, light green-grey
3008-2		KL 12	16.06	16°05.5	59°41.1	2239	1169	CC: carbonate-ooze, light green-grey
3008-3		KL 24	21.58	16°05.4	59°41.1	2240	0	device damaged, no core
3008-4		ROS	23:55	16°05.5	59°41.2	2207	12(bt)	$O^{18} + C^{13}$ samples : 3 x 50 ml
3008-5	14.03	MC	01:42	16°05.4	59°41.0	2223	19	2 big, 2 small tubes, clay/carbonate-ooze, olive-green, foraminifera.
Sta.110-3, 110-4								
3009-1	14.03	ROS	18:25	16°02.9	60°16.0	4080	12(bt)	$O^{18} + C^{13}$ samples : 3 x 50 ml
3009-2	15.03	MC	04:00	16°12.6	60°16.8	4071	35	2 big, 2 small tubes, clay/carbonate ooze, olive-green, fluffy Layer

Oman Upwelling

Sta.112								
3010-1	16.03	ROS	14:55	17°45.1	58°09.0	808	12(bt.)	$O^{18} + C^{13}$ samples : 3 x 50 ml
3010-2		MC	18:56	17°45.0	58°09.0	3166	30	1 small tube, Corg and Dinoflag. samples
3010-3		MC	21:08	17°45.0	58°09.0	3165	30	1 small tube, Corg, carbonate ooze olive-green, 0-2 cm brown-green

Sta.113

3011-1	17.03	SL 12	19:34	16°32.1	55°19.9	2636	1081	CC: carbonate-ooze, olive-green, foraminifera, H_2S
3011-2	18.03	KL 24	01:27	16°31.9	55°19.9	2624	2040	CC: carbonate-ooze, olive-green
3011-3	18.03	MC	05:01	16°31.9	55°19.9	2624	22	carbonate-ooze, olive-green, foraminifera rare, fluffy layer
3011-4	18.03	ROS	08:24	16°31.9	55°19.9	2596	12(bt.)	$O^{18} + C^{13}$ samples : 3 x 50 ml

Gulf of Aden

Sta.114

3012-1	19.03	SL 12	08:24	14°32.4	51°45.1	1539	789	CC: clay/carbonate-ooze, surface lost
3012-1		MC	09:45	14°32.4	51°44.9	1538	32	carbonate-ooze, foraminifera, olive-green
3012-1		ROS	14:45	14°32.8	51°46.1	1517	12(bt.)	$O^{18} + C^{13}$ samples : 3 x 50 ml

Sta.115

3013-1	20:03	SL 12	10:13	13°18.5	48°47.0	1717	972	CC: carbonate-ooze, gray green
3013-2		MC	11:37	13°18.6	48°47.0	1731	27	2 big, 2 small tubes,carbonate-ooze, gray green, foraminifera
3013-3		ROS	14:31	13°18.3	48°46.9	1702	12(bt.)	$O^{18} + C^{13}$ samples: 3 x 50 ml

Sta.116

3014-1	21.03	SL 12	01:59	12°51.8	47°26.1	1646	1134	CC: carbonate-ooze, olive green
3014-2		MC	03:13	12°51.7	47°26.1	1626	23	2 big, 2 small tubes, 1 surface sample, carbonate-ooze, olive green, foraminifers

Sta.117

3015-1	21.03	SL 12	20:51	12°17.2	44°37.4	736	847	CC: dark green clayey mud, pteropods

8 Concluding Remarks

Firstly, we thank the masters of RV METEOR captain H. Bruns and captain M. Kull and crews for their skilled work who enabled us to obtain data sets of great interest and importance. We also acknowledge very much the help of Mrs. U. Wahl and I. Breitinger who run the coordinator's office, C. Leven for his support while preparing the report and captain Schmickler's crew at the "Leitstelle". We all appreciated the excellent organization provided by Contiways Reisen, Hamburg, represented by Mrs. Neiss and Mrs. I. Weigert. Last but not least we thank the German diplomatic representatives in various countries where their help was neccessary.

Financial support for the cruise and scientific data analysis was supplied by the Deutsche Forschungsgemeinschaft (DFG - He 697/17) and the BMBF (JGOFS-Indik).

9 References

ALMGREN, T., D. DYRSEN and S. FONDELIUS (1983): Determination of alkalinity and total carbonate. In: K. GRASSHOFF, M. ERHARD and K. KREMLING (eds.): Methods of seawater analysis. Verlag Chemie, Weinheim/Deerfield/Florida/Basel, 99-123.

ALMOGI-LABIN, A. (1982): Stratigraphic and paleoceanographic significance of late Quaternary pteropods from deep-sea cores in the Gulf of Aqaba (Elat) and northernmost Red Sea.- Marine Micropaleontology, 7, 53-72.

ALMOGI-LABIN, A et al. (in press): Response of Red Sea deep-water agglutinated foraminifera to water-mass changes during Late Quaternary. Marine Micropal.

ANDERSON, L. and D. DYRSSEN (1994): Alkalinity and total carbonate in the Arabian Sea. Carbonate depletion in the Red Sea and Persian Gulf. Marine Chemistry, **47**, 195-202.

ANSCHUTZ, P. and G. BLANC (1995): Geochemical dynamics of the Atlantis II Deep (Red Sea): silica behavior. Marine Geology, **128**, 25 - 36.

AURAS, A., D. KROON, G. GANSSEN, CH. HEMLEBEN, and J. VAN HINTE (1989): Distributional pattern of planktonic foraminifera and pteropods in surface waters and top core sediments of the Red Sea and adjacent areas controlled by the monsoonal regime and other ecological factors. Deep Sea Res., **36**, 10, 1515-1533,.

BÄCKER, H. and H. RICHTER (1973): Die rezente hydrothermal-sedimentäre Lagerstätte Atlantis II-Tief im Roten Meer. Geol. Rundsch., **62/3**, 697-741.

BANGE H.W., U.H. BARTELL, S. RAPSOMANIKIS and M.O. ANDREAE (1994): Methane in the Baltic and North Seas and a reassessment of the marine emissions of methane. Global Biogeochem. Cycles, **8**, 465-480.

BARNETT, P.R.O., J. WATSON and D. CONNELLY (1984). A multiple corer for taking virtually undisturbed samples from shelf, bathyal and abyssal sediments. Oceanol. Acta, 7, 399-408.

BAUER, S., G.L. HITCHCOCK and D.B. OLSON (1991): Influence of monsoonally-forced Ekman dynamics upon surface layer depth and plankton biomass distribution in the Arabian Sea. Deep Sea Res., **38**, 513-553.

BETHOUX, J.P. (1988): Red Sea geochemical budgets and exchanges with the Indian Ocean. J. Mar. Chem., **24**, 83-92.

BERGER, W.H., V.S. Smetacek and G. Wefer (1989): Ocean productivity and paleoproductivity - an overview. In: BERGER, W.H., V.S. SMETACEK and G. WEFER (eds.): Productivity of the ocean: Present and past. Life Sciences Research Report, **44**, 1-34.

BILLETT, D.M.S., R.S. LAMPITT, A.L. RICE and R.F.C. MANTOURA (1983): Seasonal sedimentation of phytoplankton to the deep-sea benthos. Nature (Lond.), **302**, 520-522.

BÉ, A.W.H. and D.S. TOLDERLUND (1971): Distribution and ecology of living planktonic foraminifera in surface waters of the Atlantic and Indian Oceans. In: FUNNEL, B.M. and W.R. RIEDEL (eds.): Micropaleontology of the Oceans. Cambridge University Press (London).

BÉ, A.W.H. and W.H. HUTSON (1977): Ecology of planktonic foraminifera and biogeographic patterns of life and fossil assemblages in the Indian Ocean. Micro-paleontology, **23(4)**, 369-414.

BONSANG B., M. KANAKIDOU, G. LAMBERT and P. MONFRAY (1988): The marine source of C_2-C_6 aliphatic hydrocarbons. J. Atmos. Chem., **6**, 3-20.

BRACHERT, T.C. (subm.): Non-skeletal carbonate production within a deep ocean basin: The "hard layer" of the glacial Red Sea. subm. to Geol. Rundschau.

BRACHERT, T.C. and W.-C. DULLO (1994): Micrite crusts on Ladinian foreslopes of the Dolomites seen in the light of a modern scenario from the Red Sea. Abh. Geol. B.-A., **50**, 57-78.

BRACHERT, T.C. and W.-C. DULLO (1991): Laminar micrite crusts and associated foreslope processes, Red Sea. Journal of Sedimentary Petrology, **61/3**, 354-363.

BROCK, J., S. SATHYENDRANATH, and T. PLATT (1994): A model study of seasonal mixed-layer primary production in the Arabian Sea. In: LAL, D. (ed.): Biogeochemistry of the Arabian Sea. Indian Academy of Sciences, Bangalore, 65-78.

BROECKER, W. S. and T.-H. PENG (1982): Tracers in the Sea. Eldigo Press, Palisades, New York, 690 p.

BROOK, J.C., C.R. MCCLAIN, and W.W. HAY (1992): A southwest monsoon hydrographic climatology for the northwestern Arabian Sea. J. Geophys. Res., **97** (C6), 9455-9465.

BROOK, J.C., C.R. MCCLAIN, M.E. LUTHER, and W.W. HAY (1991): The phytoplankton bloom in the northwestern Arabian Sea during the southwest monsoon 1979. J. Geophys. Res., **96** (C11), 20, 613-20,622.

BROOKS J.M., D.F. REID and B. BERNARD (1981): Methane in the upper water coulmn of the northwestern Gulf of Mexico. J. Geophys. Res., **86**, 11029-11040.

BROOKS J.M. and W.M. SACKETT (1973): Sources, sinks, and concentrations of light hydrocarbons in the Gulf of Mexico. J. Geophys. Res., **78**, 5248-5258.

BURKE R.A., J.M. BROOKS and W.M. SACKETT (1981): Light hydrocarbons in Red Sea brines and sediments. Geochom. Cosmochim. Acta, **45**, 627-634.

BURKE JR. R.A., D.F. REID, J.M. BROOKS and D.M. LAVOIE (1983): Upper water column methane geochemistry in the eastern tropical North Pacific. Limnol. Oceanogr., **28**, 19-32.

CHIPMAN, D. W., J. MARRA and T. TAKAHASHI (1993): Primary production at 47° N and 20° W in the North Atlantic Ocean: a comparison between the ^{14}C incubation method and the mixed layer carbon budget. Deep-Sea Research, **40**, 151-169.

COLBURN, J.G. (1975): The thermal structure of the Indian Ocean. 173 pp., Univ.of Hawaii, Honolulu.

CONRAD R. and W. SEILER (1988): Influence of the surface microlayer on the flux of nonconservative trace gases (CO, H_2, CH_4, N_2O) across the ocean-atmosphere interface. J. Atmos. Chem., **6**, 83-94.

COPIN-MONTÉGUT C. (1985): A method for the continuous determination of the partial pressure of carbon dioxide in the upper ocean. Marine Chemistry, **17**, 13-21.

COPIN-MONTÉGUT C. (1993): Alkalinity and carbon budgets in the Mediterranean Sea. Global biogeochemical Cycles, 7, 915-925.

COPIN-MONTÉGUT C. and B. AVRIL (1995): Tellus, in the press.

CURRIE, R.I., A.E. FISHER, and P.M. HARGREAVES (1973): Arabian Sea Upwelling. In: ZEITZSCHEL, B. (ed.): The Biology of the Indian Ocean. Springer-Verlag, New York, 37-52 pp.

DICKSON, A. G. (1981): An exact definition of total alkalinity and procedure for the estimation of alkalinity and total inorganic carbon from titration data. Deep-Sea Res., **28**, 609-623.

DICKSON A. G. and J. P. RILEY (1979): Mar. Chem., 7, 89-99.

DICKSON A. G. and F. J. MILLERO (1987). Deep Sea Res., **34**, 1733-1743.

DICKSON A. G. (1990): Deep Sea Res., **37**, 755-766.

DIETRICH, G., K. KALLE, W. KRAUSS, and G. SIEDLER (1975): Allgemeine Meereskunde. Gebr. Borntraeger, Berlin, 501 pp.

DLUGOKENCKY E.J., P.M. LANG, K.A. MASARIE and L.P. STEELE (1994): Atmospheric CH_4 records from sites in the NOAA/CMDL air sampling network. In: T.A. BODEN, D.P. KAISER, R.J. SEPANSKI and F.W. STOSS (eds.): Trends '93: A Compendium of Data on Global Change. ORNL/CDIAC-65. Carbon Dioxide Information Analysis Center, Oak Ridge National Laboratory, Oak Ridge, Tenn., U.S.A, 274-350 pp.

DOE (1994): Handbook of Methods for the Analysis of the Various Parameters of the Carbon Dioxide System in Sea Water; Version 2.0 (eds. A. G. DICKSON and C. GOYET). U.S. Department of Energy (DOE), SRGP 89-7A.

DROXLER, A.W. (1984): Late Quaternary glacial cycles in the Bahamian Deep Basins and in the adjacent Atlantic Ocean. Ph.D. Thesis (unpublished), Dept. of Marine Geology and Geophysics, Rosenstiel School of Marine and Atmospheric Science, Miami, 1-119.

DROXLER, A.W. and W. SCHLAGER (1985): Glacial versus interglacial sedimentation rates and turbidite frequency in the Bahamas. Geology, **13,** 799-802.

DROXLER, A.W., G.A. HADDAD, D.A. MUCCIARONE and J.L. CULLEN (1990): Pliocene-Pleistocene aragonite cyclic variations in holes 714A and 716B (the Maldives) compared with hole 633A (the Bahamas): Records of climate-induced $CaCO_3$ preservation at intermediate water dephts. Proceedings of the Ocean Drilling Program, Scientific Results, **115**, 539-567.

DROXLER, A.W., W. SCHLAGER, and C.C. WHALLON (1983): Quaternary aragonite cycles and oxygen-isotope record in Bahamian carbonate ooze. Geology, **11**, 235-239.

FLÜGEL, E. (1980): Die Mikrofazies der Kalke in den Trogkofel-Schichten der Karnischen Alpen. Carinthia II, Sonderheft, **36**, 51-100.

FLÜGEL, E. (1984): Permian reefs: evolution, structure, and paleoecology. 3ème Cycle Sci,. Terre: 10.1-10.20.

GASPERINI, L., B. GENSOU, E. PHILOBBOS, B. PURSER, J. REIJMER, M. RIOUAL, M. TAVIANI and M. TESSON (1992): Gulf of Suez seismic survey (M/SAbu Saleh) Sept./Oct. 1992: A first report. subm. in Giornale di Geologia.

GEVRITZ, J.L. and G.M. FRIEDMAN (1966): Deep-Sea carbonates of the Red Sea and their implications on marine lithification. Journal of Sed. Pet., **36**, 143-151.

GLASER, K.S. (1991): Late Quaternary periplatform sediments and environments on the Northeastern Nicaragua Rise, Caribbean Sea. Ph.D. Thesis (unpublished), Rice University, Houston, 1-244.

GLASER, K.S. and A.W. DROXLER (1993): Controls and development of late Quaternary periplatform carbonate stratigraphy in Walton Basin (Northeastern Nicaragua Rise, Caribbean Sea).- Paleoceanography, **8**/2, 243-274.

GOODAY, A.J. (1988): A response by benthic Foraminifera to the deposition of phytodetritus in the deep sea.- Nature, **332**, 70-73.

GOODAY, A.J. and LAMBSHEAD, P.J.D. (1989): Influence of seasonally deposited phytodetritus on benthic foraminiferal populations in the bathyal northeast Atlantic: The species responce. Marine Ecology Progress Series, **58**, 53-67.

GRASSHOFF K. (1983): Determination of oxygen. In: GRASSHOFF K., M. ERHARDT, K. KREMLING (eds.): Methods of Seawater analysis.- Verlag Chemie, Weinheim, 61-72.

GRASSHOFF, K. (1969): Zur Chemie des Roten Meeres und des Inneren Golf von Aden nach Beobachtungen von F.S. METEOR während der Indischen Ozean-Expedition 1964/65, METEOR-Forsch. Ergeb., (A), **6**, 1-76.

GUPHTA M.V.S., R. MOHAN, and A.S. MURALINATH (1995): Living coccolithophorids from the Arabian Sea. Riv. It. Paleont. Strat., v. 100, **4**, 551-574.

PAPAUD, A. and A. POISSON (1986): Distribution of dissolved CO_2 in the Red Sea and correlations with other geochemical tracers. J. Mar. Res., **44**, 385-402.

HAAKE, B., V. ITTEKKOT, T. RIXEN, V. RAMASWAMY, R.R. NAIR and W.B. CURRY (1993): Seasonality and interannual variability of particle fluxes to the deep Arabian Sea. Deep-Sea Research, **40**, 1323-1344.

HADDAD, G.A., A.W. DROXLER, D. KROON and D.W. MÜLLER (1993): Quarternary CaCO3 input and preservation within Antarctic intermediate water mineralogic and isotopic results from Holes 818B and 817A, Townsville Troug (northeast Australian margin). Proceedings of the Ocean Drilling Program, Scientific Results, **133**, 203-233.

HARTMANN, M. (1972): Sound velocity data for the hot brines and corrected depth of the interfaces in the Atlantis II Deep. Marine Geology, **12**, M16 - M20.

HARTMANN, M. (1980): Atlantis II Deep geothermal brine system. Hydrographic situation in 1977 and changes since 1965. Deep Sea Research, **27**, 161 - 171.

HEMLEBEN, CH., D. MEISCHNER, R. ZAHN, A. ALMOGI, H. ERLENKEUSER, and B. HILLER (1996): Three hundred eighty thousand year long stable isotope and faunal records from the Red Sea: Influence of global sea level change on hydrography, Palaeoceanographic Currents. Paleoceanography, **11**, 147-156.

HERMELIN, J.O.R. and G.B. SHIMMIELD (1990): The importance of the oxygen minimum zone and sediment geochemistry in the distribution of Recent benthic foraminifera in the northwest Indian Ocean. Marine Geology, **91**, 1-29.

HERMELIN, J.O.R. and G.B. SHIMMIELD (1995): Impact of productivity events on the benthic foraminiferal fauna in the Arabian Sea over the last 150,000 years. Paleoceanography, **10**, 85-116.

HOTTINGER, L. et al. (1993): Recent foraminiferida from the Gulf of Aquaba, Red Sea. Slovenska Akademija Znanosti in Umetnosti, **33**, 179 pp.

JEAN-BAPTISTE P., S. BELVISO, G. ALAUX, B.C. NGUYEN and N. MIHALOPOULOS (1990): ^{3}He and methane in the Gulf of Aden. Geochim. Cosmochim. Acta, **54**, 111-116.

JOHNSON, D. A. and C. NIGRINI (1980): Radiolarian biogeography in surface sediments of the western Indian Ocean. Marine Microplaeontology, **5**, 111-152.

KHALIL M.A.K. and R.A. RASMUSSEN (1983): Sources, sinks, and seasonal cycles of atmospheric methane. J. Geophys. Res., **88**, 5131-5144.

KHALIL M.A.K. and R.A. RASMUSSEN (1986): Interannual variability of atmospheric methane: possible effects of the El Nino-Southern Oscillation. Science, **232**, 56-58.

KULLENBERG, B. (1952): On the salinity of water contained in marine sediments.-- Medd. Oceanogr. Inst. Göteborg, 21, 1 - 38.

KUMAR, M. D., A. RAJENDRAN, K. SOMASUNDAR, V. ITTEKKOT and B. N. DESAI (1992): Process controlling carbon components in the Arabian Sea. In: B. N. DESAI (ed.) Oceanography of the Indian Ocean. Oxford and IBH Publishing, New Delhi, 313-325.

LADAGE S., R. SEIFERT, W. MICHAELIS, H. RUPP, P. HALBACH and J. MAKRIS (1991): Hydrothermal gas generation in a back-arc basin. Naturwissenschaften, **78**, 64-66.

LAMBERT G. and S. SCHMIDT (1993): Reevaluation of the oceanic flux of methane: Uncertainties and long term variations. Chemosphere, **26**, 579-589.

LAMONTAGNE R.A., J.W. SWINNERTON and V.J. LINNENBOM (1974): C_1-C_4 hydrocarbons in the North and South Pacific. Tellus, **26**, 71-77.

LAMONTAGNE R.A., J.W. SWINNERTON, V.J. LINNENBOM and W.D. SMITH (1973): Methane concentrations in various marine environments. J. Geophys. Res., **78**, 5317-5324.

LELIEVELD J., P.J. CRUTZEN and C. BRÜHL (1993): Climate effects of atmospheric methane. Chemosphere, **26**, 739-768.

LISS P.S. and L. MERLIVAT (1986):Air-sea gas exchange rates: Introduction and synthesis. In: BUAT-MENARD P. (ed.): The role of air-sea exchange in geochemical cycling. D. Reidel Publishing Company, 113-127.

LOCHTE, K. (1993): Mikrobiologie von Tiefseesedimenten. In: MEYER-REIL, L.A. and M. KÖSTER (eds.): Mikrobiologie des Meeresbodens. Jena, G.Fischer Verlag, 258-282.

LOCKE, S. and R.C. THUNELL (1988): Paleoceanographic record of the last glacial/interglacial cycle in the Red Sea and Gulf of Aden.- Pal. Pal. Pal., **64**, 163-187.

LYNCH J.M. and S.H.T. HARPER (1974): Formation of ethylene by a soil fungus. J. Gen. Microbiol., **80**, 187-195.

MAKRIS, J. and RIHM, R. (1991): Shear-controlled evolution of the Red Sea: pull apart model.- Tectonophysics, **198**, 441-466.

MALANOTTE-RIZZOLI, P. and A. HECHT (1988): Large scale properties of the Eastern Mediterranean: a review. Oceanol. Acta, **11**, 323-335.

MANGINI, A. and P. SCHLOSSER (1986): The formation of eastern Mediterranean sapropels.-- Marine Geol., **72**, 115 - 124.

MANSOURI S. and A.W. BUNCH (1989): Bacterial ethylene synthesis from 2-Oxo-4-thiobutyric acid and from methionine. J. Gen. Microbiol., **135**, 2819-2827.

MATTHEWS, D.J. (1939): Tables of velocity of sound in pure water and sea water in echo sounding and sound ranging.- Hydrographic Department, Admiralty, London.

MICHAELIS W., A. JENISCH and H.H. RICHNOW (1990): Hydrothermal petroleum generation in Red Sea sediments from the Kebrit and Shaban Deeps. Applied Geochemistry, **5**, 103-114.

MILLERO F. J. and A. POISSON (1981). Deep Sea Res., **28**, 625-629.

MILLIMAN, J.D. (1974): Marine carbonates.- (Springer Verlag), Part 1.

MILLIMAN, J.D., D.A. ROSS and T.-L. KU (1969): Precipitation and lithification of deep-sea carbonates in the Red Sea.- Journal of Sedimentary Petrology, **39**/2, 724-736.

NAGAHAMA K., T. OGAWA, T. FUJII, M. TAZAKI, S. TANASE, Y. MORINO and H. FUKUDA (1991): Purification and properties of an ethylene-forming enzyme from *Pseudimonas syringae* pv. *phaseolicola* PK2. J. Gen. Microbiol., **137**, 2281-2286.

NIGRINI, C. (1991): Composition and biostratigraphy of radiolarian assemblages from an area of upwelling (northwestern Arabian Sea. Leg 117). In: PRELL, W. J., N. NIITSUMA et al. (eds.): Proc. of the Ocean Drilling Program, Scientific Results, 117, College Station, TX (ocean Drilling Program), 89-126.

NIGRINI, C. and J. P. CAULET (1992): Late Neogene radiolarian assemblages of Indo-Pacific areas of upwelling. Micropaleontology, **38**, 139-164.

OWENS N.J.P., C.S. LAW, R.F.C. MANTOURA, P.H. BURKILL and C.A. LLEWELLYN (1991): Methane flux to the atmosphere from the Arabian Sea. Nature, **354**, 293-296.

PATZERT, W.C. (1972): Seasonal Variations in structure and circulation in the Red Sea, H.I.G Rep., Univ. of Hawaii, Honolulu, 1-58.

PEREZ, F. F. and F. FRAGA (1987): A precise and rapid analytical procedure for alkalinity determination. Marine Chemistry, **21**, 169-182.

PFANNKUCHE, O. (1993): Benthic response to the sedimentation of particulate organic matter at the BIOTRANS station, 47°N,20°W. Deep-Sea Res., **40**, 135-150.

PICKARD, G.L. and W.J. EMERY, (1990): Descriptive physical oceanography, an indroduction.- Pergamon Press, Oxford, New York, Beijing, Frankfurt, Sâo Paulo, 320 pp.

PLASS C., R. KOPPMANN and J. RUDOLPH (1992): Light hydrocarbons in surface water of the Mid-Atlantic. J. Atmos. Chem., **15**, 235-251.

PLASS-DÜLMER C., A. KEHDIM, R. KOPPMANN, F.J. JOHNEN and J. RUDOLPH (1993): Emission of light nonmethane hydrocarbons from the Atlantic into the atmosphere. Global Biochem. Cycles, 7, 211-228.

PLASS-DÜLMER C., R. KOPPMANN, M. RATTE and J. RUDOLPH (1995): Light nonmethane hydrocarbons in seawater. Global Biogeochem. Cycles, **9**, 79-100.

POISSON, A., S. MORCOS, E. SOUVERMEZOGLOU, A. PAPAUD, and A. IVANOFF (1982): Some aspects of biogeochemical cycles in the Red Sea with special references to new observations made in summer 1982. Deep Sea Res., **31**, 707-718.

POST, J. (1985): Changes in the Red Sea hydrothermal activities between 1964 and 1984.- unpubl. manuscript.

PRELL, W.L. and W.B. CURRY, (1981): Faunal and isotopic indices of monsoonal upwelling: Western Arabian Sea. Oceanological Acta, **4**, 91-98.

PRIMROSE S.B. (1977): Evaluation of the role of methional, 2-keto-4-methylthiobutyric acid and peroxidase in ethylene formation by *Escherichia coli*. J. Gen. Microbiol., **98**, 519-528.

PRIMROSE S.B. and M.J. DILWORTH (1976): Ethylene production by bacteria. J. Gen. Microbiol., **93**, 177-181.

PUCHELT, H. (1984): Forschungsfahrt Sonne 29, Rotes Meer, 8. 1. 1984 - 9. 3. 1984, Fahrtbericht.- Institut für Petrographie und Geochemie, Universität Karlsruhe, 288 pp.

QASIM, S.Z. (1982): Oceanography of the northern Arabian Sea. Deep Sea Res., **29**, 1041-1068.

RATTE M., C. PLASS-DÜLMER, R. KOPPMANN and J. RUDOLPH (1993): Production mechanism of C_2-C_4 hydrocarbons in seawater: field measurements and experiments. Global Biogeochem. Cycles, **7**, 369-378.

REIJMER, J.J.G., SCHLAGER, W. and DROXLER, A.W. (1988): Site 632: Pliocene-Pleistocene sedimentation cycles in a Bahamian basin. Proceedings of the Ocean Drilling Program, Scientific Results, **101**, 213-220.

ROBINSON, C. and P.G.LEB. WILLIAMS (1991): Development and assessment of an analytical system for the accurate and continual measurement of total dissolved inorganic carbon. Marine Chemistry, **34,** 157-175.

ROETHER, W. and R. SCHLITZER (1991): Eastern Mediterranean deep water renewal on the basis of CFM and tritium data, Dyn. Atmos. Oceans, **15**, 333-354.

ROETHER, W., P. SCHLOSSER , R. KUNTZ and W. WEISS (1992): Transient-tracer studies of the thermohaline ciruclation of the Mediterranean. In: CHARNOCK, H. (ed.): Winds and Currents of the Mediterranean Basin, Proceedings of the Workshop held at Santa Teresa, La Spezia, Italy, Sept. 1982, Reports in Meteorology and oceanography, No. 41, The Division of Applied Physics, Harvard University, Vol. II, 291-317,

ROETHER, W., M. ROUSSENOV, and R. WELL (1994): A tracer study of the thermohaline circulation of the Eastern Mediterranean. In: MALANOTTE-RIZZOLI P. AND A. R. ROBINSON (eds.): Ocean Processes in climate Dynamics: Global and Mediterranean Examples. Kluwer Acad. Pub., 371-394.

ROETHER, W., B. MANCO, B. KLEIN, D. BREGANT, D. GEORGOPOULOS, V. BEITZEL, V. KOVACEVIC and A. LUCHETTA (1996): Recent changes in Eastern Mediterranean Deep Waters. accepted, Science.

ROSSIGNOL-STRICK, M. (1985): Mediterranean Quaternary sapropels, an immediate response of the African Monsoon to variation of insolation.-- Paeogeogr. Paleoclimatol. Paleoecol., **49**, 237-263.

RUDOLPH J. and D.H. EHHALT (1981): Measurements of C_2-C_5 hydrocarbons over the North Atlantic. J. Geophys. Res., **86**, 11959-11964.

SAUNDERS, P.M. and N.P. FOFONOFF (1976): Conversion of pressure to depth in the Ocean. Deep Sea Research , **23**, 109 - 111.

SCHERBACHER, M. (1994): Vergesellschaftungen rezenter Benthosforaminiferen in Sedimenten des mittleren Roten Meeres.- Diplom thesis, unpubl., Tübingen, 36 pp.

SCHLAGER, W., J.J.G. REIJMER and A.W. DROXLER (1994): Highstand shedding of carbonate platforms.- Journal of Sedimentary Research, **64**/3, 270-281.

SCHLITZER R., W. ROETHER, H. OSTER, H.G. JUNGHANS, M. HAUSMANN, H. JOHANNSEN and A. MICHELATO (1991): Chlorofluromethane and oxygen in the Eastern Mediterranean. Deep-Sea Res., **38**, 1531-1551.

SCHMIEDL, G. (1995): Rekonstruktion der spätquartären Tiefenwasserzirkulation und Produktivität im östlichen Südatlantik anhand von benthischen Foraminiferen-vergesellschaftungen.- Berichte zur Polarforschung, **160**, 207 pp.

SCHOELL, M. (1974): Valdivia VA 01/03 Hydrographie II und III.- Bundesanstalt f. Bodenforschung, Hannover.

SCRANTON M. I. and P.G. BREWER (1977): Ocurrence of methane in the near-surface waters of the western subtropical North-Atlantic. Deep-Sea Res., **24**, 127-138.

SEIFERT R., N. DELLING, H.H. RICHNOW, S. KEMPE and W. MICHAELIS (1996): Ethene and methane in the upper water column of the subtropical Atlantic. (submitted).

SMETACEK, V. (1991): Die Primärproduktion der marinen Plankton-Algen. Spektrum der Wissenschaft, **12,** 52-63.

STOFFERS, P., R. BOTZ, and J. SCHOLTEN (1990): Isotope geochemistry of carbonate minerals in the Shaban Deep.- In: HELING (ed.): Sediments in environmental chemistry. Selected aspects and case histories. Berlin, Springer, 83-94.

SWINNERTON J.W. and R.A. LAMONTAGNE (1974): Oceanic distribution of low-molecular-weight hydrocarbons. Environm. Sci. Technol., **8**, 657-663.

SWINNERTON J.W. and V.J. LINNENBOM (1967): Determination of the C_1 to C_4 hydrocarbons in sea water by gas chromatography. J. Gas Chromat., **5**, 570-573.

TAYLOR, A. H. and J. A. STEPHENS (1993): Diurnal variations of convective mixing and the spring bloom of phytoplankton. Deep-Sea Res., **40**, 389-408.

THOMAS G.E., J.J. OLIVERO, E.J. JENSEN, W. SCHROEDER and O.B.TOON (1989): Relation between increasing methane and the presence of ice clouds at the mesopause. Nature, **338**, 490-492.

TRAGANZA, E.D., J.W. SWINNERTON and C.H. CHEEK (1979): Methane supersaturation and ATP-zooplankton blooms in near-surface waters of the Mediterranean and the subtropical North Atlantic Ocean. Deep-Sea Res., **26**,1237-1245.

VAN DE PAVERD, P.J. (1995): Recent polycystine radiolaria from the Snellius-II expedition. Academisch proefschrift, Free University Amsterdam, 351 p.

VAN STRAATEN, L.M.J.U. (1972): Holocene stages of oxygen depletion in the waters of the Adriatic Sea. In: D.J. STANLEY (ed.): The Mediterranean Sea: A Natural Sedimentation Laboratory. Dowden, Hutchinson, Ross. Stroudsburg, Pa. 631 - 643.

WELHAN, J.A. (1988): Origins of methane in hydrothermal systems. Chem. Geol., **71**, 183-198.

WHITICAR M.J., SUESS, E., WEHNER, H. (1985): Thermogenic hydrocarbons in surface sediments ot the Bransfield Strait, Antarctic Peninsula. Nature, **314**, 87-90.

WÜST; G. (1961): On the vertical circulation of the Mediterranean Sea. J. Geophys. Res., **66**, 3261-3271.

WYRTKI, K. (1973), Physical oceanography of the Indian Ocean. In: ZEITZSCHEL B. (ed.): The Biology of the Indian Ocean, Springer-Verlag, New York, 18-36.

WYRTKI, K. (1971): Oceanographic Atlas of the International Indian Ocean Expedition, National Science Foundation, Washington D.C., 531 p.

Publications from METEOR expeditions
in other reports

Gerlach, S.A., J. Thiede, G. Graf und F. Werner (1986): Forschungsschiff Meteor, Reise 2 vom 19. Juni bis 16. Juli 1986. Forschungsschiff Poseidon, Reise 128 vom 7. Mai bis 8. Juni 1986. Ber. Sonderforschungsbereich 313, Univ. Kiel, 4, 140 S.

Siedler, G., H. Schmickler, T.J. Müller, H.-W. Schenke und W. Zenk (1987): Forschungsschiff Meteor, Reise Nr. 4, Kapverden - Expedition, Oktober - Dezember 1986. Ber. Inst. f. Meeresk., 173, Kiel, 123 S.

Wefer, G., G.F. Lutze, T.J. Müller, O. Pfannkuche, W. Schenke, G. Siedler und W. Zenk (1988): Kurzbericht über die Meteor - Expedition Nr. 6, Hamburg - Hamburg, 28. Oktober 1987 - 19. Mai 1988. Berichte, Fachbereich Geowissenschaften, Universität Bremen, 4, 29 S.

Müller T.J., G. Siedler und W. Zenk (1988): Forschungsschiff Meteor, Reise Nr. 6, Atlantik 87/88, Fahrtabschnitte Nr. 1 - 3, Oktober - Dezember 1987. Ber. Inst. f. Meeresk., 184, Kiel, 77 S.

Lutze, G.F., C.O.C. Agwu, A. Altenbach, U. Henken-Mellies, C. Kothe, N. Mühlhan, U. Pflaumann, C. Samtleben, M. Sarnthein, M. Segl, Th. Soltwedel, U. Stute, R. Tiedemann und P. Weinholz (1988): Bericht über die "Meteor" -Fahrt 6-5, Dakar - Libreville, 15.1.-16.2.1988.Berichte - Reports, Geol. Paläont. Inst., Univ. Kiel, 22, 60 S.

Wefer, G., U. Bleil, P.J. Müller, H.D. Schulz, W.H.Berger, U. Brathauer, L. Brück, A. Dahmke, K. Dehning, M.L. Durate-Morais, F. Fürsich, S. Hinrichs, K. Klockgeter, A. Kölling, C. Kothe, J.F. Makaya, H. Oberhänsli, W. Oschmann, J. Posny, F. Rostek, H. Schmidt, R. Schneider, M. Segl, M. Sobiesiak, T. Soltwedel und V. Spieß (1988): Bericht über die Meteor - Fahrt M 6-6, Libreville - Las Palmas, 18.2.1988 - 23.2.1988. Berichte, Fachbereich Geowissenschaften, Universität Bremen, 3, 97 S.

Hirschleber, H., F. Theilen, W. Balzer, B. v. Bodungen und J. Thiede (1988): Forschungsschiff Meteor, Reise 7, vom 1. Juni bis 28. September 1988, Ber. Sonderforschungsbereich 313, Univ. Kiel, 10, 358 S.

METEOR-Berichte
List of publications

89-1	(1989) Meincke, J., Quadfasel, D.	GRÖNLANDSEE 1988-Expedition, Reise Nr. 8, 27. Oktober 1988 - 18. Dezember 1988. Universität Hamburg, 40 S.
89-2	(1989) Zenk, W., Müller, T.J., Wefer, G.	BARLAVENTO-Expedition, Reise Nr. 9, 29. Dezember 1988 - 17. März 1989. Universität Hamburg, 238 S.
90-1	(1990) Zeitschel, B., Lenz, J., Thiel, H., Boje, R., Stuhr, A., Passow, U.	PLANKTON'89 - BENTHOS'89, Reise Nr. 10, 19. März - 31. August 1989. Universität Hamburg, 216 S.
90-2	(1990) Roether, W., Sarnthein, M., Müller, T.J., Nellen, W., Sahrhage, D.	SÜDATLANTIK-ZIRKUMPOLARSTROM, Reise Nr. 11, 3. Oktober 1989 - 11. März 1990. Universität Hamburg, 169 S.
91-1	(1991) Wefer, G., Weigel, W., Pfannkuche	OSTATLANTIK 90 - EXPEDITION, Reise Nr. 12, 13. März - 30. Juni 1990. Universität Hamburg, 166 S.
91-2	(1991) Gerlach, S.A., Graf, G.	EUROPÄISCHES NORDMEER, Reise Nr. 13, 6. Juli - 24. August 1990. Universität Hamburg, 217 S.
91-3	(1991) Hinz, K., Hasse, L., Schott, F.	SUBTROPISCHER & TROPISCHER ATLANTIK, Reise Nr. 14/1-3, Maritime Meteorologie und Physikalische Ozeanographie, 17. September - 30. Dezember 1990. Universität Hamburg, 58 S.
91-4	(1991) Hinz, K.	SUBTROPISCHER & TROPISCHER ATLANTIK, Reise Nr. 14/3, Geophysik, 31. Oktober - 30. Dezember 1990. Universität Hamburg, 94 S.
92-1	(1992) Siedler, G., Zenk, W.	WOCE Südatlantik 1991, Reise Nr. 15, 30. Dezember 1990 - 23. März 1991. Universität Hamburg, 126 S.
92-2	(1992) Wefer, G., Schulz, H.D., Schott, F., Hirschleber, H. B.	ATLANTIK 91 - EXPEDITION, Reise Nr. 16, 27. März - 8. Juli 1991. Universität Hamburg, 288 S.

92-3	(1992) Suess, E., Altenbach, A.V.	EUROPÄISCHES NORDMEER, Reise Nr. 17, 15. Juli - 29. August 1991. Universität Hamburg, 164 S.
93-1	(1993) Meincke, J., Becker, G.	WOCE-NORD, Cruise No. 18, 2. September - 26. September 1991. NORDSEE, Cruise No. 19, 30 September - 12 October 1991. Universität Hamburg, 105 pp.
93-2	(1993) Wefer, G., Schulz, H.D.	OSTATLANTIK 91/92 - EXPEDITION, Reise Nr. 20, M 20/1 und M 20/2, 18. November 1991 - 3. Februar 1992. Universität Hamburg, 248 S.
93-3	(1993) Wefer, G., Hinz, K., Roeser, H.A.	OSTATLANTIK 91/92 - EXPEDITION, Reise Nr. 20, M 20/3, 4. Februar - 13. März 1992. Universität Hamburg, 145 S.
93-4	(1993) Pfannkuche, O., Duinker, J.C., Graf, G., Henrich, R., Thiel, H., Zeitschel, B.	NORDATLANTIK 92, Reise Nr. 21, 16. März - 31. August 1992. Universität Hamburg, 281 S.
93-5	(1993) Siedler, G., Balzer, W., Müller, T.J., Rhein, M., Onken, R., Zenk, W.	WOCE South Atlantic 1992, Cruise No. 22, 22 September 1992 - 31 January 1993. Universität Hamburg, 131 pp.
94-1	(1994) Bleil, U., Spieß, V., Wefer, G.	Geo Bremen SOUTH ATLANTIC 1993, Cruise No. 23, 4 February - 12 April 1993. Universität Hamburg, 261 pp.
94-2	(1994) Schmincke, H.-U., Rihm, O.	OZEANVULKAN 1993, Cruise No. 24, 15 April - 9 May 1993. Universität Hamburg, 88 pp.
94-3	(1994) Hieke, W., Halbach, P., Türkay, M., Weikert, H.	MITTELMEER 1993, Cruise No. 25, 12 May - 20 August 1993. Universität Hamburg, 243 pp.
94-4	(1994) Suess, E., Kremling, K., Mienert, J.	NORDATLANTIK 1993, Cruise No. 26, 24 August - 26 November 1993. Universität Hamburg, 256 pp.

94-5	(1994) Bröckel, K. von, Thiel, H., Krause, G.	ÜBERFÜHRUNGSFAHRT, Reise Nr. 0, 15. März - 15. Mai 1986. ERPROBUNGSFAHRT, Reise Nr. 1, 16. Mai - 14. Juni 1986. BIOTRANS IV, Skagerrak 86, Reise Nr. 3, 21. Juli - 28. August 1986. Universität Hamburg, 126 S.
94-6	(1994) Pfannkuche, O., Balzer, W., Schott, F.	CARBON CYCLE AND TRANSPORT OF WATER MASSES IN THE NORTH ATLANTIC - THE WINTER SITUATION, Cruise No. 27, 29 December - 26 March 1994. Universität Hamburg, 134 pp.
95-1	(1995) Zenk, W. Müller, T.J.	WOCE Studies in the South Atlantic, Cruise No. 28, 29 March - 14 June 1994. Universität Hamburg, 193 pp.
95-2	(1995) Schulz, H., Bleil, U., Henrich, R., Segl, M.	Geo Bremen SOUTH ATLANTIC 1994, Cruise No. 29, 17 June - 5 September 1994. Universität Hamburg, 323 pp.
96-1	(1996) Nellen, W. Bettac, W. Roether, W. Schnack, D. Thiel, H. Weikert, H. Zeitschel, B.	MINDIK (Band I), Reise Nr. 5, 2. Januar - 24. September 1987. Universität Hamburg, 275 S.
96-2	(1996) Nellen, W. Bettac, W. Roether, W. Schnack, D. Thiel, H. Weikert, H. Zeitschel, B.	MINDIK (Band II), Reise Nr. 5, 2. Januar - 24. September 1987. Universität Hamburg, 179 S.
96-3	(1996) Koltermann, K.P., Pfannkuche, O., Meincke, J.	JGOFS, OMEX and WOCE in the North Atlantic 1994, Cruise No. 30, 7 September - 22 December 1994. Universität Hamburg, 148 pp.
96-4	(1996) Hemleben, Ch. Roether, W. Stoffers, P.	Östliches Mittelmeer, Rotes Meer, Arabisches Meer, Cruise No. 31, 30 December 1994 - 22 March 1995. Universität Hamburg, 282 pp.